NASA CR-
141939

MCR-75-13
NAS9-14212

Final
Report

June 1975

Payload/Orbiter Contamination Control Assessment Support

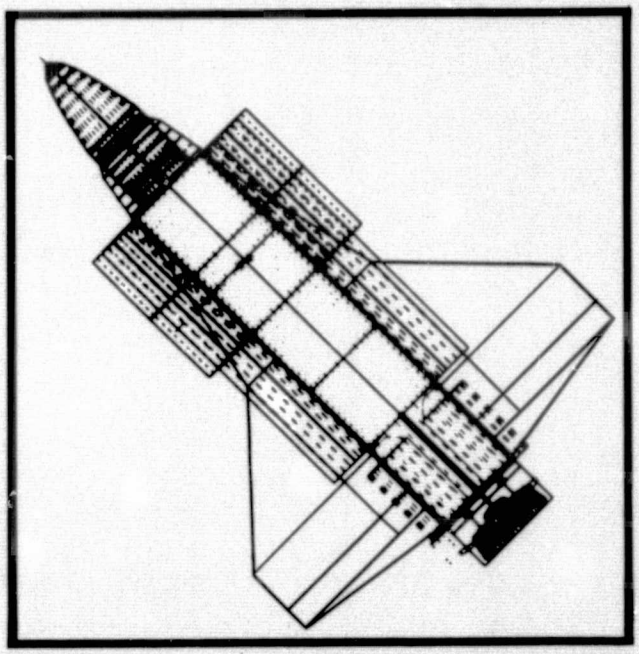

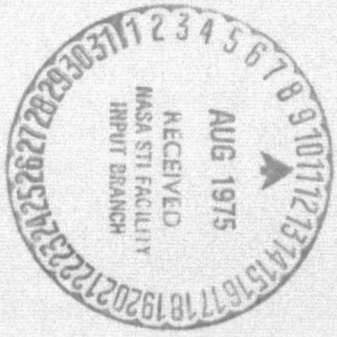

MARTIN MARIETTA

MCR 75-13
June 27, 1975

Technical Report

PAYLOAD/ORBITER CONTAMINATION CONTROL ASSESSMENT SUPPORT

Final Report

Contract NAS9-14212

Authors

R. O. Rantanen
E. B. Ress

Prepared for

Lyndon B. Johnson Space Center
Houston, Texas 77058

Martin Marietta Aerospace, Denver Division
Denver, Colorado 80201
P.O. Box 179

CONTENTS

CONTENTS (Continued)

CONTENTS (Continued)

CONTENTS (Continued)

CONTENTS (Continued)

CONTENTS (Concluded)

1. SCOPE

1.1 Purpose - The purpose of this report is to present the results achieved in performing the Payload/Orbiter Contamination Control Assessment Support study. The intent of this activity was to determine and quantify the expected on orbit contaminant environment for Space Shuttle Payloads from major Shuttle Orbiter sources. These sources are the supplemental flash evaporator vent, cabin atmosphere leakage, outgassing, and the Vernier Control System (VCS) engines. The impact of these sources was assessed through the development and use of a contamination computer model. Particular attention was given to determining the contamination control requirements which should be placed on the Shuttle Orbiter and determining the impact on Shuttle Orbiter design features such as the materials characteristics of external surfaces, use of water sublimators/evaporators for water dumps and/or heat rejection, and the Vernier Control System plume characteristics.

1.2 Scope - This report describes the development and use of a basic contamination math model of the Shuttle Orbiter which incorporates specific Shuttle Orbiter configurations and contamination sources. These configurations and sources were evaluated with respect to known Shuttle Orbiter operational surface characteristics and specific lines-of-sight which encompass the majority of viewing requirements for Shuttle payloads. The results of these evaluations are presented as summary tables for each major source. In addition, contamination minimization studies were conducted and recommendations are made, where applicable, to support the Shuttle Orbiter design and operational planning for those sources which were identified to present a significant contamination threat. These minimization studies are presented as part of this report for completeness and as a record of activities conducted.

1.3 Summary - A basic Shuttle Orbiter contamination math model has been established. This model incorporates specific Shuttle Orbiter configurations and identifies major Shuttle Orbiter contamination sources. A Shuttle Orbiter configuration was synthesized utilizing a mass transport analog to thermal radiation phenomenon for surfaces which act as uniform emitters of mass flux. The Shuttle Orbiter on orbit geometry and major source characteristics have been established consistent with previous contamination modeling activities reported in the Applicable Documents MCR-74-93, MCR-74-474, and MCR-75-202.

The current Shuttle Orbiter contamination math model has updated configuration and source changes over those presented in the above mentioned documents. The configuration and source changes which are reflected in the current model are:

a) geometric refinement of the tail section (view factors to the payload bay);

b) geometric refinement of the Orbital Manuevering System (OMS) pod structure;

c) payload bay door and radiator configuration when opened;

d) supplemental flash evaporator flowrates from 5.5 lb/hr to 15 lb/hr (2.49 kg/hr to 6.8 kg/hr) per nozzle and location;

e) detailed geometry modeling of the 900 lb Reaction Control System (RCS) engines;

f) refined VCS location and orientation;

g) wing elevon shape refinement;

h) overall wing shape and contour update; and

i) rear body flap configuration.

The modeling approach used throughout this study was to utilize independent subroutines for predictions and trade studies instead of spending excessive effort in integrating a large computer model that would require extensive input core capacity and operational time. This allowed minimum turnaround time for trade studies and a detailed checkout of each subroutine. The subroutines were developed with the latitude to be eventually integrated into a single model that would allow access of any source and required computations to assess the contamination potential of the source on a representative critical surface..

From the model development activity, predictions were established for the Shuttle Orbiter contaminant induced environment for specific lines-of-sight for all the major Shuttle Orbiter sources considered. Where these predictions exceeded

the acceptable criteria presented in Applicable Document JSC 07700 Volume X Revision C, minimization studies were performed to identify improvements or recommendations for improvements. The criteria identified in the above applicable document are presented below for reference in understanding the data presented and comparison to the predictions.

a) Fewer than 1 particle larger than 5 microns in the field-of-view of an instrument per orbit.

b) Column density for water vapor less than 10^{12} molecules/cm^2 (polar molecules).

c) Background brightness from scattering or emission less than 20th magnitude/sec^2 in the UV range.

d) Return flux of less than 10^{12} molecules/cm^2/sec.

e) Control to 1 percent absorption of UV, visible, and IR radiation by condensibles on optical surfaces.

Of these criteria, criteria b) and d) were used most often to evaluate the predicted induced environment. As based upon the predicted induced environment and the criteria, the two sources analyzed in detail in the minimization studies were the aft VCS engines and the supplemental evaporator system.

The VCS engines were also evaluated at the forward locations and at various canted orientations at the forward and baseline aft location. For all locations and orientations evaluated, the VCS engine contributions to the lines-of-sight exceeded 10^{12} molecules/cm^2 (polar molecules). Since the VCS engines work on an as required basis, there are a number of important parameters that should be considered by the payload groups to minimize the potential impact of the VCS firings upon their observation requirements. Proper selection of orbital altitude, deadband requirements, and attitude requirements can minimize the VCS impact. Gimballing of payloads will place less requirements on the VCS system. Consideration for Control Moment Gyros (CMGs) for the more sensitive payloads could be an alternate approach to minimize the VCS contribution to the induced environment.

The supplemental evaporator system was also evaluated in detail at numerous locations along the length of the Shuttle Orbiter fuselage beginning at approximately X = 600 and extending to the aft rear end heat shield below the main propulsion engines. Even though some of these locations were desirable from a contamination viewpoint, they impacted other systems (i.e., guidance and control, thermal, structures, etc.). The evaporator minimization studies showed that desirable evaporator locations (from a contamination consideration), in order of priority, were aft facing +X, X = 1519 facing $\pm$Y (lower aft corner), and between X = 600 to X = 950 underneath the payload bay doors facing $\pm$Y. Additional considerations that may impact the desirability of some of these locations were evaluated and they include ice buildup on cold Shuttle Orbiter surfaces, increased VCS usage resulting from forces generated by evaporator exhaust impingement on adjacent Shuttle Orbiter surfaces, and the flow of evaporator exhaust products through the payload bay door/ Shuttle Orbiter fuselage hinge line.

Additional studies were performed to determine the deposition potential on the Shuttle Orbiter radiator surfaces and a surface in the payload bay. Outgassing from the tail leading edge (which can look directly into the payload bay) has been analyzed and does not present a significant contamination problem. The radiator surfaces were assessed to be significantly degraded from direct impingement from VCS and RCS engines and OMS pod structure outgassing. Additional impingement on the radiator surfaces occurs from the return flux of RCS and OMS engine exhaust products and Shuttle Orbiter outgassed material.

Approaches to minimize these potential sources are delineated in the recommendations. These include materials selection and outgassing characteristic measurements and establishing on orbit operational constraints.

2. APPLICABLE DOCUMENTS

2.1 Program Documents - The following documents form a part of this report in the extent that they were used for related program information relevant to this study.

PROGRAM DOCUMENTS

MCR-73-105 Revision 1	"Thermal Radiation Analysis System", (TRASYS), NAS9-14318, May 1975, Martin Marietta Aerospace, Denver Division.
MCR-74-93	"Payload/Orbiter Contamination Control Requirement Study", NAS8-30452, May 1974, Martin Marietta Aerospace, Denver Division.
MCR-74-474	"Payload/Orbiter Contamination Control Requirement Study", NAS8-30755 Exhibit A, December 1974, Martin Marietta Aerospace, Denver Division.
MCR-75-202	"Payload/Orbiter Contamination Control Requirement Study", NAS8-30755 Exhibit B, June 1975, Martin Marietta Aerospace, Denver Division.
JSC 07700 Vol. X, Revision C	"Space Shuttle Flight and Ground System Specifications", July 3, 1974, Lyndon B. Johnson Space Center.
Minutes	"Minutes from the 4th and 5th Particle and Gas Working Group Meetings", S. Jacobs, Lyndon B. Johnson Space Center.

T-169-28 Vol VI — "Shuttle Active Thermal Control System Development Testing Water Ejector Plume Test", November 16, 1973, Summerhays, R. M., LTV, Dallas, Texas.

50M02442 Rev. W — "ATM Material Control for Contamination Due to Outgassing", March 1, 1972, George C. Marshall Space Flight Center.

3. STUDY RESULTS

3.1 Shuttle Orbiter Contamination Modeling - The general contamination modeling considerations and approaches utilized in this study for the Shuttle Orbiter are similar to those reported in the MCR-74-93, MCR-74-474, and MCR-75-202 reports identified in the Applicable Documents section. The following subsections treat specifically those considerations utilized for this study. For completeness, some of the material contained in the above identified reports is repeated.

3.1.1 Shuttle Orbiter Contamination Mathematical Model Description - Presented in Figure 1 is a logic flow diagram of the basic Shuttle Orbiter contamination math model. The flow diagram outlines the major steps and/or functions of the model. Many of the computations are presently developed as subroutines to the model. Without the subroutines, the model utilizes approximately 105K core of a CDC 6000 series computer. Addition of the noted subroutines would increase the total core requirement past 150K thus limiting its operational capability on the current computer.

There are other considerations for maintaining the model as described above. These are:

a) improved fidelity of the Shuttle Orbiter configuration (more surfaces) will increase the total computer core requirements;

b) sources such as the evaporator, VCS, and RCS do not use a radiation analog for characteristic source description, therefore, they require different subroutines for computation;

c) timelining of and positioning of the sources identified in b) have not been firmly established;

d) identification of mission profiles, temperature data, beta angles, mission duration, etc., have not been adequately defined and will require additional core storage for these data arrays;

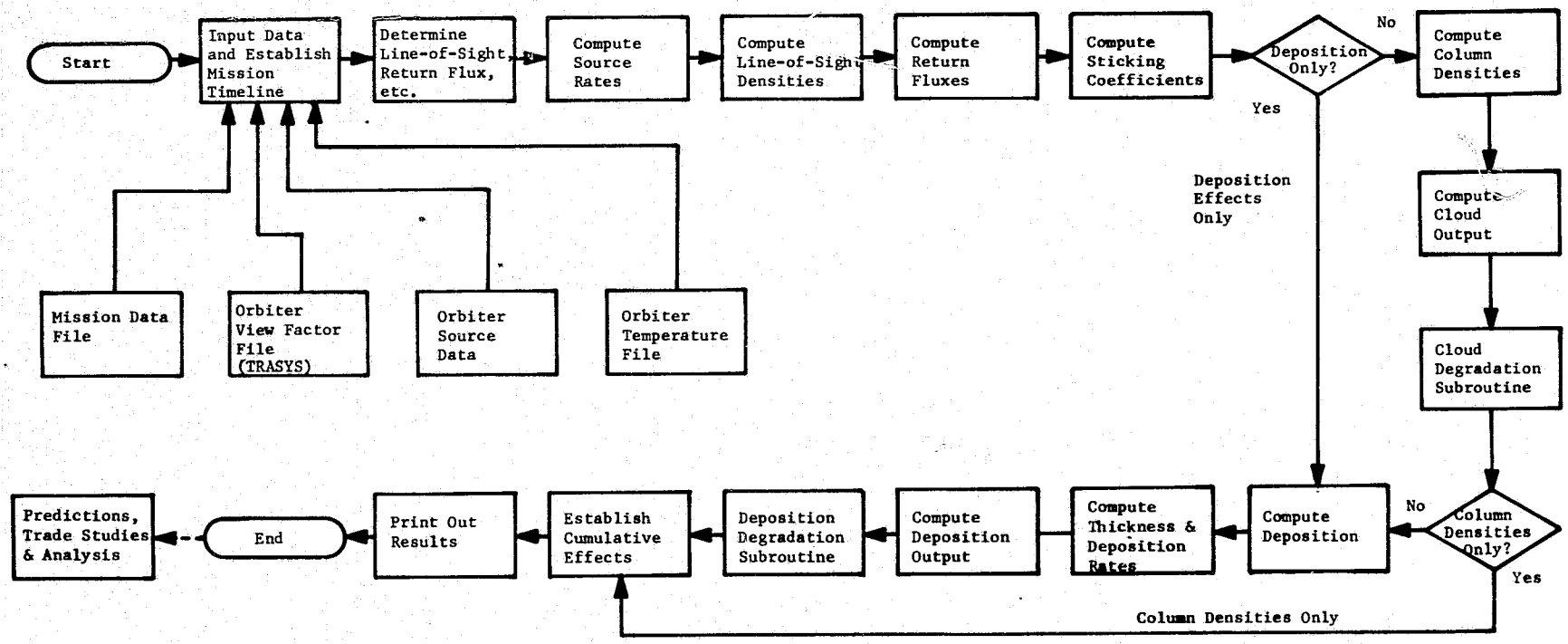

Figure 1. Preliminary Flow Diagram for the Basic Shuttle Orbiter Contamination Mathematical Model

e) the total size required, ultimate operational usage, and the necessary streamlining has yet to be determined; and

f) the need to perform timely trade studies under the current activity has precluded the cumbersome and costly usage of a large complex computer program for specific sources.

It is anticipated that the program may ultimately require extensive computer core capacity where a series of overlays (external subroutines) will have to be developed and integrated to maintain operational capability. Depending upon required geometric fidelity of the modeled Shuttle Orbiter and the number or extent of surfaces required to address the desired mission profiles, this function may also become an overlay or a separate external subroutine. This approach may be desirable since the requirement to continually address these subroutines will be quite high, therefore, minimizing the general cumbersome nature of working with a large totally integrated program which inherently increases computer use time and cost. The ultimate goal in the development of the present model and subroutines is to establish an integrated model that could be operated in a cost efficient manner. The features of the eventual model are anticipated to allow evaluation of each identified major source individually or together and to be able to select the computations desired for the evaluation.

The following subsections discuss and present a description of the various aspects in the development and the data contained in the math model. These are presented for general understanding, interpretation of data presented, and analyses conducted during the contract period.

3.1.2 Surface Description - The Shuttle Orbiter was three dimensionally synthesized on a CDC 6500 computer using a Scope 3.4.1 Operating System. The basic Shuttle Orbiter configuration(s) are synthesized by utilizing a mass transport analog to thermal radiation for surfaces which act as uniform emitters (Lambertian) of mass flux as reported in the Applicable Document MCR-75-105, Revision 1 (TRASYS). The maximum number of surfaces and/or nodes that can be defined using this technique is 1100. Depending upon the number of nodes available for surface definition and the number of surfaces to be described, the minimum area size must be considered as a variable.

The Shuttle Orbiter was described geometrically by 60 basic surface shapes. These surfaces were further subdivided into a total of 194 nodes. Table A-I in Appendix A presents a summary of these surfaces by indicating general area, name of surface, type of geometric surface used, surface number, number of nodes, and node numbers. The physical shape of the surfaces input to the model to define the configurations are drawn graphically by scale computer plots from a Cathode Ray Tube (CRT) display. These graphical displays are used only to verify the location and geometrical shape of any specific surface or relationship between surfaces or contaminant sources and do not form an integral portion of the basic model. These graphical displays will be further discussed in the following subsection.

Three different computer listings or formats are developed from TRASYS with respect to the configuration modeling. These listings provide visibility to all the geometric considerations used is establishing the Shuttle Orbiter contamination model. A set of each of the different computer listings is presented in Appendix A with accompanying descriptive text. The information presented in Appendix A is representative of the development of the Shuttle Orbiter contamination modeling effort to date.

3.1.3 Graphic Displays - The physical shapes of the surfaces input to the computer to define the modeled configuration are drawn to scale on a CRT display. The CRT display is a portion of the TRASYS system and is used to verify the location and geometrical shape of any specific surface or relationship between surfaces or contamination sources. Figures 2 through 5 are current computer drawn CRT displays of the Shuttle Orbiter input configuration used in the contamination model. Figures 2 through 5 present a top view, side view, end view, and three dimensional view, respectively.

Figure 6 demonstrates an important aspect in the development of the computer model in that specific surfaces can be displayed whether they are a source or a receiver. The spatial interaction can be shown without addressing the entire configuration. This latter point is useful in surface mapping a configuration for surface and/or material categorization and location studies prior to input into the contamination model for assessment. Once all of the Shuttle Orbiter surfaces and

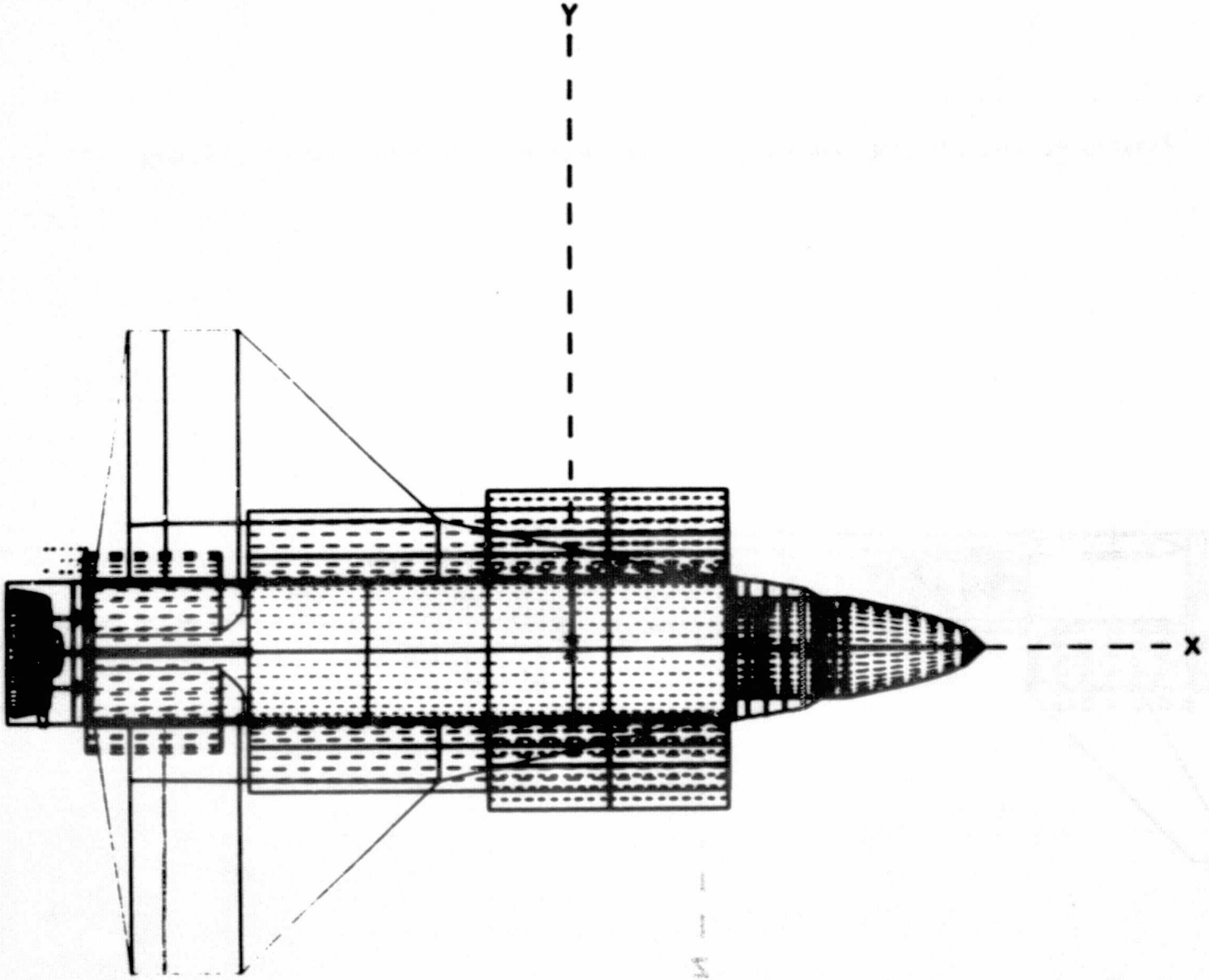

Figure 2. Graphic Display of Top View of the Current Modeled Shuttle Orbiter

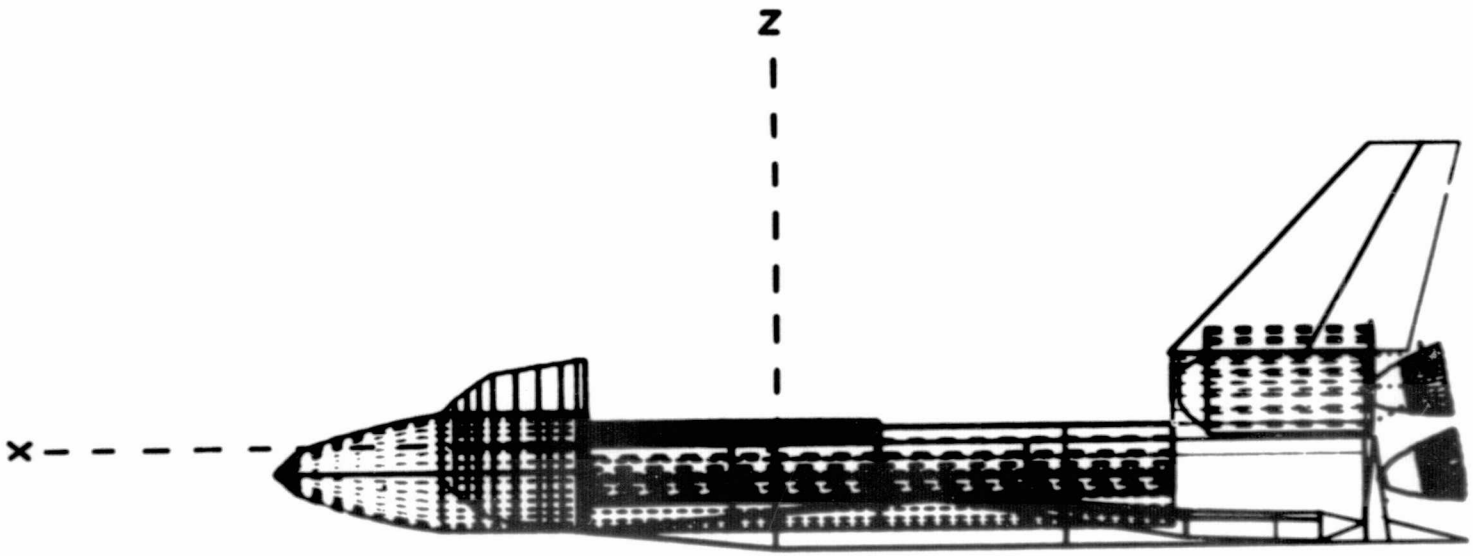

Figure 3. Graphic Display of a Side View of the Current Modeled Shuttle Orbiter

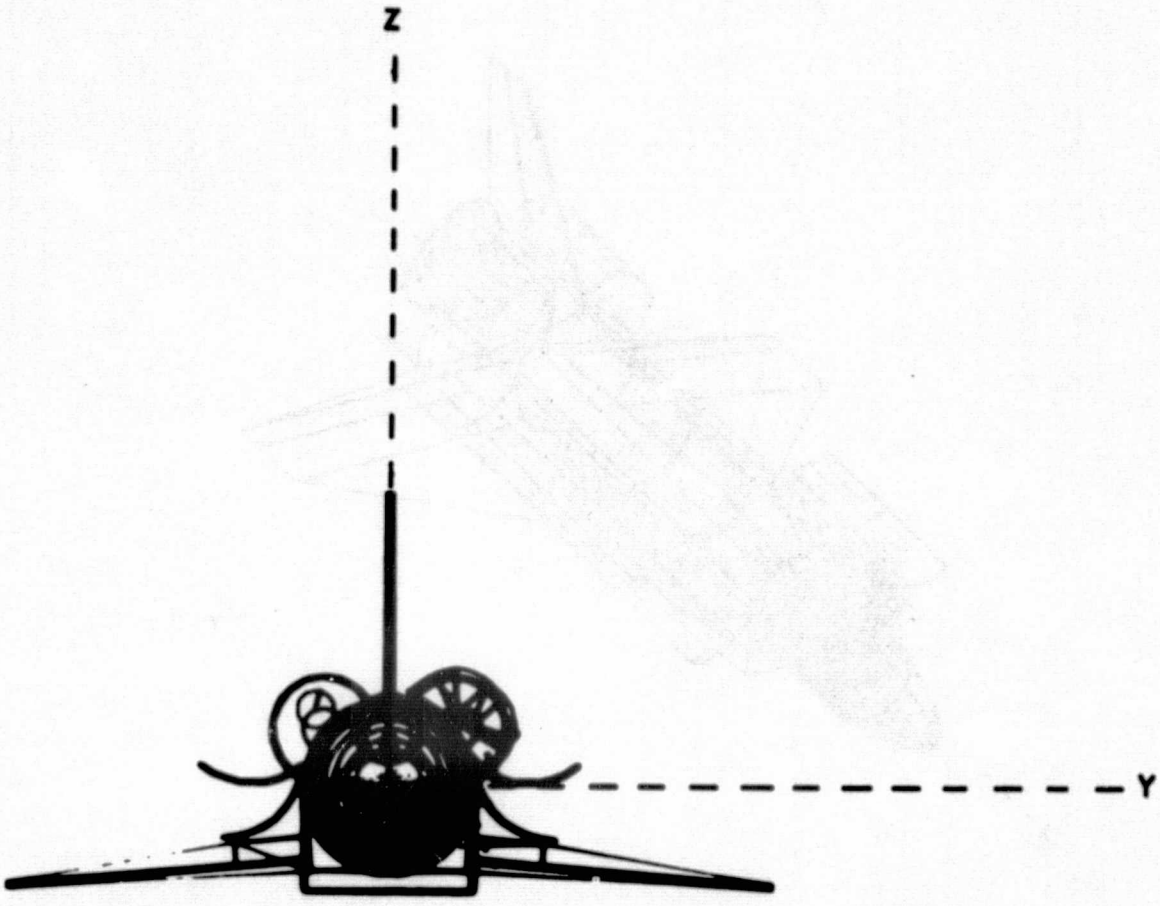

Figure 4. Graphic Display of an End View of the Current Modeled Shuttle Orbiter

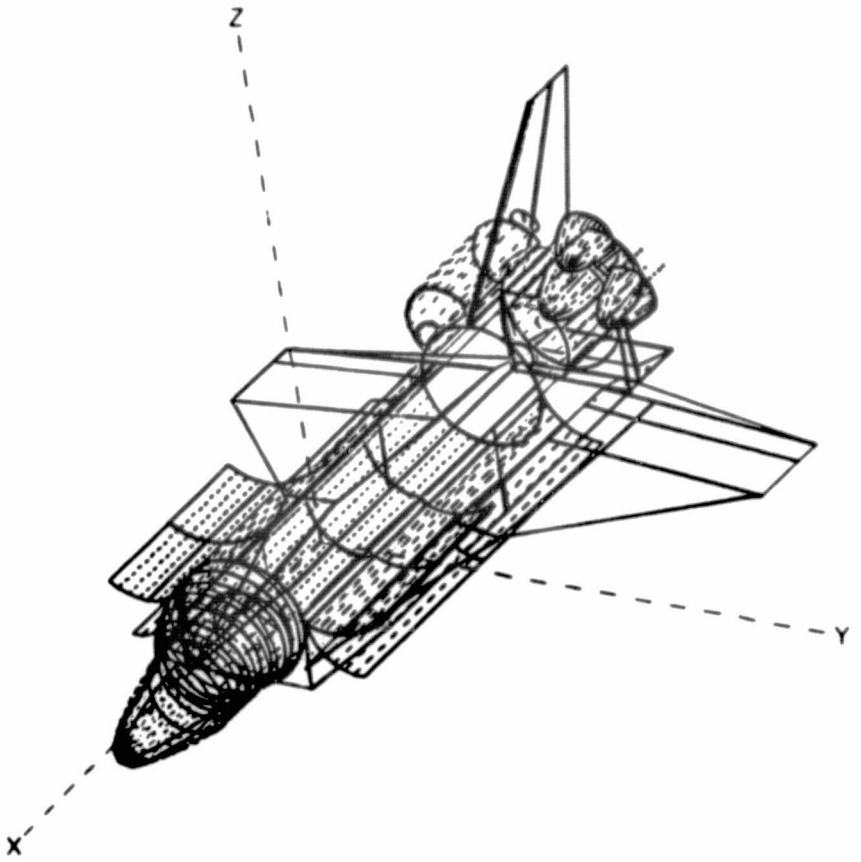

Figure 5. Graphic Display of a Three Dimensional View of the Current Modeled Shuttle Orbiter

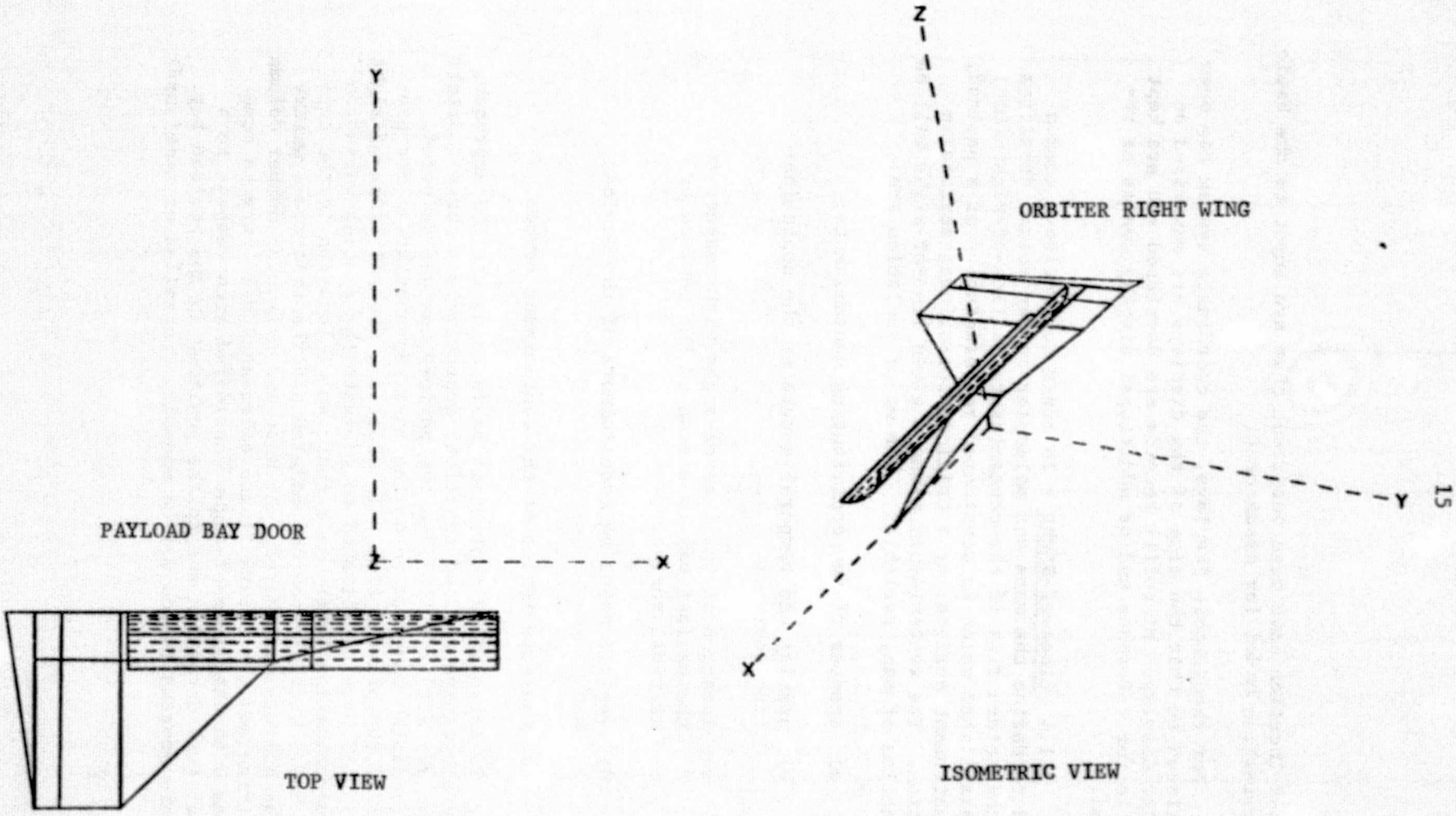

Figure 6. Graphic Display of Isolated Surfaces of Interest.

sources location have been verified, they are input to the basic contamination model for assessment.

For the graphic displays, the coordinate system has been positioned so that the size of the displays are maximized on the CRT display. Microfilm records are developed and are kept on file for reference and/or additional display copies as required.

3.1.4 Lines-of-Sight - In order to provide a common basis to define the mass and molecular number column densities and the return flux of the contaminants, a line-of-sight (LOS) is established which is considered representative of a payload, an instrument surface, or a critical operational surface in question. The contaminants along a given line-of-sight will be a function of many variables. The major variables are:

a) species of the contributing contaminants;

b) spatial and temporal nature of the contamination sources;

c) location of the line-of-sight with respect to the payload bay (position of the payload or critical surface);

d) vehicle pointing requirements of the payload; and

e) characteristics of the contaminant source.

To establish a consistent basis using the LOS approach, a representative payload position, approximately three-quarters of the way aft (X = 1107) in the payload bay was selected. This position was felt to be the most representative for payloads at the present time. In addition, several lines-of-sight at X = 735 were established to evaluate the spatial variation in contamination levels as a function of location in the payload bay. With the sources modeled and the relative symmetry of the sources considered, the mass and molecular number column densities and the return fluxes calculated will vary to some degree with the lines-of-sight considered with respect to a normal (+Z) direction and to the position in the payload bay. As more sources (which may be manually controlled or timelined)

are added to the model, the contaminants along any given line-of-sight with respect to locations in the payload bay can be expected to show larger spatial variations. Payloads with line-of-sight pointing requirements that are not along the +Z axis will see larger spatial variations of the contaminant environment.

For a baseline, nine lines-of-sight were established originating at X = 1107. The majority of outgassing, off-gassing, and leakage analyses was performed for these nine lines-of-sight. These lines-of-sight are identified as:

a) LOS 1A, zero degree line-of-sight (in the +Z direction);

b) LOS 2A, 50 degrees off of +Z towards $\pm$Y;

c) LOS 3A, 25 degrees off of +Z towards $\pm$Y;

d) LOS 4A, 50 degrees off of +Z towards $\pm$Y plus 45 degrees towards +X (aft);

e) LOS 5A, 50 degrees off of +Z towards -X (forward); and

f) LOS 6A, 50 degrees off of +Z towards +X (aft).

These lines-of-sight are graphically depicted in Figures 7 through 12 along with the LOS designation number. LOS 2A, LOS 3A, and LOS 4A actually represent two lines-of-sight each. These are symmetrical and can be analyzed by evaluating only one of the two for each LOS.

At X = 1107, several additional lines-of-sight were evaluated mainly for the evaporator as a source. These lines-of sight are:

a) LOS 7A, 65 degrees off of +Z towards -X (forward); and

b) LOS 8A, 90 degrees off of +Z towards -X (forward) parallel to the X axis one meter above the skin line.

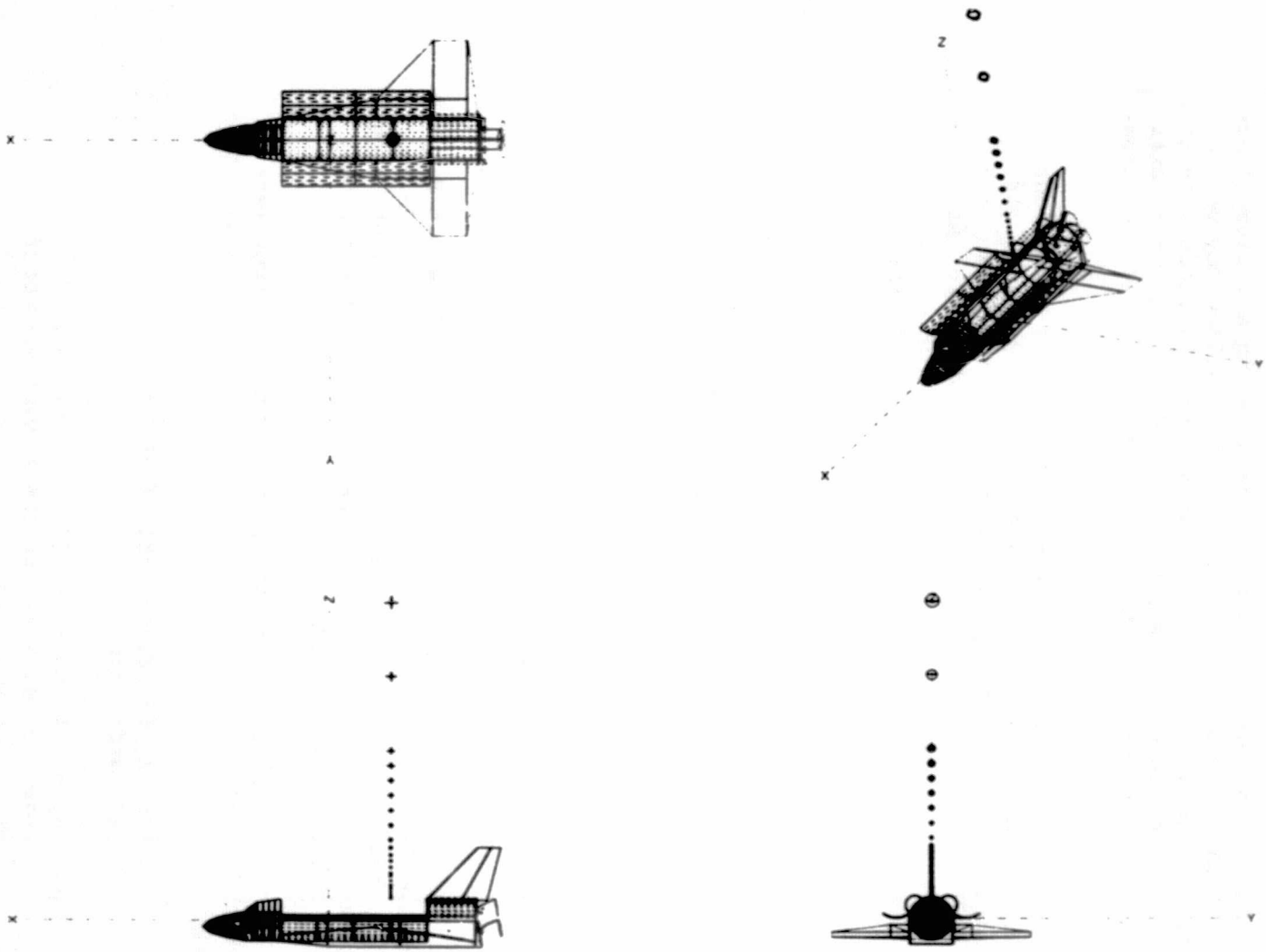

Figure 7. Zero Degree Line-of-Sight - LOS 1A

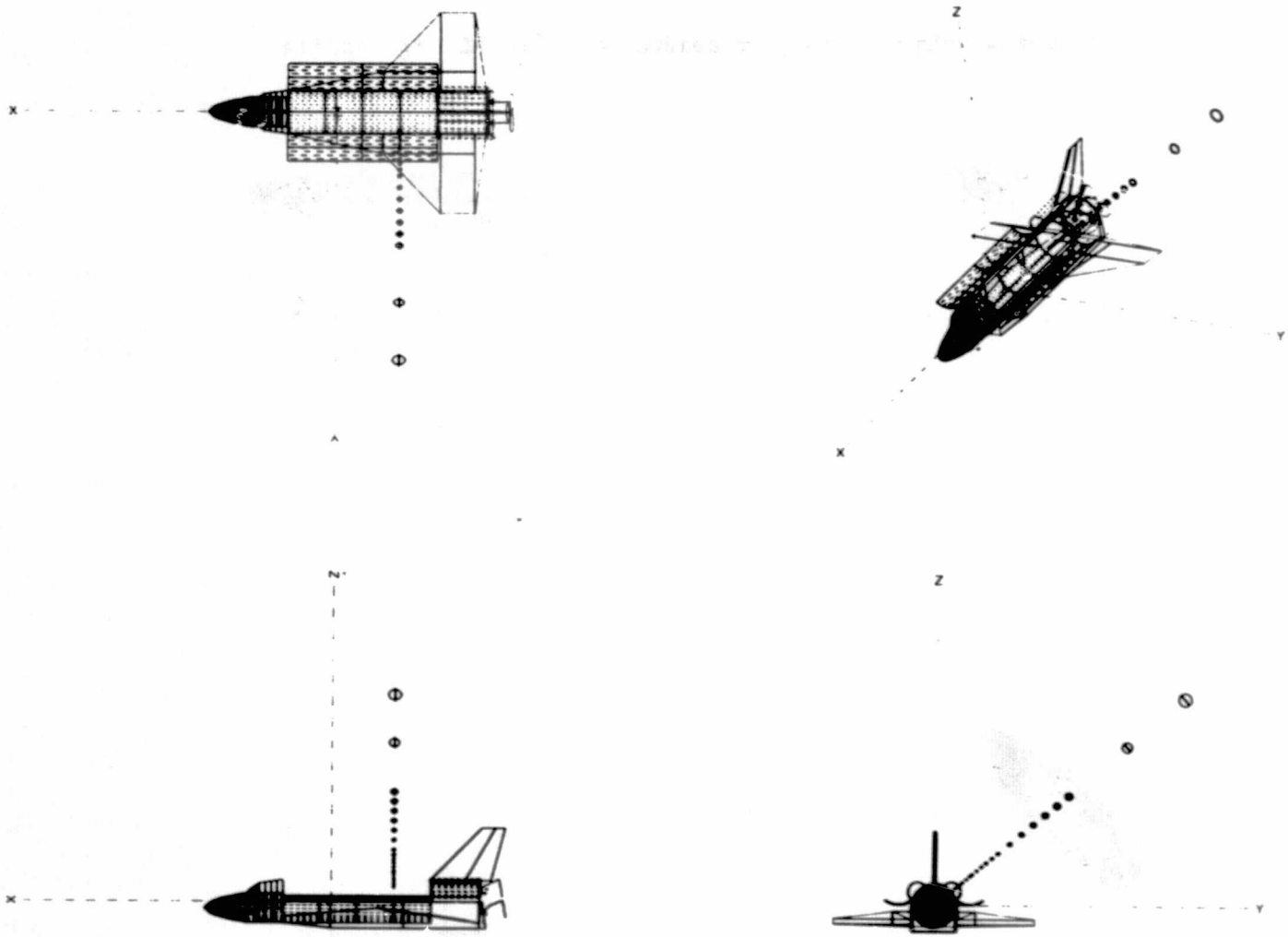

Figure 8. Fifty Degree ±Y Line-of-Sight - LOS 2A

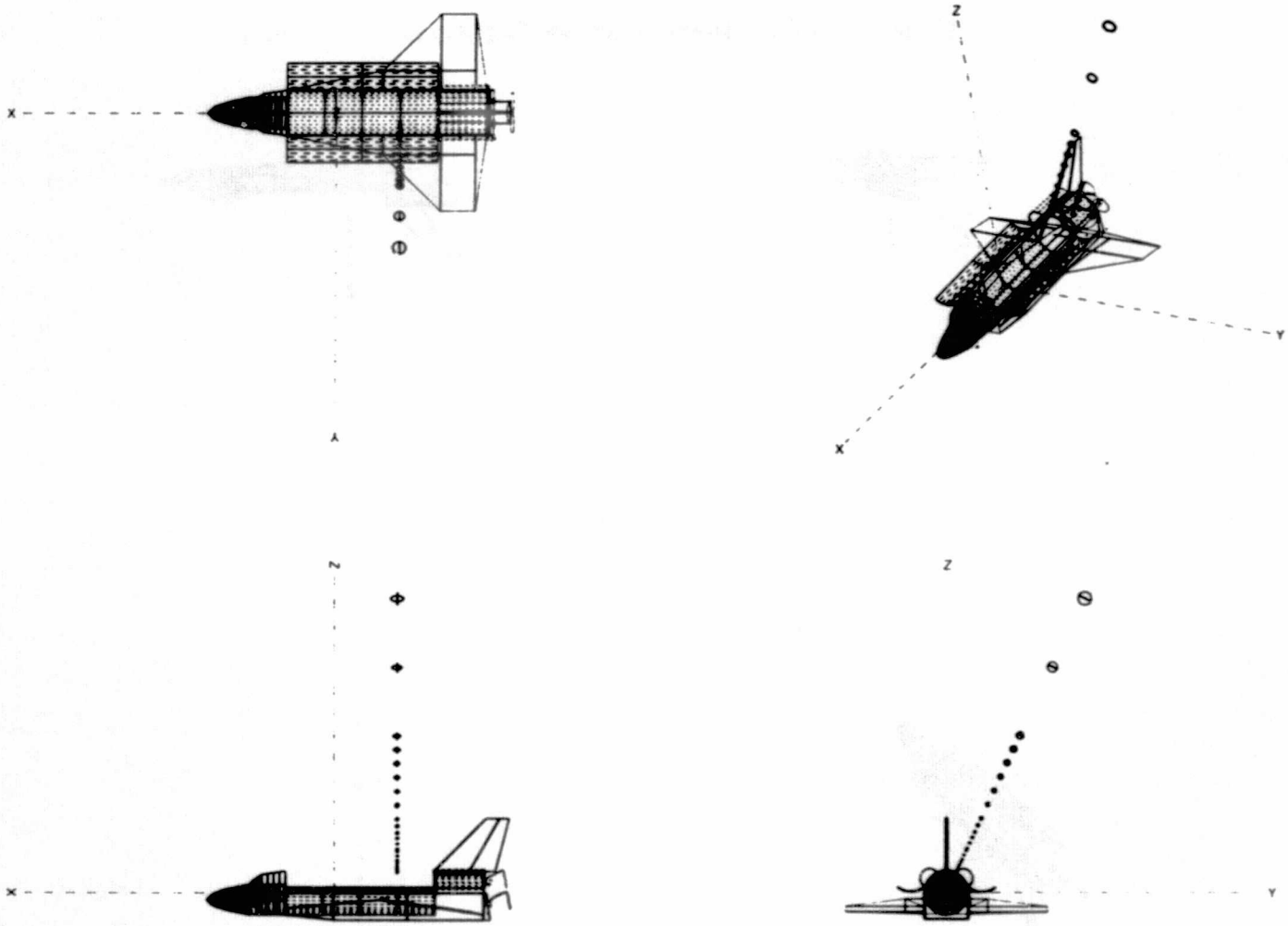

Figure 9. Twenty-five Degree ±Y Line-of-Sight - LOS 3A

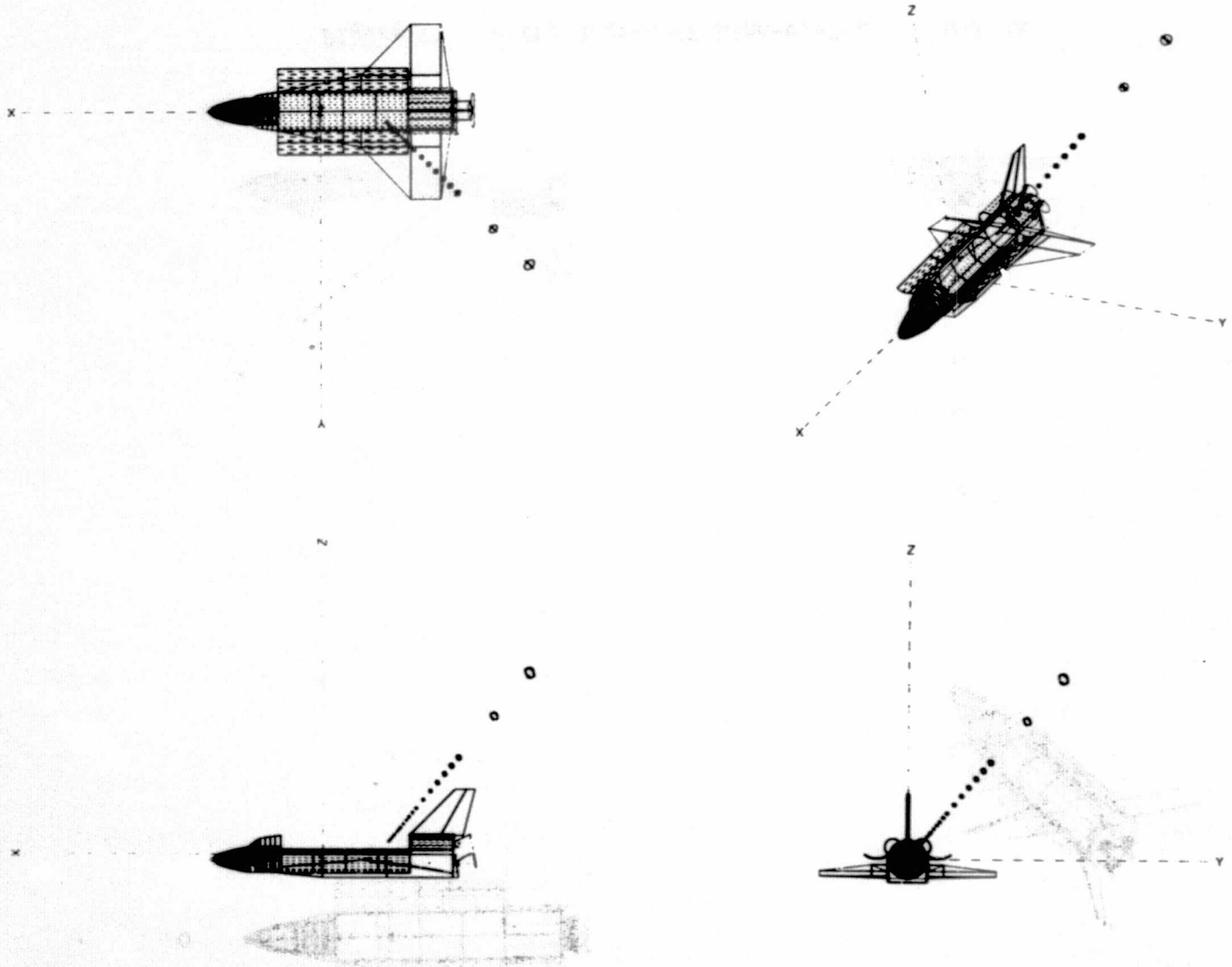

Figure 10. Forty-five Degrees off ±Y Towards +X and Fifty Degrees off +Z Line-of-Sight - LOS 4A

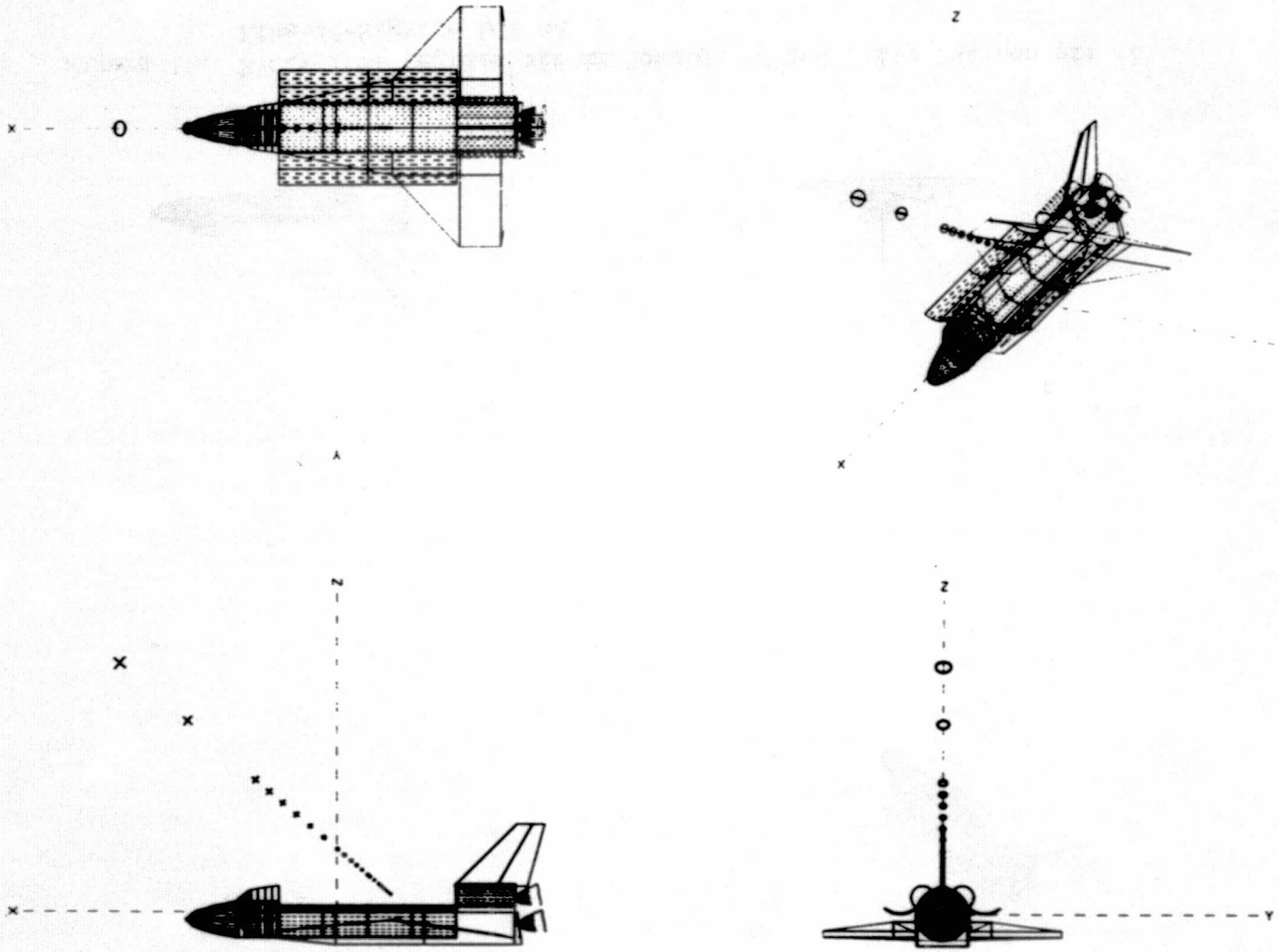

Figure 11. Fifty Degree -X Line-of-Sight - LOS 5A

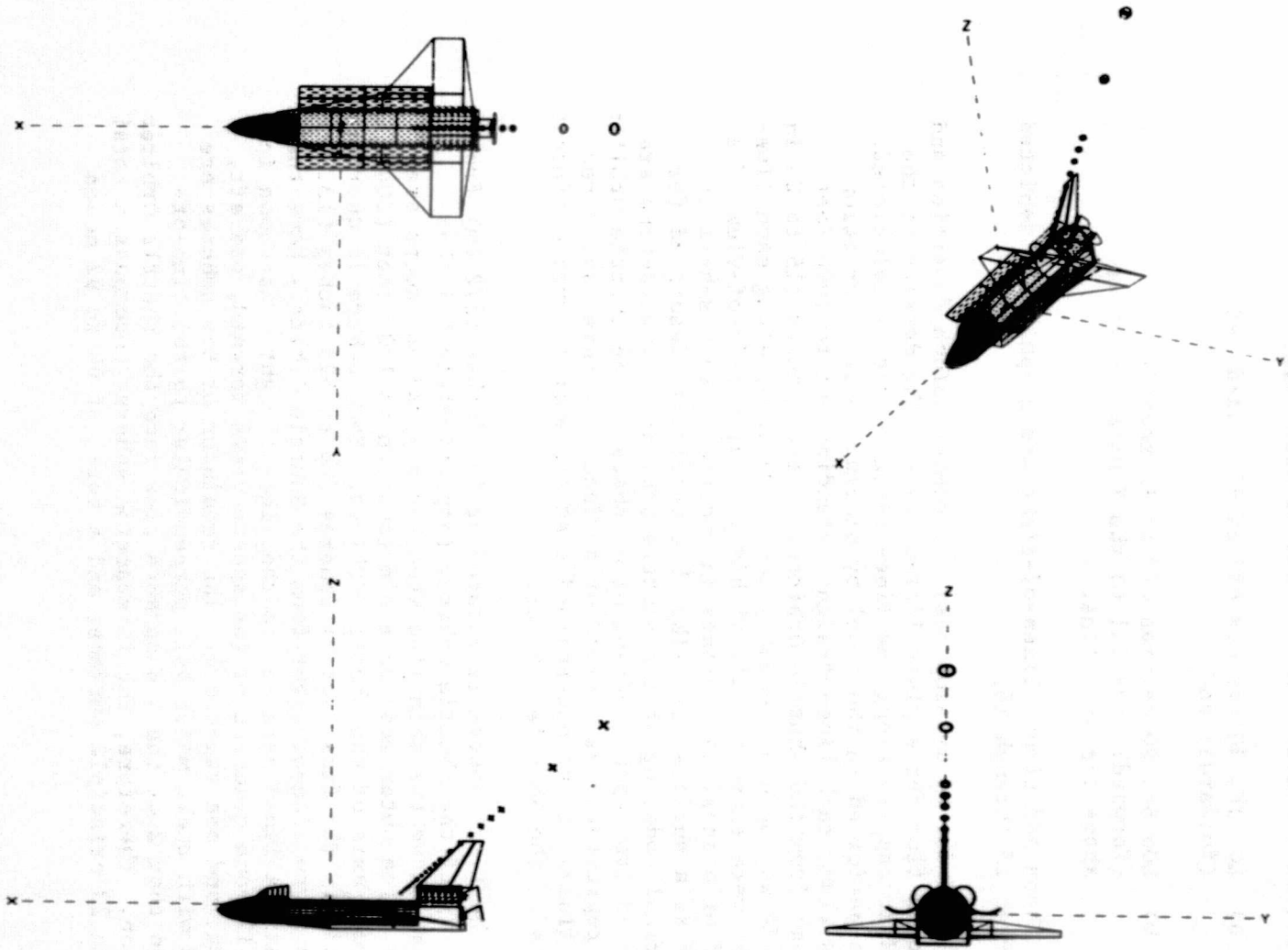

Figure 12. Fifty Degree +X Line-of-Sight - LOS 6A

During the course of this study, several lines-of-sight in the forward part of the payload bay at X = 735 were analyzed for specific sources. These lines-of-sight are:

a) LOS 5F, 50 degrees off of +Z towards -X (forward); and

b) LOS 8F, 90 degrees off of +Z towards -X (forward) parallel to the X axis one meter above the skin line.

These additional lines-of-sight are graphically depicted in Figures 13 through 16.

In order to develop mass and number column densities and the return flux for a given line-of-sight, the density of the induced atmosphere along the line-of-sight must be calculated. This is performed in the model by placing small interaction spheres along each line-of-sight extending out to 1000 feet (304.8 m) from the Shuttle Orbiter. These spheres (15 to 23 in number depending upon geometry considerations) along each line-of sight were sized to fall within typical fields-of-view of a payload or a sensitive surface in question. Each sphere is treated as a surface just like that previously described for geometrical modeling of the Shuttle Orbiter. View factors are calculated from each quadrant of a sphere to the Shuttle Orbiter and/or representative payload or surface. In this way, directional fluxes can be ascertained that are emitted from different portions of the Shuttle Orbiter.

The first sphere is located at 107 inches (272 cm) from the X axis of the Shuttle Orbiter (approximately 5 inches (12.7 cm) above the skin line when the payload bay doors are closed). The outer most sphere's location is 1000 feet (304.8 m) from the X axis of the Shuttle Orbiter. Each sphere is quartered into nodes. The first set of spheres (up to 523 inches (1328 cm) along a given line-of-sight from the Shuttle Orbiter) have their major axis aligned parallel to the line-of-sight. As shown in Figure 17, one quadrant of the sphere views forward, one aft, one port, and one starboard. The remainder of the spheres are aligned with their major axis perpendicular to the line-of-sight so that 2 of the 4 quadrants view into the Shuttle Orbiter direction. Therefore, the interaction spheres encompass a total of 15 to 23 principle surfaces and a total of 60 to 92 nodes

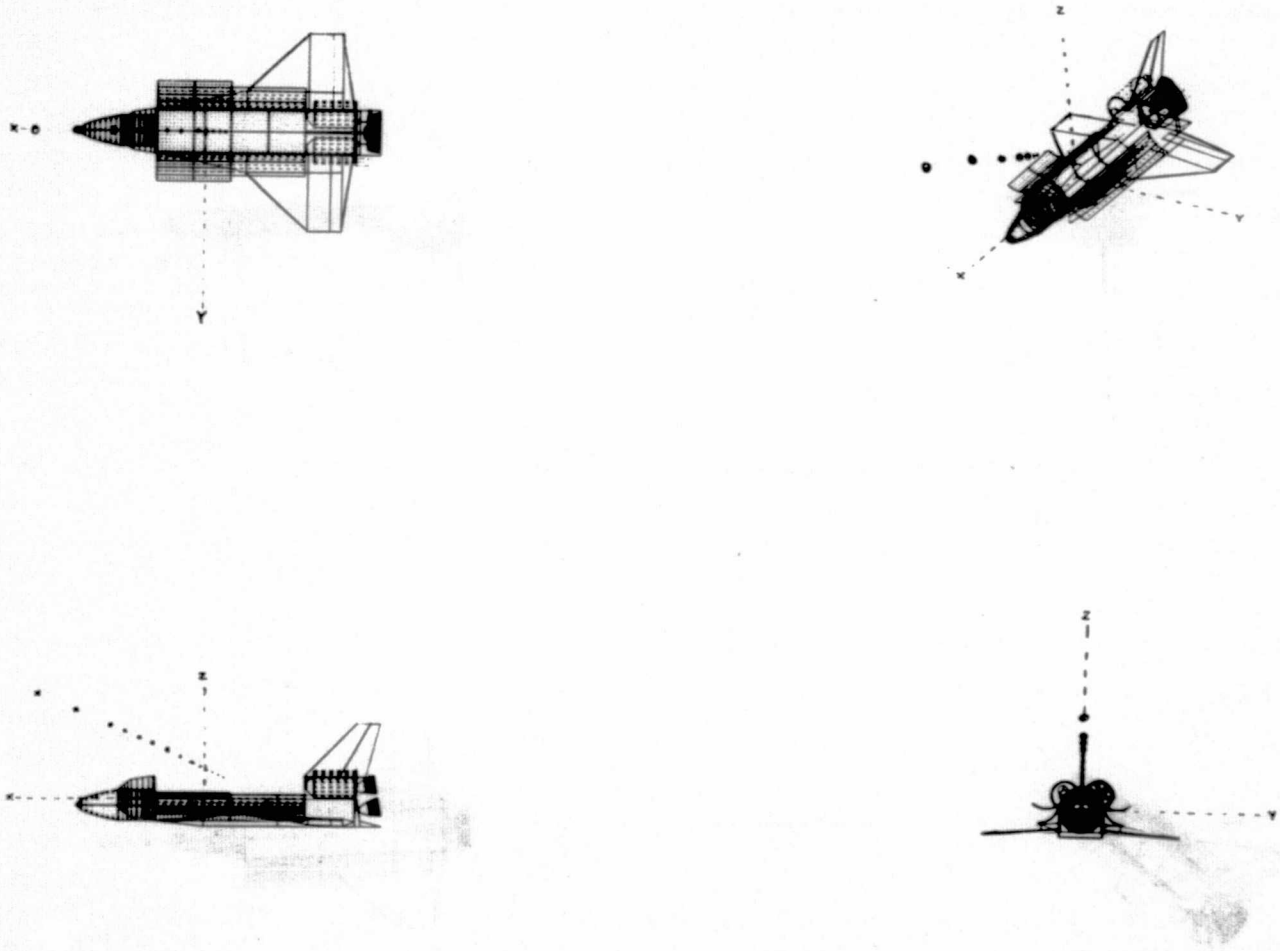

Figure 13. Sixty-five Degrees -X Line-of-Sight - LOS 7A

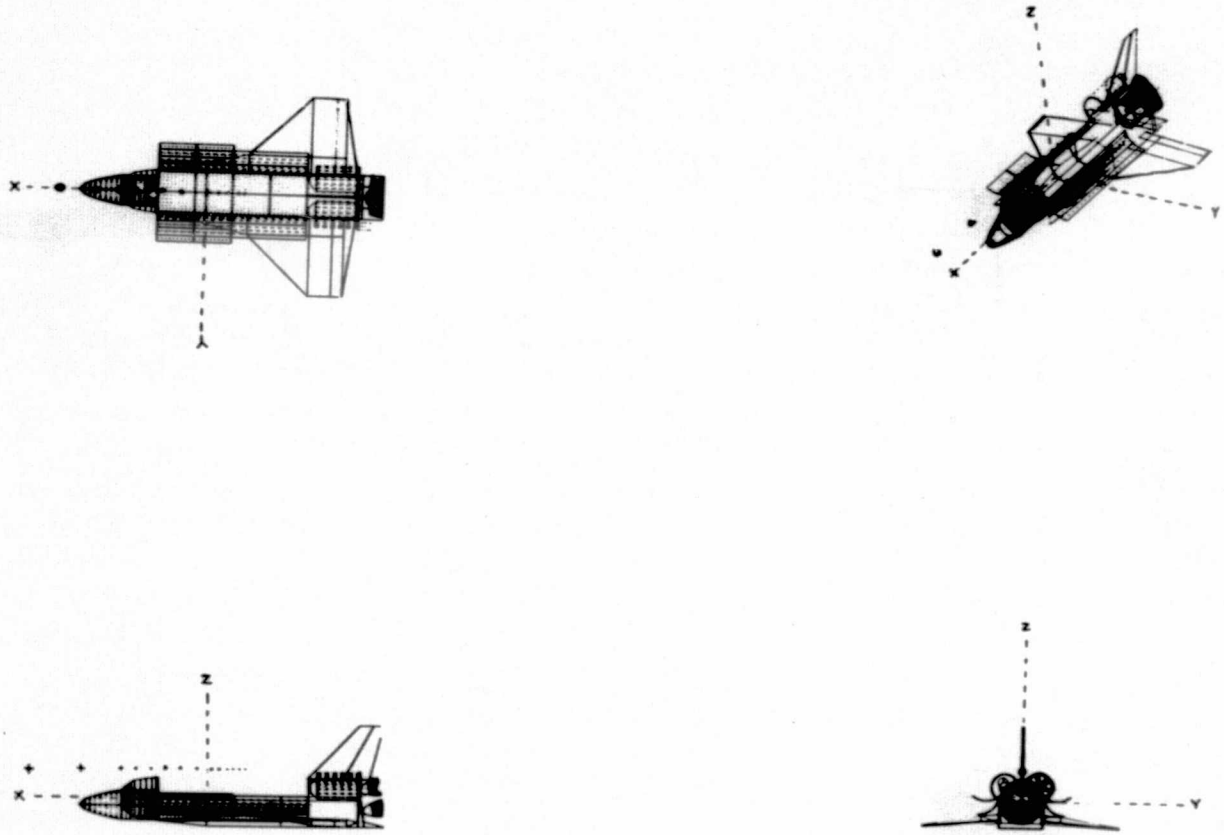

Figure 14. Ninety Degree -X Line-of-Sight - LOS 8A

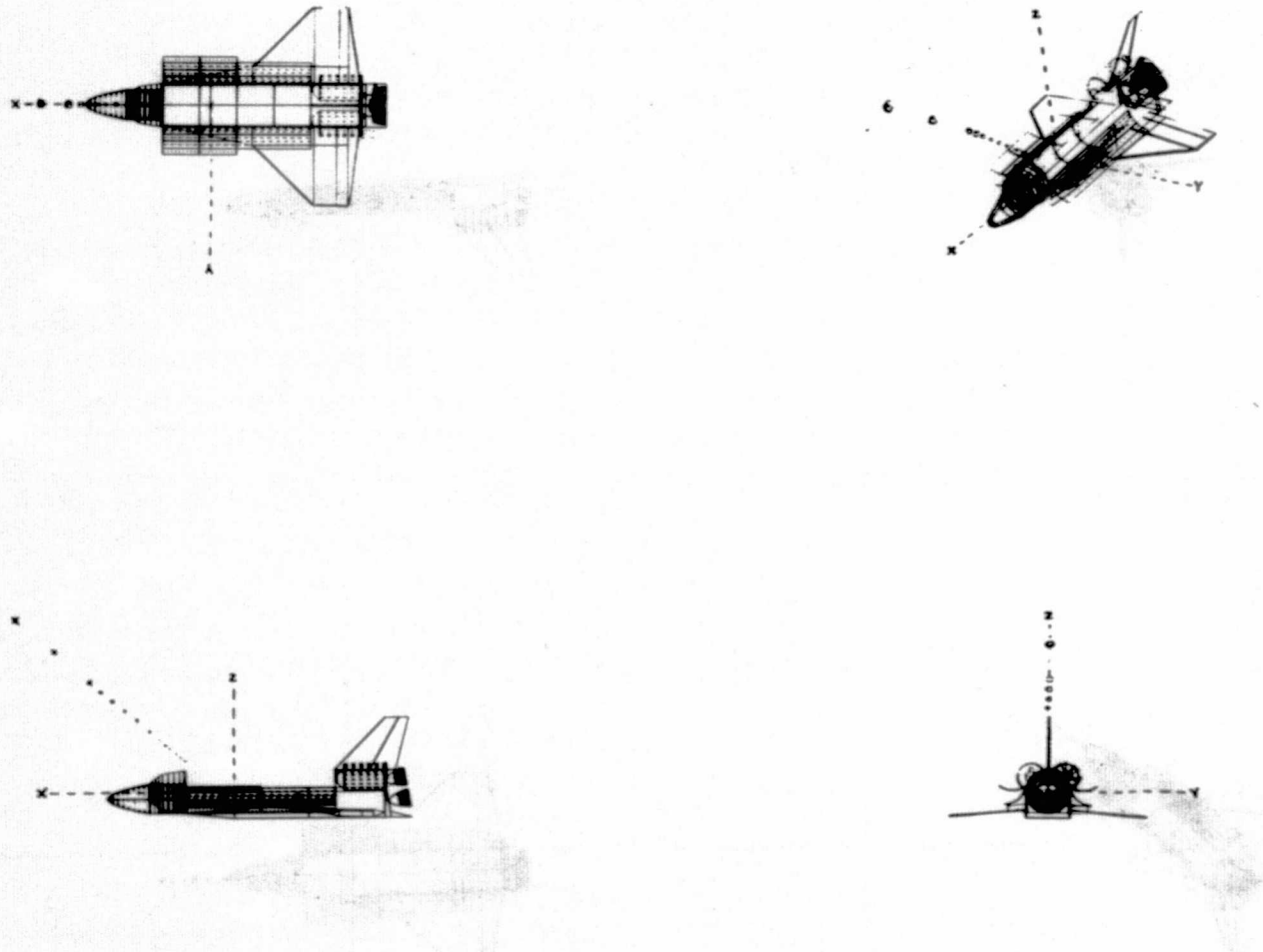

Figure 15. Fifty Degree -X Line-of-Sight - LOS 5F

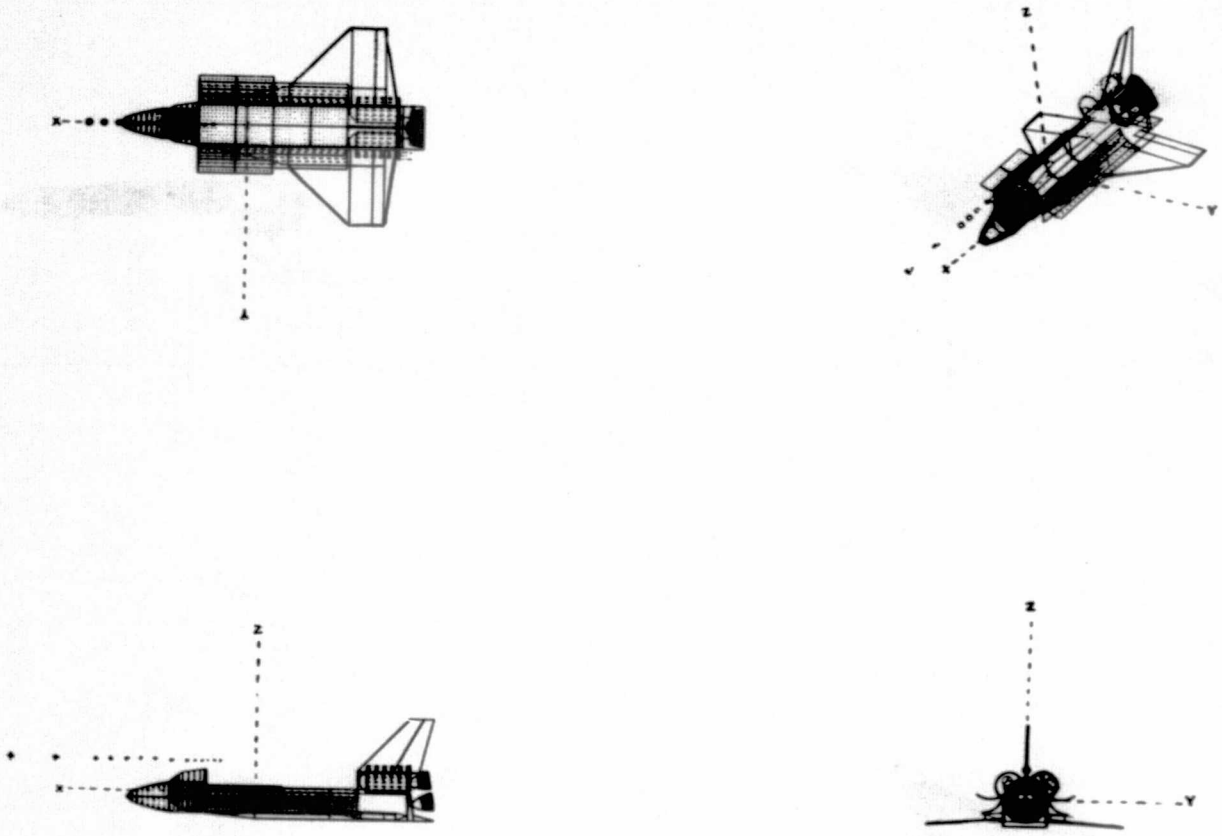

Figure 16. Ninety Degree -X Line-of-Sight - LOS 8F

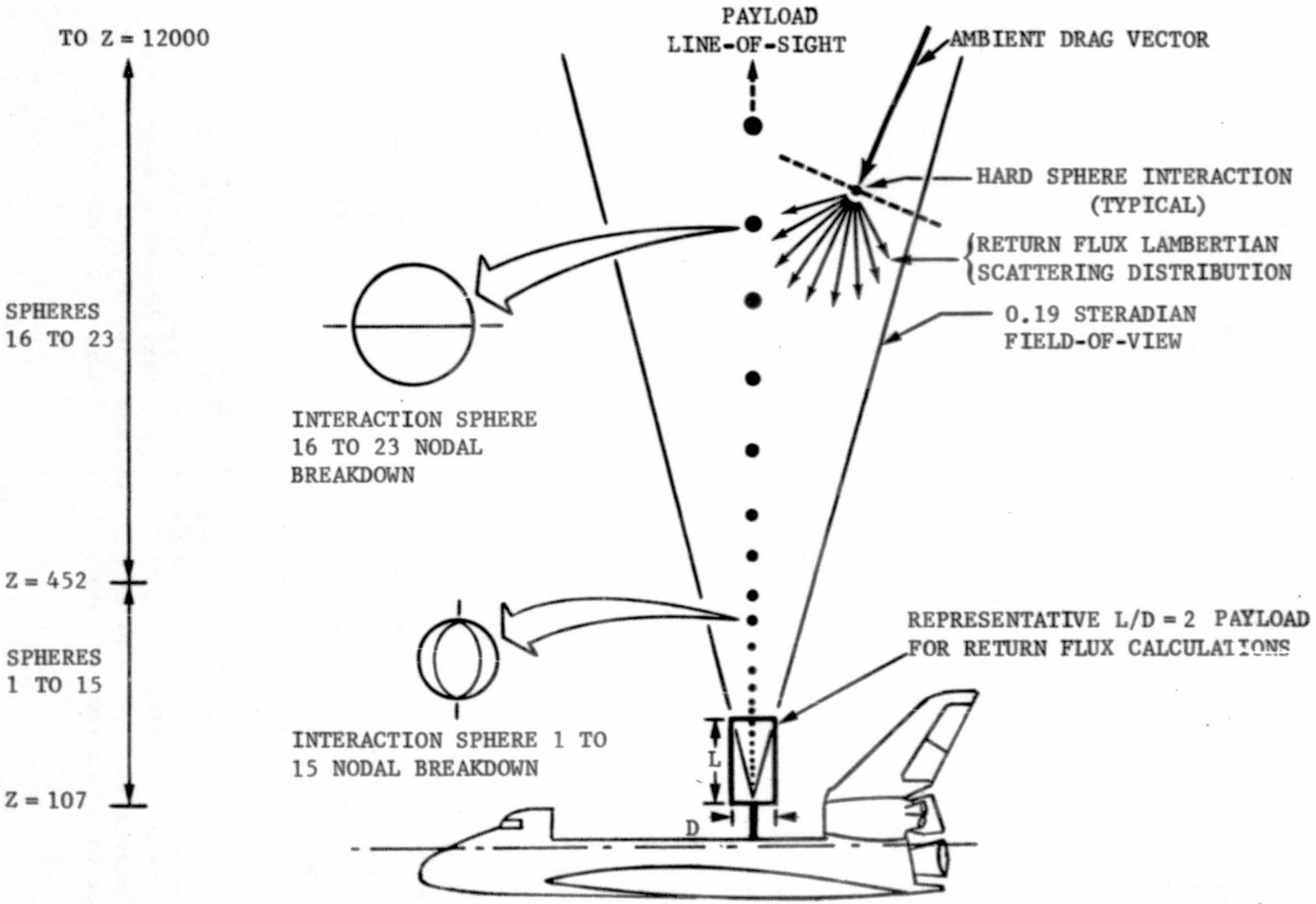

Figure 17. Interaction Sphere Orientations and Return Flux Geometry

depending on the line-of-sight in question and the resolution required. The flux and density at each point (sphere) along a line-of-sight is calculated for each Shuttle Orbiter source considered. Integration along the line-of-sight results in the mass column density (MCD). By knowing the physical makeup of the contaminants (e.g., H_2O, O_2, N_2, N_2O_4, CO_2, etc.) from each source, the mass column density can be converted into molecular number column density (NCD) for each constituent. This is also true for defining the return flux of the contaminants as they interact with the ambient atmosphere.

For simple surface geometries, the return flux is calculated from the mass column or molecular number column density. This is performed by considering the solid viewing angle of the surface, hard sphere gas-gas interactions of the contaminants with the ambient, the vehicle induced atmosphere within this field-of-view, and calculating the fraction of the induced atmosphere capable of returning to a surface within a given solid angle. For this study, the return flux has been calculated for a representative surface with a physical field-of-view of 28 degrees total viewing which equates to a solid angle of 0.19 steradians. For viewing angles up to 45 degrees and less than 28 degrees, the return flux may be calculated by ratioing the solid angle to 0.19 steradians.

In some instances, a surface may have a large field-of-view over which the mass column density varies. Also, the off axis portions of an instrument may be susceptible to contamination, such as baffled systems. Coupled with these possibilities, the density of the induced environment does not necessarily decrease uniformly with distance along a line-of-sight. These considerations rule out a simple analytical approach to the return flux calculations and requires the geometrical relations to be established by additional computer configuration modeling to accurately assess the return flux capability. This additional analysis is highly configuration dependent and was not performed for the present task.

3.2 Shuttle Orbiter Contamination Sources - A review was conducted of available documentation for identification of Shuttle Orbiter contamination sources. As a result of this review, the identified contaminant sources were broken up into four categories. These categories are the major Shuttle Orbiter on orbit sources, other Shuttle Orbiter sources,

reflections and sublimation from Shuttle Orbiter surfaces, and boost and reentry sources. These categories were chosen to basically represent different levels of contamination, unique geometric influences, and different phases of operational activities.

In some instances, the available information was insufficient in detail to uniquely model or specifically define the source characteristics. However, based upon Skylab experience and results, those sources where detailed information was not readily available, they were treated in a manner similar to Skylab developed data.

The following subsections discuss each of the identified sources considered and presents, where applicable, the physical relationships modeled.

3.2.1 Major Shuttle Orbiter On Orbit Sources - The major Shuttle Orbiter on orbit sources considered for this study were:

a) outgassing;

b) offgassing;

c) Shuttle Orbiter cabin atmosphere leakage;

d) supplemental flash evaporator vents;

e) Vernier Control Subsystem (VCS) 25 lb vernier engines; and

f) the return flux.

These sources represent the largest contributors to the induced on orbit environment either steady state or transient in nature. The contaminant quantities, source locations, emission rates, chemical composition, and emission patterns are identified in the following subsections for these sources.

In this study, the difference between outgassing and offgassing is defined as follows. Outgassing is that contribution which comes from the material bulk characteristics and is long term in nature. Offgassing is related to the volatiles which are either adsorbed or absorbed by the material and/or carried in the preparation of a material and evaporate very rapidly when initially exposed to vacuum.

The other contaminant sources mentioned later in this subsection must eventually be quantitatively analyzed and considered in a total Shuttle Orbiter/payload contamination analyses. At present, their impact has been assessed to be less significant than the identified major sources or design and test data is insufficient at this time to perform more than a qualitative assessment.

3.2.1.1 Outgassing - The molecular emission from nonmetallic materials exposed to the vacuum environment of space may contribute significantly to the contaminant environment of the Shuttle Orbiter and payloads. The majority of deposition observed on Skylab was the result of outgassing from nonmetallic materials. Even though these materials were basically controlled to specifications contained in the Applicable Document, 50M02442, the long term nature of the bulk outgassing rate will contribute significantly to the deposition on spacecraft surfaces.

Although the majority of the Shuttle Orbiter surfaces will be covered with carbon and/or ceramic coated silica tiles, the adhesive covering required to bond these materials will represent an identified outgassing source. In addition, when a payload becomes operational, the payload bay doors will be open exposing a significant area of the Shuttle Orbiter which will not be ceramic tiles and thus expose additional nonmetallic materials (which will be carefully selected for low outgassing characteristics).

The current Shuttle Orbiter Thermal Protection Subsystem (TPS) consists of materials applied externally to the primary structural shell covering approximately 11,600 ft^2 (1077.7 m^2) out of a total of 12,961 ft^2 (1204.1 m^2). In addition to relatively small areas such as thermal pane windows and thermal seals, the major portion consists of three separate types of material coverings including Low Temperature Reusable Surface Insulation (LRSI), High Temperature Reusable Surface Insulation (HRSI), and Reinforced Carbon-Carbon (RCC). The LRSI and HRSI are very similar in composition except for approximately 3000 ft^2 (278.7 m^2) of the LRSI which has been recently changed to NOMEX 12 and has yet to be evaluated. The tiles are coated with a RSI ceramic coating (hydrophobic treatment with silicone resin) and are bonded to the Shuttle Orbiter structural shell with Room Temperature Vulcanized (RTV) 560 adhesive 0.0075 $\pm$0.002 inches in thickness. Joint gaps between each individual

tile of 0.050 $\pm$0.015 inches allow for tile expansion during periods of high temperature extremes and provide "escape routes" for outgassed material to the external environment. These tile expansion gaps also have the capability to trap or adsorb material as a result of ground handling, External Tank (ET) ablation processes, Solid Rocket Booster Motor (SRBM) staging, and provide in general a geometry where trapped material may slowly diffuse. This latter condition could be important in assessing the short term outgassing characteristics and the long term outgassing of the bonding material.

HRSI is used basically on the Shuttle Orbiter lower surfaces, the nose cone area, and the vertical stabilizer leading edge (4555 ft^2 or 423.2 m^2) while the LRSI covers essentially all of the Shuttle Orbiter upper surfaces (6482 ft^2 or 602.2 m^2). RCC is used only in areas of very high temperature extremes (greater than 2300°F) such as the nose cone and leading edges of the Shuttle Orbiter wings (563 ft^2 or 52.3 m^2). By far, the largest outgassant source from the TPS will be the RTV 560 adhesive used with the RSI tiles. RTVs have been found to characteristically demonstrate an initial steady-state outgassing rate (OGR) of approximately 1 x 10^{-8} g/cm^2/second at 100°C. However, this rate will be attenuated due to tile geometry and adhesive location and could be further reduced by curing and/or vacuum exposure time. Previous study activities reported in the Applicable Documents MCR-74-93 and MCR-74-474 assumed an average surface outgassing rate of 5 x 10^{-10} g/cm^2/second at 100°C for the entire surface of the Shuttle Orbiter. Simulation testing at MSFC (Reference 1) of a section of TPS has since indicated that this tile configuration has a characteristic outgassing rate of 5 x 10^{-10} g/cm^2/second at 100°C which confirms related outgassing contamination data presented in the above mentioned Applicable Documents. This rate has been used in this study and represents the baseline outgassing rate until changes occur in the planned materials for the Shuttle Orbiter TPS structure at which time new tests will be required to identify the characteristic outgassing rate for the TPS.

During nearly all the orbital operations, the payload bay doors will be in an open position allowing the active thermal control system space radiators to be constantly exposed to space. In modeling these surfaces, a steady-state outgassing rate of 5 x 10^{-10} g/cm^2/second at 100°C was also assumed since the overall outgassing characteristics for this surface are as yet not established.

For specific payloads requiring particular cleanliness levels, the payload bay inboard cavity lower half will be enclosed with a payload bay liner for contamination control and insulation. This will most likely be a fabric liner consisting of some adhesives. The forward and aft ends of the payload bay will be covered with multilayered insulation material. The outgassing rates of the liner and bay end materials exposed to vacuum are inherently dependent upon several factors including surface temperature variations and extremes, accumulative exposure times to space environment, physical and chemical characteristics of the individual materials, and precure procedures employed. To accurately describe the source characteristics of these surfaces, specific tests must be conducted. Therefore, for modeling purposes in this study, the steady-state outgassing rate of 5×10^{-10} g/cm^2/second at 100°C was again assumed to be representative of outgassing as a contaminant source for these surfaces.

Skylab contamination modeling indicated that the outgassing rate of vacuum exposed nonmetallic material varies exponentially with surface temperature and exposure time described by the relationship:

$$OGR = OGR_{100} \left(e^{-t/\tau}\right) \left(e^{\frac{T-100}{29}}\right)$$

where; OGR = Outgassing rate in g/cm^2/second,

OGR_{100} = Initial steady-state OGR at 100°C in g/cm^2/second,

t = Time in hours of vacuum exposure,

τ = Time in hours for OGR to decay to 1/e (0.368) of its initial value. For space vehicles having orbits similar to Skylab, $\tau \simeq 4100$ hours,

T = Temperature of the outgassing surface in °C.

The temperature function $e^{\frac{T-100}{29}}$ follows an equivalent activation energy temperature dependence near 8000 calories/mole for low temperatures. At higher temperatures, the activation energy falls between 10 and 15 Kcal/mole. Preliminary

results of the TPS panel test at MSFC indicates an activation energy near 15 Kcal/mole for a limited temperature range of 70 to 125°C.

Molecules outgassing from a surface generally demonstrate a distribution of the Lambert cosine law ($\cos \theta / r^2$, where θ is the angle from the surface normal and r is the distance from the surface to the point of interest within the distribution). Outgassing will be a continuous source of contamination throughout the entire on orbit periods of the Shuttle missions. The velocity at which the outgassants leave a surface will depend upon the surface temperature and the molecular weight of the outgassed molecules. The most probable velocity for outgassed molecules will be:

$$v = \left(\frac{2R_o T}{M}\right)^{1/2} = 129\sqrt{\frac{T}{M}}$$

where;

v = Velocity of the outgassants in meters/second,

T = Temperature of the outgassants in degrees Kelvin,

M = Molecular weight of the outgassants (M = 100) was assumed for this study.

The major constituents and molecular weights of the outgassants are of course dependent upon the materials used on the Shuttle Orbiter and the payloads. These include RTVs from binders, paints and sealants, and breakdown of long hydrocarbon organic chains. Because of the wide variety of potential outgassants an average molecular weight of 100 was assumed for this study.

3.2.1.2 Offgassing - Most nonmetallic materials such as RTVs demonstrate a period of relatively high mass loss upon initial vacuum exposure before reaching a characteristic steady-state outgassing rate. The initial offgassing rate and subsequent decay rate as a function of time is a strong function of manufacturing processes, assembly, ground handling, launch activity exposure, and material application procedures. The offgassing rate from mission to mission may decrease with time and continued vacuum exposure.

The desorption rate of these adsorbed and absorbed volatile species decay to a characteristic steady-state outgassing rate in 20 to 60 hours. An offgassing rate of $2.5 \times 10^{-9} g/cm^2/$ second at $100^{o}C$ was used in the model and was assumed to be uniformly distributed over the entire Shuttle Orbiter external surfaces. This value is assumed to represent the offgassing rate near the 10 hour point on orbit and is a factor of 5 higher than the steady-state outgassing rate at $100^{o}C$ measured during the MSFC TPS testing.

The actual initial offgassing rate and time dependence will be determined from additional TPS testing being planned at MSFC. Preliminary results from the first MSFC test (Reference 1) have shown this high rate loss period continues for approximately 40 hours at which point it approaches the steady-state outgassing rate. The actual rate of the volatile species was not available from the first TPS test.

As with outgassing, the offgassing rate is a function of the surface temperature. Therefore, the offgassing rate at any temperature is assume to be:

$$OFR_T = OFR_{100^{o}C} \, e^{(T-100)/29}$$

where;

OFR_T = Offgassing rate as a function of surface temperature in $g/cm^2/second$,

$OFT_{100^{o}C} = 2.5 \times 10^{-9} g/cm^2/second$ at $100^{o}C$ at 10 hours,

T = Temperature of the offgassing surface in ^{o}C.

Other parameters of offgassing will be similar to those of outgassing. The plume distribution emitted from the source surface will be a $\cos \theta / r^2$ function and the molecules will be emitted with a velocity of:

$$v = 129 \sqrt{\frac{T}{M}}$$

where;

v = Velocity of the offgassing molecules in meter/second,

T = Temperature of the offgassants in degrees Kelvin,

M = Molecular weight of the offgassants (M = 18) was assumed for this study.

3.2.1.3 Leakage - Leakage from the crew compartments of the Shuttle Orbiter will continuously emerge from structural seams, hatches, microscopic cracks, and seals around support hardware such as instrumentation feed-throughs. The crew compartments will be pressurized to 14.7 psia (one atmos.) with O_2 and N_2 with the nominal leakage rate estimated to be approximately 7 lbs/day (3.18 kg/day). The Skylab leak rate was specified to 14 lbs/day (6.35 kg/day) and the measured value during the mission was approximately 3.75 lbs/day (1.70 kg/day). However, the Skylab internal environment pressure was approximately 5 psia (0.34 atmos.)

Leakage contaminants from these compartments will consist primarily of: 1) normal atmospheric gases, 2) internal materials and black box outgassing products, 3) astronaut by-products, 4) frictional erosion creating particles from materials subject to abrasion, and 5) evaporation from liquid sources.

The normal cabin atmosphere leakage will not condense on most of the Shuttle Orbiter and Shuttle Orbiter/payload surfaces since these gases have desorption rates that exceed impingement rates of these gases. However, the potential of condensation will exist for cryogenically cooled surfaces as employed in infrared telescope payloads and associated subsystems. The second source of leakage products is from outgassed materials in the crew compartment interior. Total contribution from this source to the contaminant environment should be negligible. The third source, astronaut by-products, are elements and compounds such as CO_2 emitted orally and dermally plus flatus and some fecal and urine products which escape their containers and should also present no problem. The fourth source, frictional erosion particles, will in the majority of cases be too large to pass through microscopic leakage orifices and will be removed from the cabin atmosphere through the Environmental Control Life Support System (ECLSS) debris filters. The last source identified is vapor evaporated from liquid

sources. Much of this moisture will be collected by the ECLSS condensate system along with various condensibles and water soluble products in the atmosphere (although approximately 0.076 lb/day (0.03 kg/day) of water vapor will be allowed to leak overboard).

Since the bulkhead between the cabin area and the payload bay area represents the largest probable area for cabin leakage, the leakage was modeled assuming that the total 7 lbs/day (3.18 kg/day) leakage from the forward payload bay bulkhead. This includes a 40 inch (101.6 cm) diameter Extravehicular Activity (EVA) hatch, a 16 inch (40.64 cm) diameter window, and numerous instrumentation feedthroughs which leak through this area. The effluents were assumed to be emitted in a $\cos \theta / r^2$ distribution in an aft direction from this surface. The actual amount that will leak from this area will require a further analysis of the cabin structure for most probable leakage points. Of the 7 lbs/day (3.18 kg/day) leakage, the following constituents and fraction of mass flow rate were modeled:

Constituent	Mass Flow Rate	
O_2	1.625 lb/day	0.74 kg/day
N_2	5.229 lb/day	2.37 kg/day
H_2	0.076 lb/day	0.03 kg/day
CO_2	0.070 lb/day	0.03 kg/day

Leakage will be emitted in molecular form having a most probable velocity based on the molecular weight (M) of the individual constituents and assuming a cabin environment temperature of 25 °C where:

$$v = \left(\frac{2R_o T}{M} \right)^{1/2} = 2220 \sqrt{\frac{1}{M}}$$

v = 413 meters/second (assuming average M = 29)

3.2.1.4 Supplemental Flash Evaporator - During the normal Shuttle Orbiter on orbit fuel cell operation, the fuel cell will generate on demand up to approximately 312 lbs (141.5 kg) of excess H_2O/day which will be expelled overboard through

the supplemental evaporator vent system. The evaporator system will flash evaporate the excess water vapor to space through two nonpropulsive supersonic nozzles. The evaporator operates on an as required basis dependent upon the temperature difference between the incoming and out-going coolant. At a particular temperature difference, the evaporator operates in a pulsed mode until the temperature difference is within acceptable limits. The exact location for these nozzles is as yet to be determined. Therefore, a number of locations were extensively investigated in this study. The results of each location evaluation are discussed in detail in subsection 3.4.2. Through preliminary vacuum chamber testing of a candidate evaporator vent system at JSC (Applicable Document T-169-28 Vol VI) and from a semi-empirical analysis, the plume distribution from any one of the supersonic nozzles at a 16 lb/hr (7.26 kg/hr) flow rate was determined to be:

$$\dot{m} = 2.05 \left[\frac{\cos^6 (1.01\,\theta)}{(r^2)} \right] \qquad \text{for } 0^\circ \leq \theta \leq 36.8^\circ$$

and

$$\dot{m} = \left[\frac{0.540}{(r^2)} \right] e^{-0.0773\,(\theta - 36.8^\circ)} \qquad \text{for } 36.8^\circ < \theta \leq 148^\circ$$

where;

$\dot{m}$ = Mass flux rate per unit area in $g/cm^2/second$,

θ = Angle from evaporator vent nozzle axis in degrees,

r = Distance from nozzle exit plane to point of interest in centimeters.

The plume distribution is depicted in Figure 18 for a nominal flowrate of 16 lb/hr (7.26 kg/hr). This test indicated that the fraction of mass expanding to angles greater than 90 degrees varies between 0.001 and 0.002 for differing nozzle lengths.

Molecular velocities of the expelled water vapor were modeled using the mean radial velocity relationship:

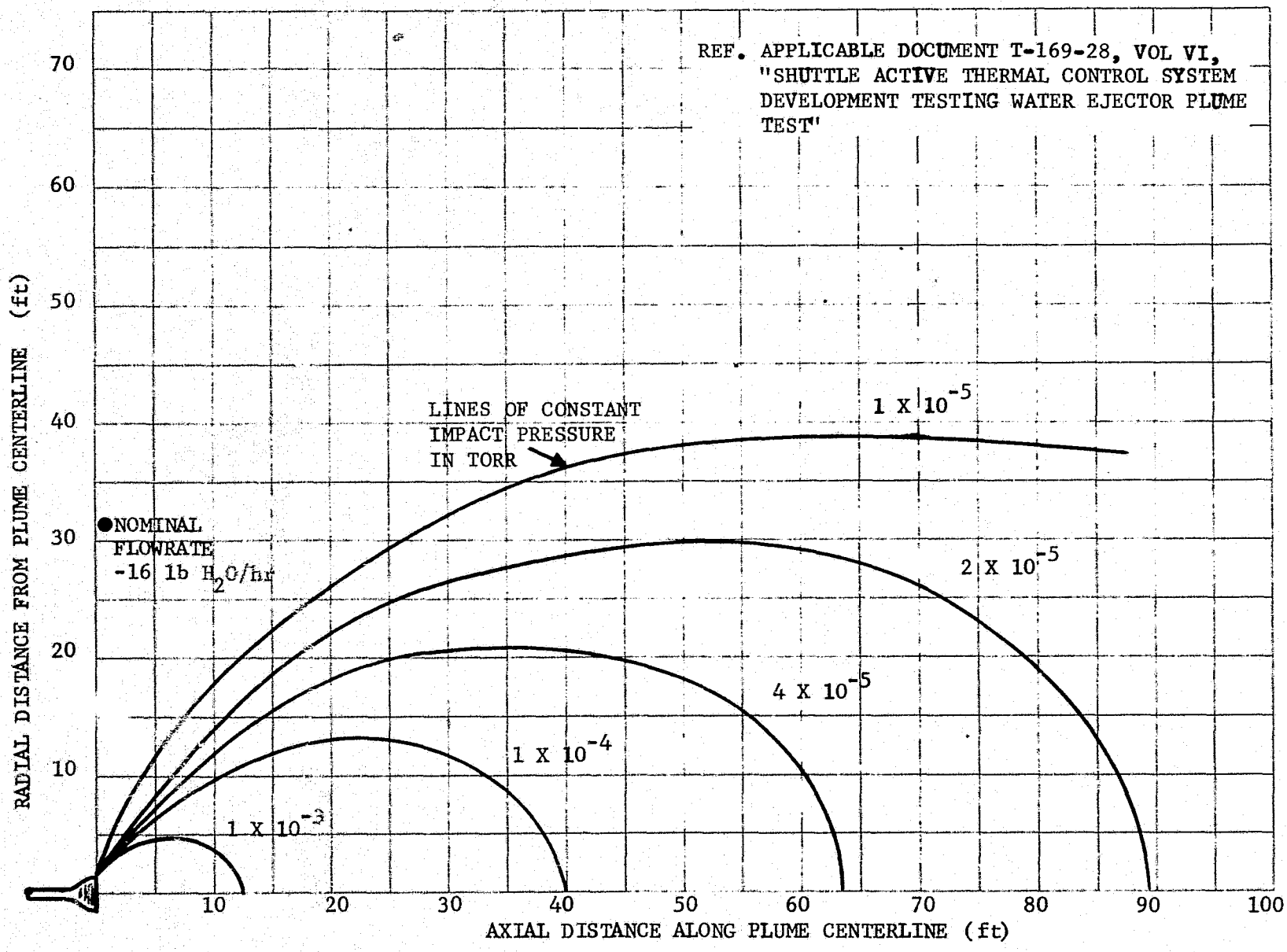

Figure 18. Impact Pressure Data - Supersonic Evaporator Nozzle

$$v = \sqrt{\frac{2\gamma RT}{(\gamma - 1)M}}$$

where: $\gamma = c_p / c_v = 1.4$,

R = Universal Gas Constant,

T = 273 degrees Kelvin,

M = Molecular weight (M=18, water)

therefore; $v_{273^oK} = 1003$ meters/second

During the course of this study, a different evaporator system than tested was selected for the flight hardware. When this hardware becomes available for testing, updated data concerning the evaporator system will be reevaluated. It is felt, however, that the data presented herein is representative of the new evaporator system and the data presented may be indicative of the new evaporator performance.

Figure 19 schematically shows the evaporator vent locations evaluated for this study. The evaporator vent location at X = 1392 is presented in the major sources summary table in subsection 3.2.1.7 as the baseline location. Other locations evaluated are discussed in subsection 3.4.2.

3.2.1.5 Vernier Control Subsystem (VCS) Engines - The VCS engines considered for this study were the six 25 lb (nominal) thrust vernier engines. Figure 20 shows the location and orientation of these engines. Two verniers are located forward of the cabin, one on each side. These engines exhaust primarily down (35 degrees off of -Z toward ±Y). There are no surfaces in the direct field-of-view of these engines. However, in side and back flow, these engines can contribute to mass column densities for certain lines-of-sight and distances from the Shuttle Orbiter.

Four verniers are located aft near the Orbital Maneuvering System (OMS) with two engines on each side of the Shuttle Orbiter. Each set of these verniers are positioned such that one engine each on both sides thrusts in the downward direction (-Z direction). The remaining verniers thrust in the port (-Y) and the starboard (+Y) direction. These rear vernier engines have the capability of directly impinging upon principle Shuttle Orbiter surfaces.

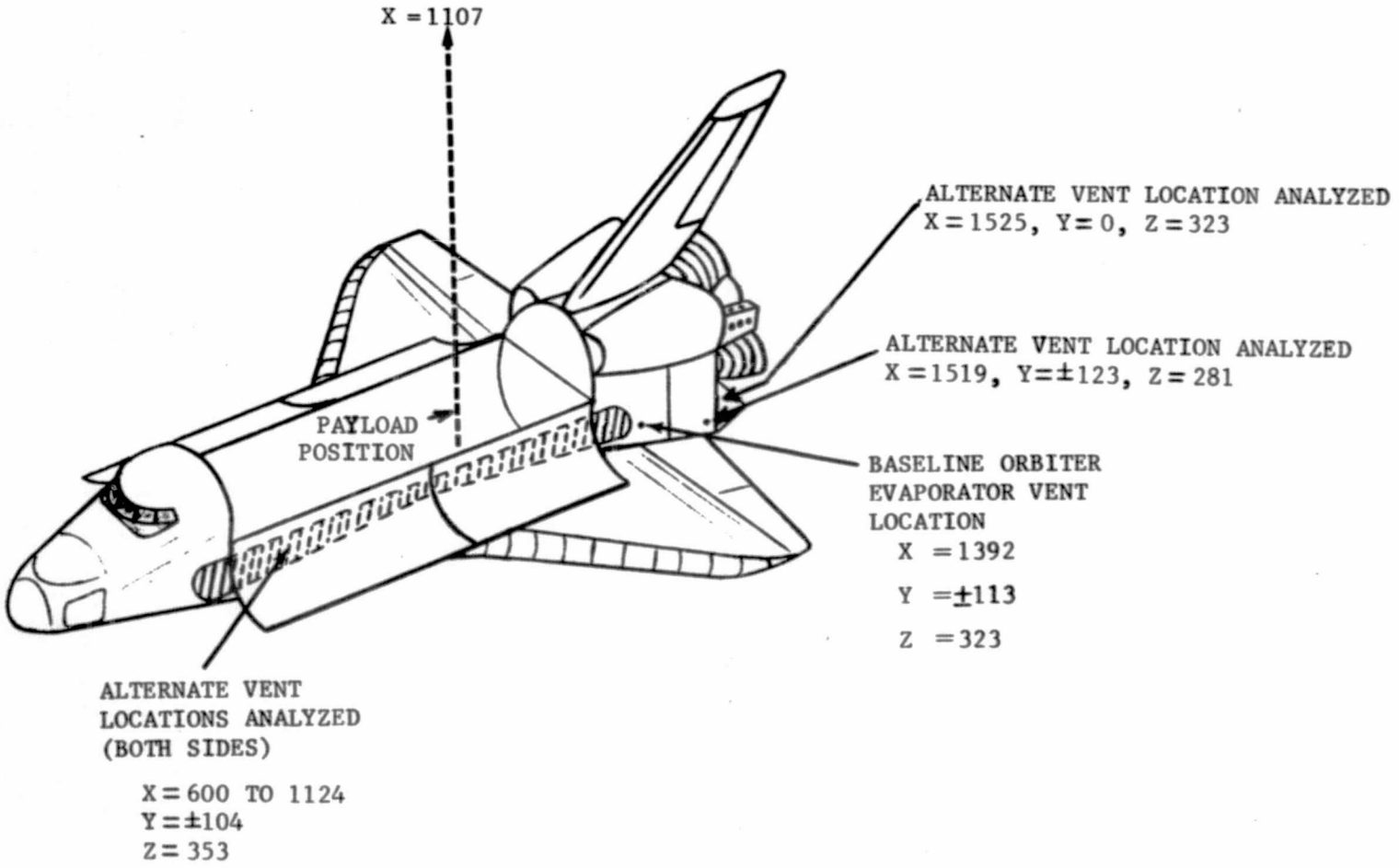

Figure 19. Shuttle Orbiter Baseline and Alternate Evaporator Vent Locations

VERNIER NO.	VEHICLE STA. NO. X	Y	Z
1	323.5	46.0	373.5
2	323.5	-46.0	373.5
3	1565.0	-134.0	459.0
4	1565.0	-118.0	457.0
5	1565.0	118.0	457.0
6	1565.0	134.0	459.0

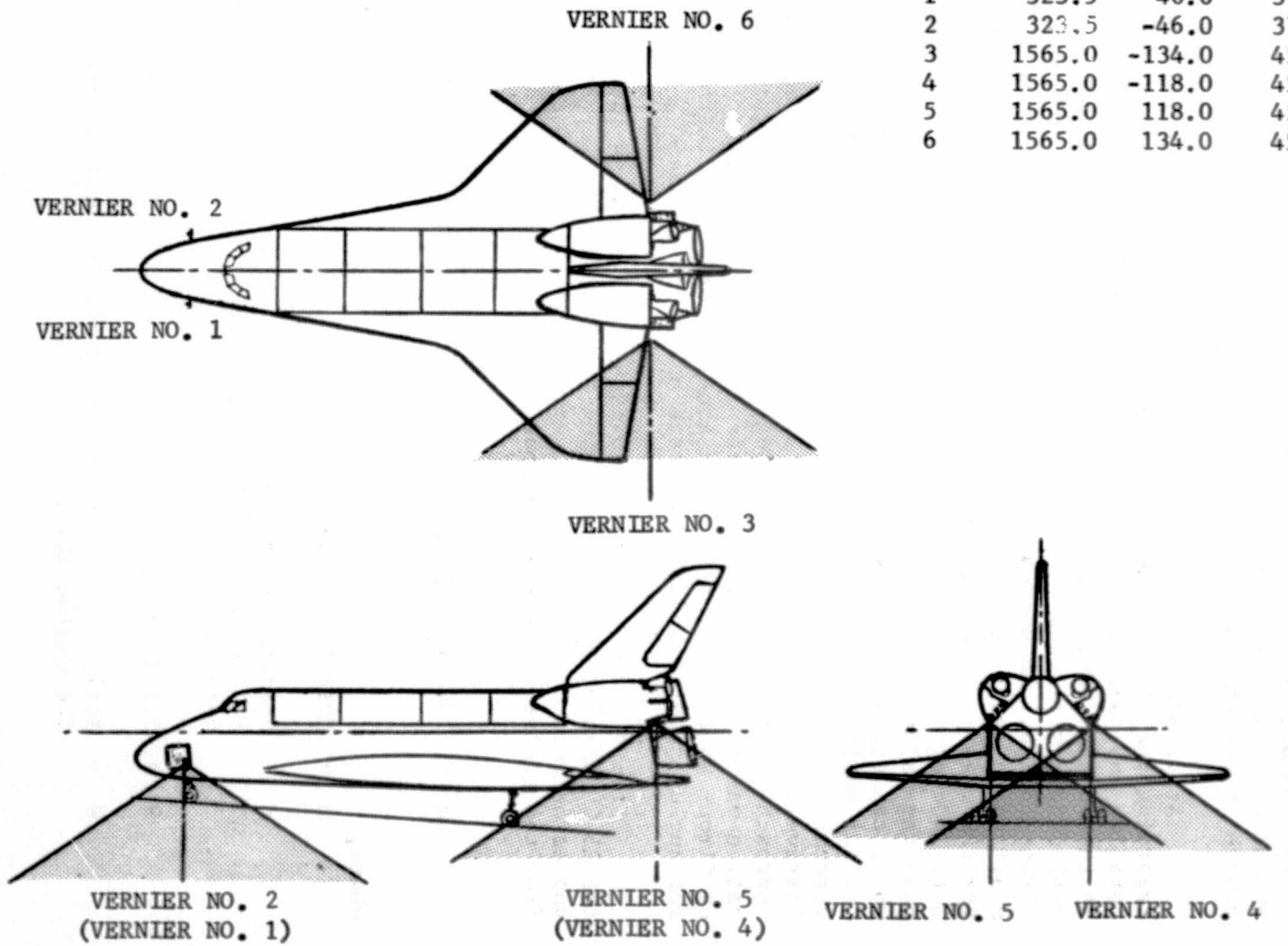

Figure 20. Vernier Engine Locations

In particular, the thrusters can impinge upon a considerable amount of wing area thus presenting an additional contaminant source in reflection.

At present, there is insufficient information available regarding the specific design of these engines to justify a detailed analysis of the exhaust flow fields beyond that used in this study. Modeling of the flow fields was based upon a scaled down version of the Skylab Marquardt R-4D N_2O_4/MMH 100 lb thrust engine. An approach developed by Simons (Reference 2) was modified to establish a closed form analytical representation for the mass contained in the engine flow field for angles from 0 to 140 degrees from the engine centerline. These angles encompass the major portion of the vernier engine flow field mass which can either be reflected or deposited on adjacent Shuttle Orbiter surfaces and contribute significantly to the induced environment. Beyond 140 degrees, the experimental data of Chirivella and Simon (Reference 3) indicates the mass flux may approach a constant value becoming independent of θ. This observation was injected into the present study by modifying the model of Simons so that it predicted a constant mass flux in the plume for angles greater than 140 degrees up to 180 degrees.

From the modified approach of Simons, the mass flux from the 25 lb vernier RCS engines using the R-4D similarity for angles between 0 and 40 degrees and between 40 and 140 degrees from the engine centerline becomes:

$$\dot{m} = 23.2/r^2 \left[\cos\left(\frac{\pi}{2} \cdot \frac{\theta}{\theta_1}\right)\right]^{8.65} \quad \text{for } 0^\circ \leq \theta \leq 40^\circ$$

where;

$\dot{m}$ = Mass flux rate per unit area in $g/cm^2/second$,

r = Distance rrom the exit plane of the engine nozzle to the point of interest within the plume in centimeters,

θ_1 = 115 degrees,

θ = Angle in degrees between 0 and 40 degrees from the engine axis.

$$\dot{m} = \left(5.81/r^2\right) \; e^{-0.0467\ (\theta - 40^o)} \quad \text{for } 40^o < \theta \leq 140^o$$

where;

$\dot{m}$ = Mass flux rate per unit area in $g/cm^2/second$,

r = Distance from the exit plane of the engine nozzle to the point of interest within the plume in centimeters,

θ = Angle from the centerline of the engine in degrees for angles greater than 40 degrees and less than or equal to 140 degrees.

For the back flow regions, the mass flux between 140 degrees and 180 degrees from the engine centerline becomes:

$$\dot{m} = 5.81/r^2 \; e^{-4.67} \quad \text{for } 140^o < \theta \leq 180^o$$

where;

$\dot{m}$ = Mass flux rate per unit area in $g/cm^2/second$,

r = Distance from the exit plane of the engine nozzle to the point of interest within the plume in centimeters.

A mean velocity of 3,505 m/second was assumed for this study. An estimate of the species concentrations in the VCS engine plumes for an oxidizer to fuel ratio of 1.636 (Reference 4) is given below:

Constituent	Mole Fraction
CO	0.12861
CO_2	0.04160
H	0.01163
H_2	0.16313
H_2O	0.33876
NO	0.00062
N_2	0.30933
O	0.00027
OH	0.00582
O_2	0.00023

No consideration was given in this study to condensation in the flow fields of the vernier engines. As mentioned previously, these results are subject to the assumption that the Shuttle Orbiter vernier engines are similar in design to the scaled down Skylab R-4D engines. Depending upon the Shuttle Orbiter VCS engine injector design, the resulting flow fields will be subject to changes as a result of oxidizer to fuel striation, thus providing unique flow fields which may not be adequately represented by the Skylab R-4D plume description. However, reasonably good contamination effects data from Skylab RCS engines inflight deposition measurements and correlation with pre-Skylab mission ground test programs exists to base a preliminary VCS engine contamination impact analysis for the Shuttle Orbiter and payloads. In order to further establish validity of this approach, data from a Marquardt 25 lb thrust R1E-3 engine analysis was reviewed and is presented below.

a) Marquardt 25 lb Thrust R1E-3 Engine - A preliminary investigation of the Marquardt 25 lb thrust R1E-3 engine flow field and a comparison to the flow field used in the VCS plume modeling efforts were performed. The R1E-3 engine exhaust has been modeled by the Method of Characteristics (MOC) program (Reference 5). The preliminary calculations using the R1E-3 flow field distribution show that this engine located at the aft -Z VCS location produces molecular column densities for LOS 1A and LOS 4A about 20% higher than the present modeled VCS engine flow fields.

This is reasonably good correlation and lends support to the Skylab R-4D plume modeling approach used in this study for the VCS engine as well as the 900 lb RCS and 6000 lb OMS engines. The final selection of the VCS engine will dictate the actual flow fields to be used in a final analysis of the VCS engine contamination potential.

3.2.1.6 Return Flux - With some Shuttle payloads planning to operate at considerably lower orbital altitudes (200 km) than Skylab (435 km) and with anticipated cryogenically cooled payloads, the returned contaminants as a result of interacting with the ambient orbital environment may represent a significant contaminant source.

The return flux of contaminants will be a function of a number of variables. These are:

a) the molecular size and weight of the contaminants leaving the Shuttle Orbiter and payloads;

b) the velocity at which the contaminants leave the Shuttle Orbiter and payloads;

c) the density and molecular size of the ambient atmosphere at a give orbital altitude;

d) the orbital altitude;

e) the attitude of the Shuttle Orbiter and the payload with respect to the velocity vector of the ambient atmosphere;

f) the temperature of the surfaces of the Shuttle Orbiter and the payloads;

g) the source locations and flux rates which comprise the induced environment; and

h) the field-of-view of the payload, instrument, and surface in question.

Figure 21 indicates how the return flux rate varies as a function of orbital altitude for a median ambient density atmosphere assuming the contaminants in the return flux have a molecular weight of 18. As in the case of outgassing where the molecular weight was assumed to be 100, there will be a condition where the return flux reaches a maximum and then begins to decrease with orbital altitude. This is discussed in subsection 3.3.1. At Skylab altitudes (435 km), the return flux is a factor of 52.7 less than at a 200 km altitude for a given mass column density along a line-of-sight. The return flux is directly related to the number density of the ambient atmosphere. The median density at a given altitude is used in the modeling. This value will vary between orbital daytime and high sunspot activity and for orbital nighttime and low sunspot activity. At 200 km, the ambient molecular density can vary between 10^9 to 10^{10} molecules/cm^3. At 435 km, the molecular density may vary between 10^7 to 10^8 molecules/cm^3. A median density of 4.8×10^6 molecules/cm^3 at 700 km, 1.3×10^8 molecules/cm^3 at 435 km, and 6.85×10^9 molecules/cm^3 at 200 km has been used in all the return flux calculations presented in this report.

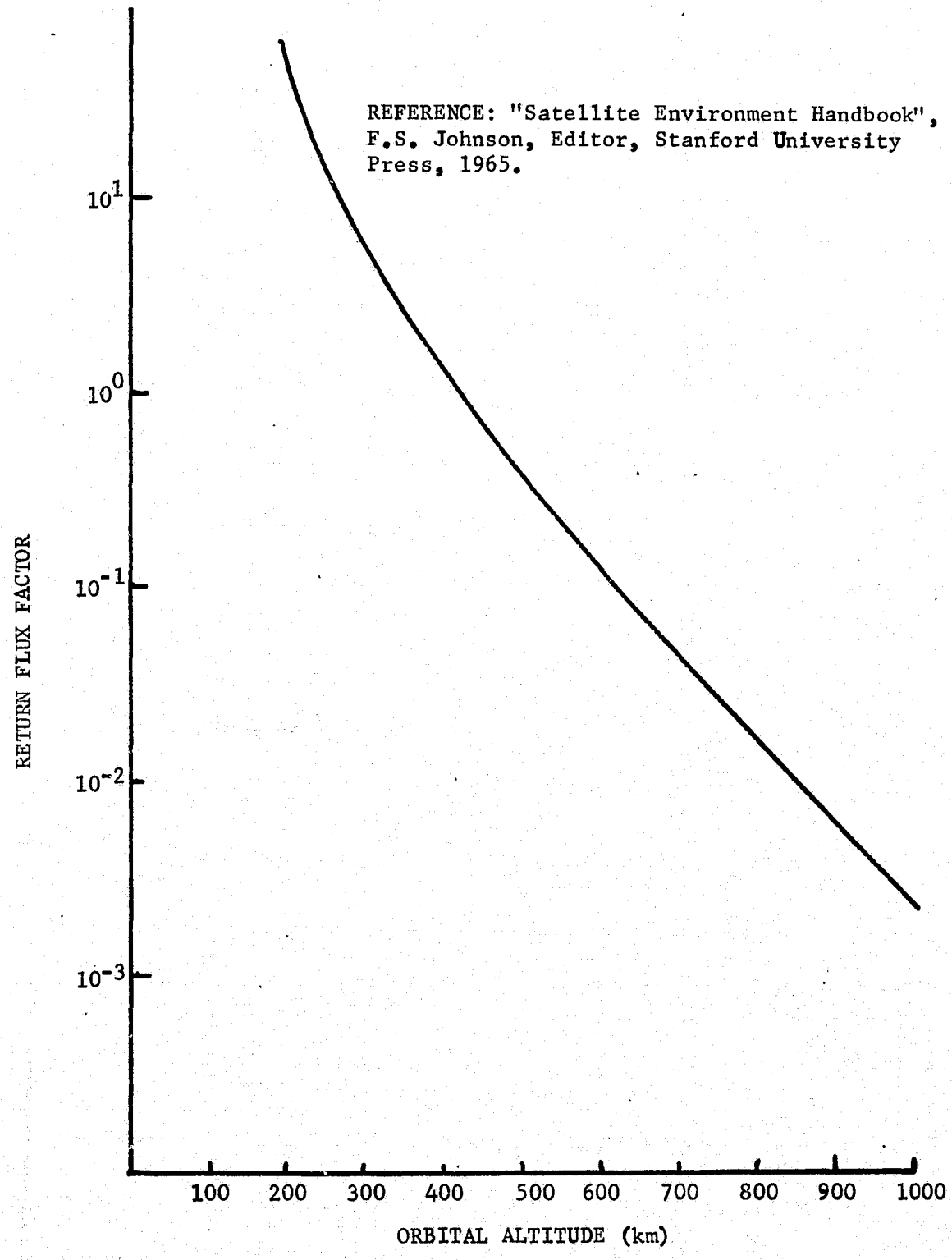

Figure 21. Return Flux as a Function of Orbital Altitude Normalized to 435 Kilometers

The density of the induced environment is calculated at each line-of-sight sphere location and is allowed to interact with the ambient atmosphere so that the return flux distribution as based upon a hard sphere interaction for a specific contaminant molecule is established at this point. The scattered molecules are emitted in a cos θ distribution that is aligned along the velocity vector or equivalently, with respect to the ambient molecule direction. Through geometry considerations, the fraction of the scattered contaminant molecules that can reach a representative surface or payload is then determined.

For any given line-of-sight, the return flux of contaminants for that line-of-sight will vary throughout an orbit. When the Shuttle Orbiter has solar oriented surfaces in attitudes similar to Skylab, they will see the maximum return flux as the Shuttle Orbiter comes from orbital midnight to orbital noon. The point of orbital sunrise will be the point of maximum return flux when the velocity vector is aligned along the line-of-sight towards the payload bay. This would also be the period of maximum mass column density since the Shuttle Orbiter and payload surfaces are warming due to solar exposure and are outgassing at their highest rate.

Just the opposite will be true for those surfaces whose viewing requirements require anti-solar lines-of-sight. In this case, maximum return flux will occur at orbital sunset when the mass column density is near a minimum since the Shuttle Orbiter and payload surfaces will be cooling and not outgassing as heavily. Before more detailed analysis for the return flux can be performed, the pointing requirements for an instrument and payload with respect to the velocity vector and the vehicle must be accurately determined.

3.2.1.7 Summary of Major Sources - Presented in Table I is a summary of the major sources modeled in this study. This summary presents the duration/frequency, constituents, plume shape function, velocity, and size parameter for each of the sources modeled.

Those secondary sources such as reflections and sublimation from the Shuttle Orbiter surfaces are a function of the modeled geometry, a cos θ/r^2 distribution in reflection, the flowrate defined by the particular source, and a corresponding

Table I. Major Sources Summary

Major Sources	Duration/ Frequency	Flowrate	Constituents	Plume Shape Function	Velocity	Size Parameter
Outgassing	Continuous	$\left[5.0e^{-t/4100} e^{(T-100)/29} \times 10^{-10}\right]$ g/cm^2/sec	Hydrocarbon chain fragments RTV's, etc.	$\cos\theta / r^2$	12.9 $\sqrt{T}$ m/sec	Molecular Avg. M = 100
Offgassing	Continuous for first 100 hours on-orbit	$\left[3.87e^{-0.14t} + 3.0e^{-.055t}\right] e^{(T-100)/29} \times 10^{-9}$ g/cm^2/sec	Water light gases Volatiles	$\cos\theta / r^2$	30.4 $\sqrt{T}$ m/sec	Molecular Avg. M = 18
Evaporator (2) *	As Reqd.	13.6 kg/hr total	Water	$\cos^6(1.01\theta)/r^2$ $[0^o \leq \theta \leq 36.8^o]$ $\frac{e^{-.0773(\theta-36.8^o)}}{r^2}$ $[36.8^o < \theta \leq 148^o]$	1012 m/sec	Molecular M = 18
Cabin Atmosphere Leakage	Continuous	3.18 kg/day	O_2 N_2 CO_2 H_2O	$\cos\theta / r^2$	2220 $\sqrt{\frac{1}{M}}$ m/sec	Molecular Avg. M = 29
RCS Vernier Engines**	As Reqd.	40.8 g/min Avg. 40 msec pulse ea. 4.8 sec--Y-POP attitude at 200 km	H_2O N_2 H_2 CO CO_2 H	$\frac{(\cos \frac{\pi \cdot \theta}{2\theta_i})^{8.65}}{r^2}$ $[0^o \leq \theta \leq 40^o]$ $\frac{e^{.0467(\theta-40^o)}}{r^2}$ $[40^o < \theta \leq 140^o]$ $\frac{e^{-4.67}}{r^2}$ $[140^o < \theta \leq 180^o]$	3505 m/sec	Molecular
Ambient Reflection	~10 to 30 min per orbit	Varies with above sources & orbital attitude	Any of the above sources	$\cos\theta / r^2$ from collision points	Varies with all above sources Max = 7.65 km/sec	Varies with all above sources

* Plume reflections off of structural surfaces (e.g. wings, experiment bay doors) are equivalent to a source equal to the plume impingement rate with a $\cos\theta/r^2$ distribution and a velocity of $30.4\sqrt{T}$ m/sec from the surface where T = surface temp.

** RCS plume reflections off of structural surfaces are assumed to have a rate equal to the plume impingement rate with a $\cos\theta/r^2$ distribution and a velocity equal to $129\sqrt{\frac{T}{M}}$ where T = surface temperature.

plume shape function as given in Table I. These sources are not defined discretely since the geometrical relationships of the model preclude listing all the surface interactions in this report to define this type source.

3.2.2 Other Sources - Other sources that were considered for specific analysis were the RCS 900 lb (nominal) thrust engines and the OMS 6000 lb (nominal) thrust engines. Their location for the aft port side of the Shuttle Orbiter are shown schematically in Figure 22.

The flow fields of the 900 lb RCS engines were analytically modeled in the same manner as the VCS engines. The mass flow equations for the RCS 900 lb engines are:

$$\dot{m} = \frac{1400 \cos^{10}\left(\frac{\pi}{2} \cdot \frac{\theta}{125}\right)}{r^2} \qquad \text{for } 0^\circ \leq \theta \leq 60^\circ$$

and

$$\dot{m} = \frac{61.32e^{-0.064(\theta-60)}}{r^2} \qquad \text{for } 60^\circ < \theta \leq 180^\circ$$

where

$\dot{m}$ = Mass flux rate per unit area in $g/cm^2/second$,

r = Distance from the exit plane of the engine nozzle to the point of interest within the plume in centimeters,

θ = Angle off of the engine axis in degrees.

The velocity of the molecular species was assumed to be 3505 m/second, as for the case with the VCS.

The flow fields of the 6000 lb OMS engines were analytically modeled in a like manner to the VCS and RCS. The mass flow equations for the OMS engines are:

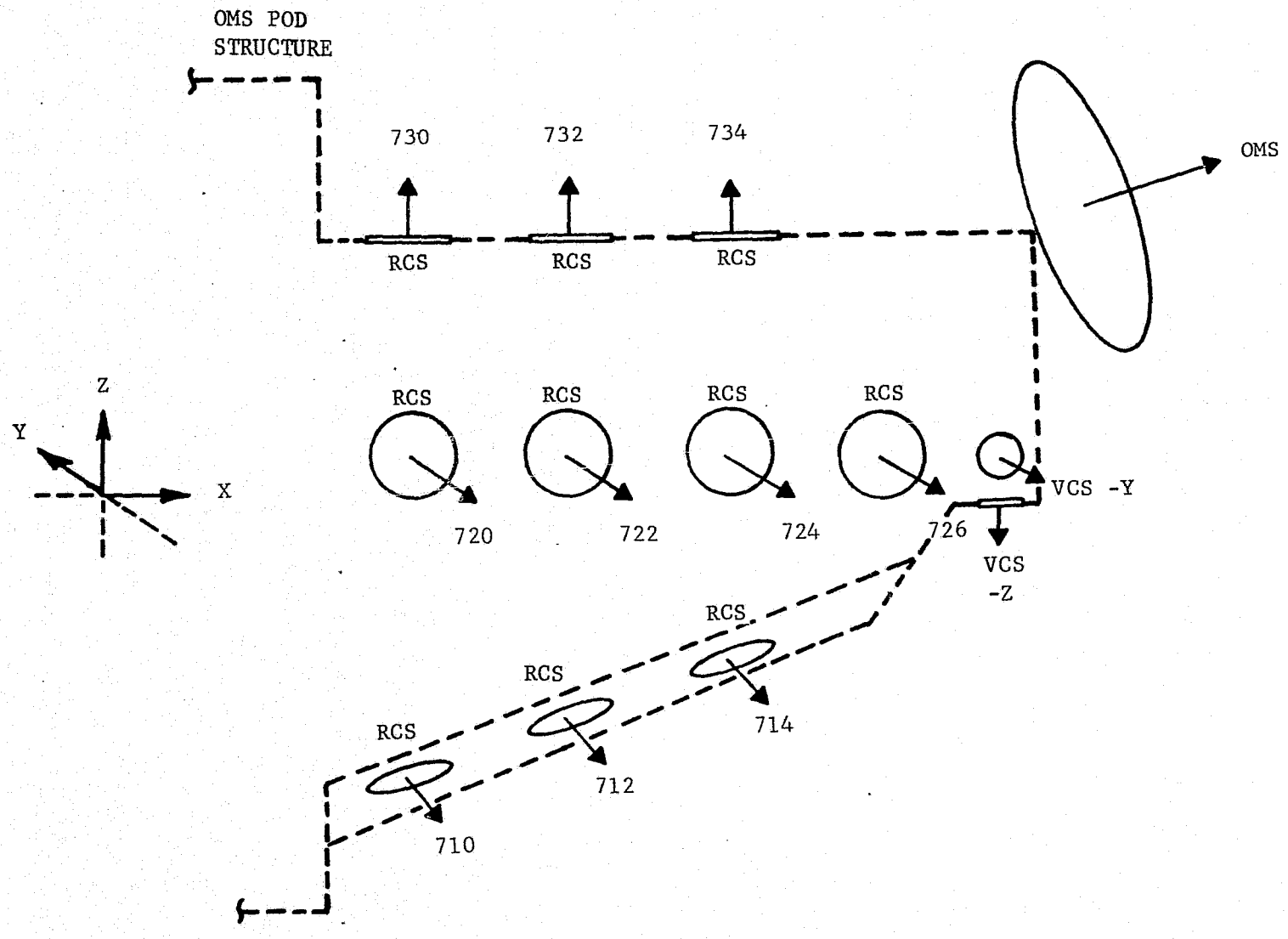

Figure 22. Shuttle Orbiter Aft Engine Cluster Geometric Relationships and Nodal Breakdown

$$\dot{m} = \left[\frac{1.39 \times 10^4}{r^2}\right] \left[\cos^{10}\left(\frac{\pi}{2} \cdot \frac{\theta}{170}\right)\right] \quad \text{for } 0^\circ \leq \theta \leq 30^\circ$$

$$\dot{m} = \left[\frac{9.55 \times 10^3}{r^2}\right] e^{-0.14\ (\theta - 30^\circ)} \quad \text{for } 30^\circ < \theta \leq 140^\circ$$

$$\dot{m} = \left[\frac{9.55 \times 10^3}{r^2}\right] e^{-15.4} \quad \text{for } 140^\circ < \theta \leq 180^\circ$$

where

$\dot{m}$ = Mass flux rate per unit area in $g/cm^2/second$,

r = Distance from the exit plane of the engine nozzle to the point of interest within the plume in centimeters.

θ = Angle off of engine axis in degrees.

The nominal velocity of the exhaust effluents has been determined from gas dynamic relationships to be 3694 m/second assuming a γ (c_p/c_v) of 1.2.

The RCS and OMS engines will be used during major orbital manuevers with the payload bay doors open. The major impact of these engines was preliminarily evaluated on the payload bay door radiator surfaces during this study and is presented in subsection 3.5.4.

Other sources that may require additional studies consist of sources deemed secondary in nature compared to the major on orbit sources presented above; these can occur during on orbit, launch, and reentry mission phases. Those additional sources on orbit include such items as propellant system and hydraulic leakage, fuel cell vents, and airlock/EVA system effluents.

Of the launch sources which include an assortment of compartment vents, engines and system vents, the Solid Rocket Booster separation motors and the External Fuel tank insulation ablation products may be the most significant contaminant sources.

This is true for two reasons: first, the products from each of these sources can impinge upon the Shuttle Orbiter external surfaces during launch and secondly, the exhaust products from each have the capability to deposit on the Shuttle Orbiter surfaces. The result is that these two sources can alter the surface properties of the external surfaces directly and/or become an additional on orbit source through sublimation of the deposits. Particles from these sources can also be trapped on the Shuttle Orbiter exterior surfaces and later be sloughed off during subsequent on orbit periods.

The sources that occur during reentry which have not been included in the model but will be included in future studies are:

a) Auxiliary Power Unit System exhaust outlets;

b) Ammonia Evaporator Vent;

c) primary evaporator vent

d) APU steam generator; and

e) hydraulic leakage.

These reentry sources combined with the residual contaminants present from launch and on orbit could possibly create a detrimental contamination source(s) for subsequent missions. Depending on cleaning requirements and refurbishment procedures, these additional residual sources or those acquired during cleaning/refurbishment must eventually be considered as sources in the modeling of subsequent flights where the total contaminant environment is evaluated and ultimately compared to the current contamination control criteria for compliance.

3.2.3 Reflection and Sublimation from Shuttle Orbiter Surfaces - The Shuttle Orbiter configuration geometrically presents a source that Skylab essentially did not have. The Shuttle Orbiter wings and the payload bay doors present surfaces where contamination source effluents can be reflected from or deposit upon and sublimate. The operational nature of the Shuttle Orbiter essentially precludes any vents being located on the bottom side. Therefore, the majority of active sources

are all located on the top side where the payloads are also positioned. The Shuttle Orbiter wings and payload doors will act as secondary contamination sources for surface outgassing, offgassing, evaporator venting, and VCS engine firings.

Although these surfaces will be warm on orbit and deposition from sources which produce H_2O, CO_2, O_2, N_2, etc., will not occur on these surfaces, the surfaces are capable of reflecting contaminants into lines-of-sight. In particular, the cryogenically cooled payloads may under certain conditions condense these low molecular weight contaminants on their external operational surfaces and change the physical properties of the cryogenic surfaces. Of particular significance are the VCS engines, all of the four rear position 25 lb thrust forward flow fields are capable of impinging on portions of the Shuttle Orbiter wings and payload bay doors when they are open. Experience from Skylab has shown that bipropellant engines such as currently planned for the Shuttle Orbiter will deposit contaminants and under certain conditions will sublimate with time. On Skylab, 0.2% of the mass flux from docking manuevers using the R4-D engines on the Command Service Module that impinged on Quartz Crystal Microbalance (QCM) surfaces at approximately 10^3C condensed. The condensed engine contaminant desorbed to 1/e of the deposited material in 72 hours and the resulting deposition that did not sublime was approximately 20% of the original deposit.

The reflection of plume impingement from both the evaporator system and the VCS were considered as a $\cos \theta / r^2$ distribution with respect to the normal of the surface at a rate equal to the plume impingement rate. The reemission velocities were modeled as the most probable velocity based upon the temperature of the emitting surface and the molecular weight of the engine exhaust effluents.

where;

$$v = \left(\frac{2R_o T}{M} \right)^{1/2}$$

$v = 30.4 \sqrt{T}$ for an assumed molecular weight of 18,

where;

v = Velocity in meters/second,

T = Temperature in degrees Kelvin.

This treatment of surface reflected species was arrived at following a literature survey of experimental work and contacts with investigators in this field. The following observations are pertinent to the decision to model the scattered molecules as described above:

a) Molecules with large dipole moments (H_2O, CO_2, etc.) have long interaction times with a surface, thus allowing for more complete accommodation with a surface. The result is diffuse emissions.

b) Molecules with incident energies less than 1 to 2 eV exhibit diffuse scattering with surfaces. These energies correspond to velocities of 1000 to 3000 meters/second for the molecules of interest. The engine molecular exhaust products are near 3500 meters/second and the evaporator exhaust near 1000 meters/second and thus fall close to this energy range.

c) A rough surface causes diffuse scattering of impinging molecules.

d) Contamination on a surface (even fractions of a monolayer) tends to drive specular scattering to diffuse scattering. Significant contamination results in total diffuse scattering.

e) For the previous conditions, the scattered molecules have velocities indicative of the surface temperature impinged upon which implies complete accommodation.

f) Low incident impingement angles can introduce lobular scattering (approaching specular) for a very clean surface with none of the above conditions.

g) Specular scattering of molecules is very hard to obtain and requires ultra-high vacuum conditions, atomically smooth, well characterized surfaces, no contamination, and a unique gas and surface combination.

h) The portion of the plumes impinging on the wing surfaces that can contribute to the lines-of-sight are in the near molecular and free molecular flow regime, thus approximating experimental conditions from which the results were obtained for the decision making process.

i) For regions of the plume that are viscous (continuum) or in the transition flow region from viscous to molecular and are impinging on the Shuttle Orbiter wing surfaces, the angle of incidence is near perpendicular. This would also allow diffuse scattering or sublimation from these surfaces which is also a diffuse process.

Therefore, the available data appears to strongly support a cosine (diffuse) scattering from the Shuttle Orbiter surfaces (in particular the wings) for the conditions anticipated on orbit.

In summary, since all of the engines and vents evaluated must necessarily be above the Shuttle Orbiter wings, the capability of reflecting these effluents in most instances into the lines-of-sight exists. The net effect is a concentration of the overboard sources to the payload side of the vehicle.

3.2.4 Boost and Reentry Contamination Sources - During launch and reentry the Shuttle Orbiter will be exposed to various contamination phenomena which dictate certain contamination control measures to insure the integrity of sensitive payloads within the payload bay. The first steps in protecting sensitive payloads will be the use of a properly designed and attached payload bay liner which is a payload option. In addition, proper operation and timelining of the active payload bay vents and effective payload bay door seals will be important initial steps towards prevention of contaminants impacting the stowed payloads. The following additional precautionary measures are suggested.

a) insure that all sensitive payloads have aperture doors and that they provide an integral seal for the payload during boost and reentry and can be used as on orbit protective covers to minimize compromising the payload in the advent of an anomalous high contamination period;

b) data acquired by the inflight contamination monitor package to be flown on the early Shuttle Orbiter flights should be reviewed to determine additional protective devices required for sensitive payloads to be flown on ensuing missions; where applicable sensitive instruments should supply their own deposition indicators to determine when the instrument deposition characteristics are within acceptable limits; and

c) delay cooling of sensitive elements until the environment is acceptable (as indicated by deposition monitors).

3.3 Shuttle Orbiter Induced Environment Predictions - This subsection presents a series of baseline tabular predictions for the modeled major Shuttle Orbiter sources contribution to the lines-of-sight (LOS 1A through 6A) identified previously. These baseline tabular results can be evaluated against the current applicable contamination control criteria for the on orbit induced environment as defined in Applicable Document JSC 07700 Volume X, Revision C. The applicable contamination control criteria are presented below for ease in assessment of the following tables and to understand how the Shuttle Orbiter induced environment relates to the current criteria.

a) Fewer than 1 particle larger than 5 microns in the field-of-view of in instrument per orbit.

b) Column density for water vapor less than 10^{12} molecules/cm^2 (polar molecules).

c) Background brightness from scattering or emission less than 20th magnitude/sec^2 in the UV range.

d) Return flux of less than 10^{12} molecules/cm^2/second.

e) Control to 1 percent absorption from UV, visible, and RI radiation by condensibles on optical surfaces.

The major Shuttle Orbiter sources presented in the following tables are outgassing, offgassing, cabin atmosphere leakage, supplemental evaporator, and VCS 25 lb thrust engines. Minimization studies have been performed for the two sources which deviate significantly from the above criteria. These sources are the evaporator and the VCS 25 lb thrust engines. The minimization studies are presented in subsection 3.4 and are discussed in detail therein.

The return flux values presented for the orbital altitudes of 700 km, 435 km, and 200 km represent the range of orbital altitudes anticipated for many of the Shuttle missions. The 435 km case has been selected since it relates directly to the Skylab mission orbital altitude from which comparisons can be made, as applicable, to specific data obtained from the Skylab Program.

As presented in Figure 17, the return flux is based on a total field-of-view of 28 degrees (0.19 steradians) and corresponds to a physical acceptance situation where L/D = 2 (length to diameter ratio of a telescope tube). To determine the return flux for angles greater than 28 degrees, the return flux can be multiplied by the ratio of the field-of-view in steradians to 0.19. This method will be accurate for viewing angles from 0 to 45 degrees. The values of return flux presented in the following tables refer to the maximum return flux for the case where the velocity vector is parallel to the corresponding line-of-sight and excludes any contribution from the ambient atmosphere. The total return flux impact is an integration of the return flux over a given mission profile. The values presented can be related to the above contamination control criteria for return flux evaluation.

3.3.1 Outgassing Induced Environment Predictions - Table II presents the outgassing environment predictions for the lines-of-sight 1A through 6A.

Table II. Outgassing Induced Environment Predictions for the Shuttle Orbiter Configuration

Predicted Parameters / Line-of-Sight		MCD (g/cm^2)	NCD ($mol./cm^2$)	Return Flux (Max)** ($mol./cm^2/second$)		
				700 km	435 km	200 km
LOS 1A	Max	3.1(-11)*	2.0(11)	3.4(9)	9.1(10)	~0
	Min	1.4(-12)	8.8(9)	1.5(8)	4.1(9)	~0
LOS 2A	Max	2.2(-11)	1.4(11)	2.4(9)	6.7(10)	~0
	Min	1.4(-12)	8.8(9)	1.5(8)	4.1(9)	~0
LOS 3A	Max	2.7(-11)	1.7(11)	2.9(9)	7.9(10)	~0
	Min	1.4(-12)	8.8(9)	1.5(8)	4.1(9)	~0
LOS 4A	Max	2.8(-11)	1.7(11)	3.0(9)	7.9(10)	~0
	Min	1.2(-12)	7.2(9)	1.3(8)	3.5(9)	~0
LOS 5A	Max	2.4(-11)	1.5(11)	2.7(9)	7.3(10)	~0
	Min	1.3(-12)	8.1(9)	1.4(8)	3.8(9)	~0
LOS 6A	Max	3.8(-11)	2.4(11)	4.1(9)	1.1(11)	~0
	Min	1.1(-12)	6.6(9)	1.2(8)	3.1(9)	~0

* $(-11) = 10^{-11}$

** Return flux predictions are for a 0.19 steradian field-of-view surface. Predictions for surfaces with differing fields-of-view will vary accordingly.

The outgassing rate was assumed to be 5 x 10^{-10} g/cm^2/ second at 100°C. This rate was also measured during testing of a segment of Shuttle TPS panel at MSFC and thus corresponds to a steady-state value for the Shuttle Orbiter surface. Table II includes predictions for a maximum and minimum vehicle surface temperature. These temperatures correspond to a hot and cold portion of an orbit or a hot and cold vehicle attitude. The number column density is seen to vary from 10^9 to 10^{11} molecules/ cm^2. For specific orbital attitudes, the external Shuttle Orbiter surface temperatures may result in small changes from these predicted values. Figure 23 graphically displays the density as a function of distance away from the Shuttle Orbiter for three lines-of-sight. Integration under these curves yields the mass column densities as depicted in Table II.

The return flux values of the outgassing molecules at 200 km are shown to be nearly zero. At 200 km, the mean free path of the outgassed molecules is less than one meter. (The average molecular weight and outgassing molecule size have been assumed to be 100 and 30Å, respectively.) Under this condition, the outgassed molecules will not be able to travel along the line-of-sight when the ambient atmosphere velocity vector is capable of allowing return flux. The return flux is inversely proportional to the mean free path (MFP) and directly proportional to the mass column density (MCD) so that the return flux is proportional to the MCD/MFP. Therefore, as the ambient density increases with a decrease in altitude, the mean free path decreases causing an increase in return flux. However, as the mean free path decreases, the chance of a molecule intercepting a line-of-sight decreases when the ambient drag vector is oriented such that it carries it away from the line-of-sight. The net result is that the mass column density decreases faster (after some decreasing altitude is reached) than the collision frequency increases. There will be a condition near 250 to 300 km that the return flux of outgassed molecules for a given mass column density is a maximum.

As can be seen from Table II, the number column density and return flux for outgassing do not exceed the applicable stated criteria for the TPS type surface material being used for the Shuttle Orbiter.

3.3.2 Offgassing Induced Environment Predictions - Table III presents the offgassing environment predictions for the lines-of-sight 1A through 6A. The presented table corresponds

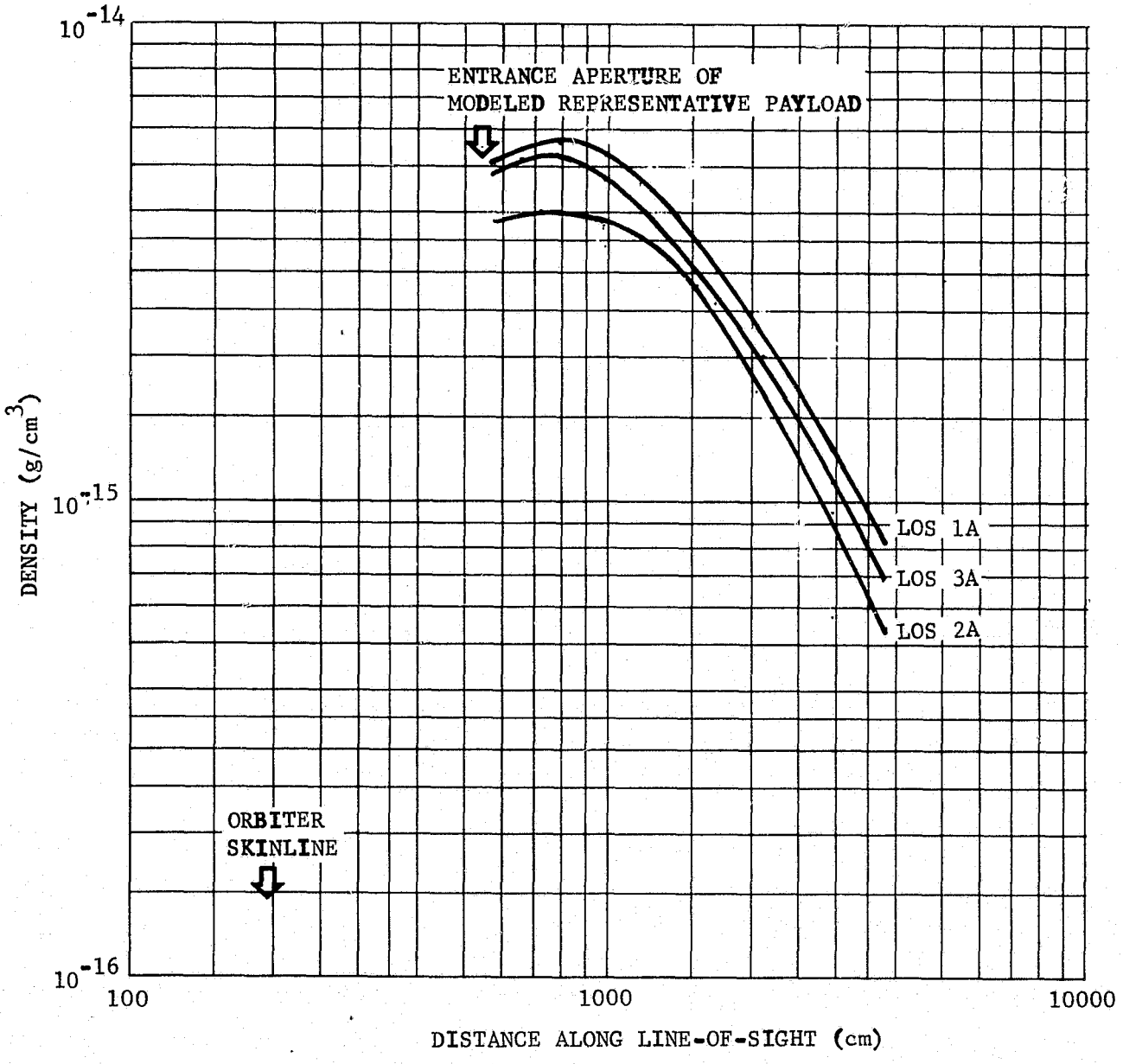

Figure 23. Density as a Function of Distance for Outgassing (LOS 1A, LOS 2A, and LOS 3A)

Table III. Offgassing Induced Environment Predictions for the Shuttle Orbiter Configuration

Predicted Parameters / Line-of-Sight		MCD (g/cm^2)	NCD ($mol./cm^2$)	Return Flux (Max)** ($mol./cm^2/second$)		
				700 km	435 km	200 km
LOS 1A	Max	6.5(-11)*	2.1(12)	1.3(9)	4.0(10)	2.0(12)
	Min	3.0(-12)	9.9(10)	6.0(7)	1.8(9)	9.0(10)
LOS 2A	Max	4.7(-11)	1.6(12)	9.3(8)	2.8(10)	1.4(12)
	Min	2.9(-12)	9.6(10)	5.7(7)	1.7(9)	8.7(10)
LOS 3A	Max	5.5(-11)	1.8(12)	1.1(9)	3.3(10)	1.7(12)
	Min	3.0(-12)	9.9(10)	6.0(7)	1.8(9)	9.0(10)
LOS 4A	Max	6.0(-11)	2.0(12)	1.2(9)	3.3(10)	1.8(12)
	Min	2.6(-12)	8.5(10)	5.3(7)	1.5(9)	7.7(10)
LOS 5A	Max	5.0(-11)	1.7(12)	1.0(9)	3.0(10)	1.6(12)
	Min	2.8(-12)	9.0(10)	5.7(7)	1.6(9)	8.3(10)
LOS 6A	Max	8.0(-11)	2.7(12)	1.6(9)	4.7(10)	2.3(12)
	Min	2.3(-12)	7.5(10)	4.7(7)	1.3(9)	6.7(10)

* $(-11) = 10^{-11}$

** Return flux predictions are for a 0.19 steradian field-of-view surface. Predictions for surfaces with differing fields-of-view will vary accordingly.

to an offgassing rate at a 10 hour point of on orbit vacuum exposure and was assumed to be 2.5 x 10^{-9}g/cm^2/second at 100°C. The table includes a maximum and minimum vehicle surface temperature profile. These temperatures correspond to a hot and cold portion of an orbit or a hot and cold vehicle attitude as in the case of outgassing. The number column density is seen to vary between 10^{11} to 10^{12} molecules/cm^2. For specific vehicle attitudes, the external surface temperatures may result in small changes from these predicted values. Figure 24 graphically displays the density as a function of distance away from the Shuttle Orbiter for three lines-of-sight. Integration under these curves yields the mass column densities as depicted in Table III.

The outgassing and offgassing rate time and temperature dependence data will be updated in subsequent modeling by utilizing results from continuing testing of the LRSI and/or HRSI configuration at MSFC.

Offgassing as opposed to outgassing will have a return flux contribution at the lower orbital altitudes (200 km) since the mean free path for the offgassants at these altitudes is considerably longer than that of the larger outgassing molecules. (The average molecular weight and offgassing molecule size have been assumed to be 18 and 3Å, respectively.)

In some cases, the number column density and return flux for offgassing approach and/or exceed the applicable contamination control criteria. However, until better test data is available, the source is considered not to present a contamination problem unless early on orbit usage of cryogenic systems is contemplated. Even in this case, operational timelining and proper attitude control will minimize this effect from this source for those susceptible payloads.

Many times it is desirable to determine the contribution from specific surfaces of the Shuttle Orbiter. Table IV shows the results of such an analysis for three lines-of-sight. This type of analysis allows detailed continuity checks of the modeling and demonstrates the versatility of the model for specific investigations. For example, the one-half mass column density distance from the vehicle for each major surface area is important for determining the emission capabilities of the molecules as background sources. This information has been used for analysis of the impact of the predicted induced environment on infrared facilities.

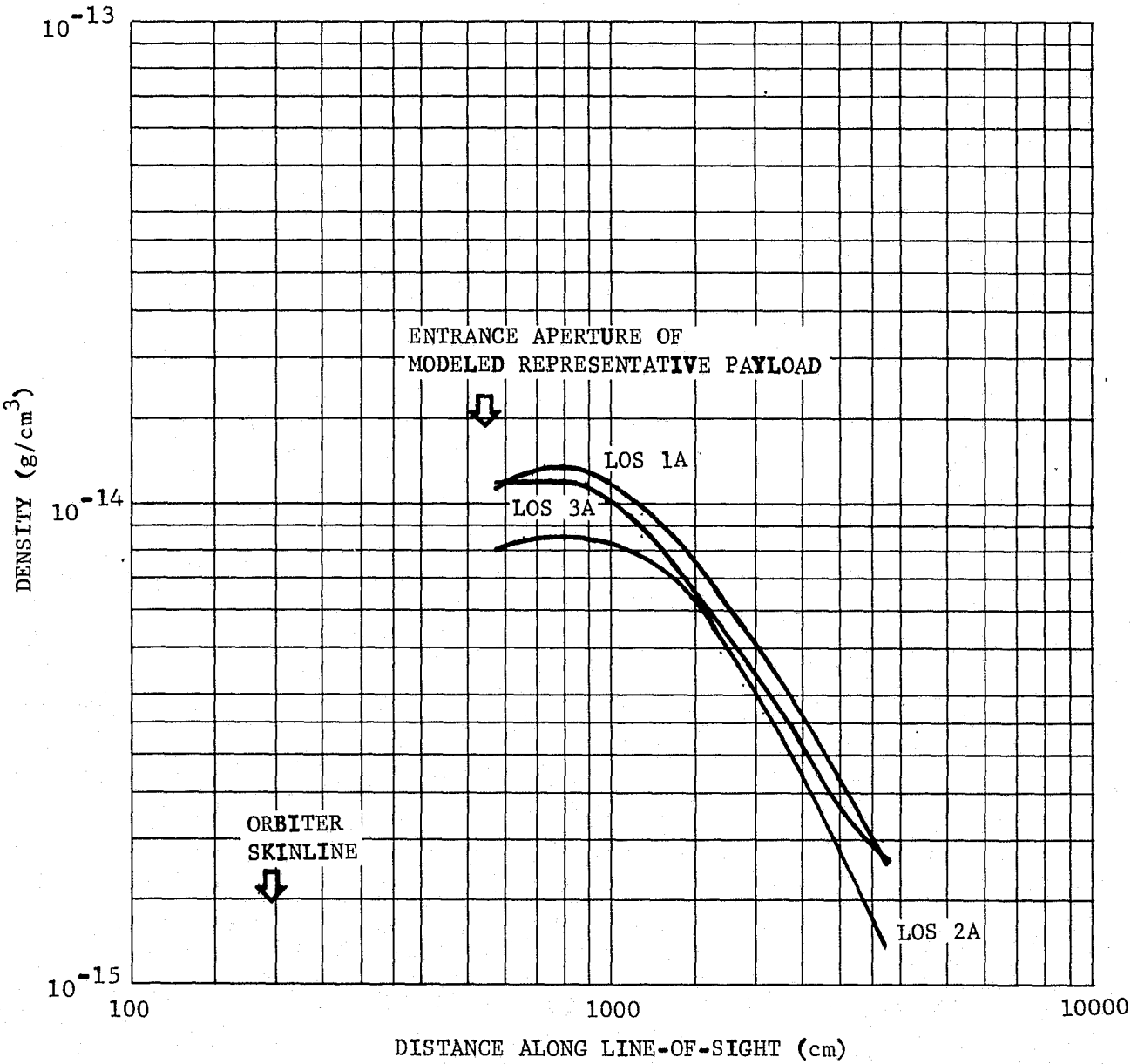

Figure 24. Density as a Function of Distance for Offgassing (LOS 1A, LOS 2A, and LOS 3A)

Table IV. Maximum and Minimum Outgassing and Offgassing Contributions to the Mass Column Density (MCD) and Distance to One-Half-MCD for Various Orbiter Surfaces

Surface	Temp. (°C)	½ MCD of LOS 1A (g/cm^2)		Distance to ½ MCD (cm)	½ MCD of LOS 2A (g/cm^2)		Distance to ½ MCD (cm)	½ MCD of LOS 5A (g/cm^2)		Distance to ½ MCD (cm)
		Out	Off		Out	Off		Out	Off	
Wings	* S=14									
Max	B=13	++ 4.7(-12)	1.0(-11)	8143	4.2(-12)	8.9(-12)	2666	2.4(-12)	5.1(-12)	7942
Min	S=-68 B=-64	3.0(-13)	6.4(-13)	7986	2.7(-13)	5.7(-13)	2661	1.6(-13)	3.4(-13)	6712
Tail	** S=UNKN									
Max	B=10	6.6(-14)	1.4(-13)	1755	3.0(-13)	6.3(-13)	5163	3.2(-14)	6.9(-14)	7384
Min	S=UNKN B=-45	8.4(-15)	1.8(-14)	1754	3.6(-14)	7.6(-14)	5137	4.1(-15)	8.8(-15)	7384
Radiator	S=4 82									
Max	B=N/A+	1.5(-12)	3.2(-12)	6468	1.7(-12)	3.5(-12)	2129	1.5(-12)	3.2(-12)	3365
Min	S=-6 38 B=N/A	7.6(-13)	1.6(-12)	6470	8.3(-13)	1.8(-12)	2126	7.7(-13)	1.6(-12)	3374
Cabin	S=73									
Max	B=60	1.3(-12)	2.7(-12)	12850	1.3(-12)	2.8(-12)	12823	5.2(-12)	1.1(-11)	8934
Min	S=-98 B=-81	2.0(-14)	4.2(-14)	12850	2.1(-14)	4.4(-14)	12823	8.1(-14)	1.7(-13)	8934
Bay	S=93									
Max	B=N/A+	9.2(-12)	1.9(-11)	2847	5.8(-12)	1.2(-11)	3369	1.1(-11)	2.3(-11)	971
Min	S=-26 B=N/A	1.8(-13)	3.9(-13)	2847	1.2(-13)	2.5(-13)	3369	2.1(-13)	4.5(-13)	971
Fuselage	S=UNKN									
Max	B=33	1.4(-11)	3.0(-11)	4878	8.6(-12)	1.9(-11)	6394	4.6(-12)	9.8(-12)	8789
Min	S=UNKN B=-68	1.3(-13)	2.8(-13)	3255	1.0(-13)	2.2(-13)	3860	6.7(-14)	1.5(-13)	3240

* S=SURFACE B=BONDLINE ** UNKN=UNKNOWN + N/A=NOT APPLICABLE ++ $4.7(-12) = 4.7 \times 10^{-12}$

In Table IV, the offgassing values presented are for the 10 hour period on orbit. To obtain values for a 24 hour period, divide the offgassing values by 2.5. The temperature data is an average for each major group. For example, the wings have several temperatures involved over their surface area. The temperature includes the average bondline temperature, if known, and the average surface temperature, if known.

The fuselage row in the table includes all surfaces not included by the other major surface areas. These are the OMS pods, the Shuttle Orbiter rear top surfaces, the large main engine bells, and the sides of the Shuttle Orbiter.

3.3.3 Cabin Atmosphere Leakage Induced Environment Predictions - Table V presents the cabin atmosphere leakage induced environment predictions for the lines-of-sight 1A through 6A for a leak rate of 3.18 kg/day. Figure 25 graphically displays the density as a function of distance away from the Shuttle Orbiter for several lines-of-sight. Integration under these curves yields the mass column densities as depicted in Table V. The number column density is seen to be in the range of 10^{13} molecules/cm^2 (10^{11} polar molecules/cm^2) for all lines-of-sight and does not exceed the stated criteria. However, the return flux from the leakage does exceed the stated criteria by an order of magnitude but is felt not to be a concern since the majority of the constituents of the leakage will not condense at the temperatures of the majority of the surfaces. The variation between the lines-of-sight is small and indicates the leakage source contributes uniformly to the portions of the lines-of-sight that are near the Shuttle Orbiter.

The pressurized cabin area leakage will be a steady-state source, unlike outgassing and offgassing. The percent of the molecular number column density constituents which make up the cabin leakage is:

a) O_2 - 23%;

b) N_2 - 75%;

c) CO_2 - 1%; and

d) H_2O - 1%.

Table V. Leakage Induced Environment Predictions for the Shuttle Orbiter Configuration

Predicted Parameters / Line-of-Sight	MCD (g/cm^2)	NCD*** ($mol./cm^2$)	Return Flux (Max)** ($mol./cm^2/second$)		
			700 km	435 km	200 km
LOS 1A	1.0(-9)*	2.2(13)	1.2(10)	3.7(11)	1.9(13)
LOS 2A	9.9(-10)	2.2(13)	1.2(10)	3.7(11)	2.0(13)
LOS 3A	1.1(-9)	2.3(13)	1.3(10)	3.9(11)	2.1(13)
LOS 4A	8.8(-10)	1.9(13)	1.1(10)	3.2(11)	1.7(13)
LOS 5A	1.6(-9)	3.5(13)	2.0(10)	5.6(11)	3.1(13)
LOS 6A	8.6(-10)	1.9(13)	1.1(10)	3.2(11)	1.7(13)

* $(-9) = 10^{-9}$

** Return flux predictions are for a 0.19 steradian field-of-view surface. Predictions for surfaces with differing fields-of-view will vary accordingly.

***Polar molecules constitute approximately 2% of the values presented.

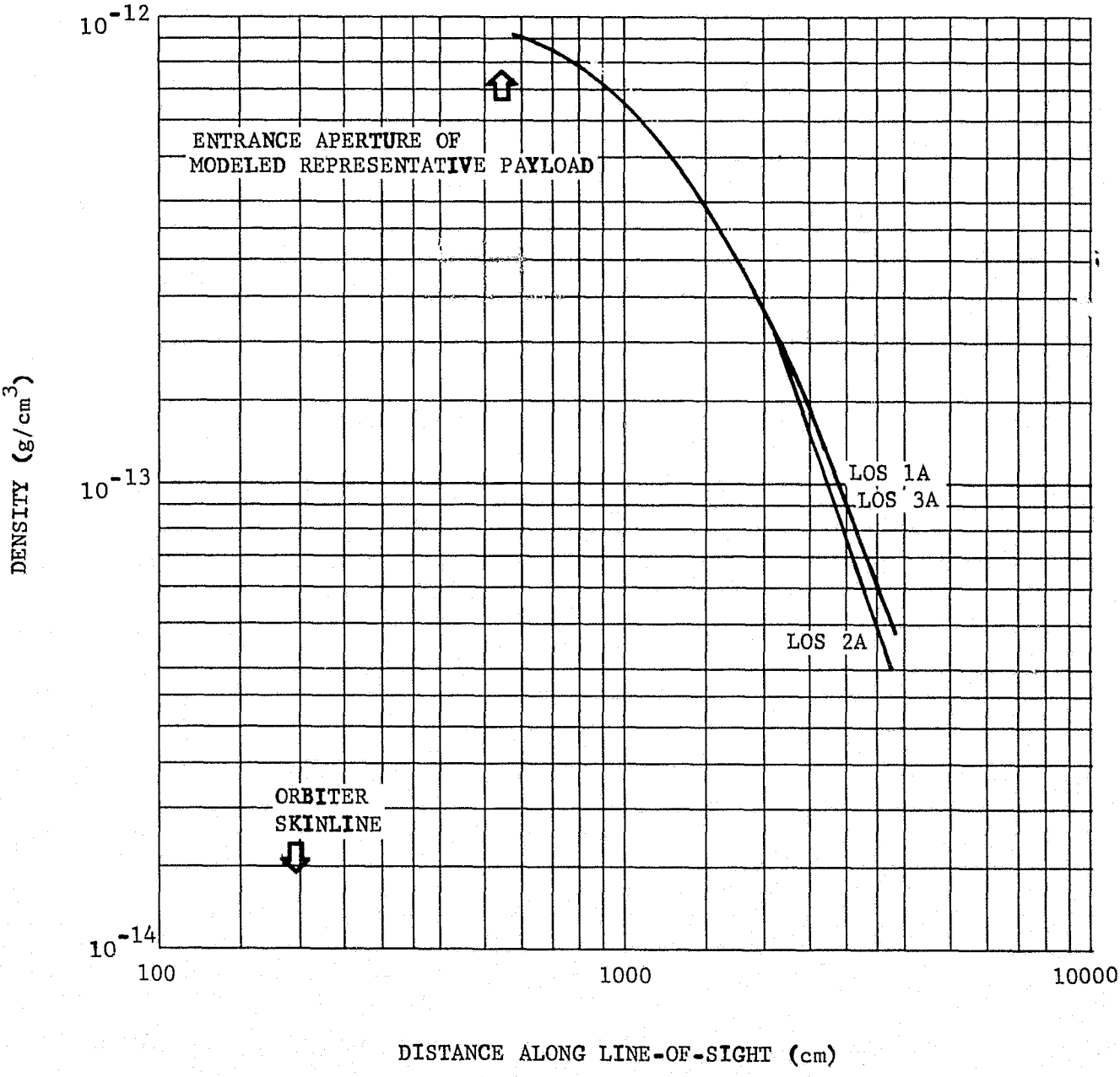

Figure 25. Density as a Function of Distance for Leakage (LOS 1A, LOS 2A, and LOS 3A)

3.3.4 Supplemental Evaporator Induced Environment Predictions - The Shuttle Orbiter supplemental evaporator system can contribute significantly to the mass column densities of lines-of-sight depending upon the evaporator vent location on the Shuttle Orbiter. For this subsection, the evaporator contributions to LOS 1A through 6A are established for the baseline evaporator vent location at X = 1392, Y = ±113 and Z = 323.

Table VI presents the evaporator induced environment predictions for a flowrate of 6.8 kg/hr/vent. The -Y evaporator vent contribution corresponds to the side of the Shuttle Orbiter the lines-of-sight view out of the (X, Z) plane. The +Y evaporator vent contribution corresponds to the evaporator vent on the other side of the Shuttle Orbiter. For lines-of-sight in the (X, Z) plane (LOS 1A, 5A, and 6A), the contributions are the same from symmetry considerations. Figure 26 graphically displays the density as a function of distance away from the Shuttle Orbiter for three lines-of-sight. Integration under these curves yields the mass column densities as depicted in Table VI.

At this location, the evaporator effluents also reflect off of the wings and are a significant contributor to the lines-of-sight. For lines-of-sight in the (X, Z) plane, this is the only contribution from the evaporator. The molecular number column densities are seen to vary between 10^{13} and 10^{14} molecules/cm^2 for the baseline evaporator location for LOS 1A through LOS 6A.

Since the evaporator's contribution to all the established lines-of-sight exceeds the applicable contamination control criteria, several alternate locations were analyzed to determine if a more suitable location could be found to minimize this contaminant source. The results of these activities are discussed in detail in the subsection 3.4.2.

3.3.5 Vernier Control System (25 lb Thrust Engines) Induced Environment Predictions - The VCS engines can contribute to the lines-of-sight at the baseline position by direct flow from the engine as well as wing reflections, as does the evaporator vent system. These contributions are instantaneous in nature, occurring only during engine on time. Reflections are considered to occur instantaneously being equivalent to a

Table VI. Shuttle Orbiter Baseline Evaporator, X = 1392, Induced Environment Predictions

Predicted Parameters / Line-of-Sight/ Evaporators	MCD (g/cm^2)			NCD ($mol./cm^2$)	Return Flux (Max) ** ($mol./cm^2$/second)		
	Direct Impingement	Wing Reflection	Total	Total	700 km	435 km	200 km
LOS 1A							
-Y Evap.	0	2.6(-9)	2.6(-9)	8.7(+13)	5.3(+10)	1.4(+12)	7.9(+13)
+Y Evap.	0	2.6(-9)	2.6(-9)	8.7(+13)	5.3(+10)	1.4(+12)	7.9(+13)
Both	0	5.2(-9)	5.2(-9)	1.7(+14)	1.1(+11)	2.9(+12)	1.6(+14)
LOS 2A							
-Y Evap.	3.3(-9)*	6.3(-9)	9.6(-9)	3.3(+14)	1.9(+11)	5.3(+12)	2.8(+14)
+Y Evap.	0	2.6(-11)	2.6(-11)	8.5(+11)	5.3(+8)	1.4(+10)	7.6(+11)
Both	3.3(-9)	6.3(-9)	9.6(-9)	3.3(+14)	1.9(+11)	5.3(+12)	2.8(+14)
LOS 3A							
-Y Evap.	4.6(-10)	6.3(-9)	6.8(-9)	2.3(+14)	1.3(+11)	4.0(+12)	2.0(+14)
+Y Evap.	0	4.9(-10)	4.9(-10)	1.6(+13)	9.9(+9)	2.8(+11)	1.4(+13)
Both	4.6(-10)	6.8(-9)	7.4(-9)	2.4(+14)	1.4(+11)	4.3(+12)	2.1(+14)
LOS 4A							
-Y Evap.	1.7(-9)	9.8(-9)	1.1(-8)	3.8(+14)	2.2(+11)	6.3(+12)	3.3(+14)
+Y Evap.	0	4.4(-12)	4.4(-12)	1.4(+11)	8.6(+7)	2.4(+9)	6.6(+9)
Both	1.7(-9)	9.8(-9)	1.1(-8)	3.8(+14)	2.2(+11)	6.3(+12)	3.3(+14)
LOS 5A							
-Y Evap.	0	1.3(-9)	1.3(-9)	4.1(+13)	2.5(+10)	6.9(+11)	3.6(+13)
+Y Evap.	0	1.3(-9)	1.3(-9)	4.1(+13)	2.5(+10)	6.9(+11)	3.6(+13)
Both	0	2.6(-9)	2.6(-9)	8.2(+13)	5.0(+10)	1.4(+12)	7.3(+13)
LOS 6A							
-Y Evap.	0	2.4(-9)	2.4(-9)	7.9(+13)	4.6(+10)	1.3(+12)	7.3(+13)
+Y Evap.	0	2.4(-9)	2.4(-9)	7.9(+13)	4.6(+10)	1.3(+12)	7.3(+13)
Both	0	4.8(-9)	4.8(-9)	1.6(+14)	9.2(+10)	2.7(+12)	1.4(+14)

* $(-9) = 10^{-9}$

** Return flux predictions are for a 0.19 steradian field-of-view surface. Predictions for surfaces with differing fields-of-view will vary accordingly.

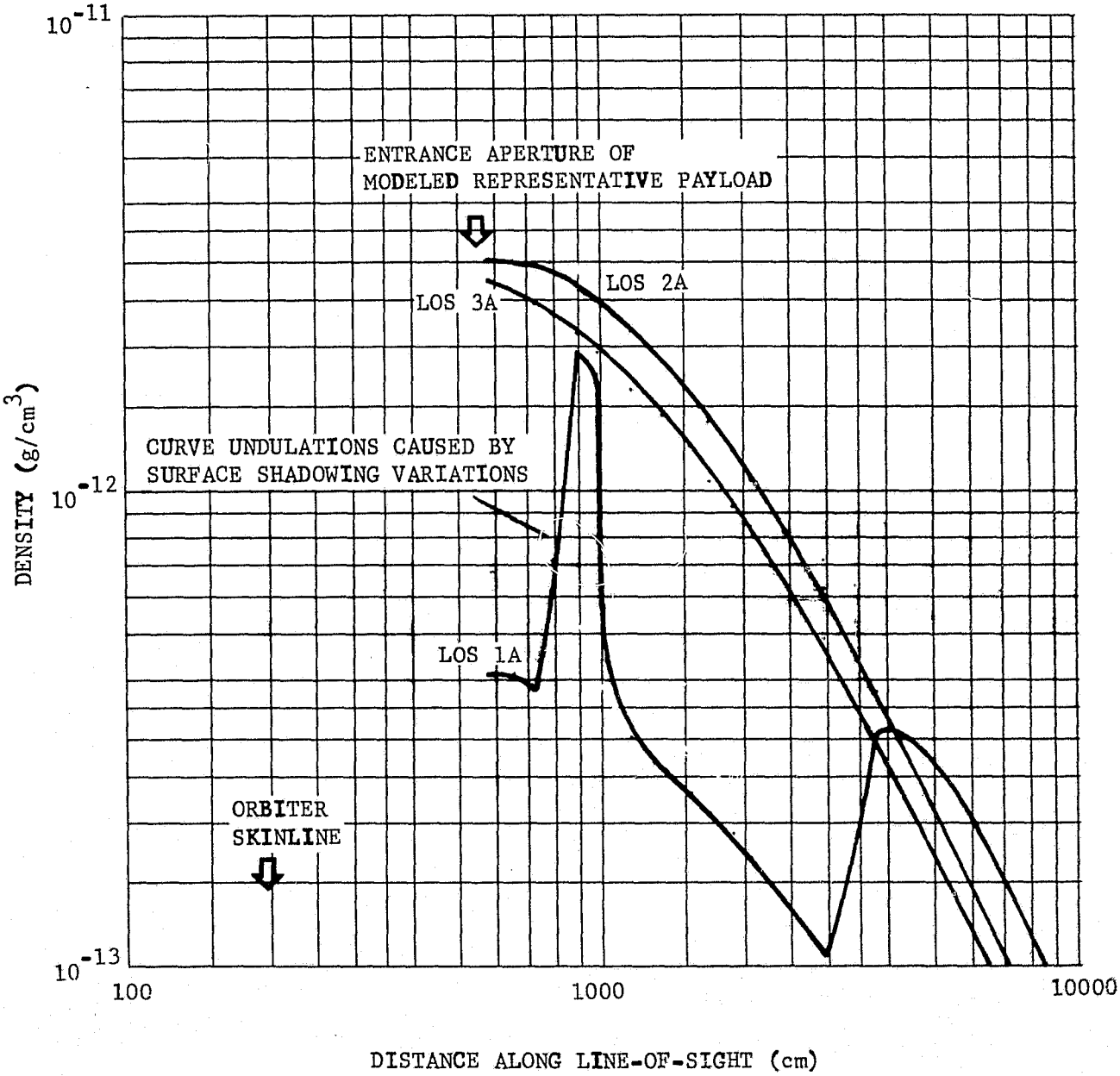

Figure 26. Density as a Function of Distance for Evaporator (LOS 1A, LOS 2A, and LOS 3A)

source equal to the plume impingement rate with a Lambertian distribution assuming thermal accomodation at the surface.

Table VII presents the VCS engines induced environment predictions. Each engine contribution is delineated since each may fire independently. The duration of each engine pulse and firing frequency depends on the orbital altitude and vehicle attitude. An indication of this firing frequency is presented in the following subsection 3.3.5.1. The engine locations are shown in Figure 20 for the baseline position. Table VII includes contributions of the VCS engines on both sides of the vehicle to the lines-of-sight. The values presented for the forward VCS engines result from backflow taking into account Shuttle Orbiter fuselage shadowing. Even though structure in the near vicinity of these engines tends to lessen the backflow contributions, it is assumed that due to skin line tracking of the engine effluents and other geometric considerations that these engines will contribute to the modeled lines-of-sight at certain distances and line-of-sight positions. Figure 27 graphically displays the density as a function of distance away from the Shuttle Orbiter for three lines-of-sight. Integration under these curves yields the mass column densities as depicted in Table VII.

The molecular number column densities vary between 10^{12} to 10^{14} molecules/cm^2 for LOS 1A through 6A. As in the case of the evaporator, the contributions to the established lines-of sight exceed the applicable contamination control criteria. Minimization studies for the VCS engines were also conducted to see if their contribution to the lines-of-sight could be minimized. These are presented in subsection 3.4.1.

The VCS engine firings or duty cycles will be highly dependent upon attitude and pointing requirements for the payload. Depending upon intended operational activities, the VCS system could or could not be of major concern. Under certain conditions the VCS engines could be considered as almost a continuous source of contamination.

3.3.5.1 VCS Duty Cycle Variations - As previously stated, the VCS firing frequency depends on orbital altitude and vehicle attitude and pointing requirements. An idea of firing frequency extremes can be ascertained from preliminary VCS duty cycle information supplied by Rockwell International (Reference 6). The

Table VII. Shuttle Orbiter VCS (25 lb Thrust) Induced Environment Predictions

Predicted Parameters / Line-of-Sight & Engine Flux Direction	MCD* (g/cm²)			NCD (mol./cm²)	Return Flux (Max)**** (mol./cm²/second)		
	Direct Impingmt.	Wing Reflection	Total	Total	700 km	435 km	200 km
LOS 1A							
AFT -Z*	2.4(-10)***	1.8(-8)	1.8(-8)	4.4(+14)	2.7(11)	7.6(12)	3.9(14)
AFT Y*	1.9(-9)	6.3(-9)	8.2(-9)	2.0(+14)	1.2(11)	3.4(12)	1.8(14)
FWD Y/Z*	1.6(-10)	0	1.6(-10)	3.9(+12)	2.3(9)	6.6(10)	3.4(12)
LOS 2A							
AFT -Z	7.3(-10)	3.3(-8)	3.4(-8)	8.3(+14)	4.9(11)	1.4(13)	7.3(14)
AFT $-Z_o$**	0	3.0(-10)	3.0(-10)	7.3(+12)	4.4(9)	1.2(11)	6.6(12)
AFT Y	2.0(-8)	1.0(-8)	3.0(-8)	7.3(+14)	6.8(11)	1.2(13)	6.6(14)
AFT Y_o	0	2.9(-10)	2.9(-10)	7.1(+12)	4.1(9)	1.2(11)	6.3(12)
FWD Y/Z	1.3(-9)	0	1.3(-9)	3.2(+13)	1.9(10)	5.4(11)	2.9(13)
FWD Y/Z_o	0	0	0	0	0	0	0
LOS 3A							
AFT -Z	3.4(-10)	3.4(-8)	3.4(-8)	8.3(+14)	4.9(11)	1.4(13)	7.3(14)
AFT $-Z_o$**	0	2.7(-9)	2.7(-9)	6.6(+13)	3.9(10)	1.1(12)	5.9(13)
AFT Y	6.2(-9)	8.9(-9)	1.5(-8)	3.7(+14)	2.2(11)	6.3(12)	3.2(14)
AFT Y_o	0	3.5(-9)	3.5(-9)	8.5(+13)	5.1(10)	1.5(12)	7.6(13)
FWD Y/Z	4.5(-10)	0	4.5(-10)	1.1(+13)	6.6(9)	1.9(11)	9.8(12)
FWD Y/Z_o	0	0	0	0	0	0	0
LOS 4A							
AFT -Z	5.4(-10)	5.8(-8)	5.9(-8)	1.4(+15)	8.5(11)	2.4(13)	1.3(15)
AFT $-Z_o$**	0	7.9(-11)	7.9(-11)	1.9(+12)	1.1(9)	3.2(10)	1.7(12)
AFT Y	2.2(-8)	1.3(-8)	3.5(-8)	8.5(+14)	5.1(11)	1.5(13)	7.6(14)
AFT Y_o	0	6.3(-11)	6.3(-11)	1.5(+12)	9.3(8)	2.7(10)	1.4(12)
FWD Y/Z	6.4(-10)	0	6.4(-10)	1.6(+13)	9.3(9)	2.7(11)	1.4(13)
FWD Y/Z_o	0	0	0	0	0	0	0
LOS 5A							
AFT -Z*	2.1(-11)	7.4(-9)	7.4(-9)	1.8(+14)	1.1(11)	3.2(12)	1.6(14)
AFT Y*	2.9(-10)	3.0(-9)	3.3(-9)	8.1(+13)	4.9(10)	1.4(12)	7.3(13)
FWD Y/Z*	1.1(-10)	0	1.1(-10)	2.7(+12)	1.6(9)	4.6(10)	2.4(12)
LOS 6A							
AFT -Z*	1.4(-10)	3.2(-8)	3.2(-8)	7.8(+14)	4.7(11)	1.3(13)	7.1(14)
AFT Y*	3.1(-9)	7.1(-9)	1.0(-8)	2.4(+14)	1.5(11)	4.1(12)	2.2(14)
FWD Y/Z*	0	0	0	0	0	0	0

* Due to symmetry of this line-of-sight with respect to verniers, contributions to it from opposite side verniers are equal to values presented.

** Contribution to line-of-sight from vernier on opposite side of vehicle (Z_o, Y_o, Y/Z_o)

*** $(-10) = 10^{-10}$

**** Return flux predictions are for a 0.19 steradian field-of-view surface. Predictions for surfaces with differing fields-of-view will vary accordingly.

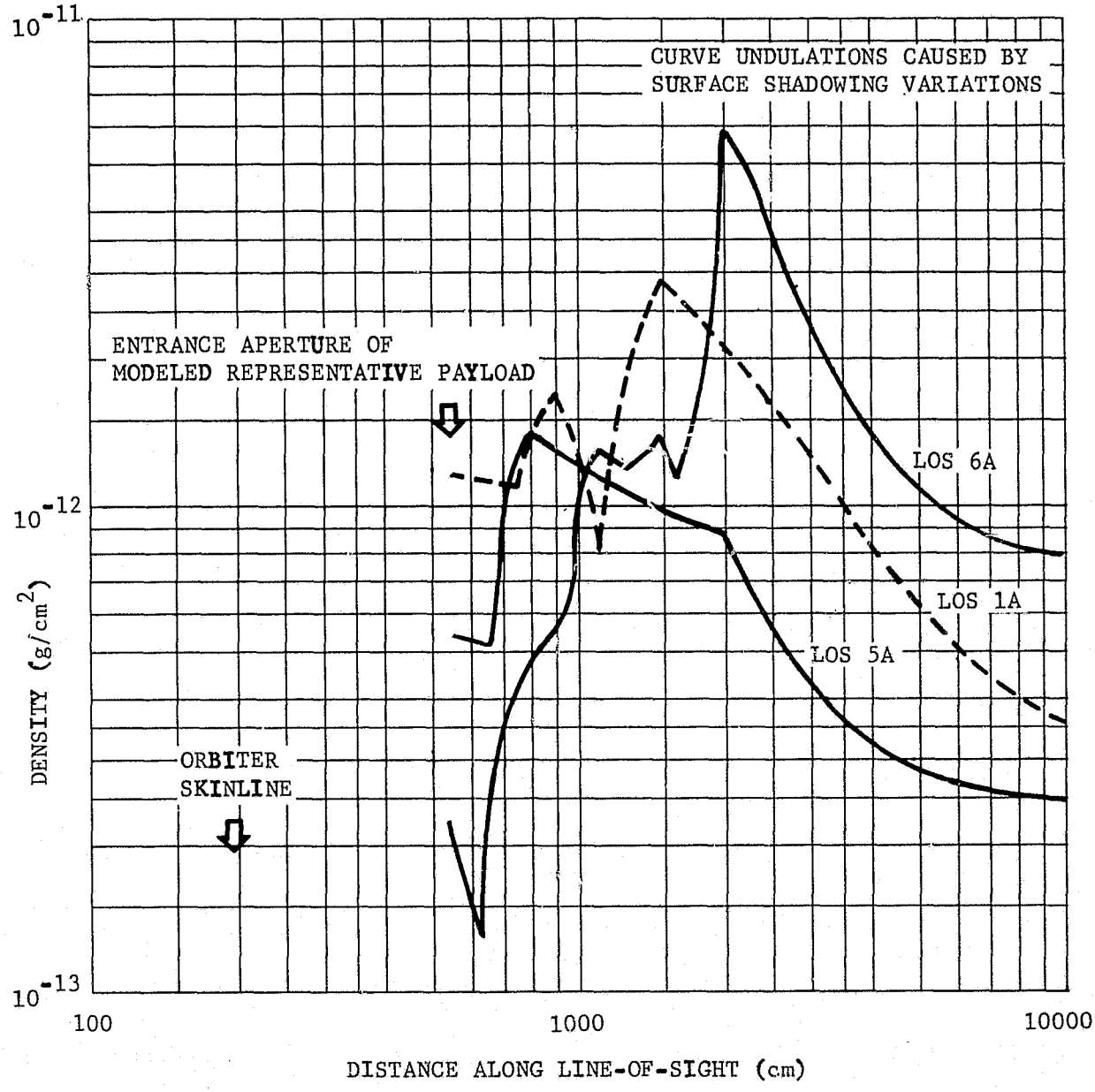

Figure 27. Density as a Function of Distance for Z Aft VCS Engine (LOS 1A, LOS 5A, and LOS 6A)

worst and best case, based on total fuel usage per orbit, were investigated for both inertial and local vertical attitudes. The time between engine firings and the duration of each firing are averages for each engine. Figures 28 and 29 show the molecular number column density as a function of time for 5% of an orbit for an inertial attitude worst and best case, respectively. Figures 30 and 31 are similar plots for local vertical worst case and best case, respectively. The time scale for the best case has been expanded so that all independent engine firings are included. These plots essentially repeat in time so that the sequence shown will apply throughout an orbit. The integrated number column density averaged over time is less than the 10^{14} molecules/cm^2 shown and will meet the criteria providing the integrated effect does not impact a given instrument or payload. However, the cyclic short high number column density periods seen in Figures 28 to 31 may be detrimental for specific payloads.

What is evident is that total fuel usage per orbit is not the only concern from a contamination viewpoint. What appears to be the most important considerations are the firing duration for each pulse and the number of pulses for a given time period. Short engine firing times result in a high frequency of pulses during an orbit. For example, the worst case inertial attitude (Figure 28) uses 29.3 lb (13.3 kg) of fuel per orbit and has the higher frequency of pulses because of the shorter pulse width required for keeping the local vertical attitude.

These duty cycles are based on a 0.3 degree deadband requirement. As the deadband limit decreases to 0.1 degree, the frequency of short pulsed firings may significantly increase. On the other hand, payloads using the Instrument Pointing System (IPS) for fine pointing will most likely require minimal usage of the VCS engines through less restrictive deadband requirements.

There are other vehicle attitudes (e.g., gravity gradient) that will require only limited VCS firings which should not significantly impact even the most sensitive payloads. Payload groups should assess their attitude requirements for a mission so that a minimum VCS duty cycle can be utilized.

3.4 Contaminant Induced Environment Minimization Studies - A major portion of this contract involved minimization studies of the contamination impact of the VCS engines and the evaporator vent as a result of their baseline locations significantly

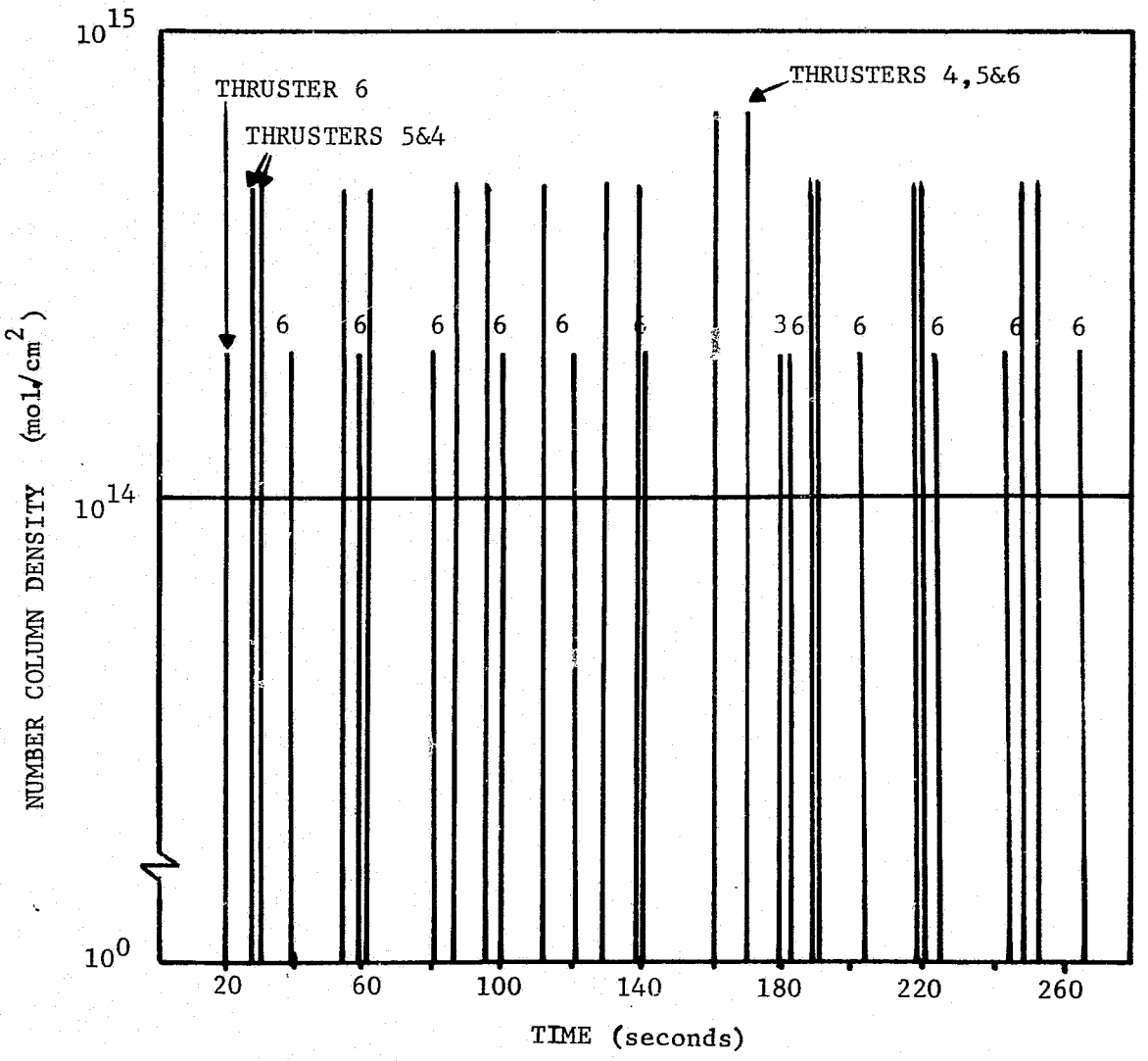

- 185 km
- 60° YAW
- 90° ROLL
- 13.32 kg/ORBIT
- AVE/PULSE = 11.35 g
- 0.3° DEADBAND
- Z LOS

Figure 28. Worst Case Inertial VCS Engine Firing Frequencies

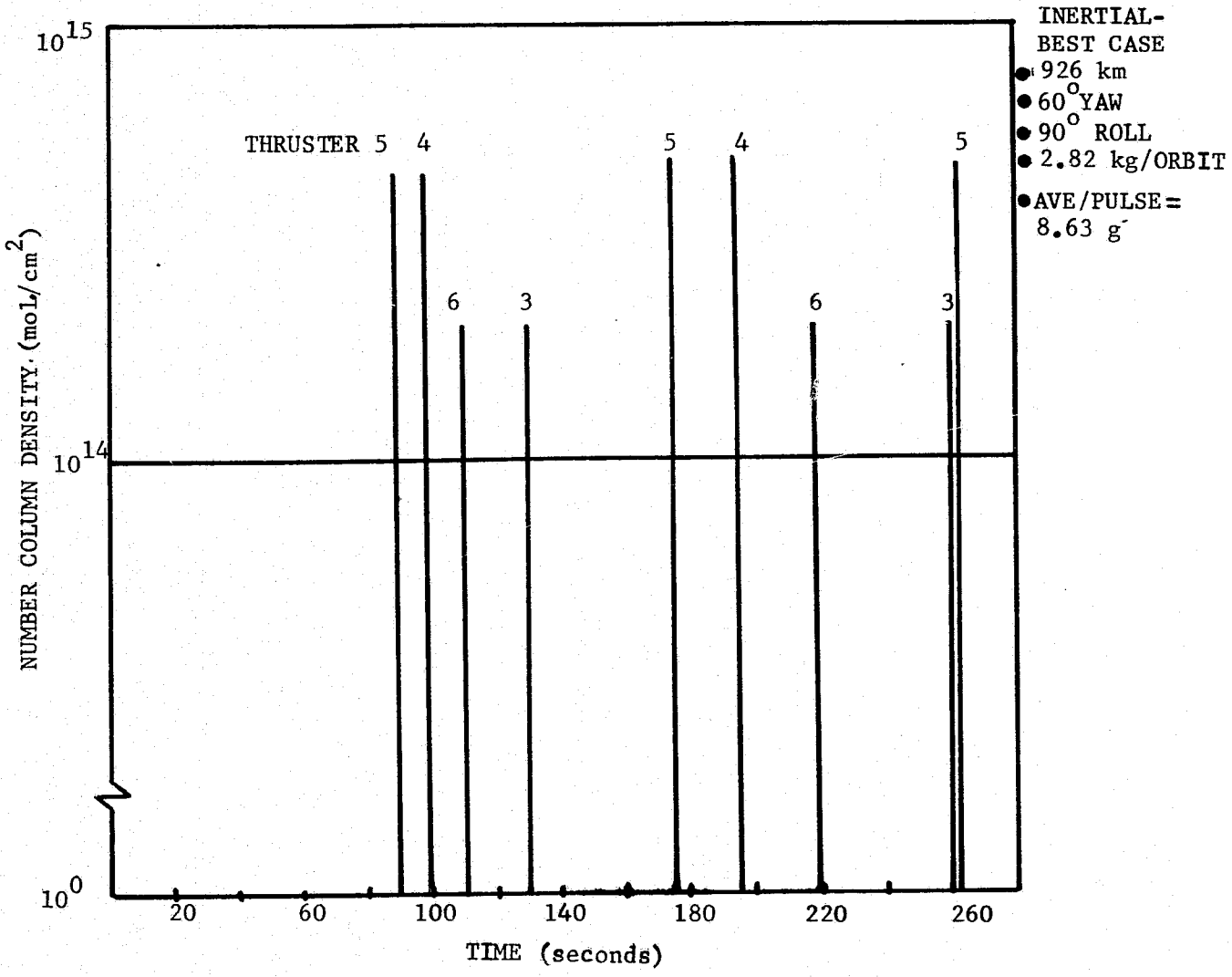

Figure 29. Best Case Inertial VCS Engine Firing Frequencies

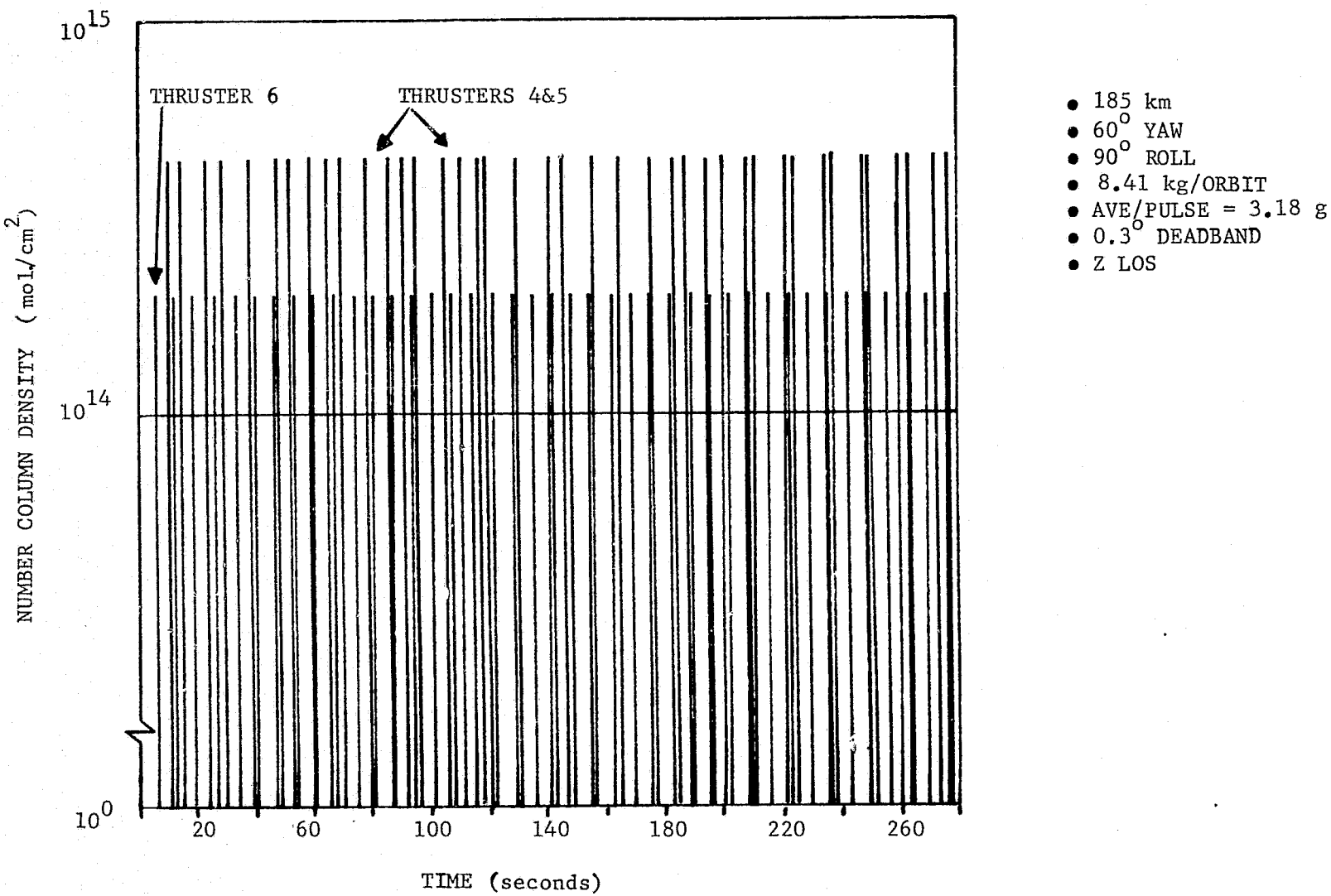

Figure 30. Worst Case Local Vertical VCS Engine Firing Frequencies

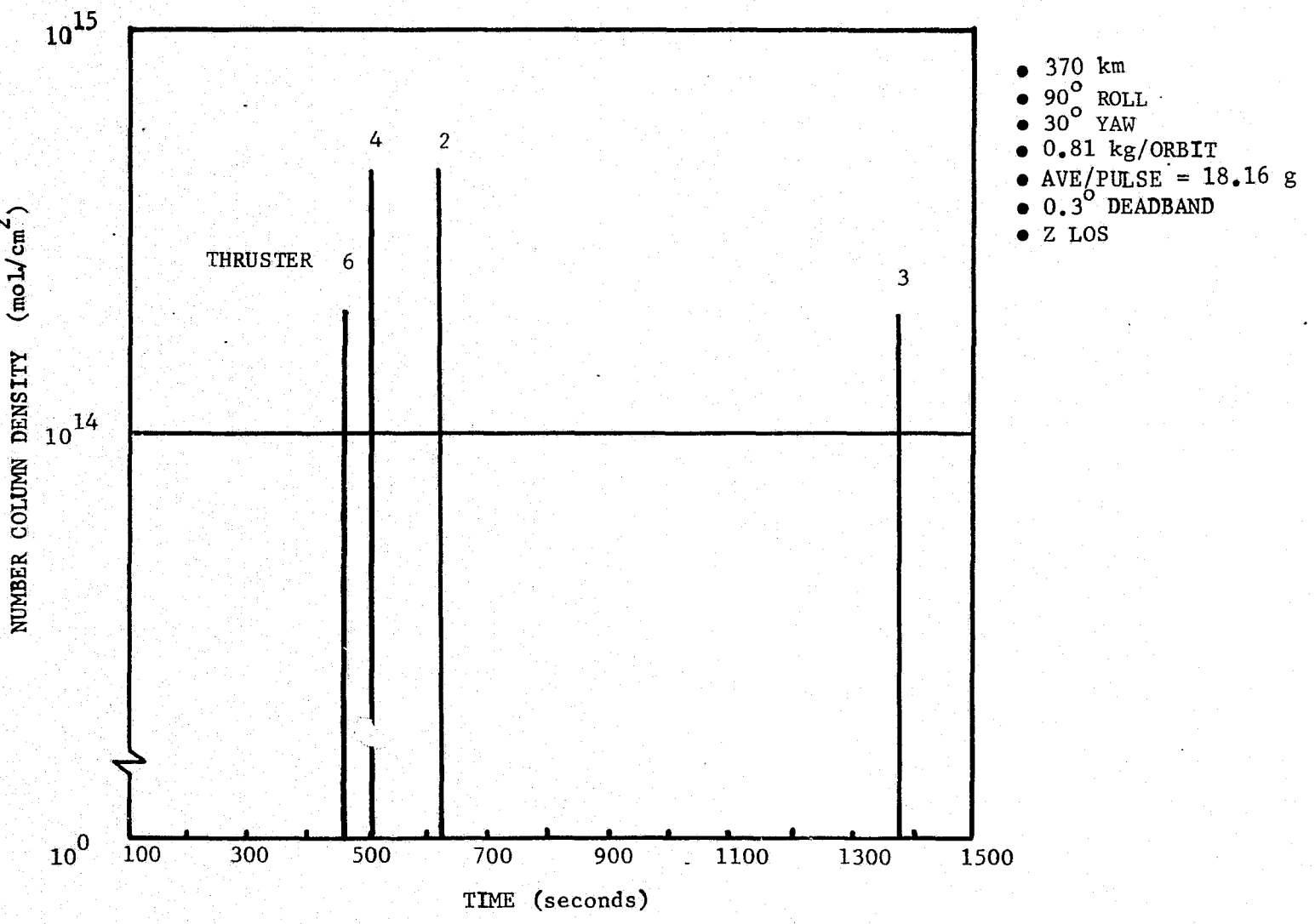

Figure 31. Best Case Local Vertical VCS Engine Firing Frequencies

exceeding certain aspects of the current contamination control criteria. The approach taken was to evaluate relocation and canting of the VCS engines and evaporator vent from their baseline locations. After a reasonable number of locations and canting combinations were evaluated it was hoped that decisions could then be made as to the best location and optimum orientation of these sources. This approach soon became complicated in that other systems became involved (e.g., guidance and control, structures - volume constraints , thermal, etc.) in that only a contamination viewpoint was not sufficient in the evaluation process. In addition, optimizing the evaporator vent location, in some instances, required additional VCS usage because of undesirable forces generated by the evaporator vent which has to be compensated for in altitude control by the VCS engines.

The predictions for the lines-of-sight in these minimization studies do not include all of the baseline lines-of-sight as presented in subsection 3.3. A limited number of these lines-of-sight were evaluated to establish a trend or to determine in a broad sense the impact of a location or orientation change. Additional lines-of-sight to the baseline lines-of-sight LOS 1A through LOS 6A were required for evaluation in specific analysis situations.

The following subsections are intended to present the analysis results of the significant contaminant minimization studies performed during the contract activity. The evaporator results have been updated for this report to include the current 15 lb/hr (6.8 kg) per nozzle evaporator flowrate (which was at 5.5 lb/hr (2.5 kg) per nozzle at the initiation of this study).

3.4.1 Vernier Control System (VCS) 25 lb Engines - The VCS engines contribute engine exhaust products to lines-of-sight by forward flow of the engine exhaust plume, backflow (greater than 90 degrees with respect to the engine axis) of the engine exhaust, or by wing reflections of the exhaust products. The wing reflections contribute significantly to all lines-of-sight and almost exclusively to lines-of-sight in the (X, Z) plane which are shielded from direct flow by Shuttle Orbiter surfaces. The forward flow and backflow primarily contribute to lines-of-sight out of the (X, Z) plane. For specific lines-of sight, the VCS engine contributions do not decrease continuously as a function of distance away from the Shuttle Orbiter

because of shadowing considerations from other surfaces between the engine and the line-of-sight in question.

The VCS contamination contribution to the induced atmosphere and surface deposition will be highly dependent on the mission profile for a specific payload. Parameters that are most important are frequency of VCS firings required to maintain a specified deadband, duration of each firing sequence, attitude of the Shuttle Orbiter during each firing, viewing direction of a payload and the Shuttle Orbiter velocity vector during each firing, payload field-of-view and exposure times, payload sensitivity to exhaust products, and payload critical surface temperatures. The contamination potential of the VCS on the payload bay door radiator surfaces is treated separately and is included in subsection 3.5.4.

The following subsections encompass the many variations possible that were investigated during this study in an effort to understand and minimize the contamination potential of the VCS engines to the lines-of-sight.

3.4.1.1 VCS Baseline Location - To date the positions of the baseline VCS locations are:

Thruster	Location			Firing Direction
	X	Y	Z	
1	323.5	46.0	373.5	35° from -Z, towards +Y
2	323.5	-46.0	373.5	35° from -Z, towards -Y
3	1565.0	-134.0	459.0	-Y
4	1565.0	-118.0	457.0	-Z
5	1565.0	118.0	457.0	-Z
6	1565.0	134.0	459.0	+Y

These locations and firing directions are schematically illustrated in Figure 20 and were used to establish the model

geometry for these studies. The VCS coordinates presented above correspond to the injector throat portions of the engines. Since the exit plane of the engine bell is required for modeling, its position was placed 6 inches (15.2 cm) downstream from the coordinates presented above.

Table VII lists the mass column density, the molecular number column density, and the maximum possible return flux at several altitudes for the baseline locations shown above. The return flux calculation is based on a median ambient atmosphere density at each altitude. Depending on sunspot activity the nighttime and daytime variations from the mean could be an order of magnitude.

3.4.1.2 Aft VCS Engine Canting - In order to reduce the VCS engine contributions to mass column densities (resulting mainly from wing reflections), the aft VCS engines were canted in the model at the baseline position to reduce the amount reflecting off of the wings. The Y facing VCS engines were canted 10 and 20 degrees from $\pm$Y towards +X (aft) and the -Z facing VCS engines 10 and 20 degrees from -Z towards +X. Calculations were made for specific lines-of-sight to determine the range of differences observed in the mass and molecular number column densities for the canted engines when compared to the baseline configuration. (See Figures 7 through 16 for line-of-sight descriptions.)

Table VIII summarizes the results for the canted engine evaluation. The results show that the Y aft engine decreases the mass column density approximately 35% and 65% for a 10 degree and 20 degree cant, respectively. The -Z aft engine decreases the mass column density by 44% and 63% for a 10 degree and 20 degree cant, respectively. The molecular column number density still exceeds 10^{12} molecules/cm^2 in all cases even though LOS 8F has the lowest number column density for engine contributions for the cases evaluated.

3.4.1.3 Elevon Canting - The wing reflection contribution from the aft VCS engines can be further reduced by canting the wing elevon down from its normal closed position. This surface receives the highest flux from the aft VCS engine exhausts and is normally at 12 degrees with respect to the X axis in a closed position. By rotating the elevon down about the Y

Table VIII. Changes in Mass Column Density (MCD) and Molecular Number Column Density (NCD) for Canted Aft VCS Engines Resulting from Wing Reflections

Line-of-Sight / Engine	LOS 1A		LOS 4A		LOS 7A		LOS 8A		LOS 5F		LOS 8F	
	MCD (g/cm^2)	NCD ($mol./cm^2$)	MCD (g/cm^2)	NCD ($mol./cm^2$)	MCD (g/cm^2)	NCD ($mol./cm^2$)	MCD (g/cm^2)	NCD ($mol./cm^2$)	MCD (g/cm^2)	NCD ($mol./cm^2$)	MCD (g/cm^2)	NCD ($mol./cm^2$)
-Z Aft (Baseline)	1.8(-8)*	4.4(14)	5.8(-8)	1.4(15)	3.3(-9)	8.1(13)	6.2(-10)	1.5(13)	4.4(-9)	1.1(14)	3.3(-10)	8.1(12)
-Z Aft 10^{o} (-Z→+X)	1.0(-8)	2.5(14)	3.2(-8)	7.9(14)	1.8(-9)	4.5(13)	3.4(-10)	8.4(12)	2.4(-9)	6.0(13)	1.8(-10)	4.5(12)
-Z Aft 20^{o} (-Z→+X)	6.6(-9)	1.6(14)	2.1(-8)	5.2(14)	1.3(-9)	3.2(13)	2.9(-10)	7.1(12)	1.6(-9)	3.9(13)	1.6(-10)	3.9(12)
± Y Aft (Baseline)	6.3(-9)	1.5(14)	1.3(-8)	3.2(14)	1.9(-9)	4.6(13)	8.3(-10)	2.0(13)	1.7(-9)	4.1(13)	4.6(-10)	1.1(13)
± Y Aft 10^{o} (Y→+X)	4.1(-9)	1.0(14)	8.5(-9)	2.1(14)	1.2(-9)	3.0(13)	5.4(-10)	1.3(13)	1.1(-9)	2.7(13)	3.0(-10)	7.3(12)
± Y Aft 20^{o} (Y→+X)	2.2(-9)	5.4(13)	4.5(-9)	1.1(14)	6.6(-10)	1.6(13)	2.9(-10)	7.1(12)	5.9(-10)	1.4(13)	1.6(-10)	3.9(12)

* $(-8) = 10^{-8}$

axis so that it is 90 degrees with respect to the X axis, it will not contribute to the wing reflections of engine exhausts. This situation was simulated in the model by removing the elevon surface. The net decrease in mass column densities was a maximum for this situation.

Table IX includes the elevon removed case to show the maximum reduction in line-of-sight column densities in conjunction with engine canting. The results show that removing the elevon as a reflecting surface did not affect the predictions for LOS 8A and 8F. These lines-of-sight do not see any appreciable contribution from this portion of the wing because of their orientation. For the remaining lines-of-sight in Table IX, the reduction in column densities varied from 30 to 80%. The resulting NCD for all combinations of elevon removal and engine canting still exceeds 10^{12} molecules/cm^2 for the lines-of-sight analyzed.

3.4.1.4 Spherical Versus Lambertian Wing Reflections - The highest wing surface impingement rate of the -Z aft VCS engine exhaust occurs at a distance near 15 ft (4.6 m) from the engine and 18 degrees off of the engine axis. The molecular densities at this point are in the 10^{12} molecules/cm^3 range which corresponds to a mean free path near 100 cm. This region is neither clear cut viscous nor molecular flow and corresponds to a transition region between these two regimes. The possibility does exist that the molecular reflections for this transition region might not follow Lambertian scattering. It might appear that with such high densities, wing reflections would approach specular thus lowering the column density predictions. This is true in some cases, although in the transition region the reflections will be a hybrid of Lambertian and specular scattering. Because of this, the engine exhaust on this wing surface area (6.5×10^4 cm^2 or 7% of total wing area) was expanded spherically symmetrically to specific lines-of-sight while the remainder of the wing was allowed to scatter diffusely (cosine). The results, compared to the total wing scattering diffusely (cosine), are presented below. There are two cases for the spherical expanded gases: one for the case of a hot gas, 3000 m/second corresponding to engine exhaust temperatures and 500 m/second corresponding to wing surface temperatures (cold gas). The actual temperature of the gas depends upon the extent of thermal accommodation capability at the wing surface and is unknown at this time.

Table IX. Effects of Elevon Canting and Aft VCS Engine Canting on Mass and Molecular Number Column Density Predictions Resulting from Wing Reflections

Line-of-Sight / VCS Engine	LOS 1A		LOS 4A		LOS 7A		LOS 8A		LOS 5F		LOS 8F	
	MCD (g/cm^2)	NCD ($mol./cm^2$)	MCD (g/cm^2)	NCD ($mol./cm^2$)	MCD (g/cm^2)	NCD ($mol./cm^2$)	MCD (g/cm^2)	NCD ($mol./cm^2$)	MCD (g/cm^2)	NCD ($mol./cm^2$)	MCD (g/cm^2)	NCD ($mol./cm^2$)
-Z Aft(Baseline)	1.8(-8)**	4.4(14)	5.8(-8)	1.4(15)	3.3(-9)	8.1(13)	6.2(-10)	1.5(13)	4.4(-9)	1.1(14)	3.3(-10)	8.1(12)
	*NE =	NE =	NE =	NE =	NE =	NE =	NE =	NE =	NE =	NE =	NE =	NE =
	4.5(-9)	1.1(14)	1.1(-8)	2.7(14)	1.1(-9)	2.7(13)	Same	Same	1.2(-9)	2.9(13)	Same	Same
-Z Aft 10^{o} (-Z→+X)	1.0(-8)	2.5(14)	3.2(-8)	7.9(14)	1.1(-9)	4.5(13)	3.4(-10)	8.4(12)	2.4(-9)	6.0(13)	1.8(-10)	4.5(12)
	NE =	NE =	NE =	NE =	NE =	NE =	NE =	NE =	NE =	NE =	NE =	NE =
	2.5(-9)	6.0(12)	5.8(-9)	1.4(14)	5.7(-10)	1.4(13)	Same	Same	6.2(-10)	1.5(13)	Same	Same
-Z Aft 20^{o} (-Z→+X)	6.6(-9)	1.6(10)	2.1(-8)	5.2(14)	1.3(-9)	3.2(13)	2.9(-10)	7.1(12)	1.6(-9)	3.9(13)	1.6(-10)	3.9(12)
	NE =	NE =	NE =	NE =	NE =	NE =	NE =	NE =	NE =	NE =	NE =	NE =
	1.6(-9)	4.0(13)	4.0(-9)	9.8(13)	4.3(-10)	1.1(13)	Same	Same	4.3(-10)	1.1(13)	Same	Same
±Y Aft(Baseline)	6.3(-9)	1.5(14)	1.3(-8)	3.2(14)	1.9(-9)	4.6(13)	8.3(-10)	2.0(13)	1.7(-9)	4.1(13)	4.6(-10)	1.1(13)
	NE =	NE =	NE =	NE =	NE =	NE =	NE =	NE =	NE =	NE =	NE =	NE =
	3.7(-9)	9.0(13)	7.7(-9)	1.9(14)	1.2(-9)	4.4(13)	Same	Same	1.0(-9)	2.5(13)	Same	Same
± Y Aft 10^{o} (Y→+X)	4.1(-9)	1.0(14)	8.5(-9)	2.1(14)	1.2(-9)	3.0(13)	5.4(-10)	1.3(13)	1.1(-9)	2.7(13)	3.0(-10)	7.3(12)
	NE =	NE =	NE =	NE =	NE =	NE =	NE =	NE =	NE =	NE =	NE =	NE =
	2.5(-9)	6.0(13)	5.0(-9)	1.2(14)	7.1(-10)	1.7(13)	Same	Same	6.5(-10)	1.6(13)	Same	Same
± Y Aft 20^{o} (Y→+X)	2.2(-9)	5.4(13)	4.5(-9)	1.1(14)	6.6(-10)	1.6(13)	2.9(-10)	7.1(12)	5.9(-10)	1.4(13)	1.6(-10)	3.9(12)
	NE =	NE =	NE =	NE =	NE =	NE =	NE =	NE =	NE =	NE =	NE =	NE =
	1.3(-9)	3.2(13)	2.7(-9)	6.6(13)	4.0(-14)	9.8(12)	Same	Same	3.6(-10)	8.7(12)	Same	Same

* NE = No Elevon

** (-8) = 10^{-8}

Lines-of-Sight	Previous Wing Lambertian Reflection, (mol./cm^2)	Hot Gas Spherical plus Wing Remainder Cosign (mol./cm^2)	Cold Gas Spherical plus Wing Remainder Cosign (mol./cm^2)
LOS 1A	4.4×10^{14}	1.8×10^{14}	3.9×10^{14}
LOS 4A	1.4×10^{15}	4.5×10^{14}	9.5×10^{14}

The above data shows that the number column density is reduced 59% and 11% for the hot and cold gas case, respectively, for LOS 1A and is reduced 68% and 32% for the hot and cold gas case, respectively, for LOS 4A. However, these values still exceed the stated criteria of 10^{12} molecules/cm^2.

Data pertaining to the Marquardt 25 pound thrust R1E-3 engine has been applied to the geometry discussed above. This data entails a Method of Characteristics (MOC) analysis of the engine flow which determines the continuum and free molecular flow regimes. Based on the results of this analysis, a smaller area of the wing is in the transition region, less than 6.5×10^3 cm^2 or less than 0.7% of the total wing area, thus further reducing the effects shown above. Therefore, the initial modeling approach, which assumes molecular flow for the engine exhaust impinging on the wing, appears to be valid and encompasses more than 99% of the wing.

3.4.1.5 Forward VCS Location - The capability does exist that all of the VCS engines could be moved to a forward location. This situation was evaluated for comparison to the aft location as discussed above. At the forward location, the -Z firing aft engine must be positioned along +Z to maintain the same attitude control.

Table X compares the aft and forward locations for LOS 1A, 2A, and 3A. Moving these engines to the selected forward position does not significantly reduce the number column density for the analyzed lines-of-sight. As a result, canting of the engines about their principle axes at this position was further investigated to see if the total number column density could be significantly reduced for the selected forward VCS positions. The evaluation of the engine canting

Table X. Comparison of Aft Location to Forward Location for VCS Engines

Position / Line-of-Sight	Y Facing Engine		Z Facing Engine	
	Aft Number Col. Density (mol./cm^2)	Fwd Number Col. Density (mol./cm^2)	Aft -Z Number Col. Density (mol./cm^2)	Fwd (+Z) Number Col. Density (mol./cm^2)
LOS 1A	2.1×10^{14}	0	4.4×10^{14}	7.8×10^{14}
LOS 2A	7.3×10^{14}	3.6×10^{14}	8.3×10^{14}	2.1×10^{14}
LOS 3A	3.7×10^{14}	1.4×10^{14}	8.3×10^{14}	5.4×10^{14}

requires several combinations of rotations. Figure 32 schematically illustrates the rotation cases analyzed and includes the forward and aft positions with no canting for clarity and comparison purposes.

Case 1 is for the aft position with both exit planes perpendicular to the major axes. Case 2 is for the forward position with both engine exit planes perpendicular to the major axes. Cases 3 and 4 are rotations at the forward location of 10 and 20 degrees, respectively, for the Y engine about the Z axis towards -X (forward) and the Z engine about the Y axis towards -X (forward). Cases 5 and 7 are rotations at the forward location of 10 and 20 degrees, respectively, for the Y engine about the X axis toward -Z and the Z engine about the X axis towards -Y. Cases 7 and 8 are combinations of cases 3 and 5 and cases 4 and 6, respectively. That is, case 7 includes a 10 degree rotation in two directions and case 8 includes a 20 degree rotation in two directions. The results are presented in Table XI.

The backflow portion of each molecular number column density is noted. This backflow portion (greater than 90 degrees off of the engine centerline) could be eliminated by effective shielding since it will be near the free molecular flow state. Figure 33 graphically presents the data in Table XI. This figure shows that overall, case 4 reduces the number column density most effectively for the three lines-of-sight considered. This case corresponds to a 20 degree rotation about Z for the Y facing engine and about Y for the Z facing engine towards -X (forward). Although moving these VCS engines forward and canting them significantly reduces the number column density, as seen in Table XI, the values still exceed 10^{12} molecules/cm^2 for the three lines-of-sight considered and for all the canting combinations investigated.

3.4.1.6 VCS Engine Summary - The VCS engines can contribute to lines-of-sight with molecular column density levels in excess of 10^{12} molecules/cm^2. This is true for all engine orientations at both an aft and a forward location. The extent to which interference to sensitive payloads can occur due to the VCS induced column densities is a strong function of altitude and attitude requirements. The engine firing frequency can range from once every 2 to 5 seconds to once or twice per orbit

Z ENGINE

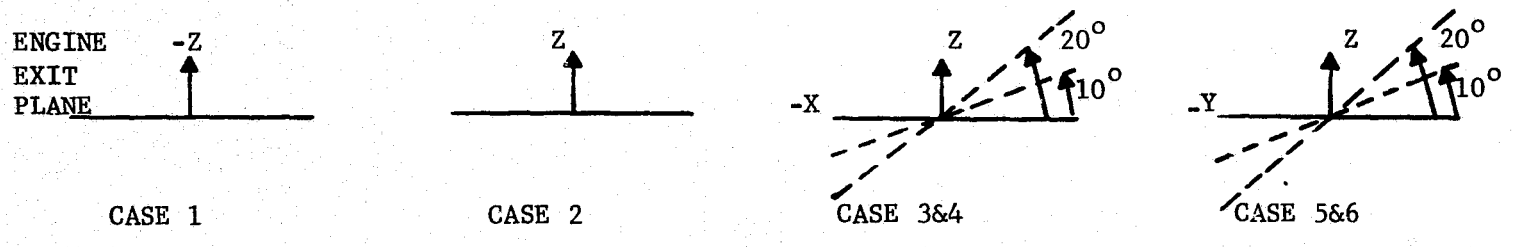

CASE 1 CASE 2 CASE 3&4 CASE 5&6

Y ENGINE

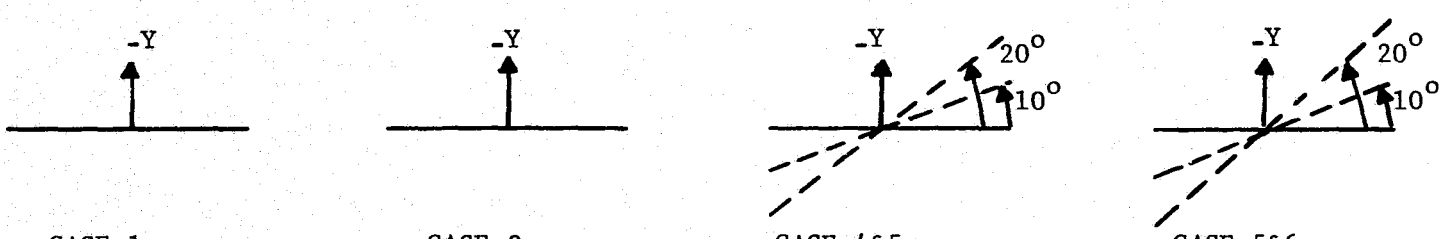

CASE 1 CASE 2 CASE 4&5 CASE 5&6

CASE 7 COMBINATION OF CASE 3&5 FOR EACH ENGINE

CASE 8 COMBINATION OF CASE 4&6 FOR EACH ENGINE

Figure 32. VCS Engine Orientations

Table XI. Predicted Molecular Number Column Densities for the 25 lb Vernier Engines at Select Locations and Cant Angles for Payload Lines-of-Sight at X = 1107

	CASE 1	CASE 2	CASE 3	CASE 4	CASE 5	CASE 6	CASE 7 (Comb. of Case 3 & 5)	CASE 8 (Comb. of Case 4 & 6)
Y Engine / Line-of-Sight at X = 1107	Aft No Cant X = 1531 Y = ±120 Z = 461	Fwd No Cant X = 323.5 Y = ±58 Z = 373	Fwd 10° Cant (Y►+X, about Z) X = 323.5 Y = ±58 Z = 373	Fwd 20° Cant (Y► +X, about Z) X = 323.5 Y = ±58 Z = 373	Fwd 10° Cant (Y ►-Z, about X) X = 323.5 Y = ±58 Z = 373	Fwd 20° Cant (Y►-Z, about X) X = 323.5 Y = ±58 Z = 373	Fwd 10° Cant (Y►+X) and (Y►-Z) X = 323.5 Y = ±58 Z = 373	Fwd 20° Cant (Y►+X) and (Y►-Z) X = 323.5 Y = ±58 Z = 373
LOS 1A	* 2.0 (14)	0	** 2.7 (13) (All B Flow)	2.1 (13) (All B Flow)	2.3 (13) (All B Flow)	1.5 (13) (All B Flow)	2.3 (13) (All B Flow)	1.6 (13) (All B Flow)
LOS 2A	3.7 (14)	1.4 (14)	7.3 (13)	5.6 (13) (9% B Flow)	6.6 (13)	3.7 (13)	6.8 (13)	4.0 (13) (10% B Flow)
LOS 3A	7.3 (14)	3.6 (14)	1.9 (14)	2.8 (13) (10% B Flow)	1.9 (14)	1.3 (14)	1.9 (14)	1.3 (14)
Z Engine / Line-of-Sight at X = 1107	Aft No Cant X = 1525 Y = ±112 Z = 442	Fwd No Cant X = 323.5 Y = ±46 Z = 423	Fwd 10° Cant (Z►+X, about Y) X = 323.5 Y = ±46 Z = 423	Fwd 20° Cant (Z►+X, about Y) X = 323.5 Y = ±46 Z = 423	Fwd 10° Cant (Z►Y, about X) X = 323.5 Y = ±46 Z = 423	Fwd 20° Cant (Z►Y, about X) X = 323.5 Y = ±46 Z = 423	Fwd 10° Cant (Z►+X) and (Z►Y) X = 323.5 Y = ±46 Z = 423	Fwd 20° Cant (Z►X) and (Z►Y) X = 323.5 Y = ±46 Z = 423
LOS 1A	4.4 (14)	7.8 (14)	4.6 (14)	2.7 (14)	7.1 (14)	5.4 (14)	4.1 (14)	2.1 (14)
LOS 2A	8.3 (14)	5.4 (14)	3.2 (14)	2.1 (14)	6.8 (14)	7.8 (14)	3.9 (14)	2.7 (14)
LOS 3A	8.3 (14)	2.1 (14)	1.5 (14)	2.4(13) (15% B Flow)	2.9 (14)	4.1 (14)	2.1 (14)	1.8 (14) (1% B Flow)

* $(14) = 10^{14}$

** B Flow = Backflow

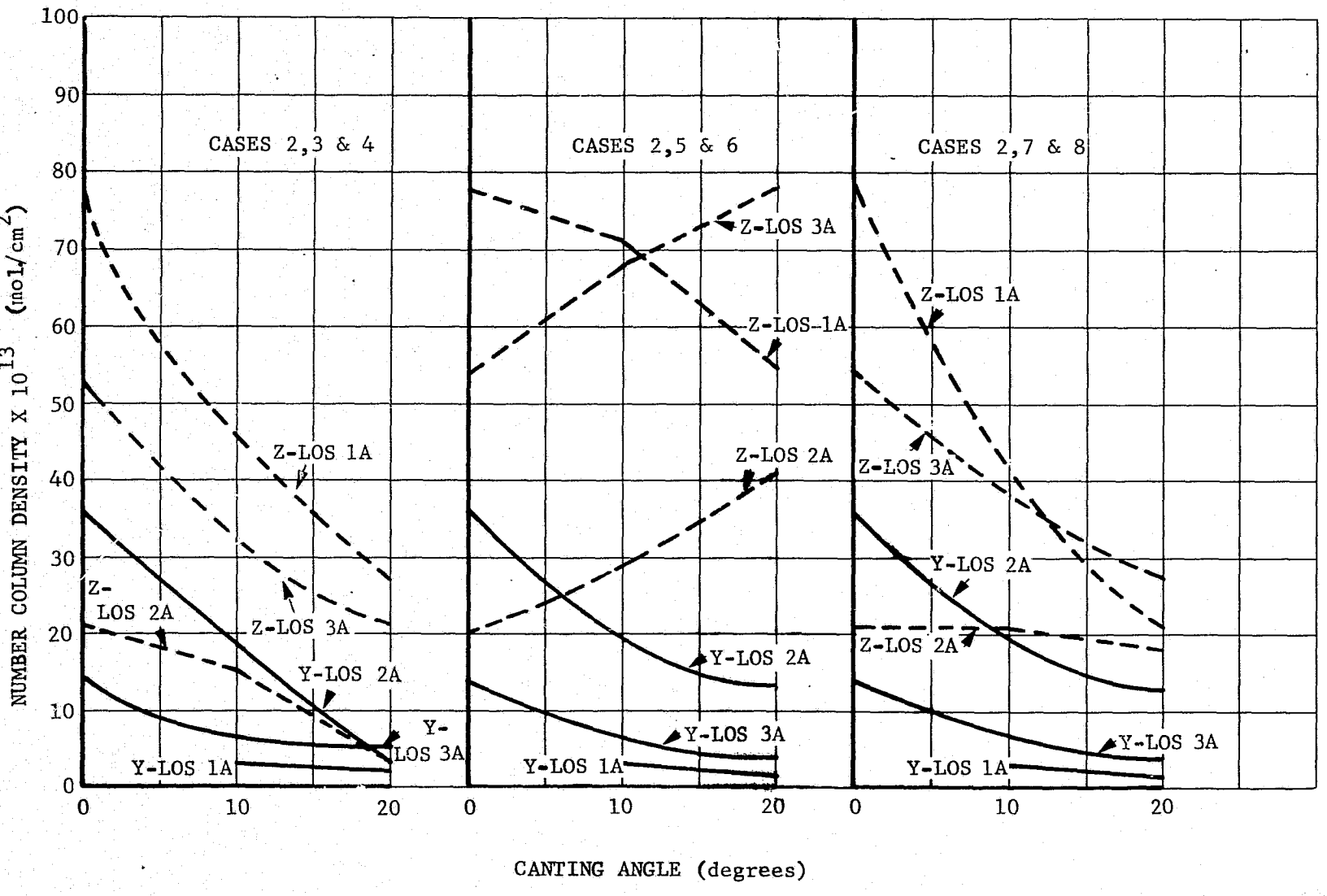

Figure 33. Canting Effects on Number Column Density for VCS Y and +Z Forward Engines

depending on the mission profile. The total fuel used per orbit is not indicative of the firing frequency. The engine pulse width per firing dictates the frequency for a given fuel consumption per orbit. The ultimate impact of the VCS 25 lb engine system will have to assessed individually for each class of payload taking into account the appropriate variables. Current studies indicate that that the VCS 25 lb thrust engines cannot meet the stated applicable criteria when firing. Therefore, meeting the intent of the criteria through minimizing engine usage requirements will be an important aspect of minimizing this contamination source influence upon various payloads. This can be accomplished through proper selection of vehicle attitudes or through payload use of a gimballed system such as the IPS.

The VCS engines not only can impact payloads, but they can also deposit on the aft, outermost portions of the Shuttle Orbiter radiators and could increase radiator ground refurbishment requirements significantly. In this case, the total fuel expended per orbit by the aft $\pm Y$ and $-Z$ engines can be directly related to the degradation potential. This is discussed in subsection 3.5.4.

3.4.2 Supplemental Evaporator Vent System - The evaporator vent system emits evaporated fuel cell water overboard as a mechanism to reject heat from the Environmental Control Life Support System (ECLSS). It can contribute exhausted water vapor to lines-of-sight by forward flow, backflow (greater than 90 degrees with respect to the evaporator vent axis), or by wing reflections of the exhausted effluents. The wing reflections for specific evaporator vent locations contribute significantly to all lines-of-sight and is the only transport mechanism to lines-of-sight in the (X,Z) plane. The position of the evaporator vents on the Shuttle Orbiter dictates the amount of wing reflection that results. Specific aft or forward locations do totally eliminate wing reflections, however, some of these positions are unacceptable due to fuselage penetration problems. For locations underneath the payload bay door, the evaporator vents can emit effluents through the payload bay door/Shuttle Orbiter fuselage seam.

The evaporator contamination contribution to the induced atmosphere and surface deposition is highly dependent upon the mission profile for a specific payload, heat rejection requirements, payload temperature, and selection of a final

evaporator vent location. Because the evaporator operation may be near continuous in nature and can be located at more positions than any other major source, it has undergone the most extensive analysis of the sources modeled to date.

The following subsections address the many trade studies performed on the evaporator during this contract. The major emphasis was to select or evaluate various positions for the evaporator vents so that the contamination potential could be ascertained and hopefully minimized. The evaporator vents are constrained to locations above the Shuttle Orbiter wings to avoid being located in high temperature areas produced during reentry. In some locations acceptable from a contamination viewpoint, the evaporator exhaust produces forces and torques on the Shuttle Orbiter by impinging on adjacent surfaces. Because of these forces, the VCS system would be required to operate at a higher rate or require greater fuel usage to maintain attitude control. Therefore, even though a specific evaporator vent location may reduce its contamination contribution, it does not necessarily reduce the total contaminatin problem.

The flow rate of the evaporator as used in this analysis was 30 lb/hr (13.6 kg) or 15 lb/hr (6.8 kg) per nozzle for the nonpropulsive configurations. Future power requirement changes may result in different flow rates as the Shuttle Program develops. In this case, ratioing the presented values will be representative of any future mass flow changes in the evaporator system.

In addition to positioning the evaporator vents at several locations, different evaporator nozzle designs were evaluated at X = 1392 (baseline location). At this location, the effects of a plugged nozzle and a nozzle using a larger exit area to throat area ratio with a zero degree lip angle were evaluated.

3.4.2.1 Evaporator Vents at X = 1392 (Baseline Position) - The evaporator vent position at X = 1392 was considered as a baseline location throughout most of this study and thus had an in depth analysis of variations at this location. Not only was the baseline supersonic nozzle configuration analyzed at this location, but also with the intent of minimizing evaporator impacts, several alternate nozzle configurations were investigated at the baseline location. At X = 1392, the evaporator effluents have the capability of reflecting off of the wing

surfaces into lines-of-sight along with contributing by direct flow from the nozzle exit plane. Figure 19 schematically illustrates this location.

Table VI lists the contribution of the X = 1392 baseline supersonic evaporator vent location to the lines-of-sight and specifies the wing reflected component and direct flow component. Since there is an evaporator vent on each side of the Shuttle Orbiter for this configuration, both contributions are shown along with the total from each vent. At this location and a 6.8 kg/hr per nozzle flow rate, the molecular number column density is in the 10^{13} to 10^{14} molecules/cm^2 range for LOS 1A through 6A. The alternate nozzle configurations analyzed at the baseline location are briefly discussed below.

a) Plugged Nozzle - An evaporator nozzle with a truncated conical surface placed in the nozzle bell chamber area can change the flowfield of the effluents. The plugged nozzle plume description, supplied by JSC (Applicable Document T-169-28, Volume VI) was evaluated for the X = 1392 location for LOS 1A. At a flowrate of 6.8 kg/hr per nozzle, the molecular number column density is 2.3×10^{14} molecules/cm^2 as compared to 1.7×10^{14} molecules/cm^2 for the standard, unplugged supersonic nozzle. Because there is no significant reduction in contaminant levels using the plugged nozzle and the fact that it could ice up and become inoperable, it has been eliminated as a possible modification.

b) Larger Area Ratio With a Zero Lip Angle Nozzle - Additional analysis was performed for another evaporator nozzle shape to determine if it would reduce the mass column density predictions. Specifically, a new nozzle concept that has an area ratio of 20:1 and a zero degree lip angle was compared to the previous nozzle configurations at the X = 1392 location. The approach employed in this nozzle design was to modify the boundary flow and plume flow coefficients by changing the physical characteristics of the nozzle shape through using analytical data developed by Simons

(Reference 2). This same flowfield description was then used to determine the exhaust fluxes on the wings and the resulting reflected material contribution to column densities for several lines-of-sight. The comparison of the baseline nozzle contribution and the new nozzle contribution are presented in Table XII. The results of the analysis indicates that such a nozzle design reduces the wing reflected component about 10 to 30% depending on the line-of-sight. This nozzle concept reduced the flux on some wing surfaces and increased it on others as compared to the baseline nozzle wing reflections. The net integrated effect is a small reduction in number column densities. The resulting values are still several orders of magnitude above the acceptable criteria of 10^{12} molecules/cm^2. In addition, the use of this nozzle would add excessive weight to the evaporator system and would be undesirable from a mass properties viewpoint.

3.4.2.2 Evaporator Vents Under the Payload Bay Doors - The evaporator vents located under the payload bay door (positions X = 594 to X = 1124 as shown by the shaded area in Figure 19) has several advantages along with some possible disadvantages. First of all, the major advantage is that the payload bay door blocks most of the effluents from the lines-of-sight and in certain regions the narrow wing in this region eliminates or significantly reduces wing reflected effluents. The major disadvantages are torques on the payload bay doors, possible ice buildup under the payload bay door, and effluents escaping through the payload bay door/Shuttle Orbiter fuselage hinge line. The effluents that escape through this hinge line could be eliminated by the use of a flexible covering or "boot".

Table XIII presents the evaporator nozzle contributions to LOS 1A for locations between X = 594 and 1124 with Z = 353 and Y = 104. The results presented in Table XIII indicate that there is a region approximately 6.1 meters in length for the 6.8 kg/hr per nozzle flowrate where an evaporator vent could be located to meet the number column density criteria of 10^{12} molecules/cm^2. If a seam line covering is used (between the payload bay door and the fuselage), this acceptable region would extend

Table XII. Number Column Densities of Baseline and Zero Lip Angle, Larger Area Ratio Evaporator Nozzle

Line-of-Sight	Baseline Nozzle ($mol./cm^2$)	New Nozzle ($mol./cm^2$)	Percent Decrease
LOS 1A	1.7×10^{14}	1.6×10^{14}	6%
LOS 4A	3.8×10^{14}	2.6×10^{14}	32%

Table XIII. Number Column Densities from Evaporator at Various Locations Under the Door for LOS 1A

X Location (Inches) / Source	594	845	924	974	1024	1124
Door Seam Contribution (mol./cm^2)	5.5×10^{11}	1.1×10^{12}	1.4×10^{12}	1.4×10^{12}	1.5×10^{12}	1.6×10^{12}
Direct Wing Contribution (mol./cm^2)	0	0	5.2×10^{11}	1.9×10^{12}	8.2×10^{12}	1.7×10^{14}
TOTAL LOS 1A (mol./cm^2)	5.5×10^{11}	1.1×10^{12}	1.9×10^{12}	3.3×10^{12}	9.7×10^{12}	1.7×10^{14}

another 2.7 meters to near X = 950. Figure 34 is a plot of molecular number column density for LOS 1A as a function of the Shuttle Orbiter X station numbers for possible evaporator vent locations. The curves presented are for flowrates of 4.5, 6.8 (baseline), and 11.4 kg/hr per nozzle. This family of curves in effect shows where and at what flowrate the criteria of 10^{12} molecules/cm^2 is exceeded. At these locations, consideration must be given to the induced forces and the accumulation created by evaporator effluent impingement upon the Shuttle Orbiter wing and door surfaces. These are analyzed in subsections 3.4.2.5 and 3.4.2.6, respectively.

3.4.2.3 Evaporator Vents at X = 1519 (Lower Aft Corner of the Fuselage) - Because wing reflected evaporator effluents are a significant contribution to the line-of-sight mass column densities, the evaporator vent was evaluated at positions such as +X (aft) venting and at X = 1519 that eliminates this contribution. Such a position at X = 1519 is in the lower aft corner of the Shuttle Orbiter, see Figure 19. In this position, the evaporator vent is lower than or even with the trailing edge of the wing. The only line-of-sight contributions that exist are direct flow from the nozzle. Therefore, the only lines-of-sight that are affected are those out of the (X, Z) plane. Another advantage of this location is that there is no significant impingement on surfaces that would produce unwanted Z direction forces although ice may accumulate on the wing trailing edge as will be discussed in subsection 3.4.2.6. Therefore, this is the only location analyzed that should not significantly increase VCS usage requirements. Table XIV presents the number column densities from such a location for several lines-of-sight. As can be seen, the (X, Z) plane has no contribution and up to approximately 30 degrees off of Z in the Y direction, the number column density is below 10^{12} molecules/cm^2. For lines-of-sight forward of X = 1107, the number column density will also be below 10^{12} molecules/cm^2.

3.4.2.4 Aft Facing Evaporator Vent Along the Longitudinal Axis Location - Another evaporator vent location evaluated was from the aft end of the Shuttle Orbiter parallel to the X axis at Y = 0 and Z = 323, see Figure 19. Since only one nozzle (propulsive) was considered at this location, the flowrate was assumed to be 13.6 kg/hr. For this case, the aft portion of the Shuttle Orbiter and the large engine bells effectively shadow the evaporator vent contribution forward of this position.

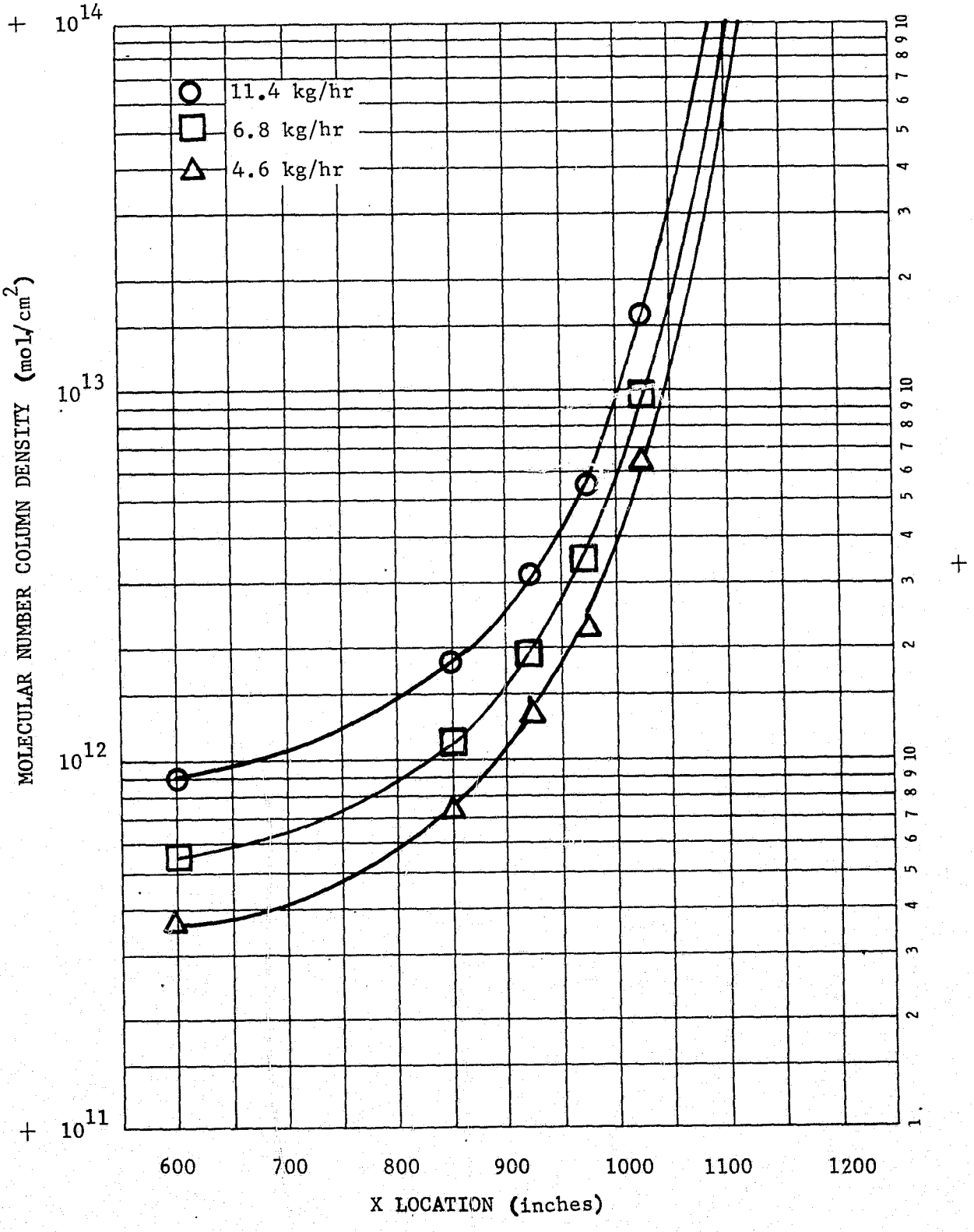

Figure 34. Evaporator Contribution to LOS 1A as a Function of X Location and Flow Rate

Table XIV. Number Column Densities for the Evaporator at X = 1519

Line of Sight	Molecular Column Density $\cdot$(mol./cm^2)
LOS 1A	0
LOS 2A	1.8×10^{13}
LOS 3A	5.6×10^{11}
LOS 4A	6.7×10^{12}

For lines-of-sight in the (Y, Z) plane extending past the aft location, there will be some contribution to these lines-of-sight. This situation was analyzed in detail to update an earlier analysis performed by Dr. R. Naumann, MSFC (Reference 6). The analysis results are different than that of Dr. Naumann's primarily because this analysis used an improved flowfield definition past 36.8 degrees off of the evaporator vent centerline.

Figure 35 shows the molecular number columm density versus angle off of the +Z axis towards +X (aft) for lines-of-sight in the (X, Z) plane originating at X = 1107 out of the payload bay. The NCD falls to 10^{12} molecules/cm^2 at 10 degrees from the vertical. LOS 4A and an additional test LOS that is 25 degrees off of Z towards Y and 45 degrees from Y towards +X (aft) were evaluated for this case to further determine the impact of this aft location. The number column densities for these lines-of-sight are 2.6×10^{13} and 7.1×10^{12} molecules/cm^2, respectively. The only lines-of-sight that are effected at all by this location are those that extend in an aft direction past approximately X = 1525. All other lines-of-sight have zero contribution from this evaporator vent location.

3.4.2.5 Forces Generated by the Evaporator Vent - Depending on the evaporator vent location, forces will be generated by impingement on adjacent Shuttle Orbiter surfaces or by the thrust of the evaporator vent itself. The forces generated by the evaporator vent will induce Shuttle Orbiter torque or drift rates and dictate increased usage of the VCS engines to achieve required deadband stability. This would be undesirable from a contamination viewpoint. Four positions were analyzed for the evaporator vent. These are X = 594, 900 to 950, 1392 (baseline), and aft (along +X). Where feasible, various cant angles of the evaporator vent were analyzed to determine if the induced forces could be reduced without significantly impacting the induced contaminant environment.

a) X = 594 Location - At this location, the effluents along the centerline of the evaporator impinges on the underside of the payload bay door. For the evaporator vent exit plane perpendicular to the Y axis, the net Z force on the vehicle for both evaporator nozzles ($\pm$Y side) is 0.49 lbs, the Y force is zero, and the X force is very near zero.

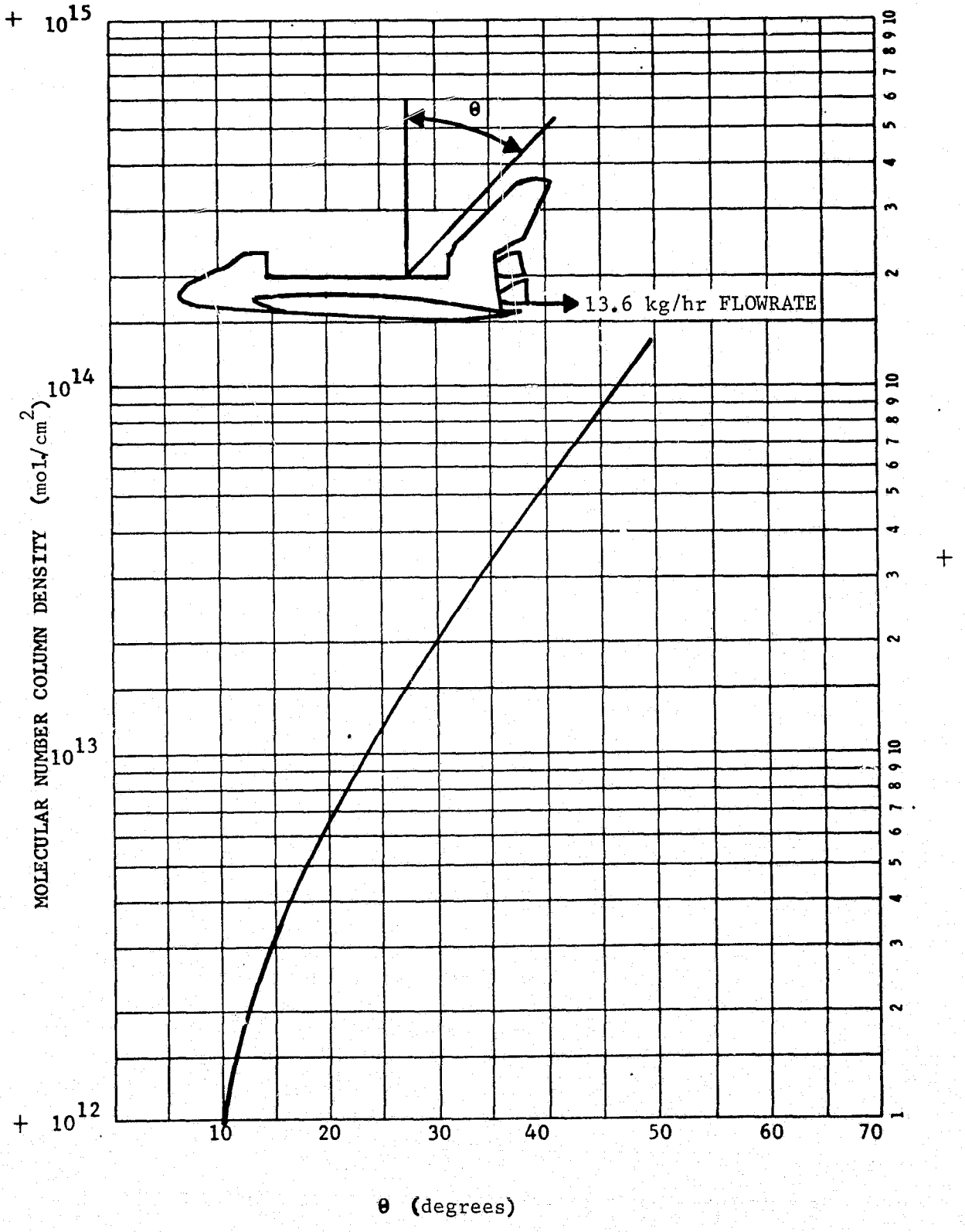

Figure 35. Molecular Number Column Density Versus Angle Off of Z Axis Towards X(Aft) For Lines-of-Sight in the (X,Z) Plane

The effect of canting the evaporator vent at this location was investigated to find an optimum cant angle to minimize the Z force component. Figure 36 shows that the optimum cant angle occurs near a 12 degree rotation towards the minus Z axis. At an angle near 20 degrees, the Z force is comparable to the no cant case (zero degrees). This 20 degree cant would reduce the possibility of ice buildup under the door by allowing the evaporator vent centerline to clear the door. Canting of the evaporator nozzles would produce undesirable Z forces that would require additional VCS engine usage.

b) X = 900 to X = 950 Location - In the region between X = 900 and X = 950, the evaporator vent contribution to LOS 1A molecular number column densities fall below 10^{12} molecules/cm^2 with a boot used for the payload bay door/Shuttle Orbiter fuselage hinge line. At this position, the force on the Shuttle Orbiter wing surface will cancel portions of the force on the door from the evaporator exhaust. For this case, the evaporator vent was positioned at various Z locations and cant angles of $\pm$12 degrees towards $\pm$Z. The resulting force for all combinations is between 0.14 and 0.16 lb in the +Z direction.

c) X = 1392 Location - At this location, the evaporator exhaust impinges on the Shuttle Orbiter wings. For the two evaporator nozzles ($\pm$Y), each with a flowrate of 6.8 kg/hr, the net -Z force has been calculated to be 0.42 lbs. This force is closer to the center of gravity than the X = 594 location and should produce smaller torques.

d) Aft Facing Evaporator Vent - At this location, the evaporator vent (facing +X) has a flowrate of 13.6 kg/hr and produces a +X force of 0.71 lb. This +X force could be on the order of the atmospheric drag force and for certain altitudes

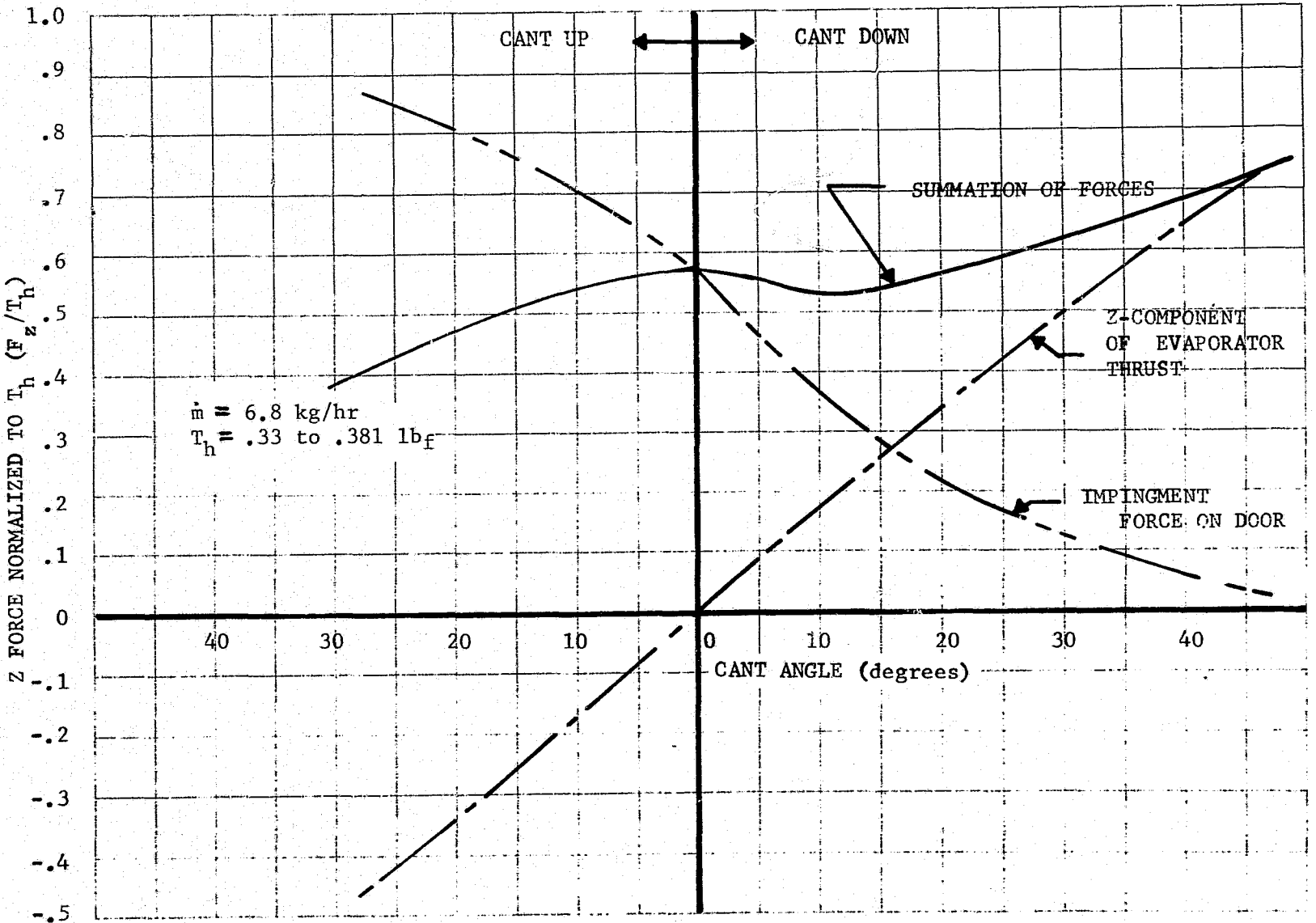

Figure 36. Evaporator Induced Forces

may require considerable VCS control to maintain the necessary altitude.

3.4.2.6 Evaporator Ice Buildup Potential - The flux of evaporator exhaust on adjacent surfaces of the Shuttle Orbiter may allow ice to form. The regions where the potential appears to be greatest from a surface temperature and geometry/distance consideration are under the payload bay door and at X = 1519. At these location, the payload bay door underside, Shuttle Orbiter wings, and elevon trailing edge can receive significant fluxes of evaporator exhaust. In addition, they have the potential of being at the lowest temperatures for specific vehicle attitudes.

The approach in analyzing this situation was to calculate the impingement flux of the evaporator effluents and the subsequent sublimation rate of ice at the lowest surface temperatures anticipated. If the water vapor impingement rate on a surface exceeds the ice sublimation rate at the given surface temperature, a potential ice buildup situation was assumed to exist. The maximum sublimation rate was calculated by the Langmuiur-Knudsen relationship and is expressed as:

$$SR = 5.83 \times 10^{-2} P_v \left(\frac{M}{T}\right)^{1/2}$$

where:

SR = Sublimation rate in g/cm^2/second,

P_v = Vapor pressure in Torr,

M = Gram molecular weight,

T = Surface temperature in degrees Kelvin.

The sublimation rate of a frost deposit is calculated assuming the ratio of the exposed frost area to the area of the surface upon which it is deposited is unity. The following subsections present the impingement rates and ice sublimation rates for several evaporator vent locations.

a) Evaporator Vents at X = 1024 Location - This position was selected because it is representative of the

impingement of the evaporator effluents on the door underside and includes a portion of the wing that will be at low temperatures. The surface temperatures were identified to be -55°C and -69°C for the door and wing, respectively, for a minimum temperature situation.

Table XV summarizes the results of the analysis for a plume centerline flux on the door and off axis for the wing surface. The results show that for the supersonic nozzle operated continuously, the net gain per day would result in 4.3 g/cm^2 of ice or frost buildup on the door. For evaporator vent locations other than X = 1024 under the door, the flux and potential ice buildup on the door would be the same. Table XV shows that the outer edge of the wing should not receive any ice buildup. Also at intermediate distances along the wing, the potential for ice buildup does not appear to exist. Small variations in flowfield and/or changes in temperature of the surfaces can increase or decrease the ice buildup significantly.

A probable evaporator operational mode is to be on for 3 seconds and off for 1 second. Under these conditions, the ice buildup on the door underside would be $1.5 \times 10^{-4} g/cm^2$ during the 3 seconds of operation. During the 1 second off time, $1.4 \times 10^{-4} g/cm^2$ would sublimate leaving $1 \times 10^{-5} g/cm^2$ at the end of a 4 second sequence. Over a 24 hour period under these assumptions, a net 0.22 g/cm^2 of ice or frost would deposit. It is this type of deposit that could randomly produce particulates during subsequent orbital activities.

b) Evaporator Vents at X = 1519 Location - At this location, the evaporator effluents can impinge on the trailing edge of the elevon which is approximately four (10.2 cm) in width. Table XVI presents the fluxes of the evaporator exhaust at points along the elevon trailing edge as measured from the Shuttle Orbiter fuselage. Also included in

Table XV. Evaporator Impingement Flux Predictions and Sublimation Rates at X=1024

Nozzle and Surface Impinged Upon	Impingement Flux ($g/cm^2/sec$)	Sublimation Rate ($g/cm^2/sec$)	Net Deposit ($g/cm^2/sec$)
Supersonic on Door	1.9×10^{-4}	1.4×10^{-4}	5.0×10^{-5}
Supersonic on Wing Edge	1.2×10^{-5}	3.4×10^{-5}	None
Supersonic on Intermediate Wing Surface	6.3×10^{-6}	3.4×10^{-5}	None

Table XVI. Evaporator Impingement Flux Predictions and Sublimation Rates at X=1519

Position Along Elevon Trailing Edge cm (inches)	Impingment Flux (g/cm^2/second)
12.7 (5)	1.0×10^{-5}
38.1 (15)	1.8×10^{-5}
119.4 (47)	1.5×10^{-5}
215.9 (85)	4.4×10^{-6}

Temperature ^{o}C (^{o}F)	Sublimation Rate (g/cm^2/second)
-70 (-94)	3.4×10^{-5}
-80 (-112)	7.4×10^{-6}
-100 (-148)	2.1×10^{-7}
-129 (-200)	1.4×10^{-10}

Table XVI is the sublimation rate of ice at various temperatures. It is shown that at temperatures near $-70^{o}C$ there is no potential for ice buildup along the elevon trailing edge while at temperatures lower than $-70^{o}C$ the potential for ice buildup exists. The actual temperature of this surface is dependent upon vehicle attitude. After establishment of the final location of the evaporator vent and detailed thermal data, the ultimate ice buildup potential of the evaporator system should be reassessed.

3.4.2.7 Supplemental Evaporator System Summary - Ideally, the supplemental evaporator would be of minimal contamination concern if it were located on the underside of the Shuttle Orbiter. However, the evaporator vents are constrained to locations above the Shuttle Orbiter wings and are, therefore, located on the same side of the Shuttle Orbiter as are the payloads and must be considered from a contamination viewpoint.

The previous subsections have dealt with the evaporator influence on lines-of-sight for the evaporator vents located at several positions. The results of these studies are summarized briefly in Table XVII. Included in the table is the location coordinates, LOS 1A contribution, forces generated, advantages, and disadvantages for each of the evaporator positions investigated.

The aft evaporator vent location, employing a single nozzle facing along +X, is the best location from contamination considerations. This location impacts the smallest fraction of lines-of-sight out of all the positions evaluated. If the thrust produced by this location causes an increase in VCS engine usage its status as an acceptable location should be reevaluated.

The next most favorable location is the X = 1519 location. The assumption here is that the evaporator vent can be positioned low enough in the aft corner so that the exhaust reflections from the top of the Shuttle Orbiter wings are eliminated. This may not be possible due to space constraints. Under this assumption, a large fraction of the lines-of-sight has mass column densities less than 10^{12} molecules/cm^2. The forces generated would also be minimized since the only surface impingement of the exhaust

Table XVII. Supersonic Evaporator Nozzle Summary

EVAPORATOR LOCATION	NCD ($mol./cm^2$) LOS 1A	FORCES	ADVANTAGES	DISADVANTAGES
X = 594 to 845 Y = ±104 Z = 353 6.8 kg/hr per vent	$5.5x10^{11}$ to $1.1x10^{12}$	0.49 lbs +Z direction on payload bay door	NCD less than 10^{12} mol./cm^2 without payload bay door hinge line sealed - no wing reflections	Door impingement produces Z forces and ice buildup on payload bay door underside which can produce undesirable ice particles; increased VCS rqmts.
X = 924 to 1124 Y = ±104 Z = 353 6.8 kg/hr per vent	$1.9x10^{12}$ to $1.6x10^{14}$ for door hinge line open $5.2x10^{11}$ to $1.6x10^{14}$ for door hinge line sealed	0.49 lb +Z direction force at X = 594; 0.14 to 0.16 +Z force at locations between X = 900 to X = 950,	From a contamination viewpoint there are no advantages.	NCD in excess of 10^{12} mol./cm^2; door impingement produces +Z forces and ice buildup on payload bay door underside; wing reflections exist for evaporator exhausts.
X = 1392 Y = ±113 Z = 323 6.8 kg/hr per vent	$1.7x10^{14}$	0.42 lbs -Z direction on orbiter wings	From a contamination viewpoint, there are no advantages.	NCD in excess of 10^{12} mol./cm^2 for all lines-of-sight - wing impingement produces -Z forces; increased VCS rqmts and VCS contamination.
X = 1519 Y = ±126 Z = 285 6.8 kg/hr per vent	0	Undetermined small X force on trailing edge of wing	NCD less than 10^{12} mol./cm^2 for significant portion of payload viewing directions; NCD is zero for lines-of-sight within ~5 degrees of (X,Z) plane - no appreciable forces generated.	NCD exceeds 10^{12} mol./cm^2 for lines-of-sight greater than 30 degrees off of Z axis towards ±Y at X = 1107 and for lines-of-sight viewing aft and over the wings for angle ~greater than 25° off Z towards Y; ice buildup on trailing edge; possible space constraints.
X = 1525 Y = 0 Z = 323 13.6 kg/hr	0	0.72 lbs + X(aft) direction	Provides the largest payload viewing area that has zero contribution to NCD for all evaporator locations evaluated; no wing reflections; entire forward and side viewing lines-of-sight have zero NCD.	X force of ~0.72 lbs; for lines-of-sight greater than 10° off of Z axis in (X,Z) plane NCD exceeds 10^{12} mol./cm^2

plume of any consequence would be on the trailing edge of the elevon. This impingement could result in ice buildup and particle generation on the elevon trailing edges near the vent exit.

The next most favorable position from an induced mass or molecular column density viewpoint is the area between X = 594 and X = 950 assuming a covering or boot is employed for the payload bay door/Shuttle Orbiter fuselage hinge line. However, the ice buildup in this region may result in undesirable particle generation during on orbit operations and induced forces may increase VCS propellant usage requirements. Any other location along the X axis between X = 950 and X = 1500 allows significant wing reflections to all lines-of-sight.

Fundamentally, there are very few positions for the evaporator vent which will allow it to meet the current applicable contamination control criteria and not impact other system operations. One basic payload option always exists for those payloads particularly sensitive to the effluents of the evaporator and that is to store the evaporator effluents during their critical periods of operation. It should be noted that this would eliminate the supplemental heat rejection capability that the evaporator supplies, thus impacting the Shuttle Orbiter thermal control system. Until final design and test of the evaporator system and location has been accomplished, the results of this analysis should be used as guidelines, where applicable, in establishing the effect of the evaporator upon the on orbit induced environment.

3.5 Additional Studies - Other studies were conducted in addition to establishing a baseline induced environment and the minimization studies of the Shuttle Orbiter supplemental evaporator and VCS engine systems. These studies consisted of providing recommendations for the MSFC Shuttle Orbiter TPS panel test and a planned JSC evaporator test, the analysis of outgassants from the tail leading edge depositing on a surface in the payload bay, and the Shuttle Orbiter radiator surface degradation analysis.

3.5.1 TPS Panel Test and Preliminary Results - The purpose of the TPS panel test conducted at MSFC was to determine the vacuum weight loss characteristics of the composite nonmetallic materials used in the construction of the Shuttle Orbiter

TPS through vacuum chamber testing of a representative TPS panel configuration. Basic recommendations for the TPS panel test were made. These recommendations included geometry, instrumentation, and desired measurements requirement to establish specific data for the Shuttle Orbiter contamination model. Results from this test are presented in Reference 1.

These results established a bulk outgassing rate of $5 \times 10^{-10} g/cm^2$/second at 100° for the TPS configuration. In addition, some correlation was achieved with the form of the sticking coefficient used in the current model.

For the majority of contaminant sources (e.g., offgassing, cabin atmosphere leakage, and evaporator), the current contamination model allows a unity sticking coefficient for a substance if the surface temperature is below the boiling point of the contaminant. At the same time, the contaminant is allowed to desorb as a function of its vapor pressure. Where vapor pressure data is available, the mass depositing is expressed as:

Net mass depositing = (mass adsorption - mass desorption)

or

$$D = (F(I-J) \cdot S(I-J) \cdot \Delta t) - (5.83 \times 10^{-2} \gamma P_v (M/T)^{1/2} \Delta t)$$

where

D = Deposition in g/cm^2

$F(I-J)$ = Flux on surface I from source J,

$S(I-J)$ = Sticking coefficient (unity or zero),

T = Temperature $^{\circ}K$ of surface I,

Δt = Time interval F(I-J) and T are constant,

γ = Desorption coefficient ($0 \leq \gamma \leq 1$),

P_v = Vapor pressure at temperature of surface I,

M = Molecular weight.

The above relationship yields the net gain of mass per unit area from a contaminant source J and is always equal to or greater than zero. It also accounts for desorption rate changes as the temperature of surface I varies with time.

Outgassing contaminant sources are characteristically a combination of molecular species for which the molecular sizes, relative abundance of each specie, and total quantity outgassed are a strong function of temperature. Vapor pressure data for each deposition outgassant specie is generally unavailable or limited at best. For polymeric contaminant sources, the problem is further complicated by the fact that the deposited material can undergo chemical reactions or can be photopolymerized in the presence of ultraviolet radiation. The result is that the vapor pressure or the desorption energy of the parent source material does not apply to the deposited outgassed species. In general, the deposited material has a larger desorption energy (and therefore greater adhesive qualities) that the parent material.

Because of the unavailability of vapor pressure or desorption energy data for this type of deposit, the current model approach is to determine the sticking coefficient as a function of the temperature difference between the source and the receiving surface. Once the deposit is determined, it is not allowed to desorb. This assumption is based on the fact the sticking coefficient is obtained from materials testing such as the Volatile Condensible Material (VCM) measurements which are long term in nature (References 7, 8, and 9) and the likelihood is high that chemical reaction or photopolymerization will occur at the surface. Both of these phenomena tend to fix the deposit. This approach was used in the Skylab modeling with apparent success.

The present sticking coefficient has the form:

$$S = \frac{TJ-TI}{K} \qquad TI < TJ$$

and

$$S = 0 \qquad TI \leq TJ$$

where

TJ = Source J temperature in ^{o}C or ^{o}K,

TI = Surface I temperature in ^{o}C or ^{o}K,

K = A constant which is a characteristic of the material.

For the majority of nonmetallic contaminant sources, the factor K has been determined to be near 200.

The sticking coefficient as described above has been found to relate the percent VCM to the percent total weight loss from materials testing with the source at 125°C and the receiving surface at 25°C. It was found to correlate with measurements made during the RTV 560 outgassing tests of the TPS panel configuration at MSFC. The TPS panel test (Reference 1) showed that for the test panel at 65.5°C and a QCM at 25°C the deposition rate was measured to be $3 \times 10^{-11} g/cm^2/second$. With the panel at 65.5°C and the QCM at -35°C, the mass deposition reading was $8 \times 10^{-11} g/cm^2/second$. The temperature differences between the panel and the QCM for the 2 cases was 40°C and 100°C, respectively. The ratio of the QCM readings was 2.7 while the ratio of the temperature differences for the two cases (which equates to the ratio of the sticking coefficients) was 2.5. This appears to be good correlation between the sticking coefficient temperature difference approach currently used in the model and the previously mentioned derived test results simulating a major Shuttle Orbiter contaminant outgassing source.

3.5.2 Supplemental Evaporator Vent Test - This test when conducted will provide a definition of the evaporator plume characteristics and the perturbations resulting from localized or adjacent Shuttle Orbiter surfaces. During this contract period; recommendations were made for instrumentation, configuration size and shape simulations, desired data, sensor locations, and modes of test operations for the evaporator test. This test will include simulation of the Shuttle Orbiter door, fuselage and wing surfaces, as well as the temperatures of these surfaces. The test has been postponed until prototype evaporator hardware can be obtained from the contractor involved. The earlier evaporator tests (Reference 6 and the

Applicable Document T-169-28, Volume VI) yielded information pertinent to the present study effort. The planned future evaporator test should yield an improved degree of refinement for the modeling activity necessary for better establishing the molecular and particulate characteristics of the flowfield.

3.5.3 Outgassing of the Tail Leading Edge on Payload Surfaces in the Payload Bay - The Shuttle Orbiter tail leading edge has a direct view into the payload bay. The tail leading edge was separated into 30 subsurfaces for resolution. The shape of the leading edge was constructed as a cylindrical surface cut in half along its main axis. For a 20 cm diameter flat surface in the payload bay located at the skinline, 4.88 meters forward of the payload bay aft end, parallel to the X axis, viewing along +Z; the tail leading edge has a total view factor of 0.0083. This represents the fraction of mass leaving the tail leading edge capable of striking the above mentioned surface. For a mass loss rate of $5 \times 10^{-10} g/cm^2$/second leaving the tail leading edge, the maximum integrated flux on the representative payload surface is $9.6 \times 10^{-13} g/cm^2$/second. After one day at this rate, the accumulative impingement becomes $8.3 \times 10^{-8} g/cm^2$/day and after 7 days it becomes $5.8 \times 10^{-7} g/cm^2$. It is unlikely that this high rate will continue for all of the exposure period. It will be dependent on sunlight exposure time per orbit and vehicle attitude. However, maximum exposure time is possible for specific mission profiles. If the accumulative impingement predicted for 7 days was all able to stick on the payload surface (which assumes cryogenic temperatures), a 58Å deposit would result if unit density is assumed for the deposited material. The only surfaces that may be degraded significantly by this level of deposition would be exposed ultraviolet optics which normally operate at temperatures far above cryogenic and would not normally have the tail in their fields-of-view. Cryogenic systems such as baffles, providing they see the tail, could condense out more material during the initial offgassing periods than that predicted above. This should be reassessed as detailed information becomes available in the future on cryogenic systems to be flown on the Shuttle Orbiter.

The rate assumed here is a steady-state rate for the RTV 560 plus tile configuration of the tail leading edge. If the initial mass loss period during early vacuum exposure has a higher emission rate of condensible species, the contamination

potential could significantly increase. Testing for condensible species during this early vacuum exposure period is currently being planned by JSC. Since this is one of the few surfaces which can view directly into the payload bay, the use of RTV 568 in place of RTV 560 should be considered since RTV 568 reportedly has a lower outgassing rate than RTV 560.

3.5.4 Shuttle Orbiter Radiator Degradation - The Shuttle Orbiter radiator system is located on the inboard sides of the payload bay doors and is currently planned to be covered with silver backed teflon material. Degradation to these surfaces can occur while the doors are open from deposition of outgassing and engine effluents along with subsequent ultraviolet photopolymerization of the deposits. The major sources analyzed for radiator surface degradation include the 25 lb thrust VCS, the 900 lb thrust RCS, the 6000 lb thrust OMS, and outgassing of the OMS pod structure. Of these sources, the $\pm$Y firing VCS and RCS engines and outgassing from the OMS pod can directly impinge upon portions of or all of the +Z facing radiator surfaces. All sources mentioned will contribute to the induced environment which may return to the radiator surfaces through interactions with the ambient atmosphere.

The following subsections address each of these sources individually. Flux and deposition rates and accumulative degradation are presented for the -Y radiator nodal surfaces illustrated in Figure 37. Due to the symmetry of the sources, the analysis applies to the +Y located radiator as well. A summary section follows the source evaluations to recapitulate the accumulative effects of these sources. As part of these studies, geometric refinements were made to the modeled OMS pod structures so that their shadowing of the VCS, RCS, and OMS engine plumes and outgassing contributions to the radiators could be more accurately established.

3.5.4.1 VCS Engine Induced Radiator Degradation - The model configuration data determined that the -Z aft VCS engine does not see any radiator surfaces because of OMS pod structure shadowing. However, the Y aft VCS engine does see the aft outer door radiator (node 785) and the outer edge of the radiator (nodes 771 and 773) as shown in Figure 37. The deposition rates on each of these nodes per second of engine firing time are:

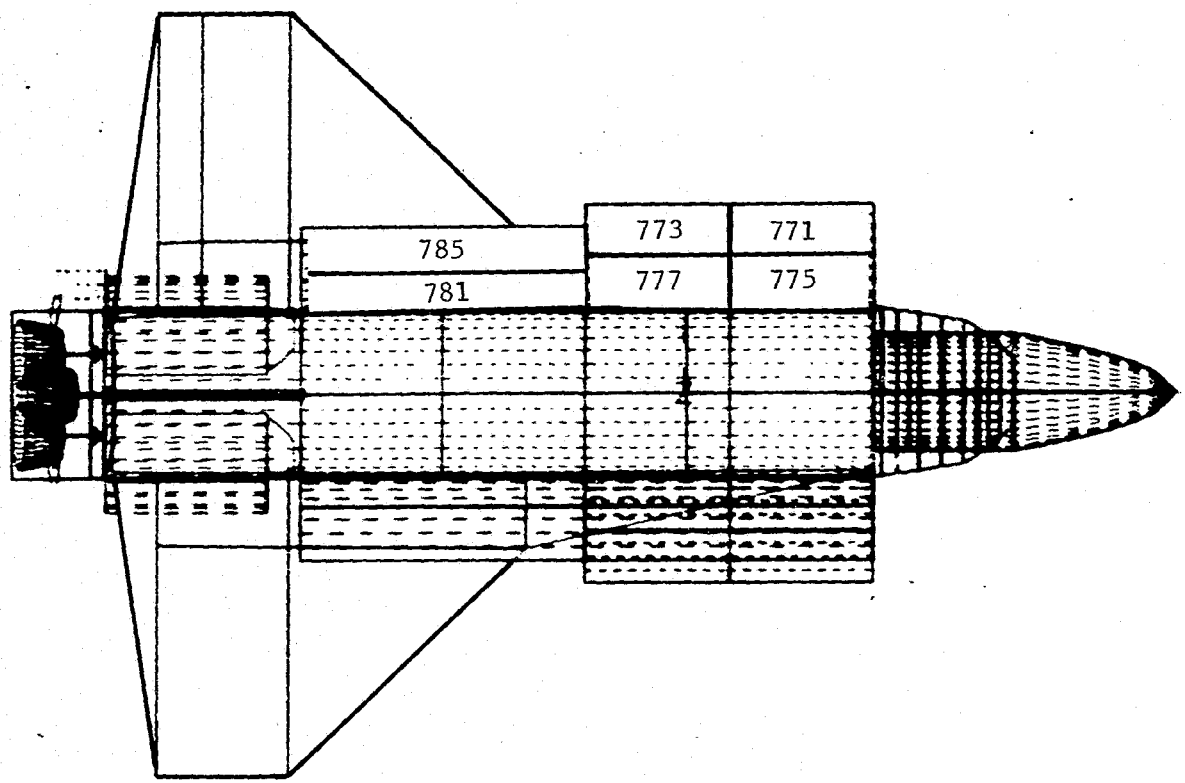

Figure 37. Top View of Radiator and Door Radiator Surface Node Designation

Node Number	Deposition Rate $g/cm^2/second$
771	3.7×10^{-11}
773	6.1×10^{-11}
785	2.1×10^{-10}

The same is true for the mirror image radiator surfaces on the other side of the vehicle.

Figure 38 shows a plot of solar absorptivity (αs) versus bipropellant engine exhausts for S13G paint (original α_s was near 0.15) and the silver backed teflon radiator surface (original α_s was near 0.08). The curve for the S13G was obtained from NASA Lewis Research Center engine testing during the Skylab Program (Reference 10). The silver backed teflon degradation curve was fitted to the S13G data in Reference 10 considering an initial α_s of 0.08. The engine testing at Lewis showed that the α_s reached a maximum level after 12 to 15 $\mu g/cm^2$ of engine exhaust deposits. The physical appearance was a yellow-orange, dry coating on the thermal control paint samples. No evidence of the original painted surface was detectable to the eye. This deposited was also accumulated in the presence of simulated ultraviolet radiation.

The worst case fuel usage attitude for the Y facing aft VCS engines to maintain a 0.3 degree deadband inertial attitude is at 100 nautical miles (185 km). This was obtained from Rockwell International VCS duty cycle calculations (Reference 11). For this case, the fuel usage per orbit of the Y facing VCS engine is 2.58 kg/orbit. The best case is a 400 nautical mile (740 km) local vertical attitude for which the Y facing VCS engine uses 0.132 kg/orbit although this is pointing vector dependent and could even be less for attitudes such as gravity gradient stablized.

Table XVIII presents the anticipated degradation of radiator nodes, 785, 771, and 773 for one orbit, one day, 7 days, and 30 days. Assuming the majority of missions require a VCS fuel usage between the worst and best case presented in Table XVIII, the radiator surfaces could degrade significantly. There are some vehicle attitudes (e.g., gravity gradient) that

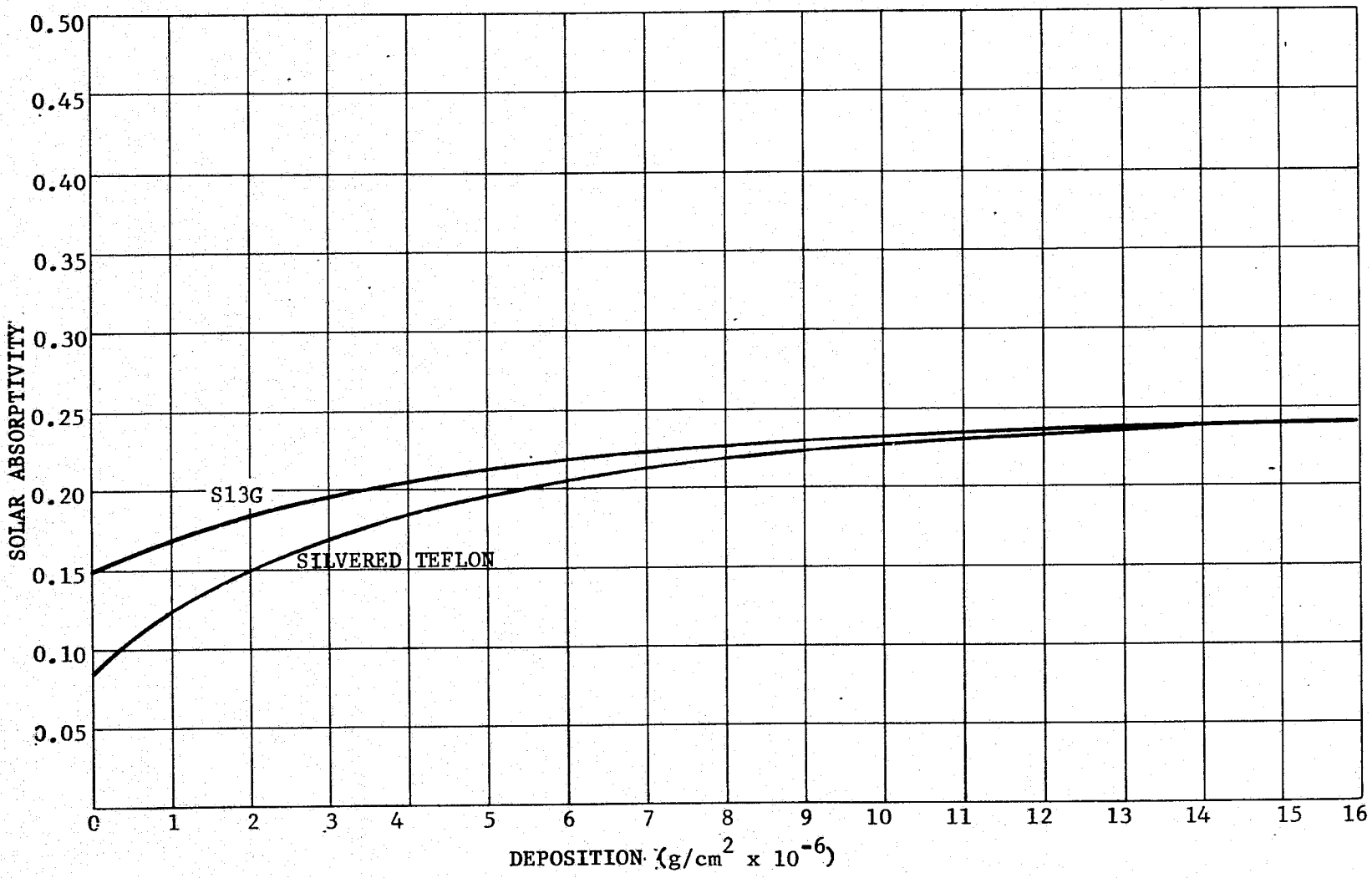

Figure 38. Absorptivity as a Function of Deposition for Bipropellent Engine Exhausts

Table XVIII. Degradation of α_s for the Shuttle Orbiter Radiators Resulting from Worst and Best Case VCS Duty Cycles

Time on Orbit / Node Number	One Orbit α_s	One Day α_s	7 Days α_s	30 Days α_s	Vehicle Attitude Parameters
					WORST CASE
785	0.08	0.085	0.135	0.21	Inertial 0.3° deadband
773	0.08	0.08	0.09	0.145	90° roll, 60° yaw, 0° pitch 16.3 orbits/day
771	0.08	0.08	0.085	0.135	185.2 km altitude Total VCS fuel 13.31 kg/orbit Y engine fuel usage 2.58 kg/orbit
					BEST CASE
785	0.08	0.08	0.08	0.086	Local Vertical 0.3° deadband
773	0.08	0.08	0.08	0.082	90° roll, 30° yaw, 0° pitch
771	0.08	0.08	0.08	0.081	14.45 orbits/day 740.8 km altitude Total VCS fuel 0.87 kg/orbit Y engine fuel usage TBD kg/orbit

will require limited VCS engine usage and should not degrade the radiators. However, in this mode, the return flux from outgassing could be a maximum resulting in comparable degradation due to outgassing if the early missions are 7 to 30 days in length. In either case, these surfaces may require cleaning (if this is possible) or replacement for subsequent missions. Subsequent missions should be less contaminating from an outgassing viewpoint. Additional testing will be required to verify this.

3.5.4.2 RCS Engine Induced Radiator Degradation - Ten aft 900 lb thrust RCS engines (3 facing +Z, 3 facing -Z, and 4 facing -Y) were positioned in the model with a high degree of fidelity. The contamination potential of these engines to the Shuttle Orbiter radiator surfaces was determined with an updated OMS pod structure in position to account for shadowing. The Y facing engines were the only RCS engines that could directly see a radiator surface. This surface was node 785, see Figure 37. The deposition rate on node 785 per second of engine firing was calculated to be 3.3×10^{-9} g/cm^2/second for each of the Y facing RCS engines assuming sticking coefficient data derived from the Lewis Research Center MMH/N_2O_4 engine tests. A typical mission that can be used to demonstrate RCS radiator degradation is Mission 19a which is a 7 day mission for the Atmospheric, Magnetospheric and Plasma in Space (AMPS) payload. For this mission, a total of 417.3 kg of fuel are consumed by the aft RCS engines. Assuming this fuel is equally distributed for the aft RCS, 139.1 kg would be used by all of the Y RCS engines and 69.6 kg for the Y engines on one side of the Shuttle Orbiter. For this fuel usage, the 900 lb RCS Y engines would operate for a possible 47 seconds. The resulting deposition on node 785 would be 2×10^{-7} g/cm^2. This deposition level would increase the α_s of node 785 from 0.08 to approximately 0.084 and should present no problem. However, from mission to mission, consideration will have to be given to potential refurbishment requirements to maintain the baseline thermal performance of the radiators.

In addition to the direct flow of engine exhausts, there will be periods when the return flux of engine exhausts to the radiators will exist. For Mission 19a mentioned above, approximately 8.0×10^{-7} g/cm^2 would deposit on the radiator for the parimary mission Z local vertical attitude. This deposit would increase the α_s of node 785 to a value near 0.12. For the case of return flux, the other radiator surfaces would degrade to a value of α_s between 0.09 and 0.11. The degradation values will significantly depend on the aft RCS fuel usage and the Shuttle Orbiter attitude and altitude.

3.5.4.3 OMS Pod Structure Outgassing Induced Radiator Degradation - Consideration of the view factors between the OMS pod structure and the Shuttle Orbiter radiator surfaces indicate that a significant flux of outgassed material could impinge on the radiator surfaces. Assuming an initial outgassing rate of 5×10^{-10} g/cm^2/second at 100°C for the OMS pod structure, the flux rate on the radiator surfaces (see Figure 37 for node position) are:

Radiator Node Number	OMS Pod Flux Rate g/cm^2/second
785	2.0×10^{-11}
781	1.5×10^{-11}
773	1.1×10^{-12}
777	6.5×10^{-13}
775	2.7×10^{-13}
771	4.5×10^{-13}

The temperature relationships between the OMS pod surfaces and the radiator surfaces varies significantly. This temperature difference throughout an orbit is required to determine the deposition levels anticipated on the radiator surfaces and the associated α_s change. Early vacuum exposure periods may exhibit a higher rate of condensibles. If this is borne out through testing, it is recommended that RTV 568 replace the RTV 560 currently baselined for the TPS bonding since it is reported to have a lower outgassing rate.

Degrading effects to the radiators can be estimated assuming all of the impinging flux is depositied and the outgassing rate stays at 5×10^{-10} g/cm^2/second continuously. After 7 days, the worse case for node 785 would be a deposit of 1.2×10^{-5} g/cm^2 of deposit. This could result in a α_s as high as 0.14 for the outgassed deposits in the presence of solar radiation (based upon thermal surface degradation witnessed on Skylab).

3.5.4.4 OMS Engine Induced Radiator Degradation - The possibility exists that the OMS engines may be used for orbital maneuvers with the radiator surfaces exposed. If this occurs, the return flux of the OMS engine exhausts can impinge upon the radiator surfaces. The degree to which this occurs will depend on OMS engine fuel usage and the Shuttle Orbiter attitude and altitude.

An estimate of the radiator degradation resulting from the OMS engines during orbital maneuvers can be obtained from Mission 19a previously discussed for the RCS engines. For this mission, the OMS engines expend 667.7 kg of fuel for forward thrust maneuvers and 3350 kg of fuel for retro maneuvers. The retro firings are the worst case for OMS engine firings since they allow a larger fraction of material to return to the Shuttle Orbiter from velocity vector considerations. It has been calculated the deposition on the radiator surfaces will be near 1×10^{-5} to 5×10^{-5} g/cm^2/second. This level of deposits will result in a α_s from 0.225 to 0.24.

3.5.4.5 Radiator Degradation Summary - All of the four major sources (VCS, RCS, and OMS engines plus OMS pod structure outgassing) can potentially degrade the Shuttle Orbiter radiator system. The direct flow from the VCS engines, RCS engines, and the OMS pod structure outgassing impact primarily one-fourth of the radiator surface area (node 785 and its counterpart on the opposite of the vehicle). The return flux from the RCS and OMS engines impact the entire surface area of the radiators. The fuel usage requirements for the VCS, RCS, and OMS engines is highly mission dependent. It may be possible to eliminate or minimize OMS and RCS engine impacts on the radiator surfaces by closing the payload bay doors during periods when these engines are required to operate. The remaining radiator degradation resulting from VCS engines and OMS pod structure outgassing would occur over 25% of the total radiator surface area.

One other potential source of contamination that can degrade the radiator surfaces is the return flux of the outgassed material from the Shuttle Orbiter surfaces. The degradation would be dependent on Shuttle Orbiter exterior temperatures, radiator surface temperatures, and Shuttle Orbiter attitude and altitude. Assuming the velocity vector is perpendicular to the radiator surfaces for hot external Shuttle Orbiter surface temperatures, the maximum possible impingement from return flux at 435 km is 1.4×10^{-11} g/cm^2/second. If this attitude was continuously held, the total impingement after one day would be 1.2×10^{-5} g/cm^2, 7 days would be 8.7×10^{-5} g/cm^2, and after 30 days would be 3.7×10^{-4} g/cm^2. The fraction that sticks to the radiators, as mentioned previously, will depend on Shuttle Orbiter external temperatures and radiator surface temperatures. The flux estimate presented for this situation is a worst case value. However, it does show that detailed mission profiles are required to determine the magnitude of the problem. The above

mentioned accumulative fluxes could be reduced by one or possibly 2 orders of magnitude through avoidance of the worst case return flux situation. However, at lower altitudes, the problem could increase about a factor of 20. As detailed mission descriptions become available, this potential problem should be assessed in detail.

3.5.5 Mission Planning to Minimize Contamination - In comparing the predicted induced environment for the identified major Shuttle Orbiter sources against current applicable on orbit contamination control criteria, it has been shown that from a preliminary analysis and design consideration certain aspects of these sources will not meet the given criteria. That is not to say that the induced optical environment from these sources cannot be effectively dealt with from a contamination control viewpoint. It does indicate that in some cases just design control influences, such as location and directional considerations, will not be adequate to meet the contamination control criteria. As a result, certain on orbit operational controls will also be required to minimize the contaminant potential of these sources in their present configuration. This is particularly true for both the flash evaporator (when at X = 1392) and the 25 lb thrust VCS engines. These on orbit operational controls will depend strongly upon the nature of the particular payload being flown. Consequently, it is envisioned that as the Shuttle Program develops, on orbit operational controls will be required to be identified in conjunction with the payloads to provide the necessary contamination controls.

In order to meet the intent of the contamination control criteria, the influences of contamination upon sensitive surfaces and instruments must be integrated into all phases of Shuttle Orbiter mission planning. Through proper mission planning with contamination control in mind, many of the predicted levels of contamination and degradation presented in this report may be minimized. Depending upon the sensitivities and susceptibilities of payloads to be flown for a given mission, some or all of the following control measures might be required to be instituted to meet the intent of the contamination control requirements.

a) delay exposure and operation of sensitive instruments until initial high offgassing period has subsided (up to 24 hours after launch;

b) select the highest feasible orbital altitudes to reduce the severity of return flux;

c) select vehicle attitudes such as gravity gradient stabilized which minimize VCS usage requirements;

d) incorporate gimballing capability into the payload designs (such as the IPS) to relax Shuttle Orbiter pointing requirements and VCS usage;

e) inhibit the supplemental evaporator system during operation or exposure of sensitive instruments;

f) fly sensitive instruments on Shuttle Orbiter vehicles that have been flown previously thus depleting a portion of the available outgassing source material;

g) close payload bay doors during OMS engine firings; and

h) employ sensitive surface covers, heater, and/or restrict geometric acceptance angles for the payloads to preclude contaminant deposition.

4. CONCLUSIONS AND RECOMMENDATIONS

4.1 Conclusions - The following are the conclusions that can be drawn from those areas that were either identified or investigated during the course of this study that presented a significant contaminant potential to the Shuttle Orbiter/payload induced environment and/or to the Shuttle Orbiter itself.

a) Supplemental Evaporator Vent Optimum Location - From contamination considerations, the optimum evaporator vent positions evaluated in order of least impact are aft facing +X, X = 1519 facing ±Y, and various X positions between 600 and 950 facing ±Y. All other locations contributed in excess of 10^{12} molecules/cm^2 to all lines-of-sight considered.

b) VCS Engine Location and Orientation - For all locations and orientations (canting angles) evaluated during this study, the VCS engines exceed the 10^{12} molecules/cm^2 criteria. The return flux exceeds the 10^{12} molecules/cm^2/second criteria.

c) Outgassing Molecular Number Column Densities and Return Flux - The molecular number column densities for all lines-of-sight considered are less than the maximum criteria of 10^{12} molecules/cm^2. The return flux values for this source are highly dependent upon the viewing angle, orbital altitude, and ambient atmosphere density variations at a specific altitude. Over the range of these three parameters, the outgassing return flux either falls below or exceeds the return flux criteria of 10^{12} molecules/cm^2/second.

d) Offgassing Molecular Number Column Densities and Return Flux - At a 10 hour on orbit point, the molecular number column densities exceed the criteria of 10^{12} molecules/cm^2 for all lines-of-sight. After 24 hours on orbit, the molecular column densities are less than the maximum criteria of 10^{12} molecules/cm^2 for all lines-of-sight. The return flux for this source is dependent upon the viewing angle, altitude, and ambient atmosphere density variations at a specific altitude. Over the range of these three parameters, the offgassing return flux either falls below or exceeds the return flux criteria of 10^{12} molecules/cm^2/second.

e) Cabin Atmosphere Leakage Molecular Number Column Densities and Return Flux - The molecular column densities of the CO_2 and H_2O components of the leakage sources (polar molecules) are less than the maximum criteria of 10^{12} molecules/cm^2 for all lines-of-sight considered. The return flux of the H_2O and CO_2 components of the leakage source are less than the return flux criteria of 10^{12} molecules/cm^2/second for the altitudes considered and a physical acceptance angle of 0.19 steradians. For viewing angles of 0.29 steradians, the return flux criteria would only be exceeded at the 200 km altitude situation. The return flux of the total leakage source exceeds 10^{12} molecules/cm^2/second.

f) Radiator Degradation - The Shuttle Orbiter radiator surfaces can be degraded from direct line-of-sight impingement of VCS and RCS engines and the OMS pod structure surface outgassants. Additionally, the radiator surfaces can degrade from the return flux of Shuttle Orbiter outgassing, RCS engine plumes, and OMS engine plumes. The extent of degradation is a strong function of VCS, RCS, and OMS engine usage, the relative temperatures of Shuttle Orbiter and radiator surfaces, and the vehicle attitude and altitude.

g) Evaporator Ice Buildup Potential - For those evaporator locations evaluated where they may impinge on cold adjacent Shuttle Orbiter surfaces, the potential for ice buildup exists. This occurs when the flux rate of evaporator water vapor exceeds the sublimation rate of ice at the temperature of the surface impinged upon. The on-off cycle of the evaporator could reduce some of the long term ice buildup at specific locations.

h) Supplemental Evaporator Vent Forces - At locations between X = 600 and X = 950, the evaporator vent produces net +Z forces. At X = 1519, the evaporator vent produces small -X forces. At the aft location (facing +X), the evaporator vent produces -X forces. For locations between X = 950 and X = 1392, the evaporator vent produces small net Z forces but is unacceptable from a contamination viewpoint because of the mass column density contribution. The forces generated may require additional VCS usage to maintain attitude control which will tend to increase overall the contaminants.

i) Tail Outgassing Into Payload Bay - The leading edge of the tail is essentially the only major surface structure that views directly into the payload bay. Depending on the early vacuum exposure outgassing rate, the leading edge of the tail could degrade sensitive payload surfaces.

j) Mission Planning - The assessment presented in this report has identified basic contamination parameters of concern for the modeled major Shuttle Orbiter contamination sources. As a result, it has been indicated that through basic design consideration complete contamination control cannot meet the applicable criteria. To achieve necessary contamination control will require operational considerations for both the Shuttle Orbiter and many of its proposed payloads, such as proper vehicle attitude selection (gravity gradient stabilized), inhibiting the evaporator vents, use of the IPS or gimballed systems to relax pointing requirements, delaying instrument operation until initial offgassing has subsided, and flying most sensitive payloads on Shuttle Orbiters that have been flown enough missions to have depleted the outgassing sources.

4.2 Recommendations - As a result of this study, the following recommendations are presented to identify those program considerations felt important for implementing or establishing the necessary contamination control for the major Shuttle Orbiter sources evaluated and identified as a contaminant potential.

a) Materials Testing - Limited nonmetallic surfaces outgassing and deposition characteristics that are essential to accurate contamination modeling and assessment are available. It is recommended that the following data be obtained during the Shuttle Orbiter Program for major nonmetallic materials that can produce significant contamination by virtue of total area of coverage, location, and temperature.

1) All data should be supplied in form of outgassing mass loss per unit area per unit time, $g/cm^2/second$.

2) The initial offgassing (e.g., light gases, H_2O, and volatiles) decay curve is required as a function of time over the temperature ranges anticipated. The anticipated precure or specific surface applications should be approximated.

3) Once the initial offgassing period has ended, the steady state outgassing rate is required over the temperature ranges anticipated. Additionally, the long term decay of the bulk outgassing rate at several temperatures is required.

4) The initial sticking coefficient as a function of the temperature of the source and the temperature of the collector is required over the range of temperatures anticipated.

5) At the end of each test, the collector should be incrementally heated to a temperature at least as high as the source to ascertain the permanency and activation energy of the deposit.

6) Residual gas analysis is required for all the above mass loss tests.

7) Ambient atmosphere readsorption quantities and subsequent behavior in vacuum as related to above testing is required.

8) Besides the testing of a material itself, there will be situations where geometry influences should be evaluated. A simulation of a representative geometry should be tested (e.g., recent TPS testing at MSFC for mass loss rate temperature and time dependence).

9) The optical properties of specific deposited components should be measured.

10) Additional data is also desirable so that effects of the deposit and the source behavior can be ascertained. This would include environmental protons, electrons, and ultraviolet radiation and their effects on the source outgassing rate and VCM deposit characteristics.

b) Cleaning and/or Refurbishment Requirements - For critical optical surfaces of the Shuttle Orbiter and payloads it is recommended that cleaning or refurbishment requirements be identified for major contaminant source deposits.

c) OMS Engine Firings - Because of the contamination threat to the Shuttle Orbiter radiator surfaces and to the payloads, it is recommended that the Shuttle Orbiter payload bay doors be closed during OMS engine firings.

d) RCS Engine Firings - Because of the contamination threat to the exposed radiator surfaces and payloads, it is recommended the Shuttle Orbiter payload bay doors be closed during extensive use of the $\pm$Y facing and +Z facing RCS aft engines.

e) Bondline Seals - For the edges of the TPS surfaces, consideration should be given to sealing these areas so that gross quantities of outgassants cannot be emitted from these areas as observed in TPS panel testing at MSFC. This is especially true for terminal edges near windows, radiator surfaces, and payload bay door edges.

f) Testing of Deposits on Radiator Surfaces - Because of the potential of engine deposits (MMH/HNO_3) and outgassing deposits from RTV 560 on the radiator surfaces, these deposits should be evaluated for α_s changes of the Shuttle Orbiter radiator surfaces through testing prior to Shuttle Orbiter flights. Simulated solar flux is required during testing to ascertain the degradation potential.

g) Evaporator Effluents - For payloads that are sensitive to the evaporator effluents, consideration should be given to the storing of water produced by the fuel cell during critical data take periods, if an acceptable evaporator nozzle location is not utilized in the design of the Shuttle Orbiter.

h) VCS Engine Effluents - For payloads sensitive to VCS engine effluents, consideration should be given for mission planning and selection of vehicle attitudes which minimize VCS requirements such as gravity gradients stabilized. The use of such attitudes in conjunction with the IPS or other gimballed system would allow for long observation periods between VCS firings (possibly as long as one orbit). Another alternative is the use of Control Moment Gyros (CMGs) for maintaining attitude control.

i) RTV 560 Replacement - For critical TPS surfaces, consideration should be given to replacing the RTV 560 bonding material with RTV 568 which has a lower bulk or characteristic outgassing rate.

j) Covering Over Shuttle Orbiter Door/Fuselage Hinge Line - If the evaporator or any other overboard vent is placed under the payload bay doors, consideration should be given to placing a boot or flexible covering over the hinge line between the Shuttle Orbiter doors and the fuselage. This would eliminate molecular and particulate material from escaping into payload viewing regions during vent operation.

k) Shuttle Orbiter External Temperature Profiles - TPS bondline and outer surface temperatures should be determined for specific points within an orbit for the majority of vehicle attitudes envisioned. These should be correlated with temperatures of payload surfaces at the same point within an orbit. With this determined, a more meaningful contamination assessment can be made. Also the temperatures of the Shuttle Orbiter radiator surfaces should be determined for specific missions.

l) Separation Rocket Booster Motors (SRBM) - The effects of SRBM separation rocket plume interactions with the Shuttle Orbiter should be determined.

m) Mission Profiles - Detailed mission profiles including parameters required for complete contamination assessment should be identified. These parameters include, Shuttle Orbiter external temperatures, attitudes, altitudes, duty cycles of each VCS, RCS, and OMS engine, evaporator flowrate requirements, and payload viewing directions and surface temperatures relative to the Shuttle Orbiter.

n) New Evaporator Systems - The development of the final evaporator design should include a review of the potential contamination problems of the evaporator. Testing of the final evaporator design is necessary to obtain plume flowfield and particulate generating characteristics. This type of testing is currently planned for the final evaporator design.

o) VCS Particulate Emissions - The VCS engine particulate or droplet generating characteristics should be determined. The size distribution, velocities, and emission direction are important in evaluating payload susceptibilities. The point at which the droplets become frozen is also important for considerations of reflection off of Shuttle Orbiter surfaces into payload lines-of-sight. The molecular effluents from these engines exceed the applicable criteria which will dictate certain control measures to be instituted to minimize field-of-view interference. These will inherently limit the impacts of generated particles from the VCS, as well.

p) Payload Impact on the Shuttle Orbiter - Spacelab and other payloads should be assessed for their contamination contribution to Shuttle Orbiter surfaces. The areas of immediate concern would be the deposition on Shuttle Orbiter radiator surfaces and the payload bay liner and view ports. This would include the periods with the payload bay doors closed and open.

5. NOTES

5.1 References - The following references are presented to support the technical and programmatic material referenced in the text of this report.

1. Naumman, R. J.: "Shuttle TPS Panel Tests Preliminary Results" Working Paper, Space Sciences Laboratory, MSFC, January 16, 1975.

2. Simons, G. A.: "Effect of Nozzle Boundary Layers on Rocket Exhaust Plumes," AIAA Journal, Vol. 10, No. 11, November 1972.

3. Chirivella, J. E. and Simon, E.: "Molecular Flux Measurements in the Back Flow Region of a Nozzle Plume," JANNAF 7th Plume Technology Meeting, April 1973.

4. Ratliff, A. W., Auden, B. J., and Thornbill, D. D.: "Analysis of Exhaust Plumes from Skylab -- Configuration R-4D Attitude Control Motors," LMSC/HREC D162171, March 1971.

5. Ratliff, A. W. and Stephens, J. T.: "A Detailed Plume Flowfield Definition of the R1E Motor for the Saturn S-IVB Auxiliary Propulsion System," LMSC/HREC D148776 - Rev. A, August 1969.

6. Naumann, R. J.: "Column Densities Resulting from Shuttle Sublimator/Evaporator Operation," NASA-TM-X-64794, October 1973.

7. Miraca, R. F. and Wittick, J. S.: "Polymers for Spacecraft Applications," N67 40270, Stanford Research Institute, September 15, 1967.

8. Campbell, W. A., et al: "A Compilation of Outgassing Data for Spacecraft Materials," NASA TND 7362.

9. Pachinaa, H. C.: "Vacuum Weight-Loss and Contamination Tests of Some Materials for Space Application," Proc. of the Fourth INTERNL. Vacuum Congress 1968.

10. Bowman, R. L., et al: "Effect of Contamination on the Optical Properties of Transmitting and Reflecting Materials Exposed to a MMH/N_2O_4 Rocket Exhaust," NASA Lewis Research Center.

11. Internal Letter from R. Budica to D. J. Simkin, "RCS Vernier Thruster Duty Cycles for Various Attitude Hold Requirements," No. 393-120-74-096, Rockwell International, November 1974.

5.2 Abbreviations - The following abbreviations were used in this report and represent terminology relevant to this study and programs used to obtain supportive data for this study.

APU	-	Auxiliary Power Unit
ATM	-	Apollo Telescope Mount
CDC	-	Control Data Corporation
CMG	-	Control Moment Gyro
CRT	-	Cathode Ray Tube
ECLSS	-	Environmental Control Life Support System
ET	-	External Tank
EVA	-	Extravehicular Activity
H_2O	-	Water
He	-	Helium
HRSI	-	High Temperature Reusable Surface Insulation
IR	-	Infrared
JSC	-	Johnson Space Center
LOS	-	Line-of-Sight
LRSI	-	Low Temperature Reusable Surface Insulation
M	-	Molecular Weight
MCD	-	Mass Column Density
MFP	-	Mean Free Path
MMH	-	Monomethyl Hydrazine
MOC	-	Method of Characteristics
MSFC	-	Marshall Space Flight Center
N_2O_4	-	Nitrogen Tetroxide
N_2	-	Nitrogen
NCD	-	Molecular Number Column Density
O_2	-	Oxygen
OFR	-	Offgassing Rate
OGR	-	Outgassing Rate
OMS	-	Orbital Maneuvering System
QCM	-	Quartz Crystal Microbalance
RCC	-	Reinforced Carbon-carbon
RCS	-	Reaction Control System
RGA	-	Residual Gas Analysis
RSI	-	Reusable Surface Insulation
RTV	-	Room Temperature Vulcanized
S	-	Sticking Coefficient
SRBM	-	Solid Rocket Booster Motor

TPS	-	Thermal Protection Subsystem
UV	-	Ultraviolet
VCS	-	Vernier Control Subsystem
VCM	-	Volatile Condensible Material
α_s	-	Solar Absorptivity
^oC	-	Degrees Centigrade
cm	-	Centimeters
e	-	2.718
eV	-	Electron Volt
^{o}	-	Degrees
^oF	-	Degrees Fahrenheit
ft	-	Feet
g	-	Gram
in	-	Inch
^oK	-	Degrees Kelvin
Km	-	Kilometer
lb	-	Pound
m	-	Mass
θ	-	Angle in degrees
μ g	-	Microgram
psi	-	Pounds per square inch

5.3 Definitions - The following definitions are presented to clarify terminology used in this report which reflect unique characterization of the principles, procedures, and methods of application that would be generally applicable to utilization of the results of this study.

a. Mass Column Density - The mass contained in a constant unit cross-sectional area extending from an origin to infinity, expressed in units of Mass/Unit Area.

b. Number Column Density - The number of molecules contained in a constant unit cross-sectional area extending from an origin to infinity, expressed in units of Molecules/Unit Area.

c. Flux - Mass flow through a unit area, expressed in units of Mass/Unit Area/Unit Time.

d. Line-of-Sight - The line being sighted from a critical surface and extending along a given direction of interest to infinity. Column densities are calculated along lines-of-sight.

e. View Factor - That fraction of the total mass leaving one surface that is capable of impinging upon another surface of interest in its field-of-view.

f. Interaction Sphere - Geometrically developed spheres along a given line-of-sight which establishes surface-to-surface relationships in its field-of-view such as distance, angular, and view factor.

g. Return Flux - The mass flow of contaminants through a unit area reflected back to a surface of interest as a result of collisions with the ambient atmosphere expressed in Mass/Unit Area/Unit Time.

h. Outgassing - That contribution to contamination which comes from the material bulk characteristics and is long term in nature.

i. Offgassing - That contribution to contamination which is related to the volatiles which are either adsorbed to the material and/or carried in the preparation of a material and boil off very rapidly when exposed to vacuum.

j. Beta Angle - That angle between the orbit plane and the earth-sun line.

APPENDIX A

Configuration Descriptions and Geometric Relationships Used in the Contamination Impact Analysis for the Shuttle Orbiter.

CONTENTS

1. SCOPE

1.1 Purpose - The purpose of this Appendix is to present a computer printout of the configuration descriptions and geometric relationships used in the contamination analyses described in the text. The information presented is representative of the development of the contamination modeling effort to date. It can be extremely useful in understanding the geometrical relationships used in the model predictions established under this study.

1.2 Scope - This Appendix presents the computer printout data generated during the Payload/Orbiter Contamination Control Assessment Support, NAS9-14212. Contained herein are the computer listings of the input surface data matrices, the view factor data matricies, and the geometric relationship data matrices for the Shuttle Orbiter configuration analyzed in this study. This configuration has been broken up into the geometrical surfaces and nodes necessary to define the principle critical surfaces. A number scheme was established based upon nodal numbers that relates the various Shuttle Orbiter surfaces to a specific surface material or function. The nodal numbers and numbering scheme are presented in tabular form along with an accompanying figure to illustrate the location of the major nodal surfaces.

2. COMPUTER PRINTOUT DESCRIPTIONS

2.1 Discussion - The computer modeling of the induced contaminant environment of the Shuttle Orbiter involved the geometric synthesis of all major surfaces. These surfaces were synthesized on a CDC 6500 digital computer using the Scope 3.4.1 Operating System by utilizing a mass transport analog to thermal radiation as reported in "Thermal Radiation Analysis System" (TRASYS), NAS9 14318, MCR 73-105, Revision 1, May 1975, Lyndon B. Johnson Space Center. For this study effort, input surfaces included the baseline Shuttle Orbiter configuration updated to known current design modifications. Vent and engine sources were modeled as geometric discs representative of a surface at the engine vent exit plane emitting with the characteristic plume distribution of the particular source.

The Shuttle Orbiter surfaces were assigned nodal numbers between 1 and 999. The Shuttle Orbiter was described geometrically by 60 basic surface shapes. These surfaces were further subdivided

Table A-I. Summary Table for the Shuttle Orbiter Geometry Breakdown

GENERAL AREA	NAME	TYPE	SURFACE NUMBER	NUMBER OF NODES	NODE NUMBERS
COCKPIT	Extreme Nose Cone	Paraboloid	122	4	122,123 124,125
	Nose Cylinder	Cylinder	320	16	320,321,322,323,324,325, 326,327,328,329,330,331, 332,333,334,335
	Hood (Partial back)	Paraboloid (Partial)	340	16	340,341,342,343,344,345, 346,347,348,349,350,351, 352,353,354,355
	Window	Paraboloid (Partial)	360	16	360,361,362,363,364,365, 366,367,368,369,370,371, 372,373,374,375
	TOTAL SURFACES = 4	TOTAL NODES = 52			
BAY	Front Bay Area Disc (Sealer)	Disc	135	1	135
	Bay Area Cylinder (Liner)	Cylinder	150	8	150,151,152,153,154,155, 156,157
	End Bay Area Disc (Sealer)	Disc	140	1	140
	+Y Side Door	Cylinder	781	8	781,782,783,784,785,786, 787,788
	-Y Side Door	Cylinder	791	8	791,792,793,794,795,796, 797,798
	+Y Radiator	Cylinder	771	8	771,772,773,774,775,776, 777,778
	-Y Radiator	Cylinder	761	8	761,762,763,764,765,766, 767,768

Table A-I. Summary Table for the Shuttle Orbiter Geometry Breakdown - continued

GENERAL AREA	NAME	TYPE	SURFACE NUMBER	NUMBER OF NODES	NODE NUMBERS
BAY	+Y Side Front Trapezoid	Trapezoid	301	1	301
	Body Side (Middle Part)	Rectangle	305	1	305
	-Y Side Front Trapezoid	Trapezoid	311	1	311
	Body Side (Middle Starboard)	Rectangle	315	1	315
	Body Bottom (Front)	Rectangle	401	1	401
	Body Bottom (Rear)	Rectangle	402	1	402
	TOTAL SURFACES = 13		TOTAL NODES = 48		
WINGS	Wing Triangle, Front, +Y	Polygon	1	1	1
	Wing Triangle, Middle Front, +Y	Polygon	2	1	2
	Wing Rectangle, Middle Front, +Y	Rectangle	143	1	143
	Wing Rectangle, Middle Back, +Y	Rectangle	3	1	3
	Wing Rectangle, Middle Back, +Y	Rectangle	144	1	144

Table A-I. Summary Table for the Shuttle Orbiter Geometry Breakdown - continued

GENERAL AREA	NAME	TYPE	SURFACE NUMBER	NUMBER OF NODES	NODE NUMBERS
WINGS	Extended Aileron Top	Rectangle	900	1	900
	Extended Aileron Inner	Rectangle	901	1	901
	Wing Triangle, Rear, +Y	Polygon	4	1	4
	Wing Triangle, Front, -Y	Polygon	10	1	10
	Wing Triangle, Middle Front, -Y	Polygon	11	1	11
	Wing Rectangle, Middle Front, -Y	Rectangle	141	1	141
	Wing Rectangle, Middle Back, -Y	Rectangle	12	1	12
	Wing Rectangle, Middle Back, -Y	Rectangle	142	1	142
	Wing Triangle, Rear, -Y	Polygon	13	1	13
	TOTAL SURFACES = 14		TOTAL NODES = 14		

Table A-I. Summary Table for the Shuttle Orbiter Geometry Breakdown - continued

GENERAL AREA	NAME	TYPE	SURFACE NUMBER	NUMBER OF NODES	NODE NUMBERS
REAR	Body Top (Rear-Starboard)	Cylinder	202	1	202
	Body Top (Rear-Port)	Cylinder	212	1	212
	Body Side (Back Port)	Rectangle	306	1	306
	Body Side (Back Starboard)	Rectangle	316	1	316
	OMS Pod C1 -Y	Cylinder	184	1	184
	OMS Pod C2 +Y	Cylinder	174	1	174
	OMS Parab -Y	Paraboloid	182	1	182
	OMS Parab +Y	Paraboloid	172	1	172
	OMS Rear Sealer	Discs & Trap	29,31,32,33, 34,35,36	7	29,31,32,33,34,35,36
	-Y OMS Front Sealer	Disc	20	1	20
	+Y OMS Front Sealer	Disc	21	1	21
	Back Rectangle 7.35 Deg	Rectangle	222	1	222
	Rear End Half Disc	Disc	22	2	22,23
	+Y Rear Side Taper	Trapezoid	145	1	145

Table A-I. Summary Table for the Shuttle Orbiter Geometry Breakdown - continued

GENERAL AREA	NAME	TYPE	SURFACE NUMBER	NUMBER OF NODES	NODE NUMBERS
REAR	Rear Bottom Edge	Rectangle	146	1	146
	Sloping Rear Flat Plate	Rectangle	147	1	147
	-Y Rear Side Taper	Trapezoid	149	1	149
	Vertical Pin Port	Trapezoid	380	1	380
	Vertical Pin (Aft-Port)	Trapezoid	385	1	385
	Vertical Pin (Starboard)	Trapezoid	390	1	390
	Vertical Pin (Aft-Starboard)	Trapezoid	395	1	395
	Vertical Pin Leading Edge	Rectangle	399	1	399
	TOTAL SURFACES = 28		TOTAL NODES = 29		
ENGINES + EVAPORATORS	OMS Engines	Disc	700	2	700,701
	OMS Engines	Disc	702	2	702,703
	Top Engine (SSME)	Paraboloid	800	4	800,801,802,803
	+Y Engine (SSME)	Paraboloid	805	4	805,806,807,808
	-Y Engine (SSME)	Paraboloid	810	4	810,811,812,813

Table A-I. Summary Table for the Shuttle Orbiter Geometry Breakdown - continued

GENERAL AREA	NAME	TYPE	SURFACE NUMBER	NUMBER OF NODES	NODE NUMBERS
ENGINES + EVAPORATORS	Back VCS +Y-Y	Disc	24	2	24,25
	Back VCS +Y-Z	Disc	26	2	26,27
	Front VCS +Y-Y	Disc	18	2	18,19
	900 lb RCS -Z 1st	Disc	710	2	710,711
	-Z 2nd	Disc	712	2	712,713
	-Z 3rd	Disc	714	2	714,715
	900 lb RCS +Y 1st	Disc	720	2	720,721
	+Y 2nd	Disc	722	2	722,723
	+Y 3rd	Disc	724	2	724,725
	+Y 4th	Disc	726	2	726,727
	900 lb RCS +Z 1st	Disc	730	2	730,731
	+Z 2nd	Disc	732	2	732,733
	+Z 3rd	Disc	734	2	734,735
	Forward Evap.	Disc	705	1	705
	Middle Evap 1	Disc	16	2	16,17
	Middle Evap 2	Disc	707	2	707,708
	Aft Evap	Disc	407	1	407

Table A-I. Summary Table for the Shuttle Orbiter Geometry Breakdown - concluded

GENERAL AREA	NAME	TYPE	SURFACE NUMBER	NUMBER OF NODES	NODE NUMBERS
ENGINES + EVAPORATORS	Aft Evap (−X)	Disc	15	1	15
	Rear Center Evaporator	Disc	740	2	741,742
	TOTAL SURFACES = 24		TOTAL NODES = 51		
	ENGINES (18)		ENGINES (42)		
	EVAPORATORS (6)		EVAPORATORS (9)		

into a total of 194 nodes. Table A-I presents a summary of these surfaces by indicating general area, name of surface, type of geometric surface used, surface number, number of nodes, and node numbers.

Figure A-1 illustrates the primary Shuttle Orbiter nodal surface number locations. Only the primary nodal surface number locations have been identified. As indicated in Table A-I, a large number of different surfaces have been used to obtain the necessary fidelity to accurately define a particular Shuttle Orbiter surface shape. Some of these surfaces are of limited use in an assessment and have not been included in Figure A-1 Those surfaces depicted to represent the majority of surfaces necessary to understand the basic content of the computer printouts and the contamination analysis and evaluation conducted during this activity.

The computer printout of the configuration view factor model consists of three data matrices which will be described in the following subsections. These data matricies are:

a) the Input Data Matrix;

b) the View Factor Data Matrix; and

c) the Geometric Relationship Data Matrix.

2.2 Input Data Matrix Description - This matrix consists of all the necessary input data required to completely describe the geometrical surfaces and configurations analyzed. Figure A-2 is an example of the format of the input data matrix for selected Shuttle Orbiter surfaces. Following is an outline description of the major items contained in this matrix (see Figure A-2):

a) nodal surface number;

b) geometric surface type - rectangle, disc, cylinder, etc.;

c) sides of surface activated - ability to emit or receive contamination;

d) surface shadowing effects;

e) surface ability to be shadowed;

f) surface rotation about major axis system;

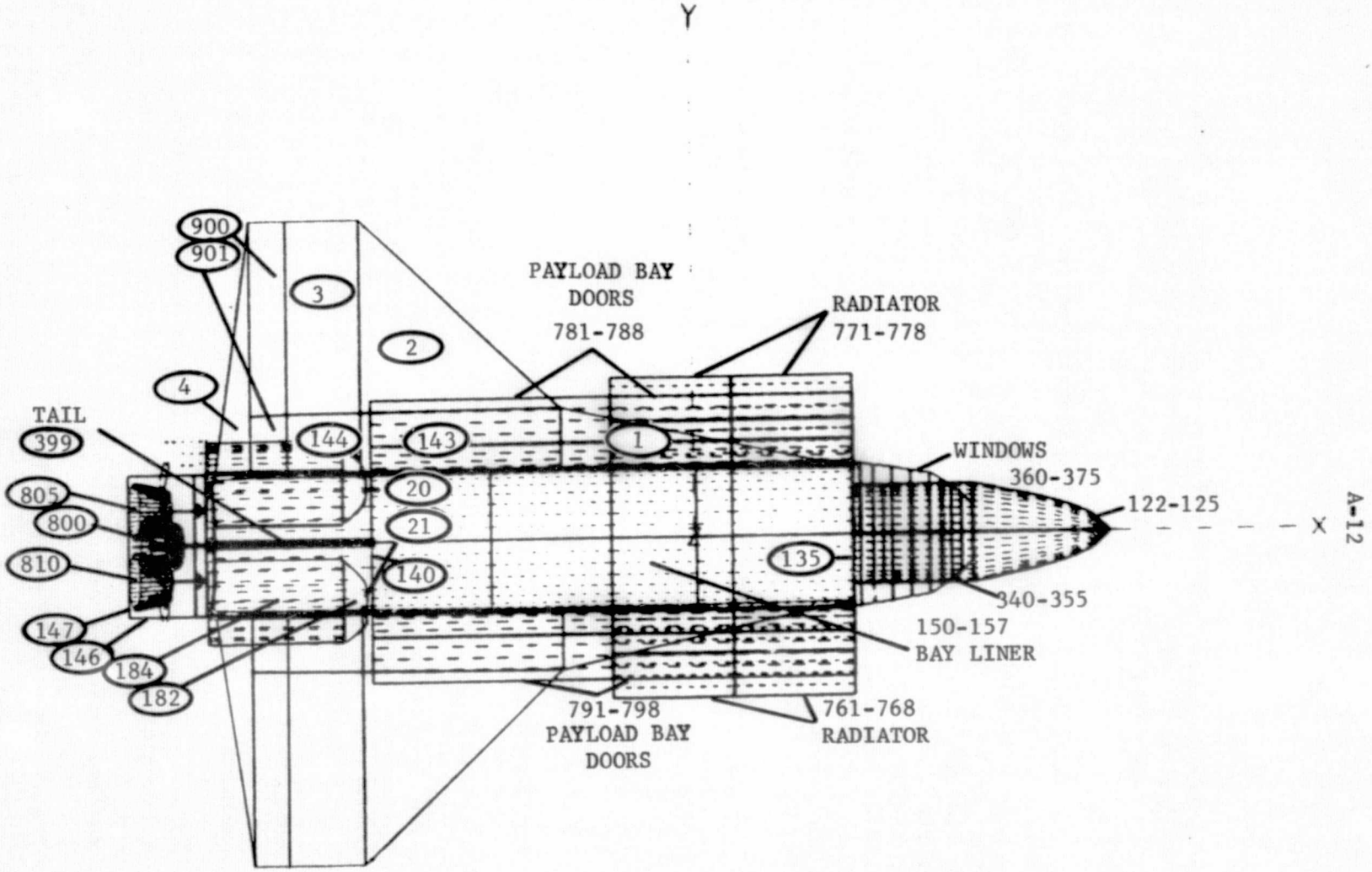

Figure A-1. Primary Shuttle Orbiter Nodal Surface Number Assignments

```
                    (a)  (b)        (c)        (d)        (e)
S       SURF=13,TYPE=POLY,ACTIVE=TOP,SHADE=BOTH,BSHADE=BOTH
        P1=-594.,0.,-102.
        P2=-644.,-300.,-30.   (g)
        P3=-644.,0.,-90.
        PROP=0.,1.
        ICON=21
        COM=* .(f). LEFT WING TAIL  EDGE  ..0 . *
S       SURF=1,TYPE=POLY,ACTIVE=TOP,SHADE=BOTH,BSHADE=BOTH
        P1=250.,0.,-75.
        P2=-192.,89.,-60.
        P3=-192.,0.,-60.
        PROP=0.,0.
        ICON=20          (h)                              (i)
        COM=*...RIGHT WING TRIANGLE RT.A.332.1024*
S       SURF=2,TYPE=POLY,ACTIVE=BOTTOM,SHADE=BOTH,BSHADE=BOTH
        PROP=0.,1.
        P1=-192.,89.,-60.
        P2=-443.,89.,-85.
        P3=-.83.,300.,-85.
        COM=*.....MIDDLE WING TRAP, RT 8 ..1.24,1292*
        ICON=20
S        SURF=14?,TYPE=RECT,ACTIVE=BOTTOM,SHADE=BOTH,BSHADE=BOTH
        P1=-1??.,0.,-60.
        P2=-443.,0.,-85.
        P3=-443.,89.,-85.
        PROP=0.,1.
        ICON=20
        COM=*B  +Y RECTANGLE WING*
S       SURF=3,TYPE=RECT,ACTIVE=BOTTOM,SHADE=BOTH,BSHADE=BOTH
        P1=-593.34,0?.,-58.333
         P2=-593.34,300.,-58.333
        P3=-443.,300.,-85.
        PROP=0.,1.
        ICON=20
        COM=*.... BACK WING RECT.  RTC .1292,1493*
S        SURF=14?,TYPE=RECT,ACTIVE=BOTTOM,SHADE=BOTH,BSHADE=BOTH
       P1=-593.34,0.,-58.333
        P2=-591..4,89.,-58.333
```

Figure A-2. Computer Printout Example of Input Data Matrix

g) point input data - three dimensional input with respect to program axis system;

h) thermal property of surface emissivity; and

i) comment - surface name and description.

2.3 View Factor Data Matrix Description - View factor output data is contained in this matrix for all modeled Lambertian surfaces capable of impinging upon susceptible surfaces of interest. Figure A-3 is an example of the view factor data matrix for selected Shuttle Orbiter suface to surface relationships. The outline below describes the main items of the view factor data matrix (reference Figure A-2):

a) Node I - emitting Lambertian surface number;

b) Node J - receiving surface number from Node I;

c) computation - verification flag of view factor calculation;

d) FE(I,J) W/SHAD - view factor fraction of mass leaving Node I capable of impinging upon Node J considering third surface shadowing;

e) FE(J,I) W/SHAD - reciprocal view factor fraction of mass leaving Node J capable of impinging upon Node I considering third surface shadowing;

f) FA(I,J) W/SHAD - view factor same as d) used internal to program;

g) F(I,J) WO/SHAD - view factor fraction of mass leaving Node I capable of impinging upon Node J if no third surface shadowing is considered.

h) SHAD. E Factor - percentage of Node I not shadowed from Node J;

i) SHAD. A Factor - same as h) internal to program; and

j) CP time - computer time required for view factor calculation accumulative for each Node I.

MODEL = RIO STEP = 1 RCS ANALYSIS 4/9/75
FORM FACTOR CALCULATION LINK.

(* INDICATES NODE PAIR HAS BEEN SUBDIVIDED)
(R INDICATES FF CALCULATED FROM J TO I)

NODE I (a)	NODE J (b)	COMPUTATION (c)	FF(I,J) W/SHAD (d)	FF(J,I) W/SHAD (e)	FA(I,J) W/SHAD (f)	F (I,J) WO/SHAD (g)	SHAD. E FACTER (h)	SHAD. A FACTOR (i)	CP TIME (SEC) (j)
5090	715	CAL.	.000002	.000159	.000002	.000035	.445607	.445607	.895
5090	723	CAL.	.000098	.000193	.000008	.000008	1.000000	1.000000	1.127
5090	722	CAL.	.000033	.000185	.000003	.000008	1.000000	1.000000	1.397
5090	724	CAL.	.000007	.000177	.000007	.000007	1.000000	1.000000	1.691
5090	720	CAL.	.000007	.000170	.000007	.000007	1.000000	1.000000	1.992
5090	731	CAL.	.000103	.000061	.000023	.000038	.333393	.333393	2.338
5090	733	CAL.	.000007	.000175	.000007	.000007	1.000000	1.000000	2.647
5090	735	CAL.	.000007	.000167	.000007	.000007	1.000000	1.000000	3.000
5090	24	CAL.	.000007	.000164	.000007	.000007	1.000000	1.000000	3.536
5090	26	CAL.	.000007	.000157	.000007	.000007	1.000000	1.000000	3.836
5090	701	CAL.	.000256	.000139	.000256	.000256	1.000000	1.000000	4.237

Figure A-3. Computer Printout Example of View Factor Data Matrix

2.4 Geometric Relationship Data Matrix Description - This data matrix supplies the computer output information on the geometrical relationships between all Shuttle Orbiter surfaces capable of viewing each other. This data is used in conjunction with the closed form mathematical source characteristics for sources other than Lambertian to determine contaminant fluxes at surfaces of interest. Figure A-4 is an example of the geometric relationship data matrix for selected Shuttle Orbiter surfaces. The outline below describes the major items depicted in Figure A-4:

a) NODE I - Source surface number;

b) NODE J - Receiving surface number from Node I;

c) F(I,J) - View Factor, fraction of mass leaving Node I (Lambertian) capable of impinging upon Node J;

d) AREA - Surface area of Node I in^2;

e) THETI - Angle that radius makes with Node I normal;

f) THETJ - Angle that radius makes with Node J normal;

g) RADIUS - Distance between Node I and Node J center points in inches;

h) NORMAL VECTOR - Node I perpendicular vector (X,Y,Z components) normalized to amplitude of Node I surface area; and

i) POSITION VECTOR - Vector (X,Y,Z components) from central axis origin to center point of Node I.

2.5 Shuttle Orbiter Data Matrices-The following subsection contain the computer printout data matrices as previously described for the Shuttle Orbiter.

Figure A-1 in the text describes the primary Orbiter nodal surface number locations. A summary listing and description of the Shuttle Orbiter nodal surfaces is contained in Figure A-5, which follows:

= RIO STEP = 1 RCS ANALYSIS 4/9/7?
SING OPERATIONS DATA

NODE J (b)	F(I,J) (c)	AREA (d)	THETI (e)	THETJ (f)	RADIUS (g)	NORMAL VECTOR I (h)			POSITION VECTOR I (i)		
723	.0u1135	2.83E+01	71.02	42.64	4.51717E+01	5.88E+00	-9.40E+00	2.60E+01	-7.47E+02	1.16E+02	3.53E+01
725	.0u1223	2.83E+01	73.13	36.44	4.13408E+01	5.88E+00	-9.40E+00	2.60E+01	-7.47E+02	1.16E+02	3.53E+01
727	.000855	2.83E+01	77.02	36.54	4.13605E+01	5.88E+00	-9.40E+00	2.60E+01	-7.47E+02	1.16E+02	3.53E+01
730	.001297	2.83E+01	36.49	30.03	7.12789E+01	5.88E+00	-9.40E+00	2.60E+01	-7.47E+02	1.16E+02	3.53E+01
732	.0u1594	2.83E+01	34.09	22.81	8.63787E+01	5.88E+00	-9.40E+00	2.60E+01	-7.47E+02	1.16E+02	3.53E+01
734	.001718	2.83E+01	35.01	16.53	6.38549E+01	5.88E+00	-9.40E+00	2.60E+01	-7.47E+02	1.16E+02	3.53E+01
7o7	.000112	2.83E+01	72.93	80.55	7.80681E+02	5.88E+00	-9.40E+00	2.60E+01	-7.47E+02	1.16E+02	3.53E+01
31	.0104+3	2.83E+01	58.31	39.19	4.50797E+01	5.88E+00	-9.40E+00	2.60E+01	-7.47E+02	1.16E+02	3.53E+01
32	.0121?6	2.83E+01	16.38	65.21	8.76773E+01	5.88E+00	-9.40E+00	2.60E+01	-7.47E+02	1.16E+02	3.53E+01
33	.0o0835	2.83E+01	40.83	47.93	5.45061E+01	5.88E+00	-9.40E+00	2.60E+01	-7.47E+02	1.16E+02	3.53E+01
34	.0119719	2.83E+01	13.59	6+.75	8.63724E+01	5.88E+00	-9.40E+00	2.60E+01	-7.47E+02	1.16E+02	3.53E+01
25	.00o+03	2.83E+01	80.96	40.96	4.45082E+01	5.88E+00	-9.40E+00	2.60E+01	-7.47E+02	1.16E+02	3.53E+01
27	.0o3+07	2.83E+01	68.87	47.08	2.30293E+01	5.88E+00	-9.40E+00	2.60E+01	-7.47E+02	1.16E+02	3.53E+01
0J0	.0224oJ	2.83E+01	57.10	30.07	9.89+90E+01	5.88E+00	-9.40E+00	2.60E+01	-7.47E+02	1.16E+02	3.53E+01
0J1	.03o9+7	2.83E+01	56.27	10.65	8.81+47E+01	5.88E+00	-9.40E+00	2.60E+01	-7.47E+02	1.16E+02	3.53E+01
22	.1o9o5o	2.83E+01	60.26	71.15	1.23?68E+02	5.88E+00	-9.40E+00	2.60E+01	-7.47E+02	1.16E+02	3.53E+01
1o3	.0301o+	2.83E+01	84.01	69.50	4.23+07E+02	5.88E+00	-9.40E+00	2.60E+01	-7.47E+02	1.16E+02	3.53E+01
101	.00o0J3	2.83E+01	82.47	68.96	5.81?67E+02	5.88E+00	-9.40E+00	2.60E+01	-7.47E+02	1.16E+02	3.53E+01
740	.000521	2.83E+01	75.01	70.06	5.09+24E+02	5.88E+00	-9.40E+00	2.60E+01	-7.47E+02	1.16E+02	3.53E+01
3oJ	.0J9150	2.83E+01	15.79	61.+5	2.41?01E+02	5.88E+00	-9.40E+00	2.60E+01	-7.47E+02	1.16E+02	3.53E+01
315	.099063	2.83E+01	16.37	58.59	2.21+05E+02	5.88E+00	-9.40E+00	2.60E+01	-7.47E+02	1.16E+02	3.53E+01
721	.J+149o	2.83E+01	29.07	63.65	8.0o+03E+01	5.88E+00	-9.40E+00	2.60E+01	-7.47E+02	1.16E+02	3.53E+01
732	.0011+8	2.83E+01	0C.95	79.33	2.12+13E+02	5.88E+00	-9.40E+00	2.60E+01	-7.47E+02	1.16E+02	3.53E+01

A-17

Figure A-4. Computer Printout Example of Geometric Relationship Data Matrix

MODEL = RIO STEP = 1 RCS ANALYSIS 4/9/75
PROCESSING OPERATIONS DATA

NODE	BCS	AREA	ALPH	EMISS	SURF. TYPE	ACTIVE	---------COMMENTS----------
5000	DISCS	1.439E+01	0.	0.	DISC	TOP	...SPECIAL DISC(DIMENSIONS=
5005	DISCS	1.035E+01	0.	0.	DISC	TOP	...SPECIAL DISC(DIMENSIONS=
5010	DISCS	2.027E+01	0.	0.	DISC	TOP	...SPECIAL DISC(DIMENSIONS=
5015	DISCS	2.498E+01	0.	0.	DISC	TOP	...SPECIAL DISC(DIMENSIONS=
5020	DISCS	3.058E+01	0.	0.	DISC	TOP	...SPECIAL DISC(DIMENSIONS=
5025	DISCS	3.683E+01	0.	0.	DISC	TOP	...SPECIAL DISC(DIMENSIONS=
5030	DISCS	4.052E+01	0.	0.	DISC	TOP	...SPECIAL DISC(DIMENSIONS=
5035	DISCS	3.684E+01	0.	0.	DISC	TOP	...SPECIAL DISC(DIMENSIONS=
5040	DISCS	6.414E+01	0.	0.	DISC	TOP	...SPECIAL DISC(DIMENSIONS=
5045	DISCS	8.127E+01	0.	0.	DISC	TOP	...SPECIAL DISC(DIMENSIONS=
5050	DISCS	1.000E+02	0.	0.	DISC	TOP	...SPECIAL DISC(DIMENSIONS=
5055	DISCS	1.215E+02	0.	0.	DISC	TOP	...SPECIAL DISC(DIMENSIONS=
5060	DISCS	1.360E+02	0.	0.	DISC	TOP	...SPECIAL DISC(DIMENSIONS=
5065	DISCS	1.834E+02	0.	0.	DISC	TOP	...SPECIAL DISC(DIMENSIONS=
5070	DISCS	2.587E+02	0.	0.	DISC	TOP	...SPECIAL DISC(DIMENSIONS=
5075	DISCS	3.437E+02	0.	0.	DISC	TOP	...SPECIAL DISC(DIMENSIONS=
5080	DISCS	4.036E+02	0.	0.	DISC	TOP	...SPECIAL DISC(DIMENSIONS=
5085	DISCS	5.017E+02	0.	0.	DISC	TOP	...SPECIAL DISC(DIMENSIONS=
5090	DISCS	5.784E+02	0.	0.	DISC	TOP	...SPECIAL DISC(DIMENSIONS=
5095	DISCS	6.106E+02	0.	0.	DISC	TOP	...SPECIAL DISC(DIMENSIONS=
5100	DISCS	1.085E+03	0.	0.	DISC	TOP	...SPECIAL DISC(DIMENSIONS=
5105	DISCS	2.877E+03	0.	0.	DISC	TOP	...SPECIAL DISC(DIMENSIONS=
5110	DISCS	2.877E+03	0.	0.	DISC	TOP	...SPECIAL DISC(DIMENSIONS=
1-5	BODY	2.547E+03	0.	0.	TRAPEZOID	TOP	+ Y REAR TAPER
146	BODY	1.955E+01	0.	0.	RECTANGLE	TOP	REAR FLAT PLATE CUT BACK
147	BODY	2.324E+02	0.	0.	RECTANGLE	TOP	SLOPING REAR FLAT PLATE
710	BODY	2.827E+01	0.	0.	DISC	BOTTOM	-Z 1ST RCS X=1519.75
711	BODY	2.827E+01	0.	0.	DISC	TOP	-Z 1ST RCS X=1519.75
712	BODY	2.827E+01	0.	0.	DISC	BOTTOM	-Z 2ND RCS X=1532.875
713	BODY	2.827E+01	0.	0.	DISC	TOP	-Z 2ND RCS X=1532.875
714	BODY	2.827E+01	0.	0.	DISC	BOTTOM	-Z 3RD RCS X=1545.375
715	BODY	2.827E+01	0.	0.	DISC	TOP	-Z 3RD RCS X=1545.375
720	BODY	2.827E+01	0.	0.	DISC	BOTTOM	+Y 1ST RCS X=1516.
721	BODY	2.827E+01	0.	0.	DISC	TOP	+Y 1ST RCS X=1516.
722	BODY	2.827E+01	0.	0.	DISC	BOTTOM	+Y 2ND RCS X=1529.
723	BODY	2.827E+01	0.	0.	DISC	TOP	+Y 2ND RCS X=1529.
724	BODY	2.827E+01	0.	0.	DISC	BOTTOM	+Y 3RD RCS X=1542.
725	BODY	2.827E+01	0.	0.	DISC	TOP	+Y 3RD RCS X=1542.
726	BODY	2.827E+01	0.	0.	DISC	BOTTOM	+Y 4TH RCS X=1555.
727	BODY	2.827E+01	0.	0.	DISC	TOP	+Y 4TH RCS X=1555.
730	BODY	2.827E+01	0.	0.	DISC	BOTTOM	+Z 1ST RCS X=1516.
731	BODY	2.827E+01	0.	0.	DISC	TOP	+Z 1ST RCS X=1516.
732	BODY	2.827E+01	0.	0.	DISC	BOTTOM	+Z 2ND RCS X=1529.
733	BODY	2.827E+01	0.	0.	DISC	TOP	+Z 2ND RCS X=1529.
734	BODY	2.827E+01	0.	0.	DISC	BOTTOM	+Z 3RD RCS X=1542.
735	BODY	2.827E+01	0.	0.	DISC	TOP	+Z 3RD RCS X=1542.

Figure A-5. Summary Listing and Description of the Orbiter Nodal Surface Assignment

MODEL = RIO STEP = 1 RCS ANALYSIS 4/9/75
PROCESSING OPERATIONS DATA

NODE	BCS	AREA	ALPH	EMISS	SURF. TYPE	ACTIVE	--------COMMENTS----------
740	BODY	2.427E+01	0.	0.	DISC	BOTTOM	-X EVAP. X=1525. CENTER BELL
741	BODY	2.827E+01	0.	0.	DISC	TOP	-X EVAP. X=1525. CENTER BELL
900	BODY	1.487E+04	0.	0.	RECTANGLE	BOTTOM	EXTENDED AILERON TOP
911	BODY	4.778E+03	0.	0.	RECTANGLE	BOTTOM	EXTENDED ALERION INNER
761	BODY	1.178E+04	0.	0.	CYLINDER	INSIDE	-Y RADIATOR
762	BODY	1.178E+04	0.	0.	CYLINDER	OUTSID	-Y RADIATOR
763	BODY	1.178E+04	0.	0.	CYLINDER	INSIDE	-Y RADIATOR
764	BODY	1.178E+04	0.	0.	CYLINDER	OUTSID	-Y RADIATOR
765	BODY	1.178E+04	0.	0.	CYLINDER	INSIDE	-Y RADIATOR
766	BODY	1.178E+04	0.	0.	CYLINDER	OUTSID	-Y RADIATOR
767	BODY	1.178E+04	0.	0.	CYLINDER	INSIDE	-Y RADIATOR
768	BODY	1.178E+04	0.	0.	CYLINDER	OUTSID	-Y RADIATOR
771	BODY	1.178E+04	0.	0.	CYLINDER	INSIDE	+Y RADIATOR
772	BODY	1.178E+04	0.	0.	CYLINDER	OUTSID	+Y RADIATOR
773	BODY	1.178E+04	0.	0.	CYLINDER	INSIDE	+Y RADIATOR
774	BODY	1.178E+04	0.	0.	CYLINDER	OUTSID	+Y RADIATOR
775	BODY	1.178E+04	0.	0.	CYLINDER	INSIDE	+Y RADIATOR
776	BODY	1.178E+04	0.	0.	CYLINDER	OUTSID	+Y RADIATOR
777	BODY	1.178E+04	0.	0.	CYLINDER	INSIDE	+Y RADIATOR
778	BODY	1.178E+04	0.	0.	CYLINDER	OUTSID	+Y RADIATOR
140	BODY	2.269E+04	-0.	-0.	DISC	TOP	END BAY AREA DISK
282	BODY	7.850E+03	0.	0.	PARABOLOID	OUTSID	1ST PARAB -Y OMS
144	BODY	4.433E+04	0.	0.	CYLINDER	OUTSID	OMS END CYLINDER RADIUS=65.
29	BODY	5.951E+03	0.	0.	TRAPEZOID	TOP	TRAP BOTTOM OMS END SEALER
31	BODY	4.149E+02	0.	0.	DISC	TOP	1ST TRIANGLE LT SIDE LOOKING B
32	BODY	8.955E+02	0.	0.	DISC	TOP	LAST TRI RT SIDE
172	BODY	7.413E+03	0.	0.	PARABOLOID	OUTSID	1ST PARAB +Y OMS
174	BODY	4.813E+04	0.	0.	CYLINDER	OUTSID	+Y OMS END CYLINDER
33	BODY	1.496E+03	0.	0.	DISC	BOTTOM	2ND TRI LEFT SIDE
34	BODY	1.312E+03	0.	0.	DISC	TOP	3RD TRI MIDLLE RT SIDE
35	BODY	8.486E+02	0.	0.	TRAPEZOID	TOP	TOP INSIDE TRAP
36	BODY	8.226E+02	0.	0.	TRAPEZOID	TOP	TOP INSIDE TRAP
24	BODY	2.827E+01	0.	0.	DISC	BOTTOM	REAR Y RCS (Y WAS 134. ALL RES
25	BODY	2.827E+01	0.	0.	DISC	TOP	REAR Y RCS (Y WAS 134. ALL RES
26	BODY	2.827E+01	0.	0.	DISC	BOTTOM	REAR Z RCS (Z WAS 57. ALL REST
27	BODY	2.827E+01	0.	0.	DISC	TOP	REAR Z RCS (Z WAS 57. ALL REST
149	BODY	2.647E+03	0.	0.	TRAPEZOID	BOTTOM	- Y. REAR SIDE TAPER...
707	BODY	2.827E+01	0.	0.	DISC	BOTTOM	......JULY 8 EVAP..3 IN. RAD.
708	BODY	2.827E+01	0.	0.	DISC	TOP	......JULY 8 EVAP..3 IN. RAD.
800	BODY	3.000E+03	0.	0.	PARABOLOID	OUTSID	TOP ENGIN
801	BODY	5.847E+03	0.	0.	PARABOLOID	OUTSID	TOP ENGIN
802	BODY	3.000E+03	0.	0.	PARABOLOID	OUTSID	TOP ENGIN
803	BODY	5.847E+03	0.	0.	PARABOLOID	OUTSID	TOP ENGIN
805	BODY	3.000E+03	0.	0.	PARABOLOID	OUTSID	+ Y ENGIN
806	BODY	5.847E+03	0.	0.	PARABOLOID	OUTSID	+ Y ENGIN
807	BODY	3.000E+03	0.	0.	PARABOLOID	OUTSID	+ Y ENGIN

Figure A-5. Summary Listing and Description of the Orbiter Nodal Surface Assignment - continued

MODEL = RIO STEP = 1 RCS ANALYSIS 4/9/75
PROCESSING OPERATIONS DATA

NODE	BCS	AREA	ALPH	EMISS	SURF. TYPE	ACTIVE	--------COMMENTS----------
618	BODY	5.647E+03	0.	0.	PARABOLOID	OUTSID	+ Y ENGIN
610	BODY	5.444E+03	0.	0.	PARABOLOID	OUTSID	-Y ENGIN...
611	BODY	5.647E+03	0.	0.	PARABOLOID	OUTSID	-Y ENGIN...
612	BODY	5.444E+03	0.	0.	PARABOLOID	OUTSID	-Y ENGIN...
613	BODY	5.647E+03	0.	0.	PARABOLOID	OUTSID	-Y ENGIN...
20	BODY	1.14[illegible]	0.	0.	DISC	TOP	...-Y OMS SEALER ...
21	BODY	1.14[illegible]	0.	0.	DISC	TOP	..+Y OMS SEALER ...
222	BODY	2.273E+04	0.	0.	RECTANGLE	BOTTOM	BACK RECT 7.350EG
22	BODY	1.[illegible]	0.	0.	DISC	BOTTOM	REAR END HALF DISK
23	BODY	1.034E+04	0.	0.	DISC	TOP	REAR END HALF DISK
227	BODY	2.827E+01	0.	0.	DISC	TOP	BACK SIDE EVAPORAT, UPDATED
15	BODY	2.827E+01	0.	0.	DISC	TOP	REAR END EVAPORATOR
10	BODY	1.887E+04	0.	0.	TRAPEZOID	BOTTOM	....LEFT FRONT WING A ...
11	BODY	4.04[illegible]	0.	0.	TRAPEZOID	TOP	......LEFT MIDDLE WING BACK.B
141	BODY	2.[illegible]	0.	0.	RECTANGLE	TOP	BS INNER WING
12	BODY	4.402E+04	0.	0.	RECTANGLE	TOP	..... LEFT BACK RECT. WING C
142	BODY	1.[illegible]	0.	0.	RECTANGLE	TOP	INNER WING C
13	BODY	1.012E+04	0.	0.	TRAPEZOID	TOP	..... LEFT WING TAIL EDGE
1	BODY	1.878E+04	0.	0.	TRAPEZOID	TOP	...FRONT WING TRIANGLE RT.A.58
2	BODY	4.04[illegible]	0.	0.	TRAPEZOID	BOTTOM	.....MIDDLE WING TRAP, RT B ..
143	BODY	2.[illegible]	0.	0.	RECTANGLE	BOTTOM	B +Y RECTANGLE WING
3	BODY	2.[illegible]	0.	0.	RECTANGLE	BOTTOM	.... BACK WING RECT. RTC .129
144	BODY	4.[illegible]	0.	0.	RECTANGLE	BOTTOM	INNER WING C RECT
4	BODY	1.312E+04	0.	0.	TRAPEZOID	BOTTOM	+Y WING TAIL EDGE
120	BODY	2.8[illegible]	-0.	-0.	CYLINDER	INSIDE	BAY AREA CYLINDER
121	BODY	2.814E+04	-0.	-0.	CYLINDER	INSIDE	BAY AREA CYLINDER
122	BODY	2.81[illegible]	-0.	-0.	CYLINDER	INSIDE	BAY AREA CYLINDER
123	BODY	2.8[illegible]	-0.	-0.	CYLINDER	INSIDE	BAY AREA CYLINDER
124	BODY	2.8[illegible]	-0.	-0.	CYLINDER	INSIDE	BAY AREA CYLINDER
125	BODY	2.81[illegible]	-0.	-0.	CYLINDER	INSIDE	BAY AREA CYLINDER
126	BODY	2.81[illegible]	-0.	-0.	CYLINDER	INSIDE	BAY AREA CYLINDER
127	BODY	2.81[illegible]	-0.	-0.	CYLINDER	INSIDE	BAY AREA CYLINDER
139	BODY	3.2[illegible]	-0.	-0.	DISC	TOP	FRONT BAY AREA DISK
127	BODY	1.[illegible]	-0.	-0.	PARABOLOID	OUTSID	VERY NOSE CONE
123	BODY	1.527E+04	-0.	-0.	PARABOLOID	OUTSID	VERY NOSE CONE
124	BODY	1.[illegible]	-0.	-0.	PARABOLOID	OUTSID	VERY NOSE CONE
125	BODY	1.[illegible]	-0.	-0.	PARABOLOID	OUTSID	VERY NOSE CONE
320	BODY	4.073E+03	-0.	-0.	CYLINDER	OUTSID	NOSE CYLINDER
321	BODY	4.073E+03	-0.	-0.	CYLINDER	OUTSID	NOSE CYLINDER
322	BODY	4.073E+03	-0.	-0.	CYLINDER	OUTSID	NOSE CYLINDER
323	BODY	4.073E+03	-0.	-0.	CYLINDER	OUTSID	NOSE CYLINDER
324	BODY	4.073E+03	-0.	-0.	CYLINDER	OUTSID	NOSE CYLINDER
325	BODY	4.073E+03	-0.	-0.	CYLINDER	OUTSID	NOSE CYLINDER
326	BODY	4.073E+03	-0.	-0.	CYLINDER	OUTSID	NOSE CYLINDER
327	BODY	4.073E+03	-0.	-0.	CYLINDER	OUTSID	NOSE CYLINDER
328	BODY	4.073E+03	-0.	-0.	CYLINDER	OUTSID	NOSE CYLINDER

Figure A-5. Summary Listing and Description of the Orbiter Nodal Surface Assignment - continued

MODEL = RIO STEP = 1 RCS ANALYSIS 4/9/75
PROCESSING OPERATIONS DATA

NODE	BCS	AREA	ALPH	EMISS	SURF. TYPE	ACTIVE	--------COMMENTS----------	
329	BODY	4.673E+03	-0.	-0.	CYLINDER	OUTSID	NOSE CYLINDER	
330	BODY	4.673E+03	-0.	-0.	CYLINDER	OUTSID	NOSE CYLINDER	
331	BODY	4.673E+03	-0.	-0.	CYLINDER	OUTSID	NOSE CYLINDER	
332	BODY	4.673E+03	-0.	-0.	CYLINDER	OUTSID	NOSE CYLINDER	
333	BODY	4.673E+03	-0.	-0.	CYLINDER	OUTSID	NOSE CYLINDER	
334	BODY	4.673E+03	-0.	-0.	CYLINDER	OUTSID	NOSE CYLINDER	
335	BODY	4.673E+03	-0.	-0.	CYLINDER	OUTSID	NOSE CYLINDER	
340	BODY	3.833E+03	-0.	-0.	PARABOLOID	OUTSID	HOOD PARTIAL BACK	
341	BODY	4.022E+03	-0.	-0.	PARABOLOID	OUTSID	HOOD PARTIAL BACK	
342	BODY	4.197E+03	-0.	-0.	PARABOLOID	OUTSID	HOOD PARTIAL BACK	
343	BODY	4.366E+03	-0.	-0.	PARABOLOID	OUTSID	HOOD PARTIAL BACK	
344	BODY	3.833E+03	-0.	-0.	PARABOLOID	OUTSID	HOOD PARTIAL BACK	
345	BODY	4.022E+03	-0.	-0.	PARABOLOID	OUTSID	HOOD PARTIAL BACK	
346	BODY	4.197E+03	-0.	-0.	PARABOLOID	OUTSID	HOOD PARTIAL BACK	
347	BODY	4.366E+03	-0.	-0.	PARABOLOID	OUTSID	HOOD PARTIAL BACK	
348	BODY	3.833E+03	-0.	-0.	PARABOLOID	OUTSID	HOOD PARTIAL BACK	
349	BODY	4.022E+03	-0.	-0.	PARABOLOID	OUTSID	HOOD PARTIAL BACK	
350	BODY	4.197E+03	-0.	-0.	PARABOLOID	OUTSID	HOOD PARTIAL BACK	
351	BODY	4.366E+03	-0.	-0.	PARABOLOID	OUTSID	HOOD PARTIAL BACK	
352	BODY	3.833E+03	-0.	-0.	PARABOLOID	OUTSID	HOOD PARTIAL BACK	
353	BODY	4.022E+03	-0.	-0.	PARABOLOID	OUTSID	HOOD PARTIAL BACK	
354	BODY	4.197E+03	-0.	-0.	PARABOLOID	OUTSID	HOOD PARTIAL BACK	
355	BODY	4.366E+03	-0.	-0.	PARABOLOID	OUTSID	HOOD PARTIAL BACK	
361	BODY	1.993E+03	-0.	-0.	PARABOLOID	OUTSID	WINDOW	
361	BODY	1.825E+03	-0.	-0.	PARABOLOID	OUTSID	WINDOW	
362	BODY	2.031E+03	-0.	-0.	PARABOLOID	OUTSID	WINDOW	
363	BODY	2.218E+03	-0.	-0.	PARABOLOID	OUTSID	WINDOW	
364	BODY	1.993E+03	-0.	-0.	PARABOLOID	OUTSID	WINDOW	
365	BODY	1.825E+03	-0.	-0.	PARABOLOID	OUTSID	WINDOW	
366	BODY	2.031E+03	-0.	-0.	PARABOLOID	OUTSID	WINDOW	
367	BODY	2.218E+03	-0.	-0.	PARABOLOID	OUTSID	WINDOW	
368	BODY	1.993E+03	-0.	-0.	PARABOLOID	OUTSID	WINDOW	
369	BODY	1.825E+03	-0.	-0.	PARABOLOID	OUTSID	WINDOW	
370	BODY	2.031E+03	-0.	-0.	PARABOLOID	OUTSID	WINDOW	
371	BODY	2.218E+03	-0.	-0.	PARABOLOID	OUTSID	WINDOW	
372	BODY	1.993E+03	-0.	-0.	PARABOLOID	OUTSID	WINDOW	
373	BODY	1.825E+03	-0.	-0.	PARABOLOID	OUTSID	WINDOW	
374	BODY	2.031E+03	-0.	-0.	PARABOLOID	OUTSID	WINDOW	
375	BODY	2.218E+03	-0.	-0.	PARABOLOID	OUTSID	WINDOW	
401	BODY	4.613E+04	.900	.900	RECTANGLE	BOTTOM	BODY BOTTOM (FRT)	4 1
402	BODY	1.436E+05	.900	.900	RECTANGLE	BOTTOM	BODY BOTTOM (REAR)	402
781	BODY	2.470E+04	0.	0.	CYLINDER	INSIDE	.....+Y SIDE DOOR.....	
782	BODY	2.470E+04	0.	0.	CYLINDER	OUTSID	.....+Y SIDE DOOR.....	
783	BODY	2.470E+04	0.	0.	CYLINDER	INSIDE	.....+Y SIDE DOOR.....	
784	BODY	2.470E+04	0.	0.	CYLINDER	OUTSID	.....+Y SIDE DOOR.....	
785	BODY	2.470E+04	0.	0.	CYLINDER	INSIDE	.....+Y SIDE DOOR.....	

Figure A-5. Summary Listing and Description of the Orbiter Nodal Surface Assignment - continued

MODEL = RIO STEP = 1 RCS ANALYSIS 4/9/75
PROCESSING OPERATIONS DATA

NODE	BOS	AREA	ALPH	EMISS	SURF. TYPE	ACTIVE	--------COMMENTS----------	
786	BODY	2.470E+00	0.	0.	CYLINDER	OUTSID	.....+Y SIDE DOOR.....	
787	BODY	2.470E+00	0.	0.	CYLINDER	INSIDE	.....+Y SIDE DOOR.....	
788	BODY	2.470E+00	0.	0.	CYLINDER	OUTSID	.....+Y SIDE DOOR.....	
791	BODY	2.413E+00	0.	0.	CYLINDER	INSIDE	... -Y SIDE DOOR....	
792	BODY	2.413E+00	0.	0.	CYLINDER	OUTSID	... -Y SIDE DOOR....	
793	BODY	2.413E+00	0.	0.	CYLINDER	INSIDE	... -Y SIDE DOOR....	
794	BODY	2.413E+00	0.	0.	CYLINDER	OUTSID	... -Y SIDE DOOR....	
795	BODY	2.413E+00	0.	0.	CYLINDER	INSIDE	... -Y SIDE DOOR....	
796	BODY	2.413E+00	0.	0.	CYLINDER	OUTSID	... -Y SIDE DOOR....	
797	BODY	2.413E+00	0.	0.	CYLINDER	INSIDE	... -Y SIDE DOOR....	
798	BODY	2.413E+00	0.	0.	CYLINDER	OUTSID	... -Y SIDE DOOR....	
301	BODY	2.994E+00	0.	0.	TRAPEZOID	TOP	+Y SIDE FRONT TRAPEZOID	
305	BODY	4.947E+00	.900	.900	RECTANGLE	TOP	BODY SIDE (MIDDLE-PORT)	305
306	BODY	5.156E+00	.900	.900	RECTANGLE	TOP	BODY SIDE (BACK-PORT)	306
311	BODY	2.994E+00	0.	0.	TRAPEZOID	BOTTOM	-Y SIDE FRONT TRAPEZOID	
315	BODY	5.078E+00	.900	.900	RECTANGLE	TOP	BODY SIDE (MIDDLE-STBD)	315
316	BODY	5.292E+00	.900	.900	RECTANGLE	TOP	BODY SIDE (BACK-STBD)	316
202	BODY	3.668E+00	.900	.900	CYLINDER	OUTSID	BODY TOP (STBD-REAR)	202
212	BODY	3.668E+00	.900	.900	CYLINDER	OUTSID	BODY TOP (PORT-REAR)	212
300	BODY	2.400E+00	.900	.900	TRAPEZOID	TOP	VERTICAL FIN (PORT)	20
305	BODY	2.394E+00	.900	.900	TRAPEZOID	TOP	VERTICAL FIN (PORT-AFT)	20
390	BODY	2.400E+00	.900	.900	TRAPEZOID	BOTTOM	VERTICAL FIN (STBD)	20
395	BODY	2.394E+00	.900	.900	TRAPEZOID	BOTTOM	VERTICAL FIN (STBD-AFT)	20
700	BODY	2.827E+01	0.	0.	DISC	TOP	..MOST FORWARD EVAPORATOR.....	
730	BODY	1.590E+03	0.	0.	DISC	BOTTOM	.......SUPER ENGINS (OMS LOCAT	
731	BODY	1.590E+03	0.	0.	DISC	TOP	.......SUPER ENGINS (OMS LOCAT	
732	BODY	1.590E+03	0.	0.	DISC	BOTTOM	.......SUPER ENGINS (OMS LOCAT	
733	BODY	1.590E+03	0.	0.	DISC	TOP	.......SUPER ENGINS (OMS LOCAT	
18	BODY	2.827E+01	0.	0.	DISC	BOTTOM	...FRONT RCS..LOOKING +/-Y AT	
19	BODY	2.827E+01	0.	0.	DISC	TOP	...FRONT RCS..LOOKING +/-Y AT	
16	BODY	2.827E+01	0.	0.	DISC	BOTTOM	...MIDDLE EVAP. LOOKING +/- Y.	
17	BODY	2.827E+01	0.	0.	DISC	TOP	...MIDDLE EVAP. LOOKING +/- Y.	
399	BODY	4.152E+03	.900	.900	RECTANGLE	TOP	VERT. FIN LDG. EDGE	2

Figure A-5. Summary Listing and Description of the Orbiter Nodal Surface Assignment - continued

2.5.1 INPUT DATA MATRIX

The following pages contain the input data computer printouts for the Shuttle Orbiter configuration.

```
MODEL = CONTAM                                          RCS ANALYSIS      4/9/75
SURFACE DATA INPUT BLOCK

INPUT CARD COL. = 12345678 1 2345678 2 2345678 3 2345678 4 2345678 5 2345678 6 2345678 7 2345678 8 EDIT NO. OLD EDIT NO.  LABEL

                  HEADER       SURFACE DATA                                                185                         AA
                  I       ICSN     =         1                                             186                         AA
                          TX       =     8.0000000000E+02                                  187                         AA
                          TY       =     0.                                                188                         AA
                          TZ       =     0.                                                189                         AA
                          ROTZ     = -180.0000                                             190                         AA
                          ROTY     =    -0.                                                191                         AA
                          ROTX     =     0.                                                192                         AA
                  I       ICSN     =         2                                             193                         AA
                          TX       =    -5.0000000000E+02                                  194                         AA
                          TY       =     0.                                                195                         AA
                          TZ       =     0.                                                196                         AA
                          ROTZ     = -180.0000                                             197                         AA
                          ROTY     =    -0.                                                198                         AA
                          ROTX     =     0.                                                199                         AA
                  I       ICSN     =         3                                             200                         AA
                          TX       =     8.0000000000E+02                                  201                         AA
                          TY       =     0.                                                202                         AA
                          TZ       =     0.                                                203                         AA
                          ROTZ     =  -90.0000                                             204                         AA
                          ROTY     =    -0.                                                205                         AA
                          ROTX     =   90.0000                                             206                         AA
                  I       ICSN     =         4                                             207                         AA
                          TX       =     4.3000000000E+02                                  208                         AA
                          TY       =     6.2900000000E+01                                  209                         AA
                          TZ       =     2.4000000000E+01                                  210                         AA
                          ROTZ     =   79.7000                                             211                         AA
                          ROTY     =   41.0000                                             212                         AA
                          ROTX     =     0.                                                213                         AA
                  I       ICSN     =         5                                             214                         AA
                          TX       =     4.3000000000E+02                                  215                         AA
                          TY       =    -6.2900000000E+01                                  216                         AA
                          TZ       =     2.4000000000E+01                                  217                         AA
                          ROTZ     =  100.0000                                             218                         AA
                          ROTY     =  -41.0000                                             219                         AA
                          ROTX     =     0.                                                220                         AA
                  I     ICSN=    6                                                         221                         AA
                        TX=-195.                                                           222                         AA
                        TY=0.                                                              223                         AA
                        TZ=14.                                                             224                         AA
                          ROTX=0.,ROTY=90.,ROTZ=0.                                         225                         AA
                  I       ICSN=7                                                           226                         AA
                          TX=-116.,TY=0.,TZ=14.                                            227                         AA
                          ROTX=0.,ROTY=90.,ROTZ=0.                                         228                         AA
                  I     ICSN=8                                                             229                         AA
                        TX=-116.,TY=0.,TZ=14.                                              230                         AA
                          ROTX=0.,ROTY=90.,ROTZ=0.                                         231                         AA
                  I     ICSN=9                                                             232                         AA
                        TX=156.,TY=0.,TZ=14.                                               233                         AA
                          ROTX=0.,ROTY=-90., ROTZ=0.                                       234                         AA
                  I     ICSN=10                                                            235                         AA
```

MODEL = CONTAM RCS ANALYSIS 4/9/75
SURFACE DATA INPUT BLOCK

```
INPUT CARD COL. = 12345678 1 2345678 2 2345678 3 2345678 4 2345678 5 2345678 6 2345678 7 2345678 8 EDIT NO. OLD EDIT NO.  LABEL
                  TX=120.,TY=0.,TZ=14.                                                                          256        AA
                     ROTX=0.,ROTY=90.,ROTZ=0.                                                                   257        AA
               I   ICSN = 11                                                                                    258        AA
                  TX=-47..,TY=-76.14,TZ=65.56                                                                   259        AA
                     ROTX=0.,ROTY=90.,ROTZ=0.                                                                   260        AA
               I   ICSN=12                                                                                      261        AA
                  TX=-47..,TY=+76.14,TZ=65.56                                                                   262        AA
                  ROTX=0., ROTY=90.0,ROTZ=0.                                                                    263        AA
               I   ICSN=13                                                                                      264        AA
                   TX=-76.,TY=0.,TZ=30.                                                                         265        AA
                  ROTX=0.0,ROTY=-90.,ROTZ=0.                                                                    266        AA
               I   ICSN=14                                                                                      267        AA
                  TX=-717.,TY=0.0,TZ=-50.                                                                       268        AA
                  ROTX=0.0,ROTY=-90.,ROTZ=0.                                                                    269        AA
               I      ICSN=15                                                                                   270        AA
                      TX=-711..TY=0.0,TZ=0.0                                                                    271        AA
                      ROTX=0.0,  ROTY=+97.35,   ROTZ=0.0                                                        272        AA
               I    ICSN=16                                                                                     273        AA
                   TX=-771.63,TY=101.38,TZ=100.63                                                               274        AA
                  ROTY=103.,ROTX=11.,ROTZ=0.                                                                    275        AA
               I   ICSN=17                                                                                      276        AA
                   TX=-765.,TY=-66.,TZ=70.5                                                                     277        AA
                  ROTX=0.,ROTY=-74.153,ROTZ=12.241                                                              278        AA
               I    ICSN=20                                                                                     279        AA
                   TX=0.,TY=102.,TZ=0.                                                                          280        AA
                   ROTX=-9.,ROTY=0.,ROTZ=0.                                                                     281        AA
               I    ICSN=21                                                                                     282        AA
                   TX=0.,TY=-102.,TZ=0.                                                                         283        AA
                   ROTX=90.,ROTY=0.,ROTZ=0.                                                                     284        AA
               I      ICSN=25                                                                                   285        AA
                      TX=0.,TY=0.,TZ=0.                                                                         286        AA
                      ROTX=0.,ROTY=0.,ROTZ=0.                                                                   287        AA
               I      ICSN=26                                                                                   288        AA
                      TX=-719.75,TY=117.5,TZ=21.87                                                              289        AA
                      ROTX=20.,ROTY=12.,ROTZ=0.                                                                 290        AA
               I      ICSN=27                                                                                   291        AA
                      TX=-732.875,TY=116.25,TZ=24.125                                                           292        AA
                      ROTX=20.,ROTY=12.,ROTZ=0.                                                                 293        AA
               I      ICSN=28                                                                                   294        AA
                      TX=-745.375,TY=115.625,TZ=35.000                                                          295        AA
                      ROTX=20.,ROTY=12.,ROTZ=0.                                                                 296        AA
              RCS        DISC                                                                                   297        AA
              S       SURFN= 30.0,TYPE=DISC,SHADE=NO,BSHADE=BOTH,ACTIVE=TCP                                     298        AA
                      P1=0.,0.,107.                                                                             299        AA
                      P2=0.,2.14,107.                                                                           300        AA
                      P3=2.14,0.,107.                                                                           301        AA
                      P4=2.14,0.,107.                                                                           302        AA
                      PROP=1.,1.                                                                                303        AA
                      COM=*    ...SPECIAL DISC(DIMENSIONS=SPHERES)..NO. 1..*                                    304        AA
              S       SURFN= 31.0,TYPE=DISC,SHADE=NO,BSHADE=BOTH,ACTIVE=TCP                                     305        AA
                      P1=0.,0.,113.                                                                             306        AA
```

```
MODEL = CONTAM                                  RCS ANALYSIS     4/9/75
SURFACE DATA INPUT BLOCK

INPUT CARD COL. = 12345678 1 2345678 2 2345678 3 2345678 4 2345678 5 2345678 6 2345678 7 2345678 8 EDIT NO. OLD EDIT NO.  LABEL

                P2=0.,2.26,113.                                                        287            AA
                P3=2.26,0.,113.                                                        288            AA
                P4=2.26,0.,113.                                                        289            AA
                PROP=3.,0.                                                             290            AA
                COM=*    ...SPECIAL DISC(DIMENSIONS=SPHERES)..NO. 2..*                 291            AA
     S          SURFN= 5010,TYPE=DISC,SHADE=NO,BSHADE=BOTH,ACTIVE=TOP                  292            AA
                P1=0.,0.,127.                                                          293            AA
                P2=0.,2.54,127.                                                        294            AA
                P3=2.54,0.,127.                                                        295            AA
                P4=2.54,0.,127.                                                        296            AA
                PROP=3.,3.                                                             297            AA
                COM=*    ...SPECIAL DISC(DIMENSIONS=SPHERES)..NO. 3..*                 298            AA
     S          SURFN= 5015,TYPE=DISC,SHADE=NO,BSHADE=BOTH,ACTIVE=TOP                  299            AA
                P1=0.,0.,141.                                                          300            AA
                P2=0.,2.82,141.                                                        301            AA
                P3=2.82,0.,141.                                                        302            AA
                P4=2.82,0.,141.                                                        303            AA
                PROP=3.,0.                                                             304            AA
                COM=*    ...SPECIAL DISC(DIMENSIONS=SPHERES)..NO. 4..*                 305            AA
     S          SURFN= 5020,TYPE=DISC,SHADE=NO,BSHADE=BOTH,ACTIVE=TOP                  306            AA
                P1=0.,0.,156.                                                          307            AA
                P2=0.,3.12,156.                                                        308            AA
                P3=3.12,0.,156.                                                        309            AA
                P4=3.12,0.,156.                                                        310            AA
                PROP=3.,0.                                                             311            AA
                COM=*    ...SPECIAL DISC(DIMENSIONS=SPHERES)..NO. 5..*                 312            AA
     S          SURFN= 5025,TYPE=DISC,SHADE=NO,BSHADE=BOTH,ACTIVE=TOP                  313            AA
                P1=0.,0.,170.                                                          314            AA
                P2=0.,3.40,170.                                                        315            AA
                P3=3.40,0.,170.                                                        316            AA
                P4=3.40,0.,170.                                                        317            AA
                PROP=3.,0.                                                             318            AA
                COM=*    ...SPECIAL DISC(DIMENSIONS=SPHERES)..NO. 6..*                 319            AA
     S          SURFN= 5030,TYPE=DISC,SHADE=NO,BSHADE=BOTH,ACTIVE=TOP                  320            AA
                P1=0.,0.,192.                                                          321            AA
                P2=0.,3.84,192.                                                        322            AA
                P3=3.84,0.,192.                                                        323            AA
                P4=3.84,0.,192.                                                        324            AA
                PROP=3.,3.                                                             325            AA
                COM=*    ...SPECIAL DISC(DIMENSIONS=SPHERES)..NO. 7..*                 326            AA
     S          SURFN= 5035,TYPE=DISC,SHADE=NO,BSHADE=BOTH,ACTIVE=TOP                  327            AA
                P1=0.,0.,214.                                                          328            AA
                P2=0.,4.24,214.                                                        329            AA
                P3=4.24,0.,214.                                                        330            AA
                P4=4.24,0.,214.                                                        331            AA
                PROP=3.,0.                                                             332            AA
                COM=*    ...SPECIAL DISC(DIMENSIONS=SPHERES)..NO. 8..*                 333            AA
     S          SURFN= 5040,TYPE=DISC,SHADE=NO,BSHADE=BOTH,ACTIVE=TOP                  334            AA
                P1=0.,0.,226.                                                          335            AA
                P2=0.,4.52,226.                                                        336            AA
                P3=4.52,0.,226.                                                        337            AA
```

```
MODEL = CONTAM                              RCS ANALYSIS      4/9/75
SURFACE DATA INPUT BLOCK

INPUT CARD COL. = 12345678 1 2345678 2 2345678 3 2345678 4 2345678 5 2345678 6 2345678 7 2345678 8 EDIT NO. OLD EDIT NO.  LABEL

          P4=4.52,0.,226.                                                   338        AA
          PROP=0.,0.                                                        339        AA
          COM=*    ...SPECIAL DISC(DIMENSIONS=SPHERES)..NO. 9..*            340        AA
    S     SURFN= 5045,TYPE=DISC,SHADE=NO,BSHADE=BOTH,ACTIVE=TOP             341        AA
          P1=0.,0.,254.                                                     342        AA
          P2=0.,5.08,254.                                                   343        AA
          P3=5.08,0.,254.                                                   344        AA
          P4=5.08,0.,254.                                                   345        AA
          PROP=0.,0.                                                        346        AA
          COM=*    ...SPECIAL DISC(DIMENSIONS=SPHERES)..NO.10..*            347        AA
    S     SURFN= 5050,TYPE=DISC,SHADE=NO,BSHADE=BOTH,ACTIVE=TOP             348        AA
          P1=0.,0.,283.                                                     349        AA
          P2=0.,5.66,283.                                                   350        AA
          P3=5.66,0.,283.                                                   351        AA
          P4=5.66,0.,283.                                                   352        AA
          PROP=0.,0.                                                        353        AA
          COM=*    ...SPECIAL DISC(DIMENSIONS=SPHERES)..NO.11..*            354        AA
    S     SURFN= 5055,TYPE=DISC,SHADE=NO,BSHADE=BOTH,ACTIVE=TOP             355        AA
          P1=0.,0.,311.                                                     356        AA
          P2=0.,6.22,311.                                                   357        AA
          P3=6.22,0.,311.                                                   358        AA
          P4=6.22,0.,311.                                                   359        AA
          PROP=0.,0.                                                        360        AA
          COM=*    ...SPECIAL DISC(DIMENSIONS=SPHERES)..NO.12..*            361        AA
    S     SURFN= 5060,TYPE=DISC,SHADE=NO,BSHADE=BOTH,ACTIVE=TOP             362        AA
          P1=0.,0.,346.                                                     363        AA
          P2=0.,6.92,346.                                                   364        AA
          P3=6.92,0.,346.                                                   365        AA
          P4=6.92,0.,346.                                                   366        AA
          PROP=0.,0.                                                        367        AA
          COM=*    ...SPECIAL DISC(DIMENSIONS=SPHERES)..NO.13..*            368        AA
    S     SURFN= 5065,TYPE=DISC,SHADE=NO,BSHADE=BOTH,ACTIVE=TOP             369        AA
          P1=0.,0.,382.                                                     370        AA
          P2=0.,7.64,382.                                                   371        AA
          P3=7.64,0.,382.                                                   372        AA
          P4=7.64,0.,382.                                                   373        AA
          PROP=0.,0.                                                        374        AA
          COM=*    ...SPECIAL DISC(DIMENSIONS=SPHERES)..NO.14..*            375        AA
    S     SURFN= 5070,TYPE=DISC,SHADE=NO,BSHADE=BOTH,ACTIVE=TOP             376        AA
          P1=0.,0.,452.                                                     377        AA
          P2=0.,9.04,452.                                                   378        AA
          P3=9.04,0.,452.                                                   379        AA
          P4=9.04,0.,452.                                                   380        AA
          PROP=0.,0.                                                        381        AA
          COM=*    ...SPECIAL DISC(DIMENSIONS=SPHERES)..NO.15..*            382        AA
    S     SURFN= 5075,TYPE=DISC,SHADE=NO,BSHADE=BOTH,ACTIVE=TOP             383        AA
          P1=0.,0.,523.                                                     384        AA
          P2=0.,10.46,523.                                                  385        AA
          P3=10.46,0.,523.                                                  386        AA
          P4=10.46,0.,523.                                                  387        AA
          PROP=0.,0.                                                        388        AA
```

```
MODEL = CONTAM                                   RCS ANALYSIS     4/9/75
SURFACE DATA INPUT BLOCK

INPUT CARD COL. = 12345678 1 2345678 2 2345678 3 2345678 4 2345678 5 2345678 6 2345678 7 2345678 8 EDIT NO. OLD EDIT NO.  LABEL

              COM=*    ...SPECIAL DISC(DIMENSIONS=SPHERES)..NO.16..*          389        AA
        S     SURFN= 5080,TYPE=DISC,SHADE=NO,BSHADE=BOTH,ACTIVE=TCP           390        AA
              P1=0.,0.,594.                                                   391        AA
              P2=0.,11.88,594.                                                392        AA
              P3=11.88,0.,594.                                                393        AA
              P4=11.88,0.,594.                                                394        AA
              PROP=0.,0.                                                      395        AA
              COM=*    ...SPECIAL DISC(DIMENSIONS=SPHERES)..NO.17..*          396        AA
        S     SURFN= 5085,TYPE=DISC,SHADE=NO,BSHADE=BOTH,ACTIVE=TCP           397        AA
              P1=0.,0.,665.                                                   398        AA
              P2=0.,13.30,665.                                                399        AA
              P3=13.30,0.,665.                                                400        AA
              P4=13.30,0.,665.                                                401        AA
              PROP=0.,0.                                                      402        AA
              COM=*    ...SPECIAL DISC(DIMENSIONS=SPHERES)..NO.18..*          403        AA
        S     SURFN= 5090,TYPE=DISC,SHADE=NO,BSHADE=BOTH,ACTIVE=TCP           404        AA
              P1=0.,0.,735.                                                   405        AA
              P2=0.,14.70,735.                                                406        AA
              P3=14.70,0.,735.                                                407        AA
              P4=14.70,0.,735.                                                408        AA
              PROP=0.,0.                                                      409        AA
              COM=*    ...SPECIAL DISC(DIMENSIONS=SPHERES)..NO.19..*          410        AA
        S     SURFN= 5095,TYPE=DISC,SHADE=NO,BSHADE=BOTH,ACTIVE=TCP           411        AA
              P1=0.,0.,806.                                                   412        AA
              P2=0.,16.12,806.                                                413        AA
              P3=16.12,0.,806.                                                414        AA
              P4=16.12,0.,806.                                                415        AA
              PROP=0.,0.                                                      416        AA
              COM=*    ...SPECIAL DISC(DIMENSIONS=SPHERES)..NO.20..*          417        AA
        S     SURFN= 5100,TYPE=DISC,SHADE=NO,BSHADE=BOTH,ACTIVE=TCP           418        AA
              P1=0.,0.,1159.                                                  419        AA
              P2=0.,23.18,1159.                                               420        AA
              P3=23.18,0.,1159.                                               421        AA
              P4=23.18,0.,1159.                                               422        AA
              PROP=0.,0.                                                      423        AA
              COM=*    ...SPECIAL DISC(DIMENSIONS=SPHERES)..NO.21..*          424        AA
        S     SURFN= 5105,TYPE=DISC,SHADE=NO,BSHADE=BOTH,ACTIVE=TCP           425        AA
              P1=0.,0.,1513.                                                  426        AA
              P2=0.,30.26,1513.                                               427        AA
              P3=30.26,0.,1513.                                               428        AA
              P4=30.26,0.,1513.                                               429        AA
              PROP=0.,0.                                                      430        AA
              COM=*    ...SPECIAL DISC(DIMENSIONS=SPHERES)..NO.22..*          431        AA
        S     SURFN= 5110,TYPE=DISC,SHADE=NO,BSHADE=BOTH,ACTIVE=TCP           432        AA
              P1=0.,0.,12300.                                                 433        AA
              P2=0.,30.26,12300.                                              434        AA
              P3=30.26,0.,12300.                                              435        AA
              P4=30.26,0.,12300.                                              436        AA
              PROP=0.,0.                                                      437        AA
              COM=*    ...SPECIAL DISC(DIMENSIONS=SPHERES)..NO.23..*          438        AA
      RCS        BODY                                                         439        AA
```

MODEL = CONTAP RCS ANALYSIS 4/9/75

SURFACE DATA INPUT BLOCK

```
INPUT CARD COL. = 12345678 1 2345678 2 2345678 3 2345678 4 2345678 5 2345678 6 2345678 7 2345678 8 EDIT NO. OLD EDIT NO.  LABEL
                S     SURF=145,TYPE=TRAP,ACTIVE=TOP,SHADE=BOTH,BSHADE=BOTH                                    4.0          AA
                      P1=-698.,102.,0.                                                                        4.1          AA
                      P2=-698.,102.,-125.                                                                     4.2          AA
                      P3=-726.,102.,-125.                                                                     4.3          AA
                      P4=-711.,102.,0.                                                                        4.4          AA
                       PROP=0.,0.                                                                             4.5          AA
                       COM=** Y REAR TAPER*                                                                   4.6          AA
                S     SURF=146,TYPE=RECT,ACTIVE=TOP,SHADE=BOTH,BSHADE=BOTH                                    4.7          AA
                      P1=-726.,-102.,-125.                                                                    4.8          AA
                      P2=-726.,102.,-125.                                                                     4.9          AA
                      P3=-824.,102.,-125.                                                                     4.10         AA
                       PROP=0.,0.                                                                             4.11         AA
                       COM=* REAR FLAT PLATE OUT BACK  *                                                      4.12         AA
                S     SURF=147,TYPE=RECT,ACTIVE=TOP,SHADE=BOTH,BSHADE=BOTH                                    4.13         AA
                      P1=-726.,-102.,-100.                                                                    4.14         AA
                      P2=-726.,102.,-100.                                                                     4.15         AA
                      P3=-824.,102.,-125.                                                                     4.16         AA
                       PROP=0.,0.                                                                             4.17         AA
                       COM=*   SLOPING REAR FLAT PLATE *                                                      4.18         AA
                S       SURF=710,TYPE=DISC,ACTIVE=BOTH,BSHADE=BOTH,SHADE=BOTH                                 4.19         AA
                             DIMENSIONS=0.,0.,3.,0.,360.                                                      4.20         AA
                             PROP=0.,0.                                                                       4.21         AA
                             ICSN=26                                                                          4.22         AA
                             COM=* -Z 1ST RCS X=1519.75 *                                                     4.23         AA
                S       SURF=712,TYPE=DISC,ACTIVE=BOTH,BSHADE=BOTH,SHADE=BOTH                                 4.24         AA
                             DIMENSIONS=0.,0.,3.,0.,360.                                                      4.25         AA
                             ICSN=27                                                                          4.26         AA
                             PROP=0.,0.                                                                       4.27         AA
                             COM=* -Z 2ND RCS X=1532.875 *                                                    4.28         AA
                S       SURF=714,TYPE=DISC,ACTIVE=BOTH,BSHADE=BOTH,SHADE=BOTH                                 4.29         AA
                             DIMENSIONS=0.,0.,3.,0.,360.                                                      4.30         AA
                             ICSN=28                                                                          4.31         AA
                             PROP=0.,0.                                                                       4.32         AA
                             COM=* -Z 3RD RCS X=1545.375 *                                                    4.33         AA
                S       SURF=721,TYPE=DISC,ACTIVE=BOTH,BSHADE=BOTH,SHADE=BOTH                                 4.34         AA
                             P1=-716.,148.75,59.000                                                           4.35         AA
                             P2=-716.,148.75,62.000                                                           4.36         AA
                             P3=-718.,148.75,59.000                                                           4.37         AA
                             P4=-718.,148.75,59.000                                                           4.38         AA
                             PROP=0.,0.                                                                       4.39         AA
                             COM=* +Y 1ST RCS X=1516. *                                                       4.40         AA
                S       SURF=722,TYPE=DISC,ACTIVE=BOTH,BSHADE=BOTH,SHADE=BOTH                                 4.41         AA
                             P1=-729.,148.75,59.000                                                           4.42         AA
                             P2=-729.,148.75,62.000                                                           4.43         AA
                             P3=-732.,148.75,59.000                                                           4.44         AA
                             P4=-732.,148.75,59.000                                                           4.45         AA
                             PROP=0.,0.                                                                       4.46         AA
                             COM=* +Y 2ND RCS X=1529. *                                                       4.47         AA
                S       SURF=724,TYPE=DISC,ACTIVE=BOTH,BSHADE=BOTH,SHADE=BOTH                                 4.48         AA
                             P1=-742.,148.75,59.000                                                           4.49         AA
                             P2=-742.,148.75,62.000                                                           4.50         AA
```

MODEL = CONTAM RCS ANALYSIS 4/9/75
SURFACE DATA INPUT BLOCK

```
INPUT CARD COL. = 12345678 1 2345678 2 2345678 3 2345678 4 2345678 5 2345678 6 2345678 7 2345678 8 EDIT NO. OLD EDIT NO.  LABEL
                       P3=-745.,148.75,59.000                                                                  491          AA
                       P4=-745.,148.75,59.000                                                                  492          AA
                       PROP=0.,0.                                                                              493          AA
                       COM=* +Y 3RD RCS X=1545. *                                                              494          AA
              S      SURF=726,TYPE=DISC,ACTIVE=BOTH,BSHADE=BOTH,SHADE=BOTH                                      495          AA
                       P1=-755.,148.75,59.000                                                                  496          AA
                       P2=-755.,148.75,62.000                                                                  497          AA
                       P3=-758.,148.75,59.000                                                                  498          AA
                       P4=-758.,148.75,59.000                                                                  499          AA
                       PROP=0.,0.                                                                              500          AA
                       COM=* +Y 4TH RCS X=1555. *                                                              501          AA
              S      SURF=733,TYPE=DISC,ACTIVE=BOTH,BSHADE=BOTH,SHADE=BOTH                                      502          AA
                       P1=-715.,132.50,96.5                                                                    503          AA
                       P2=-716.,132.50,96.5                                                                    504          AA
                       P3=-719.,132.50,96.5                                                                    505          AA
                       P4=-719.,132.50,96.5                                                                    506          AA
                       PROP=0.,0.                                                                              507          AA
                       COM=* +Z 1ST RCS X=1516. *                                                              508          AA
              S      SURF=737,TYPE=DISC,ACTIVE=BOTH,BSHADE=BOTH,SHADE=BOTH                                      509          AA
                       P1=-729.,132.50,96.5                                                                    510          AA
                       P2=-729.,135.50,96.5                                                                    511          AA
                       P3=-732.,132.50,96.5                                                                    512          AA
                       P4=-732.,132.50,96.5                                                                    513          AA
                       PROP=0.,0.                                                                              514          AA
                       COM=* +Z 2ND RCS X=1529. *                                                              515          AA
              S      SURF=734,TYPE=DISC,ACTIVE=BOTH,BSHADE=BOTH,SHADE=BOTH                                      516          AA
                       P1=-742.,132.50,96.5                                                                    517          AA
                       P2=-742.,135.50,96.5                                                                    518          AA
                       P3=-745.,132.50,96.5                                                                    519          AA
                       P4=-745.,132.50,96.5                                                                    520          AA
                       PROP=0.,0.                                                                              521          AA
                       COM=* +Z 3RD RCS X=1542. *                                                              522          AA
              S      SURF=741,TYPE=DISC,ACTIVE=BOTH,BSHADE=BOTH,SHADE=BOTH                                      523          AA
                       P1=-725.,0.0,-77.                                                                       524          AA
                       P2=-725.,3.0,-77.                                                                       525          AA
                       P3=-725.,0.0,-74.                                                                       526          AA
                       P4=-725.,0.0,-74.                                                                       527          AA
                       PROP=0.,0.                                                                              528          AA
                       COM=* -X  EVAP. X=1925. CENTER BELL ENGS.*                                              529          AA
              S      SURF=900,TYPE=RECT,ACTIVE=BOTTOM,SHADE=BOTH,BSHADE=BOTH                                    530          AA
                       P1=-644.,89.,-90.                                                                       531          AA
                       P2=-644.,360.,-90.                                                                      532          AA
                       P3=-592.34,360.,-88.333                                                                 533          AA
                       PROP=0.,0.                                                                              534          AA
                       ICSN=20                                                                                 535          AA
                       COM=* EXT. NDED AILERON  TOP*                                                           536          AA
              S      SURF=901,TYPE=RECT,ACTIVE=BOTTOM,SHADE=BOTH,BSHADE=BOTH                                    537          AA
                       P1=-644.,0.,-90.                                                                        538          AA
                       P2=-644.,89.,-90.                                                                       539          AA
                       P3=-592.34,89.,-88.333                                                                  540          AA
                       PROP=0.,0.                                                                              541          AA
```

MODEL = CONTAM RCS ANALYSIS 4/9/75
SURFACE DATA INPUT BLOCK

```
INPUT CARD COL. = 12345678 1 2345678 2 2345678 3 2345678 4 2345678 5 2345678 6 2345678 7 2345678 8  EDIT NO. OLD EDIT NO.  LABEL
                  ICSN=20                                                                          542                    AA
                  COM=* EXTENDED ALERION INNER*                                                    543                    AA
              S   SURF=761,SHADE=BOTH,BSHADE=BOTH,ALPHA=0.,EMISS=0.                                544                    AA
                  TRANS=0.,TRANI=0.,COM=*  -Y   RADIATOR   *                                       545                    AA
                  TYPE=CYLINDER,ACTIVE=BOTH,ALPH=101.                                              546                    AA
                  BMIN=0.,BMAX=360.,GMIN=13.62,GMAX=46.                                            547                    AA
                  NNX=2,NNY=2,ICSN=5                                                               548                    AA
                  POSITION=165.1,104.2,570.                                                        549                    AA
                  ROTZ=-128.1,ROTY=0.,ROTX=0.                                                      550                    AA
              S   SURF=771,SHADE=BOTH,BSHADE=BOTH,ALPHA=0.,EMISS=0.                                551                    AA
                  TRANS=0.,TRANI=0.,COM=*  +Y   RADIATOR   *                                       552                    AA
                  TYPE=CYLINDER,ACTIVE=BOTH,ALPH=101.                                              553                    AA
                  BMIN=0.,BMAX=360.,GMIN=13.62,GMAX=46.38                                          554                    AA
                  NNX=2,NNY=2,ICSN=5                                                               555                    AA
                  POSITION=-165.1,104.2,570.                                                       556                    AA
                  ROTZ=-141.8,ROTY=0.,ROTX=0.                                                      557                    AA
              S   SURF=  140,SHADE=BOTH,BSHADE=BOTH,ALPHA=-0.    ,EMISS=-0.                       558                    AA
                  TRANS=-0.    ,TRANI=-0.    ,COM=*  END  BAY AREA DISK          *                559                    AA
                  TYPE=DISC       ,ACTIVE=TOP     ,ALPH= 0.                                        560                    AA
                  BMIN= 0.          ,BMAX= 1.02000E+02,GMIN= 0.                                    561                    AA
                  GMAX= 3.60000E+02,NNX=     1,NNY=     1,ICSN=    -0                             562                    AA
                  POSITION=240.,0.,0.                                                              563                    AA
                  ROTZ     =    -0.     , ROTY     =    90.0000, ROTX     =     0.               564                    AA
              S   SURF=182,TYPE=PARAB,ACTIVE=OUTSIDE,SHADE=BOTH,BSHADE=BOTH                        565                    AA
                  DIMENSIONS=22.5,7.,40.,25.,238.                                                  566                    AA
                  POSITION=-470.,-78.14,55.56                                                      567                    AA
                   ROTX=180.,ROTY=-90.,ROTZ=0.                                                     568                    AA
                  PROP=0.,0.                                                                       569                    AA
                  ICS=25                                                                           570                    AA
                  COM=* 1ST PARAB -Y OMS *                                                         571                    AA
              S   SURF=184,TYPE=CYLINDER,ACTIVE=OUTSIDE,SHADE=BOTH,BSHADE=BOTH                     572                    AA
                  DIMENSIONS=65.,40.,240.,25.,238.                                                 573                    AA
                  POSITION=-470.,-78.14,55.56                                                      574                    AA
                  ROTX=180.,ROTY=-90.,ROTZ=0.                                                      575                    AA
                  PROP=0.,0.                                                                       576                    AA
                  COM=* OMS END CYLINDER RADIUS=65.*                                               577                    AA
                  ICS=25                                                                           578                    AA
              S   SURF=29,TYPE=TRAP,ACTIVE=TOP,SHADE=BOTH,BSHADE=BOTH                             579                    AA
                  P1=-710.,140.,40.                                                                580                    AA
                  P2=-710.,30.,130.                                                                581                    AA
                  P3=-710.,23.75,112.                                                              582                    AA
                  P4=-710.,120.,17.5                                                               583                    AA
                  PROP=0.,0.                                                                       584                    AA
                  COM=*TRAP BOTTOM OMS END SEALER *                                                585                    AA
                  ICSN=29                                                                          586                    AA
              S   SURF=31,TYPE=DISC,ACTIVE=TOP,SHADE=BOTH,BSHADE=BOTH                             587                    AA
                  P1=-710.,111.48,87.5                                                             588                    AA
                  P2=-710.,141.29,95.                                                              589                    AA
                  P3=-710.,150.625,98.75                                                           590                    AA
                  P4=-710.,140.,40.                                                                591                    AA
                  PROP=0.,0.                                                                       592                    AA
```

MODEL = CONTAM RCS ANALYSIS 4/9/75
SURFACE DATA INPUT BLOCK

```
INPUT CARD COL. = 12345678 1 2345678 2 2345678 3 2345678 4 2345678 5 2345678 6 2345678 7 2345678 8 EDIT NO. OLD EDIT NO.  LABEL
                  COM='1ST TRIANGLE LT SIDE LOOKING BACK'                                                    593              AA
                  ICSN=25                                                                                    594              AA
              S   SURF=32,TYPE=DISC,ACTIVE=TOP,BSHADE=BOTH,SHADE=BOTH                                        595              AA
                  P1=-710.,62.5,71.25                                                                        596              AA
                  P2=-710.,13.75,68.75                                                                       597              AA
                  P3=-710.,50.,131.25                                                                        598              AA
                  P4=-710.,78.75,138.13                                                                      599              AA
                  PROP=0.,0.                                                                                 600              AA
                  COM='LAST TRI RT SIDE '                                                                    601              AA
                  ICS=25                                                                                     602              AA
              S   SURF=172,TYPE=PARAB,ACTIVE=OUTSIDE,SHADE=BOTH,BSHADE=BOTH                                  603              AA
                  DIMENSIONS=22.5,7.,40.,-56.,156.                                                           604              AA
                  PROP=0.,0.                                                                                 605              AA
                  POSITION=-470.,78.14,65.56                                                                 606              AA
                  ROTX=0.,ROTY=-90.,ROTZ=0.                                                                  607              AA
                  ICS=25                                                                                     608              AA
                  COM=' 1ST PARAB +Y OMS'                                                                    609              AA
              S   SURF=174,TYPE=CYLINDER,ACTIVE=OUTSIDE,SHADE=BOTH,BSHADE=BOTH                               610              AA
                  DIMENSIONS=65.,40.,240.,-56.,156.                                                          611              AA
                  POSITION=-470.,78.14,65.56                                                                 612              AA
                  ROTX=0.,ROTY=-90.,ROTZ=0.                                                                  613              AA
                  PROP=0.,0.                                                                                 614              AA
                  ICS=25                                                                                     615              AA
                  COM=' +Y OMS END CYLINDER '                                                                616              AA
              S   SURF=33,TYPE=DISC,ACTIVE=BOTTOM,BSHADE=BOTH,SHADE=BOTH                                     617              AA
                  P1=-710.,46.88,68.75                                                                       618              AA
                  P2=-710.,130.,27.                                                                          619              AA
                  P3=-710.,150.,56.88                                                                        620              AA
                  P4=-710.,137.5,105.                                                                        621              AA
                  PROP=0.,0.                                                                                 622              AA
                  ICSN=25                                                                                    623              AA
                  COM='2ND TRI LEFT SIDE'                                                                    624              AA
              S   SURF=34,TYPE=DISC,ACTIVE=TOP,SHADE=BOTH,BSHADE=BOTH                                        625              AA
                  P1=-710.,41.25,84.38                                                                       626              AA
                  P2=-710.,43.13,124.375                                                                     627              AA
                  P3=-710.,76.875,138.75                                                                     628              AA
                  P4=-710.,120.625,121.875                                                                   629              AA
                  PROP=0.,0.                                                                                 630              AA
                  ICSN=25                                                                                    631              AA
                  COM='3RD TRI MIDDLE RT SIDE'                                                               632              AA
              S   SURF=35,TYPE=POLY,ACTIVE=TOP,SHADE=BOTH,BSHADE=BOTH                                        633              AA
                  P1=-710.,90.88,68.75                                                                       634              AA
                  P2=-710.,137.5,105.                                                                        635              AA
                  P3=-710.,120.625,121.875                                                                   636              AA
                  P4=-710.,81.25,84.38                                                                       637              AA
                  PROP=0.,0.                                                                                 638              AA
                  ICSN=25                                                                                    639              AA
                  COM='TOP INSIDE TRAP '                                                                     640              AA
              S   SURF=24,TYPE=DISC,ACTIVE=BOTH,BSHADE=BOTH,SHADE=BOTH                                       641              AA
                  P1=-765.,149.37,59.                                                                        642              AA
                  P2=-765.,149.37,62.                                                                        643              AA
```

MODEL = CONTAM   RCS ANALYSIS   4/9/75
SURFACE DATA INPUT BLOCK

```
INPUT CARD COL. = 12345678 1 2345678 2 2345678 3 2345678 4 2345678 5 2345678 6 2345678 7 2345678 8 EDIT NO. OLD EDIT NO.  LABEL
                  1
                P3=-768.,149.37,59.                                          644                  AA
                P4=-768.,149.37,59.                                          645                  AA
                PROP=0.,0.                                                   646                  AA
                ICSN=25                                                      647                  AA
                COM=*REAR Y RCS (Y WAS 134. ALL REST SAME)*                  648                  AA
     S          SURF=26,TYPE=DISC,ACTIVE=BOTH,SHADE=BOTH,BSHADE=BOTH         649                  AA
                P1=-765.,118.,51.                                            650                  AA
                P2=-765.,115.,51.                                            651                  AA
                P3=-768.,118.,51.                                            652                  AA
                P4=-768.,118.,51.                                            653                  AA
                PROP=0.,0.                                                   654                  AA
                ICSN=25                                                      655                  AA
                COM=*REAR Z RCS (Z WAS 57. ALL REST THE SAME)*               656                  AA
     S        SURF=149,TYPE=TRAP,ACTIVE=BOTTOM,SHADE=BOTH,BSHADE=BOTH        657                  AA
              P1=-698.,-102.,0.                                              658                  AA
              P2=-698.,-102.,-125.                                           659                  AA
              P3=-728.,-102.,-125.                                           660                  AA
              P4=-711.,-102.,0.                                              661                  AA
              PROP=0.,0.                                                     662                  AA
              COM= * - Y. REAR SIDE TAPER...*                                663                  AA
     S          SURFN=707,TYPE=DISC,ACTIVE=BOTH,SHADE=BOTH,BSHADE=BOTH       664                  AA
                P1=218.,104.,-47.                                            665                  AA
                P2=213.,104.,-50.                                            666                  AA
                P3=215.,104.,-47.                                            667                  AA
                P4=215.,104.,-47.                                            668                  AA
                PROP=0.,0.                                                   669                  AA
                COM=*......JULY 8 EVAP..3 IN. RAD. UP FRONT CLOSE UNDER WING* 670                 AA
     S        SURF=800,TYPE=PARAB,ACTIVE=OUT,SHADE=BOTH,BSHADE=BOTH          671                  AA
              DIMENSIONS=4.4,0.0,100.,0.,360.                                672                  AA
              ICSN=13                                                        673                  AA
              PROP=0.,0.                                                     674                  AA
              NNX=2,NNY=2                                                    675                  AA
              COM=* TOP  ENGIN *                                             676                  AA
     S        SURF=805,TYPE=PARAB,ACTIVE= OUT,SHADE=BOTH,BSHADE=BOTH         677                  AA
              DIMENSIONS=4.4,0.0,100.,0.,360.                                678                  AA
              ICSN=14,TY=+50.                                                679                  AA
                 PROP=0.,0.                                                  680                  AA
              NNX=2,NNY=2                                                    681                  AA
              COM = * + Y ENGIN *                                            682                  AA
     S        SURF=810,TYPE=PARAB,ACTIVE=OUT,SHADE=BOTH,BSHADE=BOTH          683                  AA
              DIMENSIONS=4.4,0.0,100.,0.,360.                                684                  AA
              ICSN = 14, TY =-50.                                            685                  AA
                 PROP=0.,0.                                                  686                  AA
              NNX=2,NNY=2                                                    687                  AA
              COM = * -Y ENGIN...*                                           688                  AA
     S        SURF=20,TYPE=DISC,ACTIVE=OUT,SHADE=BOTH,BSHADE=BOTH            689                  AA
                 DIMENSIONS=0.0,0.0,25.,125.,335.                            690                  AA
              PROP=0.,0.                                                     691                  AA
              ICSN=11                                                        692                  AA
              COM = * ...-Y OWS SEALER ...*                                  693                  AA
     S        SURF=21,TYPE=DISC,ACTIVE=OUT,SHADE=BOTH,BSHADE=BOTH            694                  AA
```

MODEL = CONTAM RCS ANALYSIS 4/9/75
SURFACE DATA INPUT BLOCK

```
INPUT CARD COL. = 12345678 1 2345678 2 2345678 3 2345678 4 2345678 5 2345678 6 2345678 7 2345678 8 EDIT NO. OLD EDIT NO. LABEL
                      DIMENSIONS=0.0,0.0,25.,29.,235.                                                    695                AA
                    PROP=0.,0.                                                                           696                AA
                    ICSN=12                                                                              697                AA
                    COM= * ..+Y OMS SEALER ...*                                                          698                AA
               S      SURF=222,TYPE=RECT,ACTIVE=BOTTOM,SHADE=BOTH,BSHADE=BOTH                            699                AA
                    P1=-723.,-102.,-125.                                                                 700                AA
                    P2=-723.,102.,-125.                                                                  701                AA
                     P3=-711.,102.,0.0                                                                   702                AA
                     PROP=0.,0.                                                                          703                AA
                     COM=*  BACK RECT   7.350EG*                                                         704                AA
               S      SURF=22,TYPE=DISC,ACTIVE=BOTH,SHADE=BOTH,BSHADE=BOTH                               705                AA
                    DIMENSIONS=0.0,0.0,102.,90.,270.                                                     706                AA
                    PROP=0.,0.                                                                           707                AA
                    ICSN=15                                                                              708                AA
                    COM=* REAR END HALF DISK*                                                            709                AA
               S      SURF=407,TYPE=DISC,ACTIVE=TOP,SHADE=BOTH,BSHADE= BOTH                              710                AA
                    P1=-592.0,113.,-77.                                                                  711                AA
                    P2=-592.0,113.,-80.                                                                  712                AA
                    P3=-595.0,113.,-77.                                                                  713                AA
                    P4=-595.0,113.,-77.                                                                  714                AA
                    PROP=0.,0.                                                                           715                AA
                    COM=*  BACK SIDE EVAPORAT, UPDATED JULY 18, 0 IN DIA.*                               716                AA
               S      SURF=15,TYPE=DISC,ACTIVE=TOP,SHADE=BOTH,BSHADE=BOTH                                717                AA
                    P1=-719.,126.,-95.                                                                   718                AA
                    P2=-719.,126.,-98.                                                                   719                AA
                    P3=-722.,126.,-95.                                                                   720                AA
                    P4=-722.,126.,-95.                                                                   721                AA
                    PROP=0.,0.                                                                           722                AA
                    COM=* REAR END EVAPORATOR*                                                           723                AA
               S      SURF=10,TYPE=POLY,ACTIVE=BOTTOM,SHADE=BOTH,BSHADE=BOTH                             724                AA
                    P1=230.,0.,-102.                                                                     725                AA
                    P2=-192.,-89.,-60.                                                                   726                AA
                    P3=-192.,0.,-60.                                                                     727                AA
                    ICSN=21                                                                              728                AA
                    PROP=0.,0.                                                                           729                AA
                    COM=*....LEFT FRONT WING  A ...*                                                     730                AA
               S      SURF=11,TYPE=POLY,ACTIVE=TOP,SHADE=BOTH,BSHADE=BOTH                                731                AA
                    P1=-192.,-89.,-60.                                                                   732                AA
                    P2=-483.,-89.,-85.                                                                   733                AA
                    P3=-483.,-366.,-85.                                                                  734                AA
                    ICSN=21                                                                              735                AA
                    PROP=0.,0.                                                                           736                AA
                    COM=*......LEFT MIDDLE WING BACK.B ... *                                             737                AA
               S      SURF=141,TYPE=RECT,ACTIVE=TOP,BSHADE=BOTH,SHADE=BOTH                               738                AA
                     P1=-192.,0.,-60.                                                                    739                AA
                    P2=-483.,0.,-85.                                                                     740                AA
                    P3=-483.,-89.,-85.                                                                   741                AA
                     ICSN=21                                                                             742                AA
                     PROP=0.,0.                                                                          743                AA
                     COM=*  MS INNER WING        *                                                       744                AA
               S      SURF=14,TYPE=RECT,ACTIVE=TOP,SHADE=BOTH,BSHADE=BOTH                                745                AA
```

MODEL = CONTAM RCS ANALYSIS 4/9/75
SURFACE DATA INPUT BLOCK

```
INPUT CARD COL. = 12345678 1 2345678 2 2345678 3 2345678 4 2345678 5 2345678 6 2345678 7 2345678 8 EDIT NO. OLD EDIT NO. LABEL
                  P1=-644.,-89.,-90.                                                                    740          AA
                  P2=-644.,-366.,-90.                                                                   741          AA
                  P3=-483.,-366.,-85.                                                                   742          AA
                  ICSN=21                                                                               743          AA
                  PROP=0.,0.                                                                            744          AA
                  COM=* ..... LEFT BACK RECT. WING C .... *                                             745          AA
              S    SURF=142,TYPE=RECT,ACTIVE=TOP,SHADE=BOTH,BSHADE=BOTH                                 746          AA
                  P1=-644.,0.,-90.                                                                      747          AA
                  P2=-644.,-89.,-90.                                                                    748          AA
                  P3=-483.,-89.,-85.                                                                    749          AA
                  ICSN=21                                                                               750          AA
                  PROP=0.,0.                                                                            751          AA
                  COM=*  INNER WING C*                                                                  752          AA
              S   SURF=13,TYPE=POLY,ACTIVE=TOP,SHADE=BOTH,BSHADE=BOTH                                   753          AA
                  P1=-698.,0.,-102.                                                                     754          AA
                  P2=-644.,-366.,-90.                                                                   755          AA
                  P3=-644.,0.,-90.                                                                      756          AA
                  PROP=0.,0.                                                                            757          AA
                  ICSN=21                                                                               758          AA
                  COM=* ..... LEFT WING TAIL  EDGE  ..0 . *                                             759          AA
              S   SURF=1,TYPE=POLY,ACTIVE=TOP,SHADE=BOTH,BSHADE=BOTH                                    760          AA
                  P1=250.,0.,-70.                                                                       761          AA
                  P2=-192.,89.,-60.                                                                     762          AA
                  P3=-192.,0.,-60.                                                                      763          AA
                  PROP= 0.,0.                                                                           764          AA
                  ICSN=21                                                                               765          AA
                  COM=*...FRONT WING TRIANGLE RT.A.332.1024*                                            766          AA
              S   SURF=2,TYPE=POLY,ACTIVE=BOTTOM,SHADE=BOTH,BSHADE=BOTH                                 767          AA
                  PROP=0.,0.                                                                            768          AA
                  P1=-192.,89.,-60.                                                                     769          AA
                  P2=-483.,89.,-85.                                                                     770          AA
                  P3=-483.,366.,-85.                                                                    771          AA
                  COM=*.....MIDDLE WING TRAP, RT B ..1024,1292*                                         772          AA
                  ICSN=21                                                                               773          AA
              S    SURF=143,TYPE=RECT,ACTIVE=BOTTOM,SHADE=BOTH,BSHADE=BOTH                              774          AA
                  P1=-192.,0.,-60.                                                                      775          AA
                  P2=-483.,0.,-85.                                                                      776          AA
                  P3=-483.,89.,-85.                                                                     777          AA
                  PROP=0.,0.                                                                            778          AA
                  ICSN=23                                                                               779          AA
                  COM=*B  +Y RECTANGLE WING*                                                            780          AA
              S    SURF=3,TYPE=RECT,ACTIVE=BOTTOM,SHADE=BOTH,BSHADE=BOTH                                781          AA
                  P1=-593.34,89.,-68.333                                                                782          AA
                   P2=-593.34,366.,-68.333                                                              783          AA
                  P3=-483.,366.,-85.                                                                    784          AA
                  PROP=0.,0.                                                                            785          AA
                  ICSN=23                                                                               786          AA
                  COM=*.... BACK WING RECT.  RTC .1292,1493*                                            787          AA
              S    SURF=144,TYPE=RECT,ACTIVE=BOTTOM,SHADE=BOTH,BSHADE=BOTH                              788          AA
                 P1=-593.34,0.,-68.333                                                                  789          AA
                  P2=-593.34,89.,-68.333                                                                790          AA
```

```
MODEL = CONIAM                                   RCS ANALYSIS     4/9/75
SURFACE DATA INPUT BLOCK

INPUT CARD COL. = 12345678 1 2345678 2 2345678 3 2345678 4 2345678 5 2345678 6 2345678 7 2345678 8 EDIT NO. OLD EDIT NO.  LABEL

           P3=-483.,39.,-85.                                                          797     AA
            PROP=0.,0.                                                                798     AA
            ICSN=20                                                                   799     AA
            COM=*   INNER WING C RECT*                                                800     AA
   S        SURF=4,TYPE=POLY,ACTIVE=BOTTOM,SHADE=BOTH,BSHADE=BOTH                     801     AA
            P1=-698.,0.,-102.                                                         802     AA
            P2=-644.,356.,-90.                                                        803     AA
            P3=-644.,0.,-90.                                                          804     AA
            PROP=0.,0.                                                                805     AA
            ICSN=20                                                                   806     AA
            COM=* +Y WING TAIL EDGE       *                                           807     AA
   S       SURFN=  150,SHADE=BOTH,BSHADE=BOTH,ALPHA=-0.    ,EMISS=-0.                 808     AA
           TRANS=-0.    ,TRANI=-0.    ,COM=*BAY AREA CYLINDER               *         809     AA
           TYPE=CYLINDER   ,ACTIVE=INSIDE ,ALPH= 1.02000E+02                          810     AA
           BMIN= 0.           ,BMAX= 7.00000E+02,GMIN= 0.                             811     AA
           GMAX= 1.80000E+02,NNX=     2,NNY=     4,ICSN=    -0                        812     AA
           POSITION=-4.70000E+02, 0.              , 0.                                813     AA
           ROTZ     =    -0.     , ROTY     =    90.0000, ROTX     =     0.           814     AA
   S       SURFN=  135,SHADE=BOTH,BSHADE=BOTH,ALPHA=-0.    ,EMISS=-0.                 815     AA
           TRANS=-0.    ,TRANI=-0.    ,COM=* FRONT BAY AREA DISK            *         816     AA
           TYPE=DISC         ,ACTIVE=TOP     ,ALPH= 0.                                817     AA
           BMIN= 0.           ,BMAX= 1.02000E+02,GMIN= 0.                             818     AA
           GMAX= 3.60000E+02,NNX=     1,NNY=     1,ICSN=    -0                        819     AA
           POSITION= 2.30000E+02, 0.              , 0.                                820     AA
           ROTZ     =    -0.     , ROTY     =   -90.0000, ROTX     =     0.           821     AA
   S       SURFN=  122,SHADE=BOTH,BSHADE=BOTH,ALPHA=-0.    ,EMISS=-0.                 822     AA
           TRANS=-0.    ,TRANI=-0.    ,COM=* VERY NOSE CONE                 *         823     AA
           TYPE=PARABOLOID,ACTIVE=OUTSIDE,ALPH= 6.13000E+00                           824     AA
           BMIN= 0.           ,BMAX= 2.00000E+02,GMIN= 0.                             825     AA
           GMAX= 3.60000E+02,NNX=     4,NNY=     1,ICSN=     1                        826     AA
           POSITION= 2.00000E+02, 0.              ,-3.00000E+01                       827     AA
           ROTZ     = -180.0000, ROTY     =   -90.0000, ROTX     =     0.             828     AA
   S       SURFN= 320,SHADE=BOTH,BSHADE=BOTH,ALPHA=-0.    ,EMISS=-0.                  829     AA
           TRANS=-0.    ,TRANI=-0.    ,COM=*   NOSE CYLINDER                *         830     AA
           TYPE=CYLINDER   ,ACTIVE=OUTSIDE,ALPH= 7.00000E+01                          831     AA
           BMIN= 0.           ,BMAX= 1.70000E+02,GMIN= 0.                             832     AA
           GMAX= 3.60000E+02,NNX=     4,NNY=     4,ICSN=     1                        833     AA
           POSITION= 4.00000E+02, 0.              ,-3.00000E+01                       834     AA
           ROTZ     = -180.0000, ROTY     =   -90.0000, ROTX     =     0.             835     AA
   S       SURFN= 340,SHADE=BOTH,BSHADE=BOTH,ALPHA=-0.    ,EMISS=-0.                  836     AA
           TRANS=-0.    ,TRANI=-0.    ,COM=*   HOOD PARTIAL BACK            *         837     AA
           TYPE=PARABOLOID,ACTIVE=OUTSIDE,ALPH= 7.03000E+00                           838     AA
           BMIN= 2.60000E+02,BMAX= 3.70000E+02,GMIN= 0.                               839     AA
           GMAX= 3.60000E+02,NNX=     4,NNY=     4,ICSN=     1                        840     AA
           POSITION= 2.00000E+02, 0.              , 0.                                841     AA
           ROTZ     = -180.0000, ROTY     =   -90.0000, ROTX     =     0.             842     AA
   S       SURFN= 360,SHADE=BOTH,BSHADE=BOTH,ALPHA=-0.    ,EMISS=-0.                  843     AA
           TRANS=-0.    ,TRANI=-0.    ,COM=* WINDOW                         *         844     AA
           TYPE=PARABOLOID,ACTIVE=OUTSIDE,ALPH= 2.38000E+01                           845     AA
           BMIN= 1.64000E+01,BMAX= 7.68000E+01,GMIN= 0.                               846     AA
           GMAX= 3.60000E+02,NNX=     4,NNY=     4,ICSN=     1                        847     AA
```

MODEL = CONTAM RCS ANALYSIS 4/9/75
SURFACE DATA INPUT BLOCK

```
INPUT CARD COL. = 12345678 1 2345678 2 2345678 3 2345678 4 2345678 5 2345678 6 2345678 7 2345678 8 EDIT NO. OLD EDIT NO. LABEL
                  POSITION= 3.852CCE+02, 0.          , 0.                                                    846          AA
                  ROTZ     = -180.0000, ROTY     =  -90.0000, ROTX     =    0.                              849          AA
              S   SURFN=  401,SHADE=BOTH,BSHADE=BOTH,ALPHA=  .900,EMISS=  .900                               850          AA
                  TRANS=-0.    ,TRANI=-0.    ,COM=*BODY BOTTOM (FRT)        4 1   *                       851          AA
                  TYPE=RECTANGLE ,ACTIVE=BOTTOM ,ALPH= 0.                                                    852          AA
                  BMIN=-1.2200DE+02,BMAX= 1.02000E+02,GMIN= 0.                                               853          AA
                  GMAX= 2.2600DE+02,NNX=     1,NNY=     1,ICSN=     1                                        854          AA
                  POSITION= 5.7000DE+02, 0.          ,-1.020000E+02                                          855          AA
                  ROTZ     =    -0.    , ROTY     =    3.3870, ROTX     =    0.                             856          AA
              S   SURFN=  402,SHADE=BOTH,BSHADE=BOTH,ALPHA=  .900,EMISS=  .900                               857          AA
                  TRANS=-0.    ,TRANI=-0.    ,COM=*BODY BOTTOM (REAR)       402   *                       858          AA
                  TYPE=RECTANGLE ,ACTIVE=BOTTOM ,ALPH=-1.2500DE+02                                           859          AA
                  BMIN=-1.02000E+02,BMAX= 1.02000E+02,GMIN= 2.2500DE+02                                      860          AA
                  GMAX= 9.3000DE+02,NNX=     1,NNY=     1,ICSN=     1                                        861          AA
                  POSITION= 5.7000DE+02, 0.          , 0.                                                    862          AA
                  ROTZ     =    -0.    , ROTY     =    -0.    , ROTX     =    0.                             863          AA
              S   SURFN=  701,TYPE=CYL,ACTIVE=BOTH,SHADE=BOTH,BSHADE=BOTH                                    864          AA
                  P1=230.,201.34,37.98                                                                       865          AA
                  P2=230.,103.,19.                                                                           866          AA
                  P3=230.,201.34,-64.02                                                                      867          AA
                  P4=-470.,201.34,-64.02                                                                     868          AA
                  PROP=0.,0.                                                                                 869          AA
                  NNX=2,NNY=2                                                                                870          AA
                  COM=*.....+Y SIDE DOOR.....*                                                               871          AA
              S   SURFN=  791,TYPE=CYL,ACTIVE=BOTH,SHADE=BOTH,BSHADE=BOTH                                    872          AA
                  P1=230.,-201.34,37.98                                                                      873          AA
                  P2=230.,-201.34,-64.02                                                                     874          AA
                  P3=230.,-103.,19.                                                                          875          AA
                  P4=-470.,-103.,19.                                                                         876          AA
                  PROP=0.,0.                                                                                 877          AA
                  NNX=2,NNY=2                                                                                878          AA
                  COM=*.... -Y SIDE DOOR....*                                                                879          AA
              S   SURFN=  301,TYPE=TRAP,BSHADE=BOTH,SHADE=BOTH,ACTIVE=TOP                                    880          AA
                  P1=230.,102.,-102.                                                                         881          AA
                  P2=4.,102.,-125.                                                                           882          AA
                  P3=4.,102.,19.                                                                             883          AA
                  P4=230.,102.,19.                                                                           884          AA
                  COM=* +Y SIDE FRONT TRAPOZOID*                                                             885          AA
                  PROP=0.,0.                                                                                 886          AA
              S   SURFN=  305,SHADE=BOTH,BSHADE=BOTH,ALPHA=  .900,EMISS=  .900                               887          AA
                  TRANS=-0.    ,TRANI=-0.    ,COM=*BODY SIDE (MIDDLE-PORT)   305 *                         888          AA
                  TYPE=RECTANGLE ,ACTIVE=TOP     ,ALPH= 1.02000E+02                                          889          AA
                  BMIN=-1.2500DE+02,BMAX= 19.        ,GMIN= 2.2500DE+02                                      890          AA
                  GMAX= 5.7200DE+02,NNX=     1,NNY=     1,ICSN=     1                                        891          AA
                  POSITION= 5.7000DE+02, 0.          , 0.                                                    892          AA
                  ROTZ     =    -0.    , ROTY     =    -0.    , ROTX     =   90.0000                        893          AA
              S   SURFN=  306,SHADE=BOTH,BSHADE=BOTH,ALPHA=  .900,EMISS=  .900                               894          AA
                  TRANS=-0.    ,TRANI=-0.    ,COM=*BODY SIDE (BACK-PORT)     306 *                        895          AA
                  TYPE=RECTANGLE ,ACTIVE=TOP     ,ALPH= 1.02000E+02                                          896          AA
                  BMIN=-1.2500DE+02,BMAX= 19.        ,GMIN= 5.7200DE+02                                      897          AA
                  GMAX= 9.3000DE+02,NNX=     1,NNY=     1,ICSN=     1                                        898          AA
```

MODEL = CONTAM RCS ANALYSIS 4/9/75
SURFACE DATA INPUT BLOCK

```
INPUT CARD COL. = 12345678 1 2345678 2 2345678 3 2345678 4 2345678 5 2345678 6 2345678 7 2345678 8 EDIT NO. OLD EDIT NO. LABEL
                  POSITION= 5.700000E+02, 0.          , 0.                                                    899          AA
                  ROTZ    =   -0.     , ROTY    =   -0.     , ROTX    =   90.0000                          900          AA
              S   SURFN=  311,TYPE=TRAP,BSHADE=BOTH,SHADE=BOTH,ACTIVE=BOTTOM                                 901          AA
                  P1=230.,102.,-102.                                                                        902          AA
                  P2=4.,102.,-125.                                                                          903          AA
                  P3=4.,102.,19.                                                                            904          AA
                  P4=230.,102.,19.                                                                          905          AA
                  COM=* -Y SIDE FRONT TRAPOZOID*                                                            906          AA
                  PROP=0.,0.                                                                                907          AA
              S   SURFN=  315,SHADE=BOTH,BSHADE=BOTH,ALPHA=  .900,EMISS=  .900                              908          AA
                  TRANS=-0.   ,TRANI=-0.   ,COM=*BODY SIDE (MIDDLE-STBD)   315 *                            909          AA
                  TYPE=RECTANGLE ,ACTIVE=TOP    ,ALPH= 1.000000E+02                                         910          AA
                  BMIN= 19.        ,BMAX= 1.250000E+02,GMIN= 2.250000E+02                                   911          AA
                  GMAX= 5.700000E+02,NMX=    1,NNY=    1,ICSN=    1                                         912          AA
                  POSITION= 5.700000E+02, 0.          , 0.                                                  913          AA
                  ROTZ    =   -0.     , ROTY    =   -0.     , ROTX    =  -90.0000                          914          AA
              S   SURFN=  316,SHADE=BOTH,BSHADE=BOTH,ALPHA=  .900,EMISS=  .900                              915          AA
                  TRANS=-0.   ,TRANI=-0.   ,COM=*BODY SIDE (BACK-STBD)     316 *                        916          AA
                  TYPE=RECTANGLE ,ACTIVE=TOP    ,ALPH= 1.000000E+02                                         917          AA
                  BMIN= 19.        ,BMAX= 1.250000E+02,GMIN= 5.720000E+02                                   918          AA
                  GMAX= 9.300000E+02,NMX=    1,NNY=    1,ICSN=    1                                         919          AA
                  POSITION= 5.700000E+02, 0.          , 0.                                                  920          AA
                  ROTZ    =   -0.     , ROTY    =   -0.     , ROTX    =  -90.0000                          921          AA
              S   SURFN=  202,SHADE=BOTH,BSHADE=BOTH,ALPHA=  .900,EMISS=  .900                              922          AA
                  TRANS=-0.   ,TRANI=-0.   ,COM=*BODY TOP (STBD-REAR)  202     *                          923          AA
                  TYPE=CYLINDER  ,ACTIVE=OUTSIDE,ALPH= 1.000000E+02                                         924          AA
                  BMIN= 7.000000E+02,BMAX= 9.300000E+02,GMIN= 2.700000E+02                                  925          AA
                  GMAX= 3.600000E+02,NMX=    1,NNY=    1,ICSN=    1                                         926          AA
                  POSITION= 5.700000E+02, 0.          , 0.                                                  927          AA
                  ROTZ    =   -0.     , ROTY    =   90.0000, ROTX    =    0.                              928          AA
              S   SURFN=  212,SHADE=BOTH,BSHADE=BOTH,ALPHA=  .900,EMISS=  .900                              929          AA
                  TRANS=-0.   ,TRANI=-0.   ,COM=*BODY TOP (PORT-REAR)  212     *                          930          AA
                  TYPE=CYLINDER  ,ACTIVE=OUTSIDE,ALPH= 1.000000E+02                                         931          AA
                  BMIN= 7.000000E+02,BMAX= 9.300000E+02,GMIN= 1.800000E+02                                  932          AA
                  GMAX= 2.700000E+02,NMX=    1,NNY=    1,ICSN=    1                                         933          AA
                  POSITION= 5.700000E+02, 0.          , 0.                                                  934          AA
                  ROTZ    =   -0.     , ROTY    =   90.0000, ROTX    =    0.                              935          AA
              S   SURFN=  385 ,SHADE=BOTH,BSHADE=BOTH,ALPHA=  .900,EMISS=  .900                              936          AA
                  TRANS=-0.   ,TRANI=-0.   ,COM=*VERTICAL FIN (PORT)     20     *                          937          AA
                  TYPE=TRAPEZOID ,ACTIVE=TOP    ,ALPH= 0.                                                   938          AA
                  BMIN= 1.484600E+02,BMAX= 3.934600E+02,GMIN= 3.000000E+01                                  939          AA
                  GMAX= 4.500000E+01,NMX=    1,NNY=    1,ICSN=    1                                         940          AA
                  POSITION= 1.658460E+03, 0.          , 4.954600E+02                                        941          AA
                  ROTZ    =   -0.     , ROTY    = -180.0000, ROTX    =   90.0000                          942          AA
              S   SURFN=  385,SHADE=BOTH,BSHADE=BOTH,ALPHA=  .900,EMISS=  .900                              943          AA
                  TRANS=-0.   ,TRANI=-0.   ,COM=*VERTICAL FIN (PORT-AFT) 20     *                          944          AA
                  TYPE=TRAPEZOID ,ACTIVE=TOP    ,ALPH= 0.                                                   945          AA
                  BMIN= 1.484600E+02,BMAX= 3.934600E+02,GMIN= 1.500000E+01                                  946          AA
                  GMAX= 3.000000E+01,NMX=    1,NNY=    1,ICSN=    1                                         947          AA
                  POSITION= 1.658460E+03, 0.          , 4.954600E+02                                        948          AA
                  ROTZ    =   -0.     , ROTY    = -180.0000, ROTX    =   90.0000                          949          AA
```

```
MODEL = CONTAM                                      RCS ANALYSIS      4/9/75
SURFACE DATA INPUT BLOCK

INPUT CARD COL. = 12345678 1 2345678 2 2345678 3 2345678 4 2345678 5 2345678 6 2345678 7 2345678 8 EDIT NO. OLD EDIT NO.  LABEL

        S     SURFN= 393,SHADE=BOTH,BSHADE=BOTH,ALPHA=  .900,EMISS=  .900          950      AA
              TRANS=-0.   ,TRANI=-0.   ,COM=*VERTICAL FIN (STBD)      20    *     951      AA
              TYPE=TRAPEZOID ,ACTIVE=BOTTOM ,ALPH= 0.                              952      AA
              BMIN= 1.48400E+02,BMAX= 3.93400E+02,GMIN= 3.00000E+01                953      AA
              GMAX= 4.50000E+01,NNX=     1,NNY=     1,ICSN=    1                   954      AA
              POSITION= 1.69840E+03, 1.00000E-01, 4.95400E+02                      955      AA
              ROTZ     =   -0.     , ROTY     = -180.0000, ROTX     =   90.0000    956      AA
        S     SURFN= 395,SHADE=BOTH,BSHADE=BOTH,ALPHA=  .900,EMISS=  .900          957      AA
              TRANS=-0.   ,TRANI=-0.   ,COM=*VERTICAL FIN (STBD-AFT) 20    *      958      AA
              TYPE=TRAPEZOID ,ACTIVE=BOTTOM ,ALPH= 0.                              959      AA
              BMIN= 1.48400E+02,BMAX= 3.93400E+02,GMIN= 1.50000E+01                960      AA
              GMAX= 3.00000E+01,NNX=     1,NNY=     1,ICSN=    1                   961      AA
              POSITION= 1.69840E+03, 1.00000E-01, 4.95400E+02                      962      AA
              ROTZ     =   -0.     , ROTY     = -180.0000, ROTX     =   90.0000    963      AA
        S      SURF=705,TYPE=DISC,ACTIVE=TOP,SHADE=BOTH,BSHADE=BOTH                964      AA
               P1=327.,85.,-72.                                                    965      AA
               P2=327.,85.,-75.                                                    966      AA
               P3=324.,85.,-72.                                                    967      AA
               P4=324.,85.,-72.                                                    968      AA
               PROP=0.,0.                                                          969      AA
               COM=*..MOST FORWARD EVAPORATOR.....LOOKING +Y,6 IN DIA.*            970      AA
        S     SURFN=700,TYPE=DISC,ACTIVE=BOTH,BSHADE=BOTH,SHADE=BOTH               971      AA
              DIMENSIONS=0.,0.,22.5,0.,360.                                        972      AA
              ICSN=16,PROP=0.,0.                                                   973      AA
              COM=*.......SUPER ENGINS (OMS LOCATION)..+Y..*                       974      AA
        S     SURFN=702,TYPE=DISC,ACTIVE=BOTH,BSHADE=BOTH,SHADE=BOTH               975      AA
              DIMENSIONS=70.,0.,22.5,0.,360.                                       976      AA
              ICSN=17,PROP=0.,0.                                                   977      AA
              COM=*.......SUPER ENGINS (OMS LOCATION)..-Y..*                       978      AA
        S     SURFN=13,TYPE=DISC,ACTIVE=BOTH,SHADE=BOTH,BSHADE=BOTH                979      AA
              P1=467.5,50.,-41.9                                                   980      AA
              P2=470.5,50.,-41.9                                                   981      AA
              P3=467.5,52.497,-47.18                                               982      AA
              P4=467.5,52.497,-47.18                                               983      AA
              PROP=0.,0.                                                           984      AA
              COM=*...FRONT RCS..LOOKING +/-Y AT 35 DEG. 7/23/74...*               985      AA
        S     SURFN=16,TYPE=DISC,ACTIVE=BOTH,SHADE=BOTH,BSHADE=BOTH                986      AA
              P1=-247.,105.,-21.                                                   987      AA
              P2=-247.,105.,-24.                                                   988      AA
              P3=-250.,105.,-21.                                                   989      AA
              P4=-250.,105.,-21.                                                   990      AA
              PROP=0.,0.                                                           991      AA
              COM=*...MIDDLE EVAP. LOOKING +/- Y.........*                         992      AA
        S     SURFN= 394,SHADE=BOTH,BSHADE=BOTH,ALPHA=  .900,EMISS=  .900          993      AA
              TRANS=-0.   ,TRANI=-0.   ,COM=*VERT. FIN LDG. EDGE      2    *      994      AA
              TYPE=RECTANGLE ,ACTIVE=TOP    ,ALPH= 0.                              995      AA
              BMIN=-6.00000E+00,BMAX= 6.00000E+00,GMIN=-5.50000E+02                996      AA
              GMAX=-2.15000E+02,NNX=     1,NNY=     1,ICSN=    1                   997      AA
              POSITION= 1.69840E+03, 0.          , 4.95400E+02                     998      AA
              ROTZ     =   -0.     , ROTY     =  -45.0000, ROTX     =    0.        999      AA
```

2.5.2 VIEW FACTOR DATA MATRIX

The following pages contain the input data computer printout for the Shuttle Orbiter configuration.

MODEL = RIO STEP = 1 RCS ANALYSIS 4/9/75
FORM FACTOR CALCULATION LINK.

5000 FF SUM = 0. ROW CP TIME = 2.228 + DISC ...SPECIAL DISC(DIMENSIONS=

5005 FF SUM = 0. ROW CP TIME = 2.422 + DISC ...SPECIAL DISC(DIMENSIONS=

5010 FF SUM = .0000 ROW CP TIME = 2.665 + DISC ...SPECIAL DISC(DIMENSIONS=

(* INDICATES NODE PAIR HAS BEEN SUBDIVIDED)
(R INDICATES FF CALCULATED FROM J TO I)

NODE I	NODE J	COMPUTATION	FE(I,J) W/SHAD	FE(J,I) W/SHAD	FA(I,J) W/SHAD	F (I,J) WO/SHAD	SHAD. E FACTOR	SHAD. A FACTOR	CP TIME (SEC)	
5015	711	CAL.	.000001	.000001	.000001	.000001	1.000000	1.000000	.414	
5015	FF SUM =	.0000	ROW CP TIME =	2.803	+ DISC	...SPECIAL DISC(DIMENSIONS=				
5020	711	CAL.	.000002	.000002	.000002	.000002	1.000000	1.000000	.326	R
5020	FF SUM =	.0000	ROW CP TIME =	3.074	+ DISC	...SPECIAL DISC(DIMENSIONS=				
5025	711	CAL.	.000003	.000004	.000003	.000003	1.000000	1.000000	.349	R
5025	FF SUM =	.0000	ROW CP TIME =	3.167	+ DISC	...SPECIAL DISC(DIMENSIONS=				
5030	711	CAL.	.000004	.000006	.000004	.000004	1.000000	1.000000	.330	R
5030	FF SUM =	.0000	ROW CP TIME =	3.310	+ DISC	...SPECIAL DISC(DIMENSIONS=				
5035	711	CAL.	.000005	.000009	.000005	.000005	1.000000	1.000000	.333	R
5035	FF SUM =	.0000	ROW CP TIME =	3.113	+ DISC	...SPECIAL DISC(DIMENSIONS=				
5040	FF SUM =	.0000	ROW CP TIME =	3.069	+ DISC	...SPECIAL DISC(DIMENSIONS=				
5045	724	CAL.	.000001	.000003	.000001	.000001	1.000000	1.000000	1.687	R
5045	726	CAL.	.000001	.000002	.000001	.000001	1.000000	1.000000	2.038	R
5045	24	CAL.	.000001	.000002	.000001	.000001	1.000000	1.000000	3.499	R

MODEL = RIO STEP = 1 RCS ANALYSIS 4/9/75
FORM FACTOR CALCULATION LINK.

(* INDICATES NODE PAIR HAS BEEN SUBDIVIDED)
(R INDICATES FF CALCULATED FROM J TO I)

NODE I	NODE J	COMPUTATION	FE(I,J) W/SHAD	FE(J,I) W/SHAD	FA(I,J) W/SHAD	F (I,J) WO/SHAD	SHAD. E FACTER	SHAD. A FACTOR	CP TIME (SEC)	
5049	FF SUM = .0000	ROW CP TIME = 4.217				+ DISC		...SPECIAL DISC(DIMENSIONS=		
5050	722	CAL.	.000002	.000007	.000002	.000002	1.000000	1.000000	1.387	R
5050	724	CAL.	.000002	.000006	.000002	.000002	1.000000	1.000000	1.744	R
5050	726	CAL.	.000002	.000005	.000002	.000002	1.000000	1.000000	2.087	R
5050	735	CAL.	.000001	.000004	.000001	.000002	.555046	.555046	3.038	R
5050	24	CAL.	.000001	.000005	.000001	.000001	1.000000	1.000000	3.605	R
5050	FF SUM = .0000	ROW CP TIME = 4.324				+ DISC		...SPECIAL DISC(DIMENSIONS=		
5055	722	CAL.	.000003	.000012	.000003	.000003	1.000000	1.000000	1.428	R
5055	724	CAL.	.000002	.000011	.000002	.000002	1.000000	1.000000	1.752	R
5055	726	CAL.	.000002	.000010	.000002	.000002	1.000000	1.000000	2.088	R
5055	735	CAL.	.000003	.000012	.000003	.000003	1.000000	1.000000	3.058	R
5055	24	CAL.	.000002	.000009	.000002	.000002	1.000000	1.000000	3.686	R
5055	FF SUM = .0000	ROW CP TIME = 4.377				+ DISC		...SPECIAL DISC(DIMENSIONS=		
5060	722	CAL.	.000004	.000021	.000004	.000004	1.000000	1.000000	1.384	R
5060	724	CAL.	.000004	.000019	.000004	.000004	1.000000	1.000000	1.684	R
5060	726	CAL.	.000003	.000017	.000003	.000003	1.000000	1.000000	1.992	R
5060	733	CAL.	.000003	.000003	.000000	.000004	.113212	.113212	2.626	R
5060	735	CAL.	.000004	.000020	.000004	.000004	1.000000	1.000000	2.971	R
5060	24	CAL.	.000003	.000016	.000003	.000003	1.000000	1.000000	3.547	R
5060	701	CAL.	.000253	.000024	.000253	.000567	.447268	.447268	4.270	
5060	FF SUM = .0003	ROW CP TIME = 4.270				+ DISC		...SPECIAL DISC(DIMENSIONS=		
5065	720	CAL.	.000003	.000020	.000003	.000006	.555929	.555929	1.144	R
5065	722	CAL.	.000005	.000033	.000005	.000005	1.000000	1.000000	1.458	R
5065	724	CAL.	.000005	.000030	.000005	.000005	1.000000	1.000000	1.765	R
5065	726	CAL.	.000004	.000027	.000004	.000004	1.000000	1.000000	2.096	R
5065	733	CAL.	.000002	.000011	.000002	.000005	.331142	.331142	2.738	R
5065	735	CAL.	.000005	.000031	.000005	.000005	1.000000	1.000000	3.058	R
5065	24	CAL.	.000004	.000025	.000004	.000004	1.000000	1.000000	3.603	R
5065	701	CAL.	.000388	.000045	.000388	.000579	.670792	.670792	4.354	
5065	FF SUM = .0004	ROW CP TIME = 4.354				+ DISC		...SPECIAL DISC(DIMENSIONS=		
5070	720	CAL.	.000007	.000039	.000007	.000007	.891175	.891175	1.094	R
5070	722	CAL.	.000007	.000061	.000007	.000007	1.000000	1.000000	1.403	R
5070	724	CAL.	.000006	.000057	.000006	.000006	1.000000	1.000000	1.705	R
5070	726	CAL.	.000005	.000052	.000006	.000006	1.000000	1.000000	1.999	R

MODEL = RIO STEP = 1 RCS ANALYSIS 4/9/75
FORM FACTOR CALCULATION LINK.

(* INDICATES NODE PAIR HAS BEEN SUBDIVIDED)
(R INDICATES FF CALCULATED FROM J TO I)

NODE I	NODE J	COMPUTATION	FE(I,J) W/SHAD	FE(J,I) W/SHAD	FA(I,J) W/SHAD	F (I,J) WO/SHAD	SHAD. E FACTOR	SHAD. A FACTOR	CP TIME (SEC)	
5070	733	CAL.	.000007	.000062	.000007	.000007	1.000000	1.000000	2.662	R
5070	735	CAL.	.000006	.000057	.000006	.000006	1.000000	1.000000	2.972	R
5070	24	CAL.	.000005	.000049	.000005	.000005	1.000000	1.000000	3.523	R
5070	701	CAL.	.000551	.000039	.000551	.000551	1.000000	1.000000	4.282	
5070	FF SUM = .0006		ROW CP TIME =		+.291		+ DISC		...SPECIAL DISC(DIMENSIONS=	
5075	720	CAL.	.000008	.000101	.000008	.000008	1.000000	1.000000	1.097	R
5075	722	CAL.	.000008	.000095	.000008	.000008	1.000000	1.000000	1.363	R
5075	724	CAL.	.000007	.000088	.000007	.000007	1.000000	1.000000	1.663	R
5075	726	CAL.	.000007	.000083	.000007	.000007	1.000000	1.000000	1.953	R
5075	733	CAL.	.000008	.000093	.000008	.000008	1.000000	1.000000	2.616	R
5075	735	CAL.	.000007	.000087	.000007	.000007	1.000000	1.000000	2.901	R
5075	24	CAL.	.000006	.000078	.000006	.000006	1.000000	1.000000	3.435	R
5075	26	CAL.	.000007	.000085	.000007	.000007	1.000000	1.000000	3.762	R
5075	701	CAL.	.000483	.000104	.000483	.000483	1.000000	1.000000	4.215	
5075	FF SUM = .0005		ROW CP TIME =		+.215		+ DISC		...SPECIAL DISC(DIMENSIONS=	
5080	720	CAL.	.000009	.000136	.000009	.000009	1.000000	1.000000	1.116	R
5080	722	CAL.	.000008	.000128	.000008	.000008	1.000000	1.000000	1.375	R
5080	724	CAL.	.000008	.000121	.000008	.000008	1.000000	1.000000	1.665	R
5080	726	CAL.	.000007	.000114	.000007	.000007	1.000000	1.000000	1.958	R
5080	733	CAL.	.000008	.000124	.000008	.000008	1.000000	1.000000	2.604	R
5080	735	CAL.	.000007	.000117	.000007	.000007	1.000000	1.000000	2.905	R
5080	24	CAL.	.000007	.000109	.000007	.000007	1.000000	1.000000	3.430	R
5080	26	CAL.	.000007	.000112	.000007	.000007	1.000000	1.000000	3.704	R
5080	701	CAL.	.000401	.000112	.000401	.000401	1.000000	1.000000	+.188	
5080	FF SUM = .0005		ROW CP TIME =		+.184		+ DISC		...SPECIAL DISC(DIMENSIONS=	
5085	720	CAL.	.000008	.000167	.000008	.000008	1.000000	1.000000	1.110	R
5085	722	CAL.	.000008	.000159	.000008	.000008	1.000000	1.000000	1.413	R
5085	724	CAL.	.000008	.000151	.000008	.000008	1.000000	1.000000	1.720	R
5085	726	CAL.	.000007	.000144	.000007	.000007	1.000000	1.000000	2.020	R
5085	733	CAL.	.000008	.000152	.000008	.000008	1.000000	1.000000	2.681	R
5085	735	CAL.	.000007	.000144	.000007	.000007	1.000000	1.000000	2.992	R
5085	24	CAL.	.000007	.000138	.000007	.000007	1.000000	1.000000	3.493	R
5085	26	CAL.	.000007	.000136	.000007	.000007	1.000000	1.000000	3.805	R
5085	701	CAL.	.000323	.000113	.000323	.000323	1.000000	1.000000	4.260	

MODEL = RIO STEP = 1 RCS ANALYSIS 4/9/75
FORM FACTOR CALCULATION LINK.

(* INDICATES NODE PAIR HAS BEEN SUBDIVIDED)
(R INDICATES FF CALCULATED FROM J TO I)

NODE I	NODE J	COMPUTATION	FE(I,J) W/SHAD	FE(J,I) W/SHAD	FA(I,J) W/SHAD	F (I,J) WO/SHAD	SHAD. E FACTER	SHAD. A FACTOR	CP TIME (SEC)	
5089	FF SUM = .0004		ROW CP TIME = .269			+ DISC		...SPECIAL DISC(DIMENSIONS=		
5090	715	CAL.	.000002	.000059	.000002	.000005	.445667	.445667	.895	R
5090	720	CAL.	.000004	.000193	.000004	.000004	1.000000	1.000000	1.127	R
5090	722	CAL.	.000004	.000185	.000004	.000004	1.000000	1.000000	1.397	R
5090	724	CAL.	.000007	.000177	.000007	.000007	1.000000	1.000000	1.691	R
5090	726	CAL.	.000007	.000170	.000007	.000007	1.000000	1.000000	1.992	R
5090	731	CAL.	.000003	.000061	.000003	.000008	.333393	.333393	2.338	R
5090	733	CAL.	.000007	.000175	.000007	.000007	1.000000	1.000000	2.647	R
5090	735	CAL.	.000007	.000167	.000007	.000007	1.000000	1.000000	3.000	R
5090	24	CAL.	.000007	.000164	.000007	.000007	1.000000	1.000000	3.336	R
5090	26	CAL.	.000007	.000157	.000007	.000007	1.000000	1.000000	3.836	R
5090	701	CAL.	.000256	.000139	.000256	.000256	1.000000	1.000000	4.237	
5090	FF SUM = .0003		ROW CP TIME = .276			+ DISC		...SPECIAL DISC(DIMENSIONS=		
5092	715	CAL.	.000005	.000141	.000005	.000005	1.000000	1.000000	.879	R
5092	720	CAL.	.000007	.000216	.000007	.000007	1.000000	1.000000	1.090	R
5092	722	CAL.	.000007	.000208	.000007	.000007	1.000000	1.000000	1.413	R
5092	724	CAL.	.000007	.000201	.000007	.000007	1.000000	1.000000	1.701	R
5092	726	CAL.	.000007	.000193	.000007	.000007	1.000000	1.000000	1.965	R
5092	731	CAL.	.000003	.000090	.000003	.000007	.446657	.446657	2.340	R
5092	733	CAL.	.000007	.000195	.000007	.000007	1.000000	1.000000	2.630	R
5092	735	CAL.	.000006	.000187	.000006	.000006	1.000000	1.000000	2.926	R
5092	24	CAL.	.000007	.000188	.000007	.000007	1.000000	1.000000	3.445	R
5092	26	CAL.	.000006	.000175	.000006	.000006	1.000000	1.000000	3.723	R
5092	701	CAL.	.000250	.000103	.000250	.000250	1.000000	1.000000	4.157	
5095	FF SUM = .0003		ROW CP TIME = .157			+ DISC		...SPECIAL DISC(DIMENSIONS=		
5100	713	CAL.	.000001	.000036	.000001	.000003	.220616	.220616	.564	R
5100	715	CAL.	.000003	.000162	.000003	.000003	1.000000	1.000000	.869	R
5100	720	CAL.	.000005	.000260	.000005	.000005	1.000000	1.000000	1.108	R
5100	722	CAL.	.000005	.000275	.000005	.000005	1.000000	1.000000	1.415	R
5100	724	CAL.	.000005	.000270	.000005	.000005	1.000000	1.000000	1.687	R
5100	726	CAL.	.000004	.000265	.000004	.000004	1.000000	1.000000	1.999	R
5100	731	CAL.	.000004	.000254	.000004	.000004	1.000000	1.000000	2.337	R
5100	733	CAL.	.000004	.000249	.000004	.000004	1.000000	1.000000	2.663	R
5100	735	CAL.	.000004	.000245	.000004	.000004	1.000000	1.000000	2.924	R
5101	24	CAL.	.000004	.000241	.000004	.000004	1.000000	1.000000	3.458	R
5100	26	CAL.	.000004	.000230	.000004	.000004	1.000000	1.000000	3.750	R
5100	701	CAL.	.000053	.000036	.000053	.000053	1.000000	1.000000	4.187	R

MODEL = RIO STEP = 1 RCS ANALYSIS 4/9/75
FORM FACTOR CALCULATION LINK.

(* INDICATES NODE PAIR HAS BEEN SUBDIVIDED)
(R INDICATES FF CALCULATED FROM J TO I)

NODE I	NODE J	COMPUTATION	FE(I,J) W/SHAD	FE(J,I) W/SHAD	FA(I,J) W/SHAD	F (I,J) WO/SHAD	SHAD. E FACTER	SHAD. A FACTOR	CP TIME (SEC)	
5100	FF SUM = .9991		ROW CP TIME = 4.228			+ DISC		...SPECIAL DISC(DIMENSIONS=		
5100	713	CAL.	.000001	.000111	.000001	.000002	.667258	.667258	.566	R
5100	715	CAL.	.000002	.000165	.000002	.000002	1.000000	1.000000	.901	R
5100	720	CAL.	.000003	.000335	.000003	.000003	1.000000	1.000000	1.115	R
5100	722	CAL.	.000003	.000301	.000003	.000003	1.000000	1.000000	1.428	R
5100	724	CAL.	.000003	.000298	.000003	.000003	1.000000	1.000000	1.701	R
5100	726	CAL.	.000003	.000295	.000003	.000003	1.000000	1.000000	1.990	R
5100	731	CAL.	.000003	.000271	.000003	.000003	1.000000	1.000000	2.306	R
5100	733	CAL.	.000003	.000268	.000003	.000003	1.000000	1.000000	2.664	R
5100	735	CAL.	.000003	.000265	.000003	.000003	1.000000	1.000000	2.939	R
5100	24	CAL.	.000003	.000292	.000003	.000003	1.000000	1.000000	3.459	R
5100	26	CAL.	.000002	.000253	.000002	.000002	1.000000	1.000000	3.755	R
5100	701	CAL.	.000010	.000017	.000010	.000010	1.000000	1.000000	4.167	R
5109	FF SUM = .9990		ROW CP TIME = 4.173			+ DISC		...SPECIAL DISC(DIMENSIONS=		
5110	711	CAL.	.000000	.000002	.000000	.000000	1.000000	1.000000	.311	R
5110	713	CAL.	.000000	.000002	.000000	.000000	1.000000	1.000000	.604	R
5110	715	CAL.	.000000	.000002	.000000	.000000	1.000000	1.000000	.888	R
5110	720	CAL.	.000000	.000005	.000000	.000000	1.000000	1.000000	1.145	R
5110	722	CAL.	.000000	.000005	.000000	.000000	1.000000	1.000000	1.432	R
5110	724	CAL.	.000000	.000005	.000000	.000000	1.000000	1.000000	1.703	R
5110	726	CAL.	.000000	.000005	.000000	.000000	1.000000	1.000000	1.978	R
5110	731	CAL.	.000000	.000004	.000000	.000000	1.000000	1.000000	2.325	R
5110	733	CAL.	.000000	.000004	.000000	.000000	1.000000	1.000000	2.623	R
5110	735	CAL.	.000000	.000004	.000000	.000000	1.000000	1.000000	2.893	R
5110	24	CAL.	.000000	.000005	.000000	.000000	1.000000	1.000000	3.411	R
5110	26	CAL.	.000000	.000004	.000000	.000000	1.000000	1.000000	3.700	R
5110	701	CAL.	.000001	.000002	.000001	.000001	1.000000	1.000000	4.002	R
5110	FF SUM = .9990		ROW CP TIME = 4.098			+ DISC		...SPECIAL DISC(DIMENSIONS=		
140	711	CAL.	.000302	.028736	.000302	.000302	1.000000	1.000000	.346	R
140	712	CAL.	.000157	.014879	.000157	.000157	1.000000	1.000000	.704	R
140	714	CAL.	.000089	.008437	.000089	.000089	1.000000	1.000000	1.264	R
140	721	CAL.	.000081	.007671	.000081	.000099	.811180	.811180	1.790	R
140	723	CAL.	.000092	.008731	.000092	.000092	1.000000	1.000000	2.267	R
140	725	CAL.	.000080	.007642	.000080	.000080	1.000000	1.000000	2.742	R
140	727	CAL.	.000068	.006430	.000068	.000068	1.000000	1.000000	3.213	R
140	733	CAL.	.000042	.004004	.000042	.000071	.599629	.599629	3.601	R
140	732	CAL.	.000046	.004333	.000046	.000068	.696734	.696734	3.998	R
140	734	CAL.	.000064	.006065	.000064	.000064	1.000000	1.000000	4.514	R
140	25	CAL.	.000059	.005631	.000059	.000059	1.000000	1.000000	5.236	R
140	27	CAL.	.000061	.005821	.000061	.000061	1.000000	1.000000	5.798	R

MODEL = RIO STEP = 1 RCS ANALYSIS 4/9/75
FORM FACTOR CALCULATION LINK.

(* INDICATES NODE PAIR HAS BEEN SUBDIVIDED)
(R INDICATES FF CALCULATED FROM J TO I)

NODE I	NODE J	COMPUTATION	FE(I,J) W/SHAD	FE(J,I) W/SHAD	FA(I,J) W/SHAD	F (I,J) WO/SHAD	SHAD. E FACTOR	SHAD. A FACTOR	CP TIME (SEC)	
145	701	CAL.	.000212	.000359	.000212	.000212	1.000000	1.000000	6.114	R
145	FF SUM = .0114		ROW CP TIME = 6.141			+ TRAP		+ 1 REAR TAPER		
146	FF SUM = 0.		ROW CP TIME = 4.643			+ RECT		REAR FLAT PLATE OUT BACK		
147	710	CAL.	.000076	.054194	.000076	.000169	.692008	.692008	.734	R
147	712	CAL.	.000079	.056892	.000079	.000118	.673278	.673278	1.458	R
147	714	CAL.	.000080	.057460	.000080	.000122	.660576	.660576	2.228	R
147	721	CAL.	.000037	.026211	.000037	.000062	.589467	.589467	2.831	R
147	723	CAL.	.000040	.028621	.000040	.000067	.596222	.596222	3.116	R
147	725	CAL.	.000043	.030783	.000043	.000071	.601542	.601542	3.573	R
147	727	CAL.	.000046	.032574	.000046	.000075	.605267	.605267	3.991	R
147	730	CAL.	.000060	.042738	.000060	.000068	.881311	.881311	4.623	R
147	732	CAL.	.000055	.039245	.000055	.000093	.586914	.586914	5.270	R
147	734	CAL.	.000067	.046223	.000067	.000099	.683521	.683521	5.963	R
147	740	CAL.	.000389	.278112	.000389	.000389	1.000000	1.000000	8.869	R
147	25	CAL.	.000047	.033653	.000047	.000077	.607952	.607952	9.324	R
147	27	CAL.	.000075	.053833	.000075	.000151	.498004	.498004	10.198	R
147	701	CAL.	.000793	.010691	.000793	.001982	.400089	.400089	10.539	R
147	FF SUM = .0019		ROW CP TIME = 10.539			+ RECT		SLOPING REAR FLAT PLATE		
710	900	CAL.	.025694	.000049	.025694	.025694	1.000000	1.000000	1.850	
710	901	CAL.	.026386	.000156	.026386	.026386	1.000000	1.000000	2.109	
710	805	CAL.	.038357	.000315	.038357	.038357	1.000000	1.000000	4.587	
710	806	CAL.	.039417	.000191	.039417	.039417	1.000000	1.000000	4.856	
710	810	CAL.	.000955	.000008	.000955	.000955	1.000000	1.000000	5.514	
710	811	CAL.	.001798	.000008	.001798	.001798	1.000000	1.000000	5.745	
710	222	CAL.	.020534	.000023	.020534	.020534	1.000000	1.000000	6.266	
710	2	CAL.	.004284	.000003	.004284	.007577	.565328	.565328	7.639	
710	3	CAL.	.020889	.000020	.020889	.020889	1.000000	1.000000	8.125	
710	144	CAL.	.004933	.000015	.004933	.012926	.381664	.381664	8.399	
710	4	CAL.	.098441	.000275	.098441	.103615	.932074	.932074	10.262	
710	806	CAL.	.008561	.000005	.008561	.027963	.306171	.306171	15.963	
710	FF SUM = .3731		ROW CP TIME = 17.356			- DISC		-Z 1ST RCS X=1519.75		
711	712	CAL.	.002540	.002540	.002540	.002540	1.000000	1.000000	.210	
711	721	CAL.	.001224	.001224	.001224	.001224	1.000000	1.000000	.928	
711	723	CAL.	.001026	.001026	.001026	.001026	1.000000	1.000000	1.206	

MODEL = RIO STEP = 1 RCS ANALYSIS 4/9/75
FORM FACTOR CALCULATION LINK.

(* INDICATES NODE PAIR HAS BEEN SUBDIVIDED)
(R INDICATES FF CALCULATED FROM J TO I)

NODE I	NODE J	COMPUTATION	FF(I,J) W/SHAD	FF(J,I) W/SHAD	FA(I,J) W/SHAD	F (I,J) WO/SHAD	SHAD. F FACTOR	SHAD. A FACTOR	CP TIME (SEC)
711	725	CAL.	.000659	.000659	.000659	.000659	1.000000	1.000000	1.502
711	727	CAL.	.000355	.000355	.000355	.000355	1.000000	1.000000	1.851
711	730	CAL.	.001280	.001280	.001280	.001280	1.000000	1.000000	2.116
711	732	CAL.	.001197	.001197	.001197	.001197	1.000000	1.000000	2.421
711	734	CAL.	.001001	.001001	.001001	.001001	1.000000	1.000000	2.763
711	775	CAL.	.000004	.000000	.000004	.000010	.362195	.362159	5.379
711	777	CAL.	.000007	.000000	.000007	.000019	.371505	.371505	5.739
711	31	CAL.	.013006	.001687	.013006	.015297	.850241	.850241	6.501
711	32	CAL.	.002909	.000092	.002909	.002909	1.000000	1.000000	7.047
711	33	CAL.	.020779	.000418	.020779	.020779	1.000000	1.000000	7.622
711	34	CAL.	.004563	.000098	.004563	.004563	1.000000	1.000000	8.185
711	25	CAL.	.000204	.000204	.000204	.000204	1.000000	1.000000	8.554
711	27	CAL.	.000480	.000480	.000480	.000540	.888357	.888357	8.861
711	300	CAL.	.027538	.000226	.027538	.027538	1.000000	1.000000	9.663
711	301	CAL.	.029156	.000141	.029156	.029156	1.000000	1.000000	9.977
711	311	CAL.	.000535	.000003	.000535	.000535	1.000000	1.000000	10.782
711	22	CAL.	.046486	.000080	.046486	.048621	.956084	.956084	11.868
711	781	CAL.	.000384	.000000	.000384	.000341	1.245448	1.245448	22.004
711	212	CAL.	.010627	.000008	.010627	.039414	.269628	.269628	27.119 *
711	380	CAL.	.008230	.000008	.008230	.070352	.116983	.116983	27.638
711	385	CAL.	.007632	.000121	.007632	.007632	1.000000	1.000000	28.493
711	701	CAL.	.025631	.000456	.025631	.025631	1.000000	1.000000	29.249
711	702	CAL.	.001715	.000030	.001715	.001715	1.000000	1.000000	29.539
711	FF SUM =	.2849	ROW CP TIME =	33.250		+ DISC		-Z 1ST RCS X=1519.75	
712	330	CAL.	.022825	.000043	.022825	.022825	1.000000	1.000000	1.749
712	331	CAL.	.020820	.000123	.020820	.020820	1.000000	1.000000	1.982
712	335	CAL.	.039592	.000325	.039592	.039592	1.000000	1.000000	4.478
712	336	CAL.	.059924	.000290	.059924	.059924	1.000000	1.000000	4.841
712	810	CAL.	.001235	.000010	.001235	.001235	1.000000	1.000000	5.411
712	811	CAL.	.001871	.000009	.001871	.001871	1.000000	1.000000	5.694
712	222	CAL.	.040194	.000044	.040194	.040194	1.000000	1.000000	6.338
712	407	CAL.	.000002	.000002	.000002	.000002	1.000000	1.000000	6.698
712	2	CAL.	.006218	.000084	.006218	.007101	.840321	.840321	7.760
712	3	CAL.	.019021	.000010	.019021	.019021	1.000000	1.000000	8.264
712	144	CAL.	.007697	.000023	.007697	.010917	.705055	.705055	8.553
712	4	CAL.	.004398	.000204	.004398	.004241	.986656	.986656	9.072
712	306	CAL.	.016725	.000039	.016725	.017482	.956700	.956700	15.469
712	FF SUM =	.4040	ROW CP TIME =	16.584		- DISC		-Z 2ND RCS X=1532.875	
713	714	CAL.	.003619	.003619	.003619	.003619	1.000000	1.000000	.241
713	721	CAL.	.001160	.001160	.001160	.001166	1.000000	1.000000	.612

MODEL = RIO STEP = 1 RCS ANALYSIS 4/9/75
FORM FACTOR CALCULATION LINK.

(* INDICATES NODE PAIR HAS BEEN SUBDIVIDED)
(R INDICATES FF CALCULATED FROM J TO I)

NODE I	NODE J	COMPUTATION	FE(I,J) W/SHAD	FE(J,I) W/SHAD	FA(I,J) W/SHAD	F (I,J) WO/SHAD	SHAD. E FACTOR	SHAD. A FACTOR	CP TIME (SEC)
713	723	CAL.	.001304	.001304	.001304	.001304	1.000000	1.000000	.895
713	725	CAL.	.001041	.001041	.001041	.001041	1.000000	1.000000	1.204
713	727	CAL.	.000604	.000604	.000604	.000604	1.000000	1.000000	1.508
713	730	CAL.	.001373	.001373	.001373	.001373	1.000000	1.000000	1.771
713	732	CAL.	.001458	.001458	.001458	.001458	1.000000	1.000000	2.078
713	734	CAL.	.001353	.001353	.001353	.001353	1.000000	1.000000	2.408
713	31	CAL.	.021397	.001494	.021397	.026977	.811684	.811684	6.023
713	32	CAL.	.007056	.000242	.007056	.007056	1.000000	1.000000	6.532
713	33	CAL.	.049089	.000957	.049089	.049089	1.000000	1.000000	7.456
713	34	CAL.	.012167	.000262	.012167	.012167	1.000000	1.000000	7.840
713	25	CAL.	.000333	.000333	.000333	.000333	1.000000	1.000000	8.333
713	27	CAL.	.000904	.000904	.000904	.001176	.768278	.768278	8.624
713	300	CAL.	.026070	.000214	.026070	.026070	1.000000	1.000000	9.352
713	301	CAL.	.033827	.000104	.033827	.033827	1.000000	1.000000	9.677
713	22	CAL.	.112355	.000194	.112355	.112355	1.000000	1.000000	12.012
713	100	CAL.	.001341	.000001	.001341	.003101	.432322	.432322	14.655
713	796	CAL.	.000754	.000001	.000754	.003500	.215327	.215327	25.212
713	780	CAL.	.008673	.000009	.008673	.066721	.129795	.129795	27.269
713	385	CAL.	.094021	.000129	.094021	.094021	1.000000	1.000000	28.088
713	701	CAL.	.033048	.000568	.033048	.033048	1.000000	1.000000	28.865
713	702	CAL.	.001467	.000026	.001467	.001467	1.000000	1.000000	29.162
713	FF SUM =	.4157	ROW CP TIME =	29.905		+ DISC		-Z 2ND RCS X=1532.875	
714	900	CAL.	.020628	.000039	.020628	.020628	1.000000	1.000000	1.672
714	901	CAL.	.016912	.000100	.016912	.016912	1.000000	1.000000	1.924
714	905	CAL.	.035098	.000298	.035098	.039098	1.000000	1.000000	4.396
714	906	CAL.	.080222	.000398	.080222	.080222	1.000000	1.000000	4.843
714	910	CAL.	.001468	.000012	.001468	.001468	1.000000	1.000000	5.374
714	811	CAL.	.002635	.000013	.002635	.002635	1.000000	1.000000	5.668
714	222	CAL.	.053210	.000658	.053210	.057513	.925192	.925192	6.744
714	407	CAL.	.000001	.000001	.000001	.000001	1.000000	1.000000	7.148
714	2	CAL.	.005733	.000004	.005733	.006876	.833764	.833764	8.174
714	3	CAL.	.017636	.000017	.017636	.017636	1.000000	1.000000	8.696
714	144	CAL.	.005555	.000016	.005555	.009478	.586096	.586096	8.953
714	4	CAL.	.076914	.000215	.076914	.080212	.958880	.958880	9.916
714	516	CAL.	.011291	.000006	.011290	.011964	.943652	.943652	15.744
714	FF SUM =	.3968	ROW CP TIME =	16.857		- DISC		-Z 3RD RCS X=1545.375	
715	721	CAL.	.000791	.000791	.000791	.000791	1.000000	1.000000	.288
715	723	CAL.	.001135	.001135	.001135	.001135	1.000000	1.000000	.589
715	725	CAL.	.001223	.001223	.001223	.001223	1.000000	1.000000	.890
715	727	CAL.	.000855	.000855	.000855	.000855	1.000000	1.000000	1.106

MODEL = RIO STEP = 1 RCS ANALYSIS 4/9/75
FORM FACTOR CALCULATION LINK.

(* INDICATES NODE PAIR HAS BEEN SUBDIVICED)
(R INDICATES FF CALCULATED FROM J TO I)

NODE I	NODE J	COMPUTATION	FE(I,J) W/SHAD	FE(J,I) W/SHAD	FA(I,J) W/SHAD	F (I,J) WO/SHAD	SHAD. E FACTOR	SHAD. A FACTOR	CP TIME (SEC)
715	730	CAL.	.001297	.001297	.001297	.001297	1.000000	1.000000	1.422
715	732	CAL.	.001598	.001598	.001598	.001598	1.000000	1.000000	1.757
715	734	CAL.	.001715	.001715	.001715	.001715	1.000000	1.000000	2.039
715	767	CAL.	.000112	.000036	.000112	.000306	.367017	.367017	3.661
715	31	CAL.	.016443	.001122	.016443	.021565	.762475	.762475	5.525
715	32	CAL.	.012136	.000383	.012136	.012136	1.000000	1.000000	6.624
715	33	CAL.	.000833	.001223	.000833	.000833	1.000000	1.000000	7.242
715	34	CAL.	.019789	.000426	.019789	.019789	1.000000	1.000000	7.389
715	25	CAL.	.000459	.000459	.000459	.000459	1.000000	1.000000	7.843
715	27	CAL.	.003447	.003447	.003447	.003447	1.000000	1.000000	8.164
715	800	CAL.	.022480	.000185	.022480	.022480	1.000000	1.000000	8.842
715	801	CAL.	.036847	.000178	.036847	.036847	1.000000	1.000000	9.175
715	22	CAL.	.109556	.000196	.109556	.116077	.943827	.943827	11.091
715	150	CAL.	.000164	.000000	.000164	.002578	.063739	.063739	13.541
715	151	CAL.	.000603	.000001	.000603	.001334	.452143	.452143	13.935
715	790	CAL.	.000321	.000000	.000321	.003008	.106628	.106628	23.719
715	380	CAL.	.009158	.000009	.009158	.063515	.144188	.144188	25.637
715	385	CAL.	.009963	.000136	.009963	.099603	1.000000	1.000000	26.632
715	701	CAL.	.041498	.000738	.041498	.041498	1.000000	1.000000	27.347
715	702	CAL.	.001148	.000020	.001148	.001148	1.000000	1.000000	27.655

715 FF SUM = .4432 ROW CP TIME = 28.411 + DISC -Z 3RD RCS X=1545.375

720	900	CAL.	.025511	.000049	.025511	.025511	1.000000	1.000000	1.360
720	901	CAL.	.001257	.000007	.001257	.001257	1.000000	1.000000	1.526
720	2	CAL.	.012277	.000009	.012277	.013255	.926182	.926182	6.019
720	3	CAL.	.027842	.000026	.027842	.027842	1.000000	1.000000	6.491
720	144	CAL.	.000773	.000002	.000773	.001001	.773027	.773027	6.676
720	4	CAL.	.008281	.000023	.008281	.008281	1.000000	1.000000	6.895
720	765	CAL.	.000129	.000000	.000129	.000692	.186118	.186118	11.490

720 FF SUM = .0776 ROW CP TIME = 13.740 - DISC +Y 1ST RCS X=1516.

721	730	CAL.	.001960	.001960	.001960	.001960	1.000000	1.000000	.621
721	732	CAL.	.001619	.001619	.001619	.001619	1.000000	1.000000	.940
721	734	CAL.	.000996	.000996	.000996	.000996	1.000000	1.000000	1.255
721	741	CAL.	.000007	.000007	.000007	.000007	1.000000	1.000000	1.641
721	901	CAL.	.001157	.000007	.001157	.003452	.335358	.335358	1.885
721	31	CAL.	.174821	.011925	.174821	.178472	.979540	.979540	5.734
721	32	CAL.	.001838	.000058	.001838	.001838	1.000000	1.000000	6.232
721	33	CAL.	.177227	.003500	.177227	.177227	1.000000	1.000000	7.883
721	34	CAL.	.003544	.000070	.003544	.003544	1.000000	1.000000	8.289
721	26	CAL.	.000191	.000191	.000191	.000191	1.000000	1.000000	8.791
721	800	CAL.	.034500	.000283	.034500	.034506	1.000000	1.000000	9.633

MODEL = RIO STEP = 1 RCS ANALYSIS 4/9/75
FORM FACTOR CALCULATION LINK.

(* INDICATES NODE PAIR HAS BEEN SUBDIVIDED)
(R INDICATES FF CALCULATED FROM J TO I)

NODE I	NODE J	COMPUTATION	FE(I,J) W/SHAD	FE(J,I) W/SHAD	FA(I,J) W/SHAD	F (I,J) WO/SHAD	SHAD. E FACTOR	SHAD. A FACTOR	CP TIME (SEC)
721	801	CAL.	.049397	.000239	.049397	.049397	1.000000	1.000000	10.179
721	805	CAL.	.019336	.000159	.019336	.021671	.892279	.892279	10.671
721	806	CAL.	.034032	.000165	.034032	.034032	1.000000	1.000000	10.947
721	810	CAL.	.011899	.000098	.011899	.011899	1.000000	1.000000	11.572
721	811	CAL.	.021345	.000103	.021345	.021345	1.000000	1.000000	11.926
721	222	CAL.	.009222	.000010	.009222	.012260	.752207	.752207	12.638
721	22	CAL.	.004548	.000008	.004548	.035122	.129503	.129503	13.017
721	19	CAL.	.000008	.000008	.000006	.000008	1.000000	1.000000	13.577
721	4	CAL.	.007209	.000020	.007209	.008278	.870963	.870963	16.036
721	580	CAL.	.006642	.000007	.006642	.070667	.093994	.093994	28.977
721	585	CAL.	.054392	.000075	.054392	.098894	.550004	.550004	29.684
721	701	CAL.	.029347	.000451	.029347	.029347	1.000000	1.000000	30.652
721	702	CAL.	.002078	.000037	.002078	.002078	1.000000	1.000000	30.985
721	FF SUM =	.6802	ROW CP TIME =	31.705		+ DISC		+Y 1ST RCS X=1516.	
722	900	CAL.	.023297	.000044	.023297	.023297	1.000000	1.000000	1.225
722	901	CAL.	.001177	.000006	.001177	.001177	1.000000	1.000000	1.384
722	771	CAL.	.000005	.000000	.000005	.000021	.227057	.227057	2.062
722	773	CAL.	.000034	.000000	.000034	.000052	.639845	.639845	2.449
722	25	CAL.	.000002	.000002	.000002	.000002	1.000000	1.000000	3.778
722	2	CAL.	.011651	.000008	.011651	.011851	.983168	.983168	6.056
722	3	CAL.	.024987	.000024	.024987	.024987	1.000000	1.000000	6.511
722	144	CAL.	.000848	.000003	.000848	.000848	1.000000	1.000000	6.734
722	4	CAL.	.007516	.000021	.007516	.007516	1.000000	1.000000	6.946
722	785	CAL.	.000597	.000001	.000597	.000605	.986904	.986904	11.746
722	787	CAL.	.000015	.000000	.000015	.000048	.313525	.313525	12.219
722	FF SUM =	.0715	ROW CP TIME =	13.999		- DISC		+Y 2ND RCS X=1529.	
723	730	CAL.	.001618	.001618	.001618	.001618	1.000000	1.000000	.496
723	732	CAL.	.001960	.001960	.001960	.001960	1.000000	1.000000	.799
723	734	CAL.	.001619	.001619	.001619	.001619	1.000000	1.000000	1.113
723	901	CAL.	.002954	.000017	.002954	.002954	1.000000	1.000000	1.709
723	31	CAL.	.071108	.004851	.071108	.076050	.935016	.935016	4.632
723	32	CAL.	.005330	.000108	.005330	.005330	1.000000	1.000000	5.139
723	33	CAL.	.120622	.002426	.120622	.120622	1.000000	1.000000	6.164
723	34	CAL.	.010080	.000217	.010080	.010080	1.000000	1.000000	6.527
723	26	CAL.	.000417	.000417	.000417	.000417	1.000000	1.000000	7.007
723	800	CAL.	.032954	.000271	.032954	.032954	1.000000	1.000000	7.636
723	801	CAL.	.054628	.000204	.054628	.054628	1.000000	1.000000	8.377
723	805	CAL.	.022183	.000181	.022183	.022183	1.000000	1.000000	8.878
723	806	CAL.	.040964	.000198	.040964	.040964	1.000000	1.000000	9.142
723	810	CAL.	.011693	.000096	.011693	.011693	1.000000	1.000000	9.765

DATE 05/20/75 TIME 15.55.41. THERMAL RADIATION ANALYSIS SYSTEM (TRASYS) CDC6500/SCOPE 3.4

MODEL = RIO STEP = 1 RCS ANALYSIS 4/9/75
FORM FACTOR CALCULATION LINK.

(* INDICATES NODE PAIR HAS BEEN SUBDIVICED)
(R INDICATES FF CALCULATED FROM J TO I)

NODE I	NODE J	COMPUTATION	FE(I,J) W/SHAD	FE(J,I) W/SHAD	FA(I,J) W/SHAD	F (I,J) WO/SHAD	SHAD. E FACTOR	SHAD. A FACTOR	CP TIME (SEC)
723	811	CAL.	.021730	.000185	.021730	.022624	.960460	.960460	10.053
723	222	CAL.	.024366	.000027	.024366	.024366	1.000000	1.000000	10.739
723	22	CAL.	.059651	.000103	.059651	.065402	.912059	.912059	11.592
723	407	CAL.	.000008	.000008	.000008	.000008	1.000000	1.000000	11.914
723	15	CAL.	.000008	.000008	.000008	.000008	1.000000	1.000000	12.143
723	143	CAL.	.000381	.000010	.000381	.000576	.661408	.661408	14.181
723	144	CAL.	.002264	.000007	.002264	.002264	1.000000	1.000000	14.443
723	4	CAL.	.000720	.000019	.000720	.000741	.868908	.868908	14.805
723	388	CAL.	.023431	.000013	.023431	.027791	.843120	.843120	25.398
723	380	CAL.	.006004	.000007	.006004	.363448	.104084	.104084	27.000
723	385	CAL.	.097910	.000135	.097910	.097910	1.000000	1.000000	27.854
723	701	CAL.	.029551	.000525	.029551	.029551	1.000000	1.000000	28.578
723	702	CAL.	.001738	.000031	.001738	.001738	1.000000	1.000000	28.918
723	FF SUM =	.6982	ROW CP TIME =	29.621		+ DISC		+Y 2ND RCS X=1529.	
724	930	CAL.	.021169	.000340	.021169	.021169	1.000000	1.000000	1.098
724	901	CAL.	.000917	.000005	.000917	.000917	1.000000	1.000000	1.224
724	771	CAL.	.000016	.000000	.000016	.000020	.794041	.794041	1.985
724	773	CAL.	.000048	.000000	.000048	.000049	.975837	.975837	2.441
724	25	CAL.	.000013	.000013	.000013	.000013	1.000000	1.000000	3.703
724	2	CAL.	.010434	.000007	.010434	.010616	.982833	.982833	5.980
724	3	CAL.	.022422	.000021	.022422	.022422	1.000000	1.000000	6.422
724	144	CAL.	.000720	.000002	.000720	.000720	1.000000	1.000000	6.650
724	4	CAL.	.000720	.000019	.000720	.000720	1.000000	1.000000	6.864
724	785	CAL.	.000532	.000001	.000532	.000532	1.000000	1.000000	11.781
724	787	CAL.	.000044	.000000	.000044	.000045	.975870	.975870	12.439
724	FF SUM =	.3645	ROW CP TIME =	14.255		- DISC		+Y 3RD RCS X=1545.	
725	730	CAL.	.000996	.000996	.000996	.000996	1.000000	1.000000	.375
725	732	CAL.	.001618	.001618	.001618	.001618	1.000000	1.000000	.690
725	734	CAL.	.001960	.001960	.001960	.001960	1.000000	1.000000	.969
725	901	CAL.	.002513	.000015	.002513	.002513	1.000000	1.000000	1.597
725	31	CAL.	.025599	.001746	.025599	.031221	.819909	.819909	4.291
725	32	CAL.	.007662	.000242	.007662	.007662	1.000000	1.000000	4.759
725	33	CAL.	.068492	.001377	.068492	.068492	1.000000	1.000000	5.904
725	34	CAL.	.013883	.000299	.013883	.013883	1.000000	1.000000	6.246
725	26	CAL.	.000935	.000935	.000935	.000935	1.000000	1.000000	6.750
725	800	CAL.	.030278	.000249	.030278	.030278	1.000000	1.000000	7.534
725	901	CAL.	.058090	.000284	.058090	.058090	1.000000	1.000000	8.086
725	805	CAL.	.021538	.000177	.021538	.021538	1.000000	1.000000	8.468
725	806	CAL.	.048370	.000282	.048370	.048370	1.000000	1.000000	8.734
725	810	CAL.	.010940	.000090	.010940	.011285	.968965	.968965	9.328

MODEL = RIO STEP = 1 RCS ANALYSIS 4/9/75
FORM FACTOR CALCULATION LINK.

(* INDICATES NODE PAIR HAS BEEN SUBDIVIDED)
(R INDICATES FF CALCULATED FROM J TO I)

NODE I	NODE J	COMPUTATION	FF(I,J) W/SHAD	FF(J,I) W/SHAD	FA(I,J) W/SHAD	F (I,J) WO/SHAD	SHAD. F FACTOR	SHAD. A FACTOR	CP TIME (SEC)
725	811	CAL.	.023639	.000114	.023639	.023639	1.000000	1.000000	9.658
725	222	CAL.	.035516	.000039	.035516	.035516	1.000000	1.000000	10.287
725	22	CAL.	.077019	.000134	.077019	.085961	.962957	.902957	11.075
725	407	CAL.	.000006	.000006	.000006	.000006	1.000000	1.000000	11.390
725	15	CAL.	.000008	.000008	.000008	.000008	1.000000	1.000000	11.614
725	143	CAL.	.000333	.000000	.000333	.000509	.654869	.654869	13.641
725	144	CAL.	.001921	.000006	.001921	.001921	1.000000	1.000000	13.958
725	4	CAL.	.000161	.000017	.000161	.000186	.867021	.867021	14.305
725	806	CAL.	.020018	.000011	.020018	.022693	.882112	.882112	25.211
725	380	CAL.	.000513	.000007	.000513	.000789	.114689	.114689	26.686
725	385	CAL.	.095071	.000131	.095071	.095071	1.000000	1.000000	27.564
725	701	CAL.	.030230	.000537	.030230	.030230	1.000000	1.000000	28.271
725	702	CAL.	.001347	.000024	.001347	.001347	1.000000	1.000000	28.557
725	FF SUM =	.6329	ROW CP TIME =	29.278		+ DISC		+Y 3RD RCS X=1545.	
726	800	CAL.	.019161	.000060	.019161	.019161	1.000000	1.000000	.916
726	801	CAL.	.000779	.000005	.000779	.000779	1.000000	1.000000	1.108
726	771	CAL.	.000019	.000000	.000019	.000019	1.000000	1.000000	1.915
726	773	CAL.	.000045	.000000	.000045	.000045	1.000000	1.000000	2.376
726	25	CAL.	.000414	.000414	.000414	.000414	1.000000	1.000000	3.641
726	2	CAL.	.009362	.000007	.009362	.009629	.982489	.982489	5.907
726	3	CAL.	.020126	.000019	.020126	.020126	1.000000	1.000000	6.358
726	144	CAL.	.000613	.000002	.000613	.000613	1.000000	1.000000	6.505
726	4	CAL.	.005937	.000017	.005937	.005937	1.000000	1.000000	6.754
726	785	CAL.	.000469	.000001	.000469	.000469	1.000000	1.000000	11.740
726	787	CAL.	.000042	.000000	.000042	.000042	.995420	.995420	12.495
726	FF SUM =	.0583	ROW CP TIME =	14.327		- DISC		+Y 4TH RCS X=1555.	
727	730	CAL.	.000539	.000539	.000539	.000539	1.000000	1.000000	.273
727	732	CAL.	.000996	.000996	.000996	.000996	1.000000	1.000000	.608
727	734	CAL.	.001618	.001618	.001618	.001618	1.000000	1.000000	.896
727	901	CAL.	.002131	.000013	.002131	.002131	1.000000	1.000000	1.515
727	31	CAL.	.011501	.000785	.011501	.014094	.782670	.782670	4.260
727	32	CAL.	.008696	.000275	.008696	.008696	1.000000	1.000000	4.731
727	33	CAL.	.040496	.000814	.040496	.040496	1.000000	1.000000	5.283
727	34	CAL.	.014936	.000322	.014936	.014936	1.000000	1.000000	5.681
727	26	CAL.	.001792	.001792	.001792	.001792	1.000000	1.000000	6.165
727	800	CAL.	.026701	.000220	.026701	.026761	1.000000	1.000000	6.951
727	801	CAL.	.060960	.000295	.060960	.060960	1.000000	1.000000	7.559
727	805	CAL.	.020039	.000105	.020039	.020039	1.000000	1.000000	7.948
727	806	CAL.	.054469	.000263	.054469	.054469	1.000000	1.000000	8.282
727	810	CAL.	.010720	.000088	.010720	.010720	1.000001	1.000000	8.867

MODEL = RIO STEP = 1 RCS ANALYSIS 4/9/75
FORM FACTOR CALCULATION LINK.

(* INDICATES NODE PAIR HAS BEEN SUBDIVIDED)
(R INDICATES FF CALCULATED FROM J TO I)

NODE I	NODE J	COMPUTATION	FE(I,J) W/SHAD	FE(J,I) W/SHAD	FA(I,J) W/SHAD	F (I,J) WO/SHAD	SHAD. E FACTOR	SHAD. A FACTOR	CP TIME (SEC)
727	811	CAL.	.024307	.000118	.024307	.024307	1.000000	1.000000	9.223
727	222	CAL.	.045030	.000349	.045030	.045030	1.000000	1.000000	9.963
727	22	CAL.	.085877	.000149	.085877	.096447	.890405	.890405	10.857
727	407	CAL.	.000005	.000005	.000005	.000005	1.000000	1.000000	11.181
727	15	CAL.	.000007	.000007	.000007	.000007	1.000000	1.000000	11.424
727	143	CAL.	.000293	.000000	.000293	.000451	.648486	.648486	13.559
727	144	CAL.	.001635	.000005	.001635	.001635	1.000000	1.000000	13.834
727	4	CAL.	.005556	.000016	.005556	.006421	.865326	.865326	14.231
727	781	CAL.	.000045	.000000	.000045	.000571	.078954	.078954	21.813
727	806	CAL.	.017863	.000010	.017863	.018476	.966785	.966785	25.210
727	383	CAL.	.006373	.000006	.006373	.050711	.125676	.125676	26.417
727	385	CAL.	.090665	.000125	.090665	.090665	1.000000	1.000000	27.258
727	701	CAL.	.023018	.000409	.023018	.023018	1.000000	1.000000	27.997
727	702	CAL.	.000918	.000016	.000918	.000918	1.000000	1.000000	28.279
727	FF SUM =	.5931	ROW CP TIME =	28.988		+ DISC		+Y 4TH RCS X=1555.	
730	741	CAL.	.000006	.000006	.000006	.000006	1.000000	1.000000	.621
730	803	CAL.	.001624	.000003	.001624	.029593	.054882	.054882	.919
730	31	CAL.	.007789	.000931	.007789	.010258	.759283	.759283	4.492
730	32	CAL.	.000266	.000008	.000266	.000266	1.000000	1.000000	4.726
730	33	CAL.	.382253	.007688	.382253	.382253	1.000000	1.000000	7.414
730	34	CAL.	.000206	.000004	.000206	.000206	1.000000	1.000000	7.616
730	25	CAL.	.000340	.000340	.000340	.000340	1.000000	1.000000	8.059
730	26	CAL.	.000851	.000851	.000851	.000851	1.000000	1.000000	8.298
730	810	CAL.	.010220	.000084	.010220	.010220	1.000000	1.000000	9.114
730	801	CAL.	.009444	.000046	.009444	.009444	1.000000	1.000000	9.447
730	805	CAL.	.019445	.000160	.019445	.019445	1.000000	1.000000	9.848
730	806	CAL.	.032980	.000159	.032980	.032980	1.000000	1.000000	10.115
730	807	CAL.	.002022	.000017	.002022	.002022	1.000000	1.000000	10.329
730	808	CAL.	.002373	.000011	.002373	.002373	1.000000	1.000000	10.570
730	810	CAL.	.000787	.000056	.000787	.000787	1.000000	1.000000	10.920
730	811	CAL.	.011874	.000057	.011874	.011874	1.000000	1.000000	11.305
730	222	CAL.	.014831	.000016	.014831	.014831	1.000000	1.000000	12.019
730	22	CAL.	.026494	.000008	.026494	.026410	.170181	.170181	12.413
730	15	CAL.	.000008	.000008	.000008	.000008	1.000000	1.000000	12.939
730	212	CAL.	.000128	.000000	.000128	.125895	.001019	.001019	28.808
730	701	CAL.	.001488	.000026	.001488	.001488	1.000000	1.000000	29.474
730	702	CAL.	.000068	.000001	.000068	.000068	1.000000	1.000000	29.736
730	FF SUM =	.9653	ROW CP TIME =	30.427		- DISC		+Z 1ST RCS X=1516.	
731	32	CAL.	.001579	.000050	.001579	.001579	1.000000	1.000000	1.917
731	34	CAL.	.015869	.000338	.015869	.015869	1.000000	1.000000	2.410

MODEL = RIO STEP = 1 RCS ANALYSIS 4/9/75
FORM FACTOR CALCULATION LINK.

(* INDICATES NODE PAIR HAS BEEN SUBDIVIDED)
(R INDICATES FF CALCULATED FROM J TO I)

NODE I	NODE J	COMPUTATION	FE(I,J) W/SHAD	FE(J,I) W/SHAD	FA(I,J) W/SHAD	F (I,J) WO/SHAD	SHAD. E FACTOR	SHAD. A FACTOR	CP TIME (SEC)
731	380	CAL.	.015257	.000015	.015257	.068029	.224268	.224268	10.441
731	385	CAL.	.071304	.000098	.071304	.082508	.866317	.866317	11.101
731	701	CAL.	.007751	.000138	.007751	.007751	1.000000	1.000000	11.527
731	702	CAL.	.000001	.000000	.000001	.000001	1.000000	1.000000	11.721
731	FF SUM =	.1122	ROW CP TIME =	12.089		+ DISC		+Z 1ST RCS X=1516.	
732	740	CAL.	.000003	.000003	.000003	.000003	1.000000	1.000000	.461
732	900	CAL.	.014300	.000027	.014300	.027424	.521436	.521436	.936
732	31	CAL.	.017843	.001217	.017843	.022843	.781134	.781134	4.470
732	32	CAL.	.000688	.000022	.000688	.000688	1.000000	1.000000	4.709
732	33	CAL.	.202886	.004080	.202886	.202886	1.000000	1.000000	6.931
732	34	CAL.	.000500	.000011	.000500	.000500	1.000000	1.000000	7.126
732	25	CAL.	.000638	.000638	.000638	.000638	1.000000	1.000000	7.560
732	26	CAL.	.001458	.001458	.001458	.001458	1.000000	1.000000	7.797
732	800	CAL.	.009605	.000079	.009605	.009605	1.000000	1.000000	8.576
732	801	CAL.	.010967	.000051	.010967	.010967	1.000000	1.000000	8.897
732	805	CAL.	.019503	.000160	.019503	.019503	1.000000	1.000000	9.266
732	806	CAL.	.037821	.000163	.037821	.037821	1.000000	1.000000	9.533
732	807	CAL.	.001431	.000012	.001431	.001431	1.000000	1.000000	9.765
732	808	CAL.	.002030	.000010	.002030	.002030	1.000000	1.000000	9.996
732	810	CAL.	.000629	.000054	.000629	.000629	1.000000	1.000000	10.257
732	811	CAL.	.012533	.000061	.012533	.012533	1.000000	1.000000	10.618
732	222	CAL.	.005761	.000056	.005761	.025356	.227215	.227215	11.366
732	22	CAL.	.028897	.000050	.028897	.041703	.692931	.692931	11.772
732	15	CAL.	.000008	.000008	.000008	.000008	1.000000	1.000000	12.289
732	3	CAL.	.008138	.000006	.008138	.031124	.262303	.262303	14.768
732	4	CAL.	.032197	.000090	.032197	.067629	.476606	.476606	15.894
732	701	CAL.	.002592	.000046	.002592	.002592	1.000000	1.000000	29.371
732	702	CAL.	.000055	.000001	.000055	.000055	1.000000	1.000000	29.641
732	FF SUM =	.4702	ROW CP TIME =	30.329		- DISC		+Z 2ND RCS X=1529.	
733	32	CAL.	.004322	.000137	.004322	.004322	1.000000	1.000000	1.780
733	34	CAL.	.033851	.000730	.033851	.033851	1.000000	1.000000	2.233
733	380	CAL.	.015134	.000015	.015134	.061683	.245410	.245410	10.329
733	385	CAL.	.082823	.000114	.082823	.082823	1.000000	1.000000	10.999
733	701	CAL.	.011886	.000211	.011886	.011886	1.000000	1.000000	11.465
733	FF SUM =	.1494	ROW CP TIME =	11.962		+ DISC		+Z 2ND RCS X=1529.	
734	740	CAL.	.000012	.000012	.000012	.000012	1.000000	1.000000	.320
734	900	CAL.	.017374	.000033	.017374	.025276	.687365	.687365	.760

MODEL = RIO STEP = 1 RCS ANALYSIS 4/9/75
FORM FACTOR CALCULATION LINK.

(* INDICATES NODE PAIR HAS BEEN SUBDIVIDED)
(R INDICATES FF CALCULATED FROM J TO I)

NODE I	NODE J	COMPUTATION	FF(I,J) W/SHAD	FF(J,I) W/SHAD	FA(I,J) W/SHAD	F (I,J) WO/SHAD	SHAD. F FACTOR	SHAD. A FACTOR	CP TIME (SEC)
734	31	CAL.	.017762	.001212	.017762	.022002	.807293	.807293	4.109
734	32	CAL.	.000838	.000026	.000838	.000838	1.000000	1.000000	4.409
734	33	CAL.	.099383	.001999	.099383	.099383	1.000000	1.000000	5.475
734	34	CAL.	.000536	.000012	.000536	.000536	1.000000	1.000000	5.663
734	25	CAL.	.001155	.001155	.001155	.001155	1.000000	1.000000	6.109
734	26	CAL.	.002359	.002359	.002359	.002359	1.000000	1.000000	6.321
734	800	CAL.	.000612	.000071	.000612	.000612	1.000000	1.000000	7.083
734	801	CAL.	.011431	.000265	.011431	.011431	1.000000	1.000000	7.452
734	805	CAL.	.018926	.000155	.018926	.018926	1.000000	1.000000	7.824
734	806	CAL.	.042378	.000205	.042378	.042378	1.000000	1.000000	8.088
734	807	CAL.	.000776	.000006	.000776	.000776	1.000000	1.000000	8.296
734	808	CAL.	.001534	.000007	.001534	.001534	1.000000	1.000000	8.514
734	810	CAL.	.006420	.000053	.006420	.006420	1.000000	1.000000	8.767
734	811	CAL.	.013059	.000163	.013059	.013059	1.000000	1.000000	9.096
734	222	CAL.	.008054	.000039	.008054	.035125	.229291	.229291	9.769
734	22	CAL.	.048349	.000064	.048349	.050632	.951152	.951152	10.411
734	15	CAL.	.000008	.000008	.000008	.000008	1.000000	1.000000	10.923
734	3	CAL.	.013360	.000013	.013360	.028108	.475308	.475308	13.557
734	4	CAL.	.054493	.000152	.054493	.063164	.862720	.862720	14.472
734	701	CAL.	.004712	.000064	.004712	.004712	1.000000	1.000000	27.801
734	702	CAL.	.000039	.000001	.000039	.000039	1.000000	1.000000	28.037
734	FF SUM =	.4361	ROW CP TIME =	28.747		- DISC		+Z 3RD RCS X=1542.	
735	32	CAL.	.005583	.000176	.005583	.005583	1.000000	1.000000	1.658
735	34	CAL.	.031742	.000684	.031742	.031742	1.000000	1.000000	2.112
735	380	CAL.	.043059	.000043	.043059	.055651	.773728	.773728	10.234
735	385	CAL.	.081440	.000112	.081440	.081440	1.000000	1.000000	10.876
735	701	CAL.	.016554	.000294	.016554	.016554	1.000000	1.000000	11.314
735	FF SUM =	.1737	ROW CP TIME =	11.834		+ DISC		+Z 3RD RCS X=1542.	
740	800	CAL.	.001936	.000016	.001936	.001936	1.000000	1.000000	2.694
740	801	CAL.	.012161	.000059	.012161	.012161	1.000000	1.000000	3.001
740	802	CAL.	.001936	.000016	.001936	.001936	1.000000	1.000000	3.191
740	803	CAL.	.012161	.000059	.012161	.012161	1.000000	1.000000	3.444
740	807	CAL.	.095225	.000782	.095225	.095225	1.000000	1.000000	4.189
740	808	CAL.	.074338	.000359	.074338	.074338	1.000000	1.000000	4.550
740	810	CAL.	.095225	.000782	.095225	.095225	1.000000	1.000000	5.160
740	811	CAL.	.074338	.000359	.074338	.074338	1.000000	1.000000	5.406
740	701	CAL.	.001270	.000023	.001270	.001270	1.000000	1.000000	13.026
740	702	CAL.	.001953	.000028	.001953	.001953	1.000000	1.000000	13.352

MODEL = RIO STEP = 1 RCS ANALYSIS 4/9/75
FORM FACTOR CALCULATION LINK.

(* INDICATES NODE PAIR HAS BEEN SUBDIVIDED)
(R INDICATES FF CALCULATED FROM J TO I)

NODE I	NODE J	COMPUTATION	FE(I,J) W/SHAD	FE(J,I) W/SHAD	FA(I,J) W/SHAD	F (I,J) NO/SHAD	SHAD. E FACTER	SHAD. A FACTOR	CP TIME (SEC)	
740	FF SUM = .0453	ROW CP TIME = 13.753				- DISC		-X EVAP. X=1525. CENTER BELL		
741	31	CAL.	.000026	.000001	.000020	.000024	.836400	.836400	3.676	
741	32	CAL.	.000038	.000001	.000038	.000038	1.000000	1.000000	4.259	
741	33	CAL.	.000062	.000001	.000062	.000062	1.000000	1.000000	4.840	
741	34	CAL.	.000045	.000001	.000045	.000045	1.000000	1.000000	5.214	
741	800	CAL.	.000787	.000006	.000787	.000787	1.000000	1.000000	6.179	
741	802	CAL.	.000787	.000006	.000787	.000787	1.000000	1.000000	6.490	
741	222	CAL.	.163858	.000180	.163980	.164272	.995787	.995787	9.733	*
741	22	CAL.	.001721	.000003	.001721	.001721	1.000000	1.000000	10.110	
741	FF SUM = .1671	ROW CP TIME = 25.074				+ DISC		-X EVAP. X=1525. CENTER BELL		
900	24	CAL.	.000034	.017713	.000034	.000034	1.000000	1.000000	.381	R
900	27	CAL.	.000033	.017590	.000033	.000033	1.000000	1.000000	.875	R
900	701	CAL.	.001269	.011867	.001269	.001395	.909935	.909935	1.364	R
900	FF SUM = .0017	ROW CP TIME = 1.364				- RECT		EXTENDED AILERON TOP		
901	24	CAL.	.000004	.000651	.000004	.000004	1.000000	1.000000	.161	R
901	25	CAL.	.000011	.001938	.000011	.000011	1.000000	1.000000	.348	R
901	27	CAL.	.000100	.016954	.000100	.000100	1.000000	1.000000	.613	R
901	701	CAL.	.001569	.004714	.001569	.004550	.344828	.344828	.962	R
901	FF SUM = .0021	ROW CP TIME = .962				- RECT		EXTENDED ALERION INNER		
761	FF SUM = 0.	ROW CP TIME = .630				- CYLN		-Y RADIATOR		
762	FF SUM = 0.	ROW CP TIME = .722				+ CYLN		-Y RADIATOR		
763	FF SUM = 0.	ROW CP TIME = .676				- CYLN		-Y RADIATOR		
764	FF SUM = 0.	ROW CP TIME = .711				+ CYLN		-Y RADIATOR		

MODEL = RIO STEP = 1 RCS ANALYSIS 4/9/75
FORM FACTOR CALCULATION LINK.
1

(* INDICATES NODE PAIR HAS BEEN SUBDIVIDED)
(R INDICATES FF CALCULATED FROM J TO I)

NODE I	NODE J	COMPUTATION	FF(I,J) W/SHAD	FF(J,I) W/SHAD	FA(I,J) W/SHAD	F (I,J) NO/SHAD	SHAD. E FACTER	SHAD. A FACTOR	CP TIME (SEC)	
765	FF SUM = 0.		ROW CP TIME =	.881		- CYLN		-Y	RADIATOR	
766	FF SUM = 0.		ROW CP TIME =	.344		+ CYLN		-Y	RADIATOR	
767	FF SUM = .0000		ROW CP TIME =	.978		- CYLN		-Y	RADIATOR	
768	FF SUM = 0.		ROW CP TIME =	.350		+ CYLN		-Y	RADIATOR	
771	24	CAL.	.000000	.000018	.000000	.000000	1.000000	1.000000	.404	R
771	FF SUM = .0000		ROW CP TIME =	1.099		- CYLN		+Y	RADIATOR	
772	FF SUM = 0.		ROW CP TIME =	.388		+ CYLN		+Y	RADIATOR	
773	24	CAL.	.000000	.000042	.000000	.000000	1.000000	1.000000	.389	R
773	791	CAL.	.000008	.000061	.000008	.000136	.060341	.060341	1.037	R
773	FF SUM = .0000		ROW CP TIME =	1.075		- CYLN		+Y	RADIATOR	
774	FF SUM = 0.		ROW CP TIME =	.358		+ CYLN		+Y	RADIATOR	
775	FF SUM = .0000		ROW CP TIME =	.960		- CYLN		+Y	RADIATOR	
776	FF SUM = 0.		ROW CP TIME =	.346		+ CYLN		+Y	RADIATOR	
777	FF SUM = .0000		ROW CP TIME =	.936		- CYLN		+Y	RADIATOR	

MODEL = RIO STEP = 1 RCS ANALYSIS 4/9/75
FORM FACTOR CALCULATION LINK.

(* INDICATES NODE PAIR HAS BEEN SUBDIVIDED)
(R INDICATES FF CALCULATED FROM J TO I)

NODE I	NODE J	COMPUTATION	FE(I,J) W/SHAD	FE(J,I) W/SHAD	FA(I,J) W/SHAD	F (I,J) WO/SHAD	SHAD. E FACTER	SHAD. A FACTOR	CP TIME (SEC)	
778	FF SUM = 0.		ROW CP TIME = .349			+ CYLN		+Y RADIATOR		
140	FF SUM = 0.		ROW CP TIME = .418			+ DISC		END BAY AREA DISK		
182	FF SUM = 0.		ROW CP TIME = .507			+ PARAB		1ST PARAB -Y OMS		
184	FF SUM = 0.		ROW CP TIME = .704			+ CYLN		OMS END CYLINDER RADIUS=65.		
29	FF SUM = 0.		ROW CP TIME = .476			+ TRAP		TRAP BOTTOM OMS END SEALER		
31	29	CAL.	.000464	.000797	.000464	.000632	.733766	.733766	.426	R
31	26	CAL.	.000121	.001770	.000121	.000212	.570268	.570268	.723	R
31	27	CAL.	.000042	.000610	.000042	.000042	1.000000	1.000000	.885	R
31	701	CAL.	.035467	.009243	.035467	.042062	.843202	.843202	1.453	
31	FF SUM = .0619		ROW CP TIME = 1.453			+ DISC		1ST TRIANGLE LT SIDE LOOKING B		
32	25	CAL.	.000275	.000709	.000275	.000275	1.000000	1.000000	.524	R
32	26	CAL.	.000374	.001824	.000374	.000374	1.000000	1.000000	.987	R
32	701	CAL.	.073213	.041199	.073213	.073213	1.000000	1.000000	2.087	
32	FF SUM = .0757		ROW CP TIME = 2.126			+ DISC		LAST TRI RT SIDE		
172	FF SUM = 0.		ROW CP TIME = .532			+ PARAB		1ST PARAB +Y OMS		
174	FF SUM = 0.		ROW CP TIME = .469			+ CYLN		+Y OMS END CYLINDER		
33	25	CAL.	.000565	.028073	.000565	.000565	1.000000	1.000000	.392	R
33	26	CAL.	.000747	.037167	.000747	.000747	1.000000	1.000000	.773	R
33	701	CAL.	.060919	.053851	.060919	.064257	.948059	.948059	1.616	

MODEL = RIO STEP = 1 RCS ANALYSIS 4/9/75
FORM FACTOR CALCULATION LINK.

(* INDICATES NODE PAIR HAS BEEN SUBDIVIDED)
(R INDICATES FF CALCULATED FROM J TO I)

NODE I	NODE J	COMPUTATION	FE(I,J) W/SHAD	FE(J,I) W/SHAD	FA(I,J) W/SHAD	F (I,J) WO/SHAD	SHAD. E FACTER	SHAD. A FACTOR	CP TIME (SEC)	
33	FF SUM = .0858	ROW CP TIME = 1.676				- DISC		2ND TRI LEFT SIDE		
34	25	CAL.	.000310	.014391	.000310	.000310	1.000000	1.000000	.413	R
34	26	CAL.	.000510	.023672	.000510	.000510	1.000000	1.000000	.751	R
34	701	CAL.	.091534	.079504	.091534	.091534	1.000000	1.000000	1.691	
34	FF SUM = .0956	ROW CP TIME = 1.695				+ DISC		3RD TRI MIDDLE RT SIDE		
35	FF SUM = 0.	ROW CP TIME = .440				+ TRAP		TOP INSIDE TRAP		
36	FF SUM = 0.	ROW CP TIME = .423				+ TRAP		TOP INSIDE TRAP		
24	2	CAL.	.008601	.000006	.008601	.008755	.982354	.982354	2.324	
24	3	CAL.	.018517	.000018	.018517	.018517	1.000000	1.000000	2.740	
24	144	CAL.	.000516	.000002	.000516	.000516	1.000000	1.000000	2.949	
24	4	CAL.	.005204	.000015	.005204	.005204	1.000000	1.000000	3.151	
24	785	CAL.	.000414	.000000	.000414	.000414	1.000000	1.000000	8.175	
24	787	CAL.	.000038	.000000	.000038	.000038	1.000000	1.000000	8.942	
24	FF SUM = .0531	ROW CP TIME = 10.763				- DISC		REAR Y RCS (Y WAS 134. ALL RES		
25	26	CAL.	.002647	.002647	.002647	.002647	1.000000	1.000000	.194	
25	600	CAL.	.023581	.000194	.023581	.023581	1.000000	1.000000	1.025	
25	601	CAL.	.000718	.000294	.000718	.000718	1.000000	1.000000	1.545	
25	605	CAL.	.018312	.000150	.018312	.018312	1.000000	1.000000	1.916	
25	606	CAL.	.057962	.000280	.057962	.057962	1.000000	1.000000	2.263	
25	610	CAL.	.010139	.000083	.010139	.010139	1.000000	1.000000	2.318	
25	611	CAL.	.024429	.000118	.024429	.024429	1.000000	1.000000	3.140	
25	222	CAL.	.050270	.000655	.050270	.059461	.899916	.899916	4.431	
25	22	CAL.	.089697	.000149	.089697	.097796	.878318	.878318	5.360	
25	407	CAL.	.000065	.000005	.000065	.000065	1.000000	1.000000	5.720	
25	15	CAL.	.000307	.000007	.000307	.000307	1.000000	1.000000	5.915	
25	143	CAL.	.000283	.000000	.000283	.000446	.642079	.642079	8.212	
25	144	CAL.	.001473	.000004	.001473	.001473	1.000000	1.000000	8.450	
25	4	CAL.	.005171	.000014	.005171	.005977	.865255	.865255	8.863	
25	701	CAL.	.000172	.000000	.000172	.000130	.130374	.130374	16.560	
25	806	CAL.	.015955	.000039	.015955	.016138	.988869	.988869	20.037	
25	380	CAL.	.017403	.000018	.017403	.046445	.374823	.374823	21.229	
25	385	CAL.	.035721	.000118	.035721	.036130	.988868	.988868	22.057	
25	701	CAL.	.011322	.000184	.011322	.011322	1.000000	1.000000	22.806	
25	702	CAL.	.000966	.000010	.000966	.000966	1.000000	1.000000	23.367	

MODEL = RIO STEP = 1 RCS ANALYSIS 4/9/75
FORM FACTOR CALCULATION LINK.

(* INDICATES NODE PAIR HAS BEEN SUBDIVIDED)
(R INDICATES FF CALCULATED FROM J TO I)

NODE I	NODE J	COMPUTATION	FE(I,J) W/SHAD	FE(J,I) W/SHAD	FA(I,J) W/SHAD	F (I,J) WO/SHAD	SHAD. E FACTER	SHAD. A FACTOR	CP TIME (SEC)	
25	FF SUM = .5730	ROW CP TIME = 23.837				+ DISC		FEAR Y RCS (Y WAS 134. ALL RES		
26	830	CAL.	.002640	.000022	.002640	.002640	1.000000	1.000000	.464	
26	801	CAL.	.014055	.000068	.014055	.014055	1.000000	1.000000	.699	
26	22	CAL.	.005103	.000009	.005103	.005383	.948081	.948081	1.843	
26	880	CAL.	.021745	.000022	.021745	.042082	.516658	.516658	8.024	
26	885	CAL.	.075639	.000104	.075639	.077703	.973435	.973435	9.345	
26	701	CAL.	.049862	.000086	.049862	.049862	1.000000	1.000000	10.109	
26	702	CAL.	.000179	.000003	.000179	.000179	1.000000	1.000000	10.386	
26	FF SUM = .2549	ROW CP TIME = 10.786				- DISC		FEAR Z RCS (Z WAS 57. ALL REST		
27	800	CAL.	.002289	.000019	.002289	.002289	1.000000	1.000000	.592	
27	801	CAL.	.008285	.000040	.008285	.008285	1.000000	1.000000	.832	
27	805	CAL.	.032715	.000269	.032715	.032715	1.000000	1.000000	1.234	
27	806	CAL.	.109936	.000532	.109936	.109936	1.000000	1.000000	1.646	
27	810	CAL.	.007038	.000058	.007038	.007038	1.000000	1.000000	2.250	
27	811	CAL.	.015470	.000075	.015470	.015470	1.000000	1.000000	2.611	
27	222	CAL.	.087834	.000097	.087834	.096752	.907829	.907829	4.191	
27	22	CAL.	.008860	.000015	.008860	.008860	1.000000	1.000000	4.611	
27	407	CAL.	.000001	.000001	.000001	.000003	.415001	.415001	4.929	
27	2	CAL.	.007526	.000005	.007526	.009183	.819612	.819612	7.095	
27	3	CAL.	.017068	.000016	.017068	.017068	1.000000	1.000000	7.592	
27	144	CAL.	.007495	.000022	.007495	.012529	.598265	.598265	7.897	
27	4	CAL.	.065947	.000184	.065947	.068952	.956422	.956422	8.764	
27	150	CAL.	.000813	.000001	.000813	.006144	.132375	.132375	9.129	
27	FF SUM = .4713	ROW CP TIME = 21.599				+ DISC		FEAR Z RCS (Z WAS 57. ALL REST		
149	FF SUM = 0.	ROW CP TIME = .201				- IRAP		- Y. REAR SIDE TAPER...		
707	FF SUM = 0.	ROW CP TIME = .311				- DISC		.....JULY 8 EVAP..3 IN. RAD.		
708	FF SUM = 0.	ROW CP TIME = .261				+ DISC		.....JULY 8 EVAP..3 IN. RAD.		
800	701	CAL.	.007986	.017296	.007986	.007986	1.000000	1.000000	.383	R

MODEL = RIO STEP = 1 RCS ANALYSIS 4/9/75
FORM FACTOR CALCULATION LINK.

(* INDICATES NODE PAIR HAS BEEN SUBDIVIDED)
(R INDICATES FF CALCULATED FROM J TO I)

NODE I	NODE J	COMPUTATION	FE(I,J) W/SHAD	FE(J,I) W/SHAD	FA(I,J) W/SHAD	F (I,J) WO/SHAD	SHAD. E FACTER	SHAD. A FACTOR	CP TIME (SEC)	
800	FF SUM = .0101	ROW CP TIME = .383				+ PARAB	TOP ENGIN			
801	701	CAL.	.007277	.026753	.007277	.007277	1.000000	1.000000	.409	R
801	FF SUM = .0035	ROW CP TIME = .409				+ PARAB	TOP ENGIN			
802	FF SUM = .0000	ROW CP TIME = .180				+ PARAB	TOP ENGIN			
803	FF SUM = .0001	ROW CP TIME = .200				+ PARAB	TOP ENGIN			
805	701	CAL.	.003520	.007623	.003520	.003520	1.000000	1.000000	.322	R
805	FF SUM = .0060	ROW CP TIME = .322				+ PARAB	+ Y ENGIN			
806	701	CAL.	.001737	.006388	.001737	.001737	1.000000	1.000000	.356	R
806	FF SUM = .0048	ROW CP TIME = .395				+ PARAB	+ Y ENGIN			
807	701	CAL.	.000506	.001097	.000506	.000506	1.000000	1.000000	.310	R
807	FF SUM = .0013	ROW CP TIME = .310				+ PARAB	+ Y ENGIN			
808	701	CAL.	.000396	.001457	.000396	.000396	1.000000	1.000000	.282	R
808	FF SUM = .0008	ROW CP TIME = .282				+ PARAB	+ Y ENGIN			
810	701	CAL.	.002278	.004934	.002278	.002278	1.000000	1.000000	.319	R
810	FF SUM = .0038	ROW CP TIME = .358				+ PARAB	-Y ENGIN...			
811	701	CAL.	.001641	.006033	.001641	.001641	1.000000	1.000000	.319	R
811	FF SUM = .0028	ROW CP TIME = .359				+ PARAB	-Y ENGIN...			

MODEL = RIO STEP = 1 RCS ANALYSIS 4/9/75
FORM FACTOR CALCULATION LINK.

(* INDICATES NODE PAIR HAS BEEN SUBDIVIDED)
(R INDICATES FF CALCULATED FROM J TO I)

NODE I	NODE J	COMPUTATION	FE(I,J) W/SHAD	FE(J,I) W/SHAD	FA(I,J) W/SHAD	F (I,J) WO/SHAD	SHAD. E FACTER	SHAD. A FACTOR	CP TIME (SEC)	
812	FF SUM = 0.		ROW CP TIME =	.272	+ PARAB	-Y ENGIN...				
813	FF SUM = 0.		ROW CP TIME =	.257	+ PARAB	-Y ENGIN...				
20	FF SUM = 0.		ROW CP TIME =	.166	+ DISC	...-Y OWS SEALER ...				
21	FF SUM = 0.		ROW CP TIME =	.136	+ DISC	..+Y OWS SEALER ...				
222	701	CAL.	.000176	.002852	.000176	.002564	.068738	.068738	.411	R
222	FF SUM = .0008		ROW CP TIME =	.411	- RECT	BACK RECT 7.350EG				
22	701	CAL.	.013038	.133976	.013038	.015520	.851045	.851045	2.427	R
22	FF SUM = .0142		ROW CP TIME =	2.427	- DISC	REAR END HALF DISK				
23	FF SUM = 0.		ROW CP TIME =	.142	+ DISC	REAR END HALF DISK				
407	FF SUM = .0008		ROW CP TIME =	.206	+ DISC	BACK SIDE EVAPORAT, UPDATED				
15	FF SUM = .0001		ROW CP TIME =	.159	+ DISC	REAR END EVAPORATOR				
10	FF SUM = 0.		ROW CP TIME =	.338	- TRAP	....LEFT FRONT WING A ...				
11	FF SUM = 0.		ROW CP TIME =	.346	+ TRAP	......LEFT MIDDLE WING BACK.B				

MODEL = RIO STEP = 1 RCS ANALYSIS 4/9/75
FORM FACTOR CALCULATION LINK.

(* INDICATES NODE PAIR HAS BEEN SUBDIVIDED)
(R INDICATES FF CALCULATED FROM J TO I)

NODE I	NODE J	COMPUTATION	FE(I,J) W/SHAD	FE(J,I) W/SHAD	FA(I,J) W/SHAD	F (I,J) WO/SHAD	SHAD. E FACTER	SHAD. A FACTOR	CP TIME (SEC)	
141	FF SUM = 0.		ROW CP TIME =	.349		+ RECT		BS INNER WING		
12	FF SUM = 0.		ROW CP TIME =	.304		+ RECT		..... LEFT BACK RECT. WING C		
142	FF SUM = 0.		ROW CP TIME =	.319		+ RECT		INNER WING C		
13	FF SUM = 0.		ROW CP TIME =	.422		+ TRAP		..... LEFT WING TAIL EDGE		
1	FF SUM = 0.		ROW CP TIME =	.380		+ TRAP		...FRONT WING TRIANGLE RT.A.58		
2	FF SUM = .0001		ROW CP TIME =	.386		- TRAP		.....MIDDLE WING TRAP, RT B ..		
143	FF SUM = .0000		ROW CP TIME =	.300		- RECT		B +Y RECTANGLE WING		
3	701	CAL.	.000404	.007948	.000404	.001179	.342172	.342172	.373	R
3	FF SUM = .0006		ROW CP TIME =	.373		- RECT		.... BACK WING RECT. RTC .129		
144	FF SUM = .0001		ROW CP TIME =	.315		- RECT		INNER WING C RECT		
4	701	CAL.	.004210	.026795	.004210	.005071	.830082	.830082	.578	R
4	FF SUM = .0056		ROW CP TIME =	.582		- TRAP		+Y WING TAIL EDGE		
150	FF SUM = .0000		ROW CP TIME =	.325		- CYLN		BAY AREA CYLINDER		

MODEL = RIO STEP = 1 RCS ANALYSIS 4/9/75
FORM FACTOR CALCULATION LINK.

(* INDICATES NODE PAIR HAS BEEN SUBDIVIDED)
(R INDICATES FF CALCULATED FROM J TO I)

NODE I	NODE J	COMPUTATION	FE(I,J) W/SHAD	FE(J,I) W/SHAD	FA(I,J) W/SHAD	F (I,J) WO/SHAD	SHAD. E FACTER	SHAD. A FACTOR	CF TIME (SEC)
151	FF SUM = .0000	ROW CP TIME =			.350		- CYLN	BAY AREA CYLINDER	
152	FF SUM = 0.	ROW CP TIME =			.335		- CYLN	BAY AREA CYLINDER	
153	FF SUM = 0.	ROW CP TIME =			.352		- CYLN	BAY AREA CYLINDER	
154	FF SUM = 0.	ROW CP TIME =			.311		- CYLN	BAY AREA CYLINDER	
155	FF SUM = 0.	ROW CP TIME =			.352		- CYLN	BAY AREA CYLINDER	
156	FF SUM = 0.	ROW CP TIME =			.345		- CYLN	BAY AREA CYLINDER	
157	FF SUM = 0.	ROW CP TIME =			.357		- CYLN	BAY AREA CYLINDER	
185	FF SUM = 0.	ROW CP TIME =			.342		+ DISC	FRONT BAY AREA DISK	
122	FF SUM = 0.	ROW CP TIME =			.194		+ PARAB	VERY NOSE CONE	
123	FF SUM = 0.	ROW CP TIME =			.204		+ PARAB	VERY NOSE CONE	
124	FF SUM = 0.	ROW CP TIME =			.191		+ PARAB	VERY NOSE CONE	
125	FF SUM = 0.	ROW CP TIME =			.191		+ PARAB	VERY NOSE CONE	

MODEL = RIO STEP = 1 RCS ANALYSIS 4/9/75
FORM FACTOR CALCULATION LINK.

(* INDICATES NODE PAIR HAS BEEN SUBDIVIDED)
(R INDICATES FF CALCULATED FROM J TO I)

NODE I	NODE J	COMPUTATION	FF(I,J) W/SHAD	FF(J,I) W/SHAD	FA(I,J) W/SHAD	F (I,J) WO/SHAD	SHAD. F FACTOR	SHAD. A FACTOR	CP TIME (SEC)	
320	FF SUM = 0.	ROW CP TIME =			.206		+ CYLN		NOSE CYLINDER	
321	FF SUM = 0.	ROW CP TIME =			.203		+ CYLN		NOSE CYLINDER	
322	FF SUM = 0.	ROW CP TIME =			.170		+ CYLN		NOSE CYLINDER	
323	FF SUM = 0.	ROW CP TIME =			.168		+ CYLN		NOSE CYLINDER	
324	FF SUM = 0.	ROW CP TIME =			.137		+ CYLN		NOSE CYLINDER	
325	FF SUM = 0.	ROW CP TIME =			.124		+ CYLN		NOSE CYLINDER	
326	FF SUM = 0.	ROW CP TIME =			.122		+ CYLN		NOSE CYLINDER	
327	FF SUM = 0.	ROW CP TIME =			.128		+ CYLN		NOSE CYLINDER	
328	FF SUM = 0.	ROW CP TIME =			.211		+ CYLN		NOSE CYLINDER	
329	FF SUM = 0.	ROW CP TIME =			.209		+ CYLN		NOSE CYLINDER	
330	FF SUM = 0.	ROW CP TIME =			.217		+ CYLN		NOSE CYLINDER	
331	FF SUM = 0.	ROW CP TIME =			.198		+ CYLN		NOSE CYLINDER	

MODEL = RIO STEP = 1 RCS ANALYSIS 4/9/75
FORM FACTOR CALCULATION LINK.

(* INDICATES NODE PAIR HAS BEEN SUBDIVIDED)
(R INDICATES FF CALCULATED FROM J TO I)

NODE I	NODE J	COMPUTATION	FE(I,J) W/SHAD	FE(J,I) W/SHAD	FA(I,J) W/SHAD	F (I,J) WO/SHAD	SHAD. E FACTER	SHAD. A FACTOR	CP TIME (SEC)	
332	FF SUM = 0.	ROW CP TIME =	.297			+ CYLN			NOSE CYLINDER	
333	FF SUM = 0.	ROW CP TIME =	.258			+ CYLN			NOSE CYLINDER	
334	FF SUM = 0.	ROW CP TIME =	.239			+ CYLN			NOSE CYLINDER	
335	FF SUM = 0.	ROW CP TIME =	.266			+ CYLN			NOSE CYLINDER	
340	FF SUM = 0.	ROW CP TIME =	.200			+ PARAB			HOOD PARTIAL BACK	
341	FF SUM = 0.	ROW CP TIME =	.197			+ PARAB			HOOD PARTIAL BACK	
342	FF SUM = 0.	ROW CP TIME =	.184			+ PARAB			HOOD PARTIAL BACK	
343	FF SUM = 0.	ROW CP TIME =	.193			+ PARAB			HOOD PARTIAL BACK	
344	FF SUM = 0.	ROW CP TIME =	.187			+ PARAB			HOOD PARTIAL BACK	
345	FF SUM = 0.	ROW CP TIME =	.189			+ PARAB			HOOD PARTIAL BACK	
346	FF SUM = 0.	ROW CP TIME =	.190			+ PARAB			HOOD PARTIAL BACK	
347	FF SUM = 0.	ROW CP TIME =	.188			+ PARAB			HOOD PARTIAL BACK	

MODEL = RIO STEP = 1 RCS ANALYSIS 4/9/75
FORM FACTOR CALCULATION LINK.

(* INDICATES NODE PAIR HAS BEEN SUBDIVIDED)
(R INDICATES FF CALCULATED FROM J TO I)

NODE I	NODE J	COMPUTATION	FF(I,J) W/SHAD	FF(J,I) W/SHAD	FA(I,J) W/SHAD	F (I,J) WO/SHAD	SHAD. E FACTOR	SHAD. A FACTOR	CP TIME (SEC)	
348	FF SUM = 0.	ROW CP TIME =			.215		+ PARAB			HOOD PARTIAL BACK
349	FF SUM = 0.	ROW CP TIME =			.176		+ PARAB			HOOD PARTIAL BACK
350	FF SUM = 0.	ROW CP TIME =			.191		+ PARAB			HOOD PARTIAL BACK
351	FF SUM = 0.	ROW CP TIME =			.214		+ PARAB			HOOD PARTIAL BACK
352	FF SUM = 0.	ROW CP TIME =			.184		+ PARAB			HOOD PARTIAL BACK
353	FF SUM = 0.	ROW CP TIME =			.192		+ PARAB			HOOD PARTIAL BACK
354	FF SUM = 0.	ROW CP TIME =			.162		+ PARAB			HOOD PARTIAL BACK
355	FF SUM = 0.	ROW CP TIME =			.178		+ PARAB			HOOD PARTIAL BACK
360	FF SUM = 0.	ROW CP TIME =			.183		+ PARAB			WINDOW
361	FF SUM = 0.	ROW CP TIME =			.182		+ PARAB			WINDOW
362	FF SUM = 0.	ROW CP TIME =			.189		+ PARAB			WINDOW
363	FF SUM = 0.	ROW CP TIME =			.186		+ PARAB			WINDOW

MODEL = RIO STEP = 1 RCS ANALYSIS 4/9/75
FORM FACTOR CALCULATION LINK.

(* INDICATES NODE PAIR HAS BEEN SUBDIVIDED)
(R INDICATES FF CALCULATED FROM J TO I)

NODE I	NODE J	COMPUTATION	FE(I,J) W/SHAD	FE(J,I) W/SHAD	FA(I,J) W/SHAD	F (I,J) WO/SHAD	SHAD. E FACTER	SHAD. A FACTOR	CP TIME (SEC)
364	FF SUM = 0.	ROW CP TIME =			.224		+ PARAB	WINDOW	
365	FF SUM = 0.	ROW CP TIME =			.190		+ PARAB	WINDOW	
366	FF SUM = 0.	ROW CP TIME =			.188		+ PARAB	WINDOW	
367	FF SUM = 0.	ROW CP TIME =			.195		+ PARAB	WINDOW	
368	FF SUM = 0.	ROW CP TIME =			.184		+ PARAB	WINDOW	
369	FF SUM = 0.	ROW CP TIME =			.191		+ PARAB	WINDOW	
370	FF SUM = 0.	ROW CP TIME =			.180		+ PARAB	WINDOW	
371	FF SUM = 0.	ROW CP TIME =			.181		+ PARAB	WINDOW	
372	FF SUM = 0.	ROW CP TIME =			.180		+ PARAB	WINDOW	
373	FF SUM = 0.	ROW CP TIME =			.189		+ PARAB	WINDOW	
374	FF SUM = 0.	ROW CP TIME =			.178		+ PARAB	WINDOW	
375	FF SUM = 0.	ROW CP TIME =			.166		+ PARAB	WINDOW	

MODEL = RIO STEP = 1 RCS ANALYSIS 4/9/75
FORM FACTOR CALCULATION LINK.

(* INDICATES NODE PAIR HAS BEEN SUBDIVIDED)
(R INDICATES FF CALCULATED FROM J TO I)

NODE I	NODE J	COMPUTATION	FE(I,J) W/SHAD	FE(J,I) W/SHAD	FA(I,J) W/SHAD	F (I,J) NO/SHAD	SHAD. E FACTER	SHAD. A FACTOR	CP TIME (SEC)	
401	FF SUM =	0.	ROW CP TIME =	.150		- RECT	BODY BOTTOM (FRT)		4 1	
402	FF SUM =	0.	ROW CP TIME =	.140		- RECT	BODY BOTTOM (REAR)		402'	
781	FF SUM =	.0000	ROW CP TIME =	.444		- CYLN	.....+Y SIDE DOOR.....			
782	FF SUM =	0.	ROW CP TIME =	.170		+ CYLN	.....+Y SIDE DOOR.....			
783	FF SUM =	0.	ROW CP TIME =	.464		- CYLN	.....+Y SIDE DOOR.....			
784	FF SUM =	0.	ROW CP TIME =	.167		+ CYLN	.....+Y SIDE DOOR.....			
785	FF SUM =	.0000	ROW CP TIME =	.463		- CYLN	.....+Y SIDE DOOR.....			
786	FF SUM =	0.	ROW CP TIME =	.129		+ CYLN	.....+Y SIDE DOOR.....			
787	FF SUM =	.0000	ROW CP TIME =	.431		- CYLN	.....+Y SIDE DOOR.....			
788	FF SUM =	0.	ROW CP TIME =	.181		+ CYLN	.....+Y SIDE DOOR.....			
791	FF SUM =	0.	ROW CP TIME =	.435		- CYLN	... -Y SIDE DOOR....			
792	FF SUM =	0.	ROW CP TIME =	.248		+ CYLN	... -Y SIDE DOOR....			

MODEL = RIO STEP = 1 RCS ANALYSIS 4/9/75
FORM FACTOR CALCULATION LINK.

(* INDICATES NODE PAIR HAS BEEN SUBDIVICED)
(K INDICATES FF CALCULATED FROM J TO I)

NODE I	NODE J	COMPUTATION	FF(I,J) W/SHAD	FF(J,I) W/SHAD	FA(I,J) W/SHAD	F (I,J) WO/SHAD	SHAD. E FACTER	SHAD. A FACTOR	CP TIME (SEC)	
793	FF SUM = 0.	ROW CP TIME =	.424		- CYLN	... -Y SIDE DOOR....				
794	FF SUM = 0.	ROW CP TIME =	.228		+ CYLN	... -Y SIDE DOOR....				
795	FF SUM = 0.	ROW CP TIME =	.151		- CYLN	... -Y SIDE DOOR....				
796	FF SUM = .0000	ROW CP TIME =	.438		+ CYLN	... -Y SIDE DOOR....				
797	FF SUM = 0.	ROW CP TIME =	.146		- CYLN	... -Y SIDE DOOR....				
798	FF SUM = 0.	ROW CP TIME =	.461		+ CYLN	... -Y SIDE DOOR....				
301	FF SUM = 0.	ROW CP TIME =	.242		+ TRAP	+Y SIDE FRONT TRAPOZOID				
305	FF SUM = 0.	ROW CP TIME =	.195		+ RECT	BODY SIDE (MIDDLE-PORT)			3.5	
306	FF SUM = .0001	ROW CP TIME =	.229		+ RECT	BODY SIDE (BACK-PORT)			3.6	
311	FF SUM = 0.	ROW CP TIME =	.266		- TRAP	-Y SIDE FRONT TRAPOZOID				
315	FF SUM = 0.	ROW CP TIME =	.113		+ RECT	BODY SIDE (MIDDLE-STBD)			3.5	
316	FF SUM = 0.	ROW CP TIME =	.132		+ RECT	BODY SIDE (BACK-STBD)			3.6	

MODEL = RIO STEP = 1 RCS ANALYSIS 4/9/75
FORM FACTOR CALCULATION LINK.

(* INDICATES NODE PAIR HAS BEEN SUBDIVIDED)
(R INDICATES FF CALCULATED FROM J TO I)

NODE I	NODE J	COMPUTATION	FE(I,J) W/SHAD	FE(J,I) W/SHAD	FA(I,J) W/SHAD	F (I,J) WO/SHAD	SHAD. E FACTER	SHAD. A FACTOR	CP TIME (SEC)		
202	FF SUM =	0.	ROW CP TIME =	.162	+ CYLN	BODY TOP (STBD-REAR)	202				
212	FF SUM =	.0000	ROW CP TIME =	.807	+ CYLN	BODY TOP (PORT-REAR)	212				
380	701	CAL.	.001257	.022168	.001257	.003211	.391395	.391395	.737	R	
380	FF SUM =	.0014	ROW CP TIME =	.737	+ TRAP	VERTICAL FIN (PORT)	20				
385	700	CAL.	.000148	.001906	.000148	.000148	1.000000	1.000000	.169	R	
385	701	CAL.	.006541	.084453	.006541	.006541	1.000000	1.000000	.541	R	
385	FF SUM =	.0081	ROW CP TIME =	.575	+ TRAP	VERTICAL FIN (PORT-AFT)	20				
390	FF SUM =	0.	ROW CP TIME =	.131	- TRAP	VERTICAL FIN (STBD)	20				
395	FF SUM =	0.	ROW CP TIME =	.127	- TRAP	VERTICAL FIN (STBD-AFT)	20				
700	FF SUM =	0.	ROW CP TIME =	.338	+ DISC	..MOST FORWARD EVAPORATOR.....					
700	FF SUM =	.0019	ROW CP TIME =	.513	- DISC	.......SUPER ENGINS (OMS LOCAT					
701	703	CAL.	.000038	.000038	.000038	.000038	1.000000	1.000000	.355		
701	FF SUM =	.5627	ROW CP TIME =	1.000	+ DISC	.......SUPER ENGINS (OMS LOCAT					
702	FF SUM =	.0002	ROW CP TIME =	.021	- DISC	.......SUPER ENGINS (OMS LOCAT					
703	FF SUM =	.0000	ROW CP TIME =	.007	+ DISC	.......SUPER ENGINS (OMS LOCAT					

MODEL = RIO STEP = 1 RCS ANALYSIS 4/9/75
FORM FACTOR CALCULATION LINK.

(* INDICATES NODE PAIR HAS BEEN SUBDIVIDED)
(R INDICATES FF CALCULATED FROM J TO I)

NODE I	NODE J	COMPUTATION	FE(I,J) W/SHAD	FE(J,I) W/SHAD	FA(I,J) W/SHAD	F (I,J) WO/SHAD	SHAD. E FACTER	SHAD. A FACTOR	CP TIME (SEC)
16	FF SUM = 0.	ROW CP TIME =			.020		- DISC	...FRONT RCS..LOOKING +/-Y AT	
19	FF SUM = 0.	ROW CP TIME =			.008		+ DISC	...FRONT RCS..LOOKING +/-Y AT	
15	FF SUM = 0.	ROW CP TIME =			.011		- DISC	...MIDDLE EVAP. LOOKING +/- Y.	
17	FF SUM = 0.	ROW CP TIME =			.026		+ DISC	...MIDDLE EVAP. LOOKING +/- Y.	
399	FF SUM = 0.	ROW CP TIME =			.011		+ RECT	VERT. FIN LOG. EDGE 2	

TOTAL CP TIME (SEC) FOR PROBLEM = 725.413

MODEL = RIO STEP = 1 RCS ANALYSIS 4/9/75
FORM FACTOR CALCULATION LINK.

FORM FACTOR SUMS FROM NODE I

NODE I -	FF SUM	NODE I -	FF SUM	NODE I -	FF SUM	NODE I -	FF SUM	NODE I -	FF SUM	NODE I -	FF SUM	NODE I -	FF SUM
5000 -	0.	5005 -	0.	5010 -	.0000009	5015 -	.0000015	5020 -	.0000021	5025 -	.0000028		
5030 -	.0000043	5035 -	.0000047	5040 -	.0000005	5045 -	.0000028	5050 -	.0000075	5055 -	.0000123		
5060 -	.0002713	5065 -	.0004157	5070 -	.0005949	5075 -	.0005412	5080 -	.0004627	5085 -	.0003840		
5090 -	.0003192	5095 -	.0002622	5100 -	.0000953	5105 -	.0000374	5110 -	.0000014	145 -	.0013586		
146 -	0.	147 -	.0018803	710 -	.3731394	711 -	.2888915	712 -	.4046348	713 -	.4196085		
714 -	.3968230	715 -	.4432020	720 -	.0775529	721 -	.6801777	722 -	.0715193	723 -	.0932144		
724 -	.0644702	725 -	.0329330	726 -	.0983484	727 -	.5980634	730 -	.5652732	731 -	.1122418		
732 -	.4702049	733 -	.1493565	734 -	.4361800	735 -	.1797206	740 -	.6482691	741 -	.1670551		
900 -	.3617030	901 -	.0321590	751 -	0.	762 -	0.	763 -	0.	764 -	0.		
765 -	0.	766 -	0.	767 -	.0030003	768 -	0.	771 -	.0000001	772 -	0.		
773 -	.0003036	774 -	0.	775 -	.0000000	776 -	0.	777 -	.0000000	778 -	0.		
140 -	0.	132 -	0.	184 -	0.	29 -	0.	31 -	.0618633	32 -	.0757417		
172 -	0.	174 -	0.	33 -	.0868060	34 -	.0958351	35 -	0.	36 -	0.		
24 -	.0930559	25 -	.5730503	26 -	.2546586	27 -	.4712872	149 -	0.	707 -	0.		
708 -	0.	800 -	.0101227	801 -	.0094535	802 -	.0000224	803 -	.0000588	805 -	.0060230		
806 -	.0046232	807 -	.0013228	808 -	.0007845	810 -	.0037651	811 -	.0028475	812 -	0.		
813 -	0.	20 -	0.	21 -	0.	222 -	.0007897	22 -	.0142138	23 -	0.		
407 -	.0000292	15 -	.0000023	10 -	0.	11 -	0.	141 -	0.	12 -	0.		
142 -	0.	13 -	0.	1 -	0.	2 -	.0000530	143 -	.0000014	3 -	.0006032		
144 -	.0001078	4 -	.0055693	150 -	.0000023	151 -	.0000006	152 -	0.	153 -	0.		
154 -	0.	155 -	0.	156 -	0.	157 -	0.	135 -	0.	122 -	0.		
123 -	0.	124 -	0.	125 -	0.	320 -	0.	321 -	0.	322 -	0.		
323 -	0.	324 -	0.	325 -	0.	326 -	0.	327 -	0.	328 -	0.		
329 -	0.	330 -	0.	331 -	0.	332 -	0.	333 -	0.	334 -	0.		
335 -	0.	340 -	0.	341 -	0.	342 -	0.	343 -	0.	344 -	0.		
345 -	0.	346 -	0.	347 -	0.	348 -	0.	349 -	0.	350 -	0.		
351 -	0.	352 -	0.	353 -	0.	354 -	0.	355 -	0.	360 -	0.		
361 -	0.	362 -	0.	363 -	0.	364 -	0.	365 -	0.	366 -	0.		
367 -	0.	368 -	0.	369 -	0.	370 -	0.	371 -	0.	372 -	0.		
373 -	0.	374 -	0.	375 -	0.	401 -	0.	402 -	0.	781 -	.0000002		
782 -	0.	783 -	0.	784 -	0.	785 -	.0000025	786 -	0.	787 -	.0000002		
788 -	0.	791 -	0.	792 -	0.	793 -	0.	794 -	0.	795 -	0.		
796 -	.0000013	797 -	0.	798 -	0.	301 -	0.	305 -	0.	306 -	.0000024		
311 -	0.	315 -	0.	316 -	0.	202 -	0.	212 -	.0000083	380 -	.0014230		
385 -	.0080869	390 -	0.	395 -	0.	705 -	0.	700 -	.0019078	701 -	.9620663		
702 -	.0002289	703 -	.0000385	18 -	0.	19 -	0.	16 -	0.	17 -	0.		
399 -	0.												

TOTAL TIME FOR FORM FACTORS725.66

2.5.3 GEOMETRIC RELATIONSHIP DATA MATRIX

The following pages contain the input data computer printouts for the Shuttle Orbiter configuration.

MODEL = RIO STEP = 1 RCS ANALYSIS 4/9/75
PROCESSING OPERATIONS DATA

NODE I	NODE J	F(I,J)	AREA	THETI	THETJ	RADIUS	NORMAL VECTOR I			POSITION VECTOR I		
5015	711	.000001	2.50E+01	85.09	66.98	4.30892E+02	-8.42E-11	-1.91E+01	-1.61E+01	-2.95E+02	1.08E+02	9.06E+01
5020	711	.000002	3.06E+01	83.11	66.34	4.31787E+02	-1.03E-10	-2.34E+01	-1.97E+01	-2.97E+02	1.20E+02	1.00E+02
5025	711	.000003	3.63E+01	81.27	67.77	4.33553E+02	-1.22E-10	-2.78E+01	-2.33E+01	-2.97E+02	1.30E+02	1.09E+02
5030	711	.000004	4.63E+01	78.41	66.93	4.37220E+02	-1.56E-10	-3.55E+01	-2.98E+01	-2.97E+02	1.47E+02	1.23E+02
5035	711	.000005	5.65E+01	75.61	66.16	4.41973E+02	-1.90E-10	-4.33E+01	-3.63E+01	-2.97E+02	1.64E+02	1.38E+02
5045	724	.000001	8.11E+01	77.10	84.25	4.57308E+02	-2.73E-10	-6.21E+01	-5.21E+01	-2.95E+02	1.95E+02	1.63E+02
5045	726	.000001	8.11E+01	77.45	84.40	4.69469E+02	-2.73E-10	-6.21E+01	-5.21E+01	-2.95E+02	1.95E+02	1.63E+02
5045	24	.000001	8.11E+01	77.76	84.59	4.79019E+02	-2.73E-10	-6.21E+01	-5.21E+01	-2.95E+02	1.95E+02	1.63E+02
5050	722	.000002	1.01E+02	73.14	81.34	4.52094E+02	-3.39E-10	-7.71E+01	-6.47E+01	-2.95E+02	2.17E+02	1.82E+02
5050	724	.000002	1.01E+02	73.60	81.58	4.64427E+02	-3.39E-10	-7.71E+01	-6.47E+01	-2.95E+02	2.17E+02	1.82E+02
5050	726	.000002	1.01E+02	74.04	81.80	4.76835E+02	-3.39E-10	-7.71E+01	-6.47E+01	-2.95E+02	2.17E+02	1.82E+02
5050	735	.000001	1.01E+02	74.90	73.27	4.58646E+02	-3.39E-10	-7.71E+01	-6.47E+01	-2.95E+02	2.17E+02	1.82E+02
5050	24	.000001	1.01E+02	74.42	82.03	4.86813E+02	-3.39E-10	-7.71E+01	-6.47E+01	-2.95E+02	2.17E+02	1.82E+02
5055	722	.000003	1.22E+02	69.79	78.80	4.66994E+02	-4.10E-10	-9.31E+01	-7.81E+01	-2.95E+02	2.38E+02	2.00E+02
5055	724	.000002	1.22E+02	70.33	79.09	4.72834E+02	-4.10E-10	-9.31E+01	-7.81E+01	-2.95E+02	2.38E+02	2.00E+02
5055	726	.000002	1.22E+02	70.85	79.37	4.85119E+02	-4.10E-10	-9.31E+01	-7.81E+01	-2.95E+02	2.38E+02	2.00E+02
5055	735	.000003	1.22E+02	71.57	77.19	4.66958E+02	-4.10E-10	-9.31E+01	-7.81E+01	-2.95E+02	2.38E+02	2.00E+02
5055	24	.000002	1.22E+02	71.28	79.04	4.94518E+02	-4.10E-10	-9.31E+01	-7.81E+01	-2.95E+02	2.38E+02	2.00E+02
5060	722	.000004	1.50E+02	65.80	75.78	4.73066E+02	-5.07E-10	-1.15E+02	-9.67E+01	-2.95E+02	2.65E+02	2.22E+02
5060	724	.000004	1.50E+02	66.43	76.14	4.85414E+02	-5.07E-10	-1.15E+02	-9.67E+01	-2.95E+02	2.65E+02	2.22E+02
5060	726	.000003	1.50E+02	67.02	76.47	4.97281E+02	-5.07E-10	-1.15E+02	-9.67E+01	-2.95E+02	2.65E+02	2.22E+02
5060	733	.000000	1.50E+02	66.97	74.34	4.66300E+02	-5.07E-10	-1.15E+02	-9.67E+01	-2.95E+02	2.65E+02	2.22E+02
5060	735	.000004	1.50E+02	67.58	74.74	4.78653E+02	-5.07E-10	-1.15E+02	-9.67E+01	-2.95E+02	2.65E+02	2.22E+02
5060	24	.000003	1.50E+02	67.21	76.79	5.06506E+02	-5.07E-10	-1.15E+02	-9.67E+01	-2.95E+02	2.65E+02	2.22E+02
5060	701	.000253	1.50E+02	67.39	39.30	5.10300E+02	-5.07E-10	-1.15E+02	-9.67E+01	-2.95E+02	2.65E+02	2.22E+02
5065	720	.000003	1.83E+02	61.21	72.47	4.77797E+02	-6.18E-10	-1.40E+02	-1.18E+02	-2.95E+02	2.93E+02	2.46E+02
5065	722	.000005	1.83E+02	61.94	72.89	4.89149E+02	-6.18E-10	-1.40E+02	-1.18E+02	-2.95E+02	2.93E+02	2.46E+02
5065	724	.000005	1.83E+02	62.63	73.31	5.00161E+02	-6.18E-10	-1.40E+02	-1.18E+02	-2.95E+02	2.93E+02	2.46E+02
5065	726	.000004	1.83E+02	63.30	73.68	5.12188E+02	-6.18E-10	-1.40E+02	-1.18E+02	-2.95E+02	2.93E+02	2.46E+02
5065	733	.000002	1.83E+02	63.00	71.96	4.81271E+02	-6.18E-10	-1.40E+02	-1.18E+02	-2.95E+02	2.93E+02	2.46E+02

MODEL = RIO STEP = 1 RCS ANALYSIS 4/9/75

PROCESSING OPERATIONS DATA

NODE I	NODE J	F(I,J)	AREA	THETI	THETJ	RADIUS	NORMAL VECTOR I			POSITION VECTOR I		
5005	735	.000035	1.83E+02	63.09	72.40	4.92586E+02	-6.18E-10	-1.40E+02	-1.18E+02	-2.93E+02	2.93E+02	2.46E+02
5005	24	.000034	1.83E+02	63.84	74.03	5.20810E+02	-6.18E-10	-1.40E+02	-1.18E+02	-2.93E+02	2.93E+02	2.46E+02
5005	791	.000388	1.83E+02	63.74	43.31	5.24073E+02	-6.18E-10	-1.40E+02	-1.18E+02	-2.93E+02	2.93E+02	2.46E+02
5070	720	.000037	2.57E+02	54.32	67.43	5.14613E+02	-8.66E-10	-1.97E+02	-1.65E+02	-3.00E+02	3.46E+02	2.91E+02
5070	722	.000007	2.57E+02	55.14	67.91	5.25152E+02	-8.66E-10	-1.97E+02	-1.65E+02	-3.00E+02	3.46E+02	2.91E+02
5070	724	.000006	2.57E+02	55.93	68.37	5.35600E+02	-8.66E-10	-1.97E+02	-1.65E+02	-3.00E+02	3.46E+02	2.91E+02
5070	726	.000006	2.57E+02	56.69	68.82	5.46049E+02	-8.66E-10	-1.97E+02	-1.65E+02	-3.00E+02	3.46E+02	2.91E+02
5070	733	.000007	2.57E+02	56.03	67.92	5.16044E+02	-8.66E-10	-1.97E+02	-1.65E+02	-3.00E+02	3.46E+02	2.91E+02
5070	735	.000006	2.57E+02	56.82	68.40	5.27072E+02	-8.66E-10	-1.97E+02	-1.65E+02	-3.00E+02	3.46E+02	2.91E+02
5070	24	.000005	2.57E+02	57.30	69.21	5.54[illegible]3E+02	-8.66E-10	-1.97E+02	-1.65E+02	-3.00E+02	3.46E+02	2.91E+02
5070	791	.000551	2.57E+02	57.26	49.49	5.58789E+02	-8.66E-10	-1.97E+02	-1.65E+02	-3.00E+02	3.46E+02	2.91E+02
5075	720	.000038	3.44E+02	48.35	63.19	5.58477E+02	-1.16E-09	-2.63E+02	-2.21E+02	-3.01E+02	4.01E+02	3.36E+02
5075	722	.000038	3.44E+02	49.22	63.08	5.68187E+02	-1.16E-09	-2.63E+02	-2.21E+02	-3.01E+02	4.01E+02	3.36E+02
5075	724	.000007	3.44E+02	50.05	64.17	5.78126E+02	-1.16E-09	-2.63E+02	-2.21E+02	-3.01E+02	4.01E+02	3.36E+02
5075	726	.000037	3.44E+02	51.86	64.63	5.87769E+02	-1.16E-09	-2.63E+02	-2.21E+02	-3.01E+02	4.01E+02	3.36E+02
5075	733	.000008	3.44E+02	49.94	64.59	5.58484E+02	-1.16E-09	-2.63E+02	-2.21E+02	-3.01E+02	4.01E+02	3.36E+02
5075	735	.000007	3.44E+02	51.78	65.20	5.68492E+02	-1.16E-09	-2.63E+02	-2.21E+02	-3.01E+02	4.01E+02	3.36E+02
5075	24	.000006	3.44E+02	51.50	65.04	5.95[illegible]7E+02	-1.16E-09	-2.63E+02	-2.21E+02	-3.01E+02	4.01E+02	3.36E+02
5075	26	.000007	3.44E+02	49.29	62.28	6.13151E+02	-1.16E-09	-2.63E+02	-2.21E+02	-3.01E+02	4.01E+02	3.36E+02
5075	791	.000483	3.44E+02	51.51	59.24	5.99013E+02	-1.16E-09	-2.63E+02	-2.21E+02	-3.01E+02	4.01E+02	3.36E+02
5080	720	.000039	4.43E+02	43.30	59.72	6.07495E+02	-1.49E-09	-3.40E+02	-2.85E+02	-3.01E+02	4.55E+02	3.82E+02
5080	722	.000008	4.43E+02	44.17	60.21	6.16818E+02	-1.49E-09	-3.40E+02	-2.85E+02	-3.01E+02	4.55E+02	3.82E+02
5080	724	.000007	4.43E+02	45.02	60.68	6.25684E+02	-1.49E-09	-3.40E+02	-2.85E+02	-3.01E+02	4.55E+02	3.82E+02
5080	726	.000007	4.43E+02	45.84	61.15	6.34688E+02	-1.49E-09	-3.40E+02	-2.85E+02	-3.01E+02	4.55E+02	3.82E+02
5080	733	.000008	4.43E+02	44.75	61.92	6.16812E+02	-1.49E-09	-3.40E+02	-2.85E+02	-3.01E+02	4.55E+02	3.82E+02
5080	735	.000007	4.43E+02	45.61	62.38	6.25541E+02	-1.49E-09	-3.40E+02	-2.85E+02	-3.01E+02	4.55E+02	3.82E+02
5080	24	.000007	4.43E+02	46.50	61.55	6.41[illegible]1E+02	-1.49E-09	-3.40E+02	-2.85E+02	-3.01E+02	4.55E+02	3.82E+02
5080	26	.000007	4.43E+02	44.58	59.97	6.61[illegible]2E+02	-1.49E-09	-3.40E+02	-2.85E+02	-3.01E+02	4.55E+02	3.82E+02
5080	791	.000401	4.43E+02	46.53	60.22	6.45[illegible]5E+02	-1.49E-09	-3.40E+02	-2.85E+02	-3.01E+02	4.55E+02	3.82E+02
5085	720	.000038	5.56E+02	39.03	56.90	6.00[illegible]9E+02	-1.87E-09	-4.26E+02	-3.57E+02	-3.02E+02	5.09E+02	4.27E+02
5085	722	.000008	5.56E+02	39.89	57.36	6.08722E+02	-1.87E-09	-4.26E+02	-3.57E+02	-3.02E+02	5.09E+02	4.27E+02
5085	724	.000008	5.56E+02	40.72	57.81	6.17[illegible]5E+02	-1.87E-09	-4.26E+02	-3.57E+02	-3.02E+02	5.09E+02	4.27E+02
5085	726	.000007	5.56E+02	41.54	58.26	6.25[illegible]2E+02	-1.87E-09	-4.26E+02	-3.57E+02	-3.02E+02	5.09E+02	4.27E+02
5085	733	.000008	5.56E+02	40.35	59.80	6.07487E+02	-1.87E-09	-4.26E+02	-3.57E+02	-3.02E+02	5.09E+02	4.27E+02
5085	735	.000007	5.56E+02	41.20	60.23	6.16[illegible]4E+02	-1.87E-09	-4.26E+02	-3.57E+02	-3.02E+02	5.09E+02	4.27E+02
5085	24	.000007	5.56E+02	42.19	58.64	6.91881E+02	-1.87E-09	-4.26E+02	-3.57E+02	-3.02E+02	5.09E+02	4.27E+02
5085	26	.000007	5.56E+02	40.53	56.13	7.12904E+02	-1.87E-09	-4.26E+02	-3.57E+02	-3.02E+02	5.09E+02	4.27E+02
5085	791	.000323	5.56E+02	42.24	64.53	6.99964E+02	-1.87E-09	-4.26E+02	-3.57E+02	-3.02E+02	5.09E+02	4.27E+02
5090	715	.000002	6.79E+02	35.62	63.33	7.67[illegible]3E+02	-2.29E-09	-5.20E+02	-4.36E+02	-3.02E+02	5.63E+02	4.72E+02
5090	720	.000008	6.79E+02	38.45	54.04	7.19[illegible]3E+02	-2.29E-09	-5.20E+02	-4.36E+02	-3.02E+02	5.63E+02	4.72E+02
5090	722	.000008	6.79E+02	36.29	55.06	7.23[illegible]6E+02	-2.29E-09	-5.20E+02	-4.36E+02	-3.02E+02	5.63E+02	4.72E+02

MODEL = RIO STEP = 1 RCS ANALYSIS 4/9/75

PROCESSING OPERATIONS DATA

NODE I	NODE J	F(I,J)	AREA	THETI	THETJ	RADIUS	NORMAL VECTOR I			POSITION VECTOR I		
5090	724	.000007	6.79E+02	37.10	56.48	7.31132E+02	-2.29E-09	-5.20E+02	-4.36E+02	-3.02E+02	5.63E+02	4.72E+02
5090	726	.000007	6.79E+02	37.90	55.90	7.38796E+02	-2.29E-09	-5.20E+02	-4.36E+02	-3.02E+02	5.63E+02	4.72E+02
5090	731	.000003	6.79E+02	35.81	57.76	7.04879E+02	-2.29E-09	-5.20E+02	-4.36E+02	-3.02E+02	5.63E+02	4.72E+02
5090	733	.000007	6.79E+02	36.66	58.15	7.12360E+02	-2.29E-09	-5.20E+02	-4.36E+02	-3.02E+02	5.63E+02	4.72E+02
5090	735	.000007	6.79E+02	37.49	58.53	7.20194E+02	-2.29E-09	-5.20E+02	-4.36E+02	-3.02E+02	5.63E+02	4.72E+02
5090	24	.000007	6.79E+02	36.53	56.26	7.44798E+02	-2.29E-09	-5.20E+02	-4.36E+02	-3.02E+02	5.63E+02	4.72E+02
5090	26	.000007	6.79E+02	37.09	56.07	7.67134E+02	-2.29E-09	-5.20E+02	-4.36E+02	-3.02E+02	5.63E+02	4.72E+02
5090	731	.000250	6.79E+02	38.60	68.15	7.48528E+02	-2.29E-09	-5.20E+02	-4.36E+02	-3.02E+02	5.63E+02	4.72E+02
5095	715	.000005	8.16E+02	32.71	63.53	8.25402E+02	-2.75E-09	-6.25E+02	-5.25E+02	-3.63E+02	6.17E+02	5.18E+02
5095	720	.000007	8.16E+02	34.36	52.76	7.74407E+02	-2.75E-09	-6.25E+02	-5.25E+02	-3.63E+02	6.17E+02	5.18E+02
5095	722	.000007	8.16E+02	33.16	53.14	7.81391E+02	-2.75E-09	-6.25E+02	-5.25E+02	-3.63E+02	6.17E+02	5.18E+02
5095	724	.000007	8.16E+02	33.95	53.53	7.88728E+02	-2.75E-09	-6.25E+02	-5.25E+02	-3.63E+02	6.17E+02	5.18E+02
5095	726	.000007	8.16E+02	34.72	53.92	7.95814E+02	-2.75E-09	-6.25E+02	-5.25E+02	-3.63E+02	6.17E+02	5.18E+02
5095	731	.000003	8.16E+02	32.65	56.46	7.63105E+02	-2.75E-09	-6.25E+02	-5.25E+02	-3.63E+02	6.17E+02	5.18E+02
5095	733	.000007	8.16E+02	33.46	56.81	7.70193E+02	-2.75E-09	-6.25E+02	-5.25E+02	-3.63E+02	6.17E+02	5.18E+02
5095	735	.000006	8.16E+02	34.26	57.16	7.77334E+02	-2.75E-09	-6.25E+02	-5.25E+02	-3.63E+02	6.17E+02	5.18E+02
5095	24	.000007	8.16E+02	35.32	54.25	8.01154E+02	-2.75E-09	-6.25E+02	-5.25E+02	-3.63E+02	6.17E+02	5.18E+02
5095	26	.000006	8.16E+02	34.08	55.49	8.24383E+02	-2.75E-09	-6.25E+02	-5.25E+02	-3.63E+02	6.17E+02	5.18E+02
5095	731	.000200	8.16E+02	35.41	71.34	8.05124E+02	-2.75E-09	-6.25E+02	-5.25E+02	-3.63E+02	6.17E+02	5.18E+02
5100	713	.000001	1.69E+03	27.28	64.50	1.13765E+03	-5.69E-09	-1.29E+03	-1.09E+03	-3.07E+02	8.88E+02	7.45E+02
5100	715	.000003	1.69E+03	22.91	64.74	1.13753E+03	-5.69E-09	-1.29E+03	-1.09E+03	-3.07E+02	8.88E+02	7.45E+02
5100	720	.000005	1.69E+03	22.20	47.20	1.08777E+03	-5.69E-09	-1.29E+03	-1.09E+03	-3.07E+02	8.88E+02	7.45E+02
5100	722	.000005	1.69E+03	22.83	47.44	1.09271E+03	-5.69E-09	-1.29E+03	-1.09E+03	-3.07E+02	8.88E+02	7.45E+02
5100	724	.000005	1.69E+03	23.45	47.68	1.09778E+03	-5.69E-09	-1.29E+03	-1.09E+03	-3.07E+02	8.88E+02	7.45E+02
5100	726	.000004	1.69E+03	24.06	47.93	1.10298E+03	-5.69E-09	-1.29E+03	-1.09E+03	-3.07E+02	8.88E+02	7.45E+02
5100	731	.000004	1.69E+03	22.29	52.93	1.07586E+03	-5.69E-09	-1.29E+03	-1.09E+03	-3.07E+02	8.88E+02	7.45E+02
5100	733	.000004	1.69E+03	22.93	53.13	1.08486E+03	-5.69E-09	-1.29E+03	-1.09E+03	-3.07E+02	8.88E+02	7.45E+02
5100	735	.000004	1.69E+03	23.56	53.33	1.09399E+03	-5.69E-09	-1.29E+03	-1.09E+03	-3.07E+02	8.88E+02	7.45E+02
5100	24	.000004	1.69E+03	24.55	48.14	1.10666E+03	-5.69E-09	-1.29E+03	-1.09E+03	-3.07E+02	8.88E+02	7.45E+02
5100	26	.000004	1.69E+03	23.87	52.22	1.13572E+03	-5.69E-09	-1.29E+03	-1.09E+03	-3.07E+02	8.88E+02	7.45E+02
5100	731	.000053	1.69E+03	24.64	82.10	1.11034E+03	-5.69E-09	-1.29E+03	-1.09E+03	-3.07E+02	8.88E+02	7.45E+02
5105	713	.000001	2.88E+03	16.91	65.06	1.46733E+03	-9.70E-09	-2.20E+03	-1.85E+03	-3.13E+02	1.16E+03	9.73E+02
5105	715	.000002	2.88E+03	17.40	65.76	1.46363E+03	-9.70E-09	-2.20E+03	-1.85E+03	-3.13E+02	1.16E+03	9.73E+02
5105	720	.000003	2.88E+03	16.67	44.68	1.42182E+03	-9.70E-09	-2.20E+03	-1.85E+03	-3.13E+02	1.16E+03	9.73E+02
5105	722	.000003	2.88E+03	17.16	44.83	1.42457E+03	-9.70E-09	-2.20E+03	-1.85E+03	-3.13E+02	1.16E+03	9.73E+02
5105	724	.000003	2.88E+03	17.66	44.99	1.42743E+03	-9.70E-09	-2.20E+03	-1.85E+03	-3.13E+02	1.16E+03	9.73E+02
5105	726	.000003	2.88E+03	18.15	45.15	1.43040E+03	-9.70E-09	-2.20E+03	-1.85E+03	-3.13E+02	1.16E+03	9.73E+02
5105	731	.000003	2.88E+03	16.69	51.55	1.40180E+03	-9.70E-09	-2.20E+03	-1.85E+03	-3.13E+02	1.16E+03	9.73E+02
5105	733	.000003	2.88E+03	17.19	51.67	1.41298E+03	-9.70E-09	-2.20E+03	-1.85E+03	-3.13E+02	1.16E+03	9.73E+02
5105	735	.000003	2.88E+03	17.69	51.80	1.42428E+03	-9.70E-09	-2.20E+03	-1.85E+03	-3.13E+02	1.16E+03	9.73E+02
5105	24	.000003	2.88E+03	18.54	45.29	1.43513E+03	-9.70E-09	-2.20E+03	-1.85E+03	-3.13E+02	1.16E+03	9.73E+02
5105	26	.000002	2.88E+03	18.12	50.94	1.46236E+03	-9.70E-09	-2.20E+03	-1.85E+03	-3.13E+02	1.16E+03	9.73E+02
5105	731	.000010	2.88E+03	18.62	88.12	1.43455E+03	-9.70E-09	-2.20E+03	-1.85E+03	-3.13E+02	1.16E+03	9.73E+02

MODEL = RIO STEP = 1 RCS ANALYSIS 4/9/75
PROCESSING OPERATIONS DATA

5110	711	.000000	2.88E+03	2.00	69.75	1.19131E+04	-9.70E-09	-2.20E+03	-1.85E+03	-3.10E+02	9.19E+03	7.71E+03
5110	713	.000000	2.88E+03	2.06	69.77	1.19104E+04	-9.70E-09	-2.20E+03	-1.85E+03	-3.10E+02	9.19E+03	7.71E+03
5110	715	.000000	2.88E+03	2.12	69.78	1.18969E+04	-9.70E-09	-2.20E+03	-1.85E+03	-3.10E+02	9.19E+03	7.71E+03
5110	720	.000000	2.88E+03	1.97	40.28	1.18851E+04	-9.70E-09	-2.20E+03	-1.85E+03	-3.10E+02	9.19E+03	7.71E+03
5110	722	.000000	2.88E+03	2.03	40.29	1.18856E+04	-9.70E-09	-2.20E+03	-1.85E+03	-3.10E+02	9.19E+03	7.71E+03
5110	724	.000000	2.88E+03	2.09	40.29	1.18860E+04	-9.70E-09	-2.20E+03	-1.85E+03	-3.10E+02	9.19E+03	7.71E+03
5110	726	.000000	2.88E+03	2.16	40.29	1.18865E+04	-9.70E-09	-2.20E+03	-1.85E+03	-3.10E+02	9.19E+03	7.71E+03
5110	731	.000000	2.88E+03	1.96	49.97	1.18434E+04	-9.70E-09	-2.20E+03	-1.85E+03	-3.10E+02	9.19E+03	7.71E+03
5110	733	.000000	2.88E+03	2.02	49.98	1.18438E+04	-9.70E-09	-2.20E+03	-1.85E+03	-3.10E+02	9.19E+03	7.71E+03
5110	735	.000000	2.88E+03	2.08	49.98	1.18443E+04	-9.70E-09	-2.20E+03	-1.85E+03	-3.10E+02	9.19E+03	7.71E+03
5110	24	.000000	2.88E+03	2.21	40.30	1.18864E+04	-9.70E-09	-2.20E+03	-1.85E+03	-3.10E+02	9.19E+03	7.71E+03
5110	26	.000000	2.88E+03	2.19	49.86	1.18459E+04	-9.70E-09	-2.20E+03	-1.85E+03	-3.10E+02	9.19E+03	7.71E+03
5110	730	.000001	2.88E+03	2.22	75.48	1.18191E+04	-9.70E-09	-2.20E+03	-1.85E+03	-3.10E+02	9.19E+03	7.71E+03
145	710	.000302	2.69E+03	79.80	36.32	8.69200E+01	0.	2.69E+03	-2.23E-08	-7.09E+02	1.02E+02	-6.25E+01
145	712	.000157	2.69E+03	81.48	39.09	9.55176E+01	0.	2.69E+03	-2.23E-08	-7.09E+02	1.02E+02	-6.25E+01
145	714	.000089	2.69E+03	82.66	42.97	1.05835E+02	0.	2.69E+03	-2.23E-08	-7.09E+02	1.02E+02	-6.25E+01
145	721	.000041	2.69E+03	68.98	68.98	1.38013E+02	0.	2.69E+03	-2.23E-08	-7.09E+02	1.02E+02	-6.25E+01
145	723	.000092	2.69E+03	69.18	69.18	1.38134E+02	0.	2.69E+03	-2.23E-08	-7.09E+02	1.02E+02	-6.25E+01
145	725	.000060	2.69E+03	69.58	69.58	1.38411E+02	0.	2.69E+03	-2.23E-08	-7.09E+02	1.02E+02	-6.25E+01
145	727	.000063	2.69E+03	70.15	70.15	1.38776E+02	0.	2.69E+03	-2.23E-08	-7.09E+02	1.02E+02	-6.25E+01
145	730	.000042	2.69E+03	79.15	11.05	1.62703E+02	0.	2.69E+03	-2.23E-08	-7.09E+02	1.02E+02	-6.25E+01
145	732	.000048	2.69E+03	79.21	12.70	1.62987E+02	0.	2.69E+03	-2.23E-08	-7.09E+02	1.02E+02	-6.25E+01
145	734	.000064	2.69E+03	79.35	15.49	1.64492E+02	0.	2.69E+03	-2.23E-08	-7.09E+02	1.02E+02	-6.25E+01
145	25	.000059	2.69E+03	70.43	70.43	1.41454E+02	0.	2.69E+03	-2.23E-08	-7.09E+02	1.02E+02	-6.25E+01
145	27	.000065	2.69E+03	82.77	20.76	1.27148E+02	0.	2.69E+03	-2.23E-08	-7.09E+02	1.02E+02	-6.25E+01
145	701	.000212	2.69E+03	90.04	58.53	1.84271E+02	0.	2.69E+03	-2.23E-08	-7.09E+02	1.02E+02	-6.25E+01
147	710	.000076	2.02E+04	51.43	59.12	1.86606E+02	-5.10E+03	-7.46E-08	1.96E+04	-7.75E+02	-7.01E-10	-1.13E+02
147	712	.000079	2.02E+04	47.78	57.97	1.87303E+02	-5.10E+03	-7.46E-08	1.96E+04	-7.75E+02	-7.01E-10	-1.13E+02
147	714	.000080	2.02E+04	44.38	57.05	1.89135E+02	-5.10E+03	-7.46E-08	1.96E+04	-7.75E+02	-7.01E-10	-1.13E+02
147	721	.000037	2.02E+04	50.23	50.77	2.35204E+02	-5.10E+03	-7.46E-08	1.96E+04	-7.75E+02	-7.01E-10	-1.13E+02
147	723	.000040	2.02E+04	48.53	50.15	2.32144E+02	-5.10E+03	-7.46E-08	1.96E+04	-7.75E+02	-7.01E-10	-1.13E+02
147	725	.000043	2.02E+04	46.89	49.66	2.29780E+02	-5.10E+03	-7.46E-08	1.96E+04	-7.75E+02	-7.01E-10	-1.13E+02
147	727	.000046	2.02E+04	45.36	49.31	2.28134E+02	-5.10E+03	-7.46E-08	1.96E+04	-7.75E+02	-7.01E-10	-1.13E+02
147	730	.000060	2.02E+04	42.91	34.95	2.54989E+02	-5.10E+03	-7.46E-08	1.96E+04	-7.75E+02	-7.01E-10	-1.13E+02
147	732	.000055	2.02E+04	41.10	34.02	2.52170E+02	-5.10E+03	-7.46E-08	1.96E+04	-7.75E+02	-7.01E-10	-1.13E+02
147	734	.000067	2.02E+04	39.35	33.28	2.49996E+02	-5.10E+03	-7.46E-08	1.96E+04	-7.75E+02	-7.01E-10	-1.13E+02
147	740	.000389	2.02E+04	70.91	33.69	6.12944E+01	-5.10E+03	-7.46E-08	1.96E+04	-7.75E+02	-7.01E-10	-1.13E+02
147	25	.000047	2.02E+04	44.37	49.32	2.27772E+02	-5.10E+03	-7.46E-08	1.96E+04	-7.75E+02	-7.01E-10	-1.13E+02
147	27	.000075	2.02E+04	39.86	35.97	2.02121E+02	-5.10E+03	-7.46E-08	1.96E+04	-7.75E+02	-7.01E-10	-1.13E+02
147	701	.000793	2.02E+04	29.13	75.34	2.46160E+02	-5.10E+03	-7.46E-08	1.96E+04	-7.75E+02	-7.01E-10	-1.13E+02
710	900	.029694	2.69E+01	50.73	63.92	2.63323E+02	-5.88E+00	9.40E+00	-2.60E+01	-7.21E+02	1.17E+02	2.22E+01

A-78

A, 7310

MODEL = RIO STEP = 1 RCS ANALYSIS 4/9/75

PROCESSING OPERATIONS DATA

NODE I	NODE J	F(I,J)	AREA	THETI	THETJ	RADIUS	NORMAL VECTOR I			POSITION VECTOR I		
710	901	.026386	2.83E+01	54.41	42.26	1.56425E+02	-5.88E+00	9.46E+00	-2.60E+01	-7.21E+02	1.17E+02	2.22E+01
710	805	.038357	2.83E+01	52.92	57.08	8.46796E+01	-5.88E+00	9.46E+00	-2.60E+01	-7.21E+02	1.17E+02	2.22E+01
710	806	.039417	2.83E+01	52.72	62.93	9.65.12E+01	-5.88E+00	9.46E+00	-2.60E+01	-7.21E+02	1.17E+02	2.22E+01
710	810	.000955	2.83E+01	83.79	31.80	1.62647E+02	-5.88E+00	9.46E+00	-2.60E+01	-7.21E+02	1.17E+02	2.22E+01
710	811	.001758	2.83E+01	81.00	27.97	1.59765E+02	-5.88E+00	9.46E+00	-2.60E+01	-7.21E+02	1.17E+02	2.22E+01
710	222	.020534	2.83E+01	74.70	84.80	1.44748E+02	-5.88E+00	9.46E+00	-2.60E+01	-7.21E+02	1.17E+02	2.22E+01
710	2	.004284	2.83E+01	81.06	72.09	4.17154E+02	-5.88E+00	9.46E+00	-2.60E+01	-7.21E+02	1.17E+02	2.22E+01
710	3	.022889	2.83E+01	60.86	67.57	3.03539E+02	-5.88E+00	9.46E+00	-2.60E+01	-7.21E+02	1.17E+02	2.22E+01
710	144	.004933	2.83E+01	70.01	57.78	2.17120E+02	-5.88E+00	9.46E+00	-2.60E+01	-7.21E+02	1.17E+02	2.22E+01
710	4	.198441	2.83E+01	59.89	11.24	1.29965E+02	-5.88E+00	9.46E+00	-2.60E+01	-7.21E+02	1.17E+02	2.22E+01
710	806	.008961	2.83E+01	84.03	85.88	2.14414E+02	-5.88E+00	9.46E+00	-2.60E+01	-7.21E+02	1.17E+02	2.22E+01
711	712	.002540	2.83E+01	70.37	70.37	1.45929E+01	5.88E+00	-9.46E+00	2.60E+01	-7.21E+02	1.17E+02	2.22E+01
711	721	.001224	2.83E+01	59.53	56.06	4.88697E+01	5.88E+00	-9.46E+00	2.60E+01	-7.21E+02	1.17E+02	2.22E+01
711	723	.001020	2.83E+01	63.11	50.30	4.87519E+01	5.88E+00	-9.46E+00	2.60E+01	-7.21E+02	1.17E+02	2.22E+01
711	725	.000659	2.83E+01	66.18	52.98	5.20771E+01	5.88E+00	-9.46E+00	2.60E+01	-7.21E+02	1.17E+02	2.22E+01
711	727	.000355	2.83E+01	73.36	57.37	5.81582E+01	5.88E+00	-9.46E+00	2.60E+01	-7.21E+02	1.17E+02	2.22E+01
711	730	.001230	2.83E+01	31.87	12.54	7.61532E+01	5.88E+00	-9.46E+00	2.60E+01	-7.21E+02	1.17E+02	2.22E+01
711	732	.001197	2.83E+01	35.50	12.41	7.61161E+01	5.88E+00	-9.46E+00	2.60E+01	-7.21E+02	1.17E+02	2.22E+01
711	734	.001001	2.83E+01	40.78	18.24	7.62069E+01	5.88E+00	-9.46E+00	2.60E+01	-7.21E+02	1.17E+02	2.22E+01
711	775	.000014	2.83E+01	79.17	89.48	8.63945E+02	5.88E+00	-9.46E+00	2.60E+01	-7.21E+02	1.17E+02	2.22E+01
711	777	.000037	2.83E+01	79.46	89.35	6.89703E+02	5.88E+00	-9.46E+00	2.60E+01	-7.21E+02	1.17E+02	2.22E+01
711	31	.013506	2.83E+01	37.00	73.23	3.88524E+01	5.88E+00	-9.46E+00	2.60E+01	-7.21E+02	1.17E+02	2.22E+01
711	32	.002919	2.83E+01	9.37	83.66	9.28401E+01	5.88E+00	-9.46E+00	2.60E+01	-7.21E+02	1.17E+02	2.22E+01
711	33	.020779	2.83E+01	25.96	78.04	5.41160E+01	5.88E+00	-9.46E+00	2.60E+01	-7.21E+02	1.17E+02	2.22E+01
711	34	.004565	2.83E+01	6.04	82.99	9.19.60E+01	5.88E+00	-9.46E+00	2.60E+01	-7.21E+02	1.17E+02	2.22E+01
711	25	.000204	2.83E+01	77.14	60.31	6.45946E+01	5.88E+00	-9.46E+00	2.60E+01	-7.21E+02	1.17E+02	2.22E+01
711	27	.000480	2.83E+01	69.99	55.71	5.11837E+01	5.88E+00	-9.46E+00	2.60E+01	-7.21E+02	1.17E+02	2.22E+01
711	800	.027538	2.83E+01	53.06	24.74	1.01702E+02	5.88E+00	-9.46E+00	2.60E+01	-7.21E+02	1.17E+02	2.22E+01
711	801	.029156	2.83E+01	59.20	28.00	1.04937E+02	5.88E+00	-9.46E+00	2.60E+01	-7.21E+02	1.17E+02	2.22E+01
711	811	.000535	2.83E+01	99.00	27.97	1.59765E+02	5.88E+00	-9.46E+00	2.60E+01	-7.21E+02	1.17E+02	2.22E+01
711	22	.046406	2.83E+01	55.01	83.39	1.21939E+02	5.88E+00	-9.46E+00	2.60E+01	-7.21E+02	1.17E+02	2.22E+01
711	751	.000004	2.83E+01	82.37	87.10	4.27754E+02	5.88E+00	-9.46E+00	2.60E+01	-7.21E+02	1.17E+02	2.22E+01
711	212	.010627	2.83E+01	53.98	91.25	1.51589E+02	5.88E+00	-9.46E+00	2.60E+01	-7.21E+02	1.17E+02	2.22E+01
711	340	.003234	2.83E+01	10.92	61.29	2.44773E+02	5.88E+00	-9.46E+00	2.60E+01	-7.21E+02	1.17E+02	2.22E+01
711	345	.007632	2.83E+01	20.70	60.07	2.35295E+02	5.88E+00	-9.46E+00	2.60E+01	-7.21E+02	1.17E+02	2.22E+01
711	701	.025631	2.83E+01	41.01	52.42	1.02620E+02	5.88E+00	-9.46E+00	2.60E+01	-7.21E+02	1.17E+02	2.22E+01
711	702	.001715	2.83E+01	60.16	72.29	2.22109E+02	5.88E+00	-9.46E+00	2.60E+01	-7.21E+02	1.17E+02	2.22E+01
712	900	.022825	2.83E+01	51.42	63.37	2.72616E+02	-5.88E+00	9.46E+00	-2.60E+01	-7.34E+02	1.16E+02	2.84E+01
712	901	.020824	2.83E+01	56.24	44.00	1.78706E+02	-5.88E+00	9.46E+00	-2.60E+01	-7.34E+02	1.16E+02	2.84E+01
712	805	.039592	2.83E+01	51.25	63.06	8.70156E+01	-5.88E+00	9.46E+00	-2.60E+01	-7.34E+02	1.16E+02	2.84E+01
712	806	.039924	2.83E+01	47.40	64.47	9.14802E+01	-5.88E+00	9.46E+00	-2.60E+01	-7.34E+02	1.16E+02	2.84E+01
712	810	.001235	2.83E+01	82.59	36.19	1.68138E+02	-5.88E+00	9.46E+00	-2.60E+01	-7.34E+02	1.16E+02	2.84E+01
712	811	.001871	2.83E+01	79.20	28.85	1.55954E+02	-5.88E+00	9.46E+00	-2.60E+01	-7.34E+02	1.16E+02	2.84E+01
712	222	.040194	2.83E+01	73.09	79.52	1.48242E+02	-5.88E+00	9.46E+00	-2.60E+01	-7.34E+02	1.16E+02	2.84E+01

MODEL = RIO STEP = 1 RCS ANALYSIS 4/9/75
PROCESSING OPERATIONS DATA

NODE I	NODE J	F(I,J)	AREA	THETI	THETJ	RADIUS	NORMAL VECTOR I			POSITION VECTOR I		
712	407	.000002	2.83E+01	68.30	88.99	1.78763E+02	-5.88E+00	9.46E+00	-2.60E+01	-7.34E+02	1.16E+02	2.84E+01
712	2	.000018	2.83E+01	81.47	71.08	4.31514E+02	-5.88E+00	9.46E+00	-2.60E+01	-7.34E+02	1.16E+02	2.84E+01
712	3	.019021	2.83E+01	61.32	67.15	3.14938E+02	-5.88E+00	9.46E+00	-2.60E+01	-7.34E+02	1.16E+02	2.84E+01
712	144	.007697	2.83E+01	70.97	56.14	2.31947E+02	-5.88E+00	9.46E+00	-2.60E+01	-7.34E+02	1.16E+02	2.84E+01
712	4	.094346	2.83E+01	43.04	15.06	1.41144E+02	-5.88E+00	9.46E+00	-2.60E+01	-7.34E+02	1.16E+02	2.84E+01
712	306	.016725	2.83E+01	82.54	80.46	2.28788E+02	-5.88E+00	9.46E+00	-2.60E+01	-7.34E+02	1.16E+02	2.84E+01
713	714	.033619	2.83E+01	74.33	74.33	1.42796E+01	5.88E+00	-9.46E+00	2.60E+01	-7.34E+02	1.16E+02	2.84E+01
713	721	.001100	2.83E+01	64.15	48.19	4.89097E+01	5.88E+00	-9.46E+00	2.60E+01	-7.34E+02	1.16E+02	2.84E+01
713	723	.003304	2.83E+01	69.68	43.36	4.52246E+01	5.88E+00	-9.46E+00	2.60E+01	-7.34E+02	1.16E+02	2.84E+01
713	725	.001041	2.83E+01	69.34	43.73	4.51261E+01	5.88E+00	-9.46E+00	2.60E+01	-7.34E+02	1.16E+02	2.84E+01
713	727	.000604	2.83E+01	74.23	47.90	4.86361E+01	5.88E+00	-9.46E+00	2.60E+01	-7.34E+02	1.16E+02	2.84E+01
713	730	.001373	2.83E+01	32.72	20.69	7.27764E+01	5.88E+00	-9.46E+00	2.60E+01	-7.34E+02	1.16E+02	2.84E+01
713	732	.001458	2.83E+01	33.70	14.00	7.03127E+01	5.88E+00	-9.46E+00	2.60E+01	-7.34E+02	1.16E+02	2.84E+01
713	734	.001393	2.83E+01	37.42	14.40	7.02695E+01	5.88E+00	-9.46E+00	2.60E+01	-7.34E+02	1.16E+02	2.84E+01
713	31	.021897	2.83E+01	46.43	52.58	4.00103E+01	5.88E+00	-9.46E+00	2.60E+01	-7.34E+02	1.16E+02	2.84E+01
713	32	.007650	2.83E+01	9.37	74.21	8.94340E+01	5.88E+00	-9.46E+00	2.60E+01	-7.34E+02	1.16E+02	2.84E+01
713	33	.049689	2.83E+01	31.18	62.57	5.28495E+01	5.88E+00	-9.46E+00	2.60E+01	-7.34E+02	1.16E+02	2.84E+01
713	34	.012107	2.83E+01	4.98	74.00	8.82786E+01	5.88E+00	-9.46E+00	2.60E+01	-7.34E+02	1.16E+02	2.84E+01
713	25	.000333	2.83E+01	78.27	51.82	5.37235E+01	5.88E+00	-9.46E+00	2.60E+01	-7.34E+02	1.16E+02	2.84E+01
713	27	.000954	2.83E+01	67.60	52.60	3.69765E+01	5.88E+00	-9.46E+00	2.60E+01	-7.34E+02	1.16E+02	2.84E+01
713	800	.020070	2.83E+01	54.41	30.05	9.91128E+01	5.88E+00	-9.46E+00	2.60E+01	-7.34E+02	1.16E+02	2.84E+01
713	801	.033827	2.83E+01	58.24	22.70	9.55-69E+01	5.88E+00	-9.46E+00	2.60E+01	-7.34E+02	1.16E+02	2.84E+01
713	22	.112355	2.83E+01	57.55	77.31	1.21453E+02	5.88E+00	-9.46E+00	2.60E+01	-7.34E+02	1.16E+02	2.84E+01
713	150	.001341	2.83E+01	88.90	60.25	4.11518E+02	5.88E+00	-9.46E+00	2.60E+01	-7.34E+02	1.16E+02	2.84E+01
713	746	.000754	2.83E+01	74.60	69.08	4.98649E+02	5.88E+00	-9.46E+00	2.60E+01	-7.34E+02	1.16E+02	2.84E+01
713	380	.003673	2.83E+01	13.09	61.42	2.42820E+02	5.88E+00	-9.46E+00	2.60E+01	-7.34E+02	1.16E+02	2.84E+01
713	305	.094021	2.83E+01	16.33	59.41	2.28700E+02	5.88E+00	-9.46E+00	2.60E+01	-7.34E+02	1.16E+02	2.84E+01
713	701	.033048	2.83E+01	35.83	57.61	9.12852E+01	5.88E+00	-9.46E+00	2.60E+01	-7.34E+02	1.16E+02	2.84E+01
713	702	.001467	2.83E+01	60.37	75.77	2.10250E+02	5.88E+00	-9.46E+00	2.60E+01	-7.34E+02	1.16E+02	2.84E+01
714	900	.020628	2.83E+01	51.94	62.70	2.82116E+02	-5.88E+00	9.46E+00	-2.60E+01	-7.47E+02	1.16E+02	3.53E+01
714	901	.010912	2.83E+01	57.80	45.17	1.83656E+02	-5.88E+00	9.46E+00	-2.60E+01	-7.47E+02	1.16E+02	3.53E+01
714	815	.035098	2.83E+01	50.86	68.68	9.29245E+01	-5.88E+00	9.46E+00	-2.60E+01	-7.47E+02	1.16E+02	3.53E+01
714	806	.000222	2.83E+01	42.67	66.55	8.95117E+01	-5.88E+00	9.46E+00	-2.60E+01	-7.47E+02	1.16E+02	3.53E+01
714	810	.001468	2.83E+01	81.34	40.59	1.66750E+02	-5.88E+00	9.46E+00	-2.60E+01	-7.47E+02	1.16E+02	3.53E+01
714	811	.002639	2.83E+01	77.90	30.69	1.54433E+02	-5.88E+00	9.46E+00	-2.60E+01	-7.47E+02	1.16E+02	3.53E+01
714	222	.053210	2.83E+01	72.77	74.82	1.53864E+02	-5.88E+00	9.46E+00	-2.60E+01	-7.47E+02	1.16E+02	3.53E+01
714	407	.000001	2.83E+01	68.72	89.29	1.92107E+02	-5.88E+00	9.46E+00	-2.60E+01	-7.47E+02	1.16E+02	3.53E+01
714	2	.005733	2.83E+01	81.22	71.20	4.45122E+02	-5.88E+00	9.46E+00	-2.60E+01	-7.47E+02	1.16E+02	3.53E+01
714	3	.017630	2.83E+01	61.62	66.62	3.26249E+02	-5.88E+00	9.46E+00	-2.60E+01	-7.47E+02	1.16E+02	3.53E+01
714	144	.000555	2.83E+01	71.15	56.23	2.45498E+02	-5.88E+00	9.46E+00	-2.60E+01	-7.47E+02	1.16E+02	3.53E+01
714	4	.070914	2.83E+01	45.02	17.98	1.53117E+02	-5.88E+00	9.46E+00	-2.60E+01	-7.47E+02	1.16E+02	3.53E+01
714	306	.011293	2.83E+01	82.98	80.81	2.42804E+02	-5.88E+00	9.46E+00	-2.60E+01	-7.47E+02	1.16E+02	3.53E+01
714	721	.000791	2.83E+01	70.49	64.39	5.26695E+01	5.88E+00	-9.46E+00	2.60E+01	-7.47E+02	1.16E+02	3.53E+01

MODEL = RIO STEP = 1 RCS ANALYSIS 4/9/75
PROCESSING OPERATIONS DATA

NODE I	NODE J	F(I,J)	AREA	THETI	THETJ	RADIUS	NORMAL VECTOR I			POSITION VECTOR I		
715	723	.001135	2.83E+01	71.02	42.64	4.91717E+01	5.88E+00	-9.46E+00	2.60E+01	-7.47E+02	1.16E+02	3.53E+01
715	725	.001223	2.83E+01	73.13	36.44	4.13408E+01	5.88E+00	-9.46E+00	2.60E+01	-7.47E+02	1.16E+02	3.53E+01
715	727	.000859	2.83E+01	77.02	36.54	4.13665E+01	5.88E+00	-9.46E+00	2.60E+01	-7.47E+02	1.16E+02	3.53E+01
715	730	.001297	2.83E+01	36.49	30.83	7.12789E+01	5.88E+00	-9.46E+00	2.60E+01	-7.47E+02	1.16E+02	3.53E+01
715	732	.001598	2.83E+01	34.09	22.81	8.63987E+01	5.88E+00	-9.46E+00	2.60E+01	-7.47E+02	1.16E+02	3.53E+01
715	734	.001715	2.83E+01	35.61	16.50	6.38849E+01	5.88E+00	-9.46E+00	2.60E+01	-7.47E+02	1.16E+02	3.53E+01
715	707	.000112	2.83E+01	72.93	80.55	7.80581E+02	5.88E+00	-9.46E+00	2.60E+01	-7.47E+02	1.16E+02	3.53E+01
715	31	.010443	2.83E+01	58.31	39.19	4.50797E+01	5.88E+00	-9.46E+00	2.60E+01	-7.47E+02	1.16E+02	3.53E+01
715	32	.012136	2.83E+01	16.38	65.21	8.78773E+01	5.88E+00	-9.46E+00	2.60E+01	-7.47E+02	1.16E+02	3.53E+01
715	33	.006833	2.83E+01	40.83	47.93	5.45961E+01	5.88E+00	-9.46E+00	2.60E+01	-7.47E+02	1.16E+02	3.53E+01
715	34	.019789	2.83E+01	13.59	64.75	8.63724E+01	5.88E+00	-9.46E+00	2.60E+01	-7.47E+02	1.16E+02	3.53E+01
715	25	.000459	2.83E+01	80.96	40.56	4.45582E+01	5.88E+00	-9.46E+00	2.60E+01	-7.47E+02	1.16E+02	3.53E+01
715	27	.003447	2.83E+01	63.87	47.00	2.30293E+01	5.88E+00	-9.46E+00	2.60E+01	-7.47E+02	1.16E+02	3.53E+01
715	800	.002480	2.83E+01	57.10	36.07	9.89690E+01	5.88E+00	-9.46E+00	2.60E+01	-7.47E+02	1.16E+02	3.53E+01
715	801	.003847	2.83E+01	56.27	16.85	8.81447E+01	5.88E+00	-9.46E+00	2.60E+01	-7.47E+02	1.16E+02	3.53E+01
715	22	.169950	2.83E+01	60.26	71.15	1.23488E+02	5.88E+00	-9.46E+00	2.60E+01	-7.47E+02	1.16E+02	3.53E+01
715	150	.000194	2.83E+01	84.01	60.50	4.23607E+02	5.88E+00	-9.46E+00	2.60E+01	-7.47E+02	1.16E+02	3.53E+01
715	151	.000603	2.83E+01	82.47	68.96	5.81167E+02	5.88E+00	-9.46E+00	2.60E+01	-7.47E+02	1.16E+02	3.53E+01
715	746	.000321	2.83E+01	75.01	70.06	5.09624E+02	5.88E+00	-9.46E+00	2.60E+01	-7.47E+02	1.16E+02	3.53E+01
715	360	.000158	2.83E+01	15.79	61.45	2.41701E+02	5.88E+00	-9.46E+00	2.60E+01	-7.47E+02	1.16E+02	3.53E+01
715	365	.000063	2.83E+01	16.37	58.59	2.21865E+02	5.88E+00	-9.46E+00	2.60E+01	-7.47E+02	1.16E+02	3.53E+01
715	701	.001498	2.83E+01	29.07	63.65	8.06403E+01	5.88E+00	-9.46E+00	2.60E+01	-7.47E+02	1.16E+02	3.53E+01
715	702	.001148	2.83E+01	60.95	79.33	2.12413E+02	5.88E+00	-9.46E+00	2.60E+01	-7.47E+02	1.16E+02	3.53E+01
720	900	.002512	2.83E+01	48.40	53.29	2.50238E+02	-1.80E-10	2.83E+01	6.14E-22	-7.14E+02	1.49E+02	5.90E+01
720	901	.001257	2.83E+01	93.24	30.86	1.60031E+02	-1.80E-10	2.83E+01	6.14E-22	-7.14E+02	1.49E+02	5.90E+01
720	2	.012277	2.83E+01	75.94	66.21	4.14299E+02	-1.80E-10	2.83E+01	6.14E-22	-7.14E+02	1.49E+02	5.90E+01
720	3	.002842	2.83E+01	54.62	58.63	2.97459E+02	-1.80E-10	2.83E+01	6.14E-22	-7.14E+02	1.49E+02	5.90E+01
720	144	.000773	2.83E+01	92.46	48.17	2.32353E+02	-1.80E-10	2.83E+01	6.14E-22	-7.14E+02	1.49E+02	5.90E+01
720	4	.008281	2.83E+01	100.93	6.72	1.65540E+02	-1.80E-10	2.83E+01	6.14E-22	-7.14E+02	1.49E+02	5.90E+01
720	785	.000129	2.83E+01	87.03	70.20	4.35877E+02	-1.80E-10	2.83E+01	6.14E-22	-7.14E+02	1.49E+02	5.90E+01
721	730	.001960	2.83E+01	66.57	23.43	4.08495E+01	1.80E-10	-2.83E+01	-6.14E-22	-7.14E+02	1.49E+02	5.90E+01
721	732	.001619	2.83E+01	67.73	29.03	4.28172E+01	1.80E-10	-2.83E+01	-6.14E-22	-7.14E+02	1.49E+02	5.90E+01
721	734	.000996	2.83E+01	70.40	34.27	4.84687E+01	1.80E-10	-2.83E+01	-6.14E-22	-7.14E+02	1.49E+02	5.90E+01
721	741	.000007	2.83E+01	42.83	87.03	2.02538E+02	1.80E-10	-2.83E+01	-6.14E-22	-7.14E+02	1.49E+02	5.90E+01
721	901	.001197	2.83E+01	86.76	30.86	1.80031E+02	1.80E-10	-2.83E+01	-6.14E-22	-7.14E+02	1.49E+02	5.90E+01
721	31	.174821	2.83E+01	13.35	77.28	2.04403E+01	1.80E-10	-2.83E+01	-6.14E-22	-7.14E+02	1.49E+02	5.90E+01
721	32	.001833	2.83E+01	31.29	87.03	8.67169E+01	1.80E-10	-2.83E+01	-6.14E-22	-7.14E+02	1.49E+02	5.90E+01
721	33	.177027	2.83E+01	32.91	81.42	3.01508E+01	1.80E-10	-2.83E+01	-6.14E-22	-7.14E+02	1.49E+02	5.90E+01
721	34	.003544	2.83E+01	41.53	86.03	7.66100E+01	1.80E-10	-2.83E+01	-6.14E-22	-7.14E+02	1.49E+02	5.90E+01
721	26	.000191	2.83E+01	58.23	82.13	5.84.00E+01	1.80E-10	-2.83E+01	-6.14E-22	-7.14E+02	1.49E+02	5.90E+01
721	800	.034506	2.83E+01	4.98	18.87	1.28259E+02	1.80E-10	-2.83E+01	-6.14E-22	-7.14E+02	1.49E+02	5.90E+01
721	801	.049397	2.83E+01	27.89	14.42	1.27192E+02	1.80E-10	-2.83E+01	-6.14E-22	-7.14E+02	1.49E+02	5.90E+01
721	805	.019336	2.83E+01	54.27	55.72	1.33183E+02	1.80E-10	-2.83E+01	-6.14E-22	-7.14E+02	1.49E+02	5.90E+01
721	806	.034032	2.83E+01	63.03	57.25	1.37617E+02	1.80E-10	-2.83E+01	-6.14E-22	-7.14E+02	1.49E+02	5.90E+01

MODEL = RIO STEP = 1 RCS ANALYSIS 4/9/75

PROCESSING OPERATIONS DATA

NODE I	NODE J	F(I,J)	AREA	THETI	THETJ	RADIUS	NORMAL VECTOR I			POSITION VECTOR I		
721	810	.011899	2.83E+01	31.31	36.51	2.08068E+02	1.80E-10	-2.83E+01	-6.14E-22	-7.14E+02	1.49E+02	5.90E+01
721	811	.012345	2.83E+01	37.06	32.51	2.03524E+02	1.80E-10	-2.83E+01	-6.14E-22	-7.14E+02	1.49E+02	5.90E+01
721	222	.009222	2.83E+01	39.27	86.59	1.92130E+02	1.80E-10	-2.83E+01	-6.14E-22	-7.14E+02	1.49E+02	5.90E+01
721	22	.004548	2.83E+01	9.03	85.77	1.49329E+02	1.80E-10	-2.83E+01	-6.14E-22	-7.14E+02	1.49E+02	5.90E+01
721	15	.000000	2.83E+01	81.60	81.60	1.59760E+02	1.80E-10	-2.83E+01	-6.14E-22	-7.14E+02	1.49E+02	5.90E+01
721	4	.007209	2.83E+01	79.07	6.72	1.65540E+02	1.80E-10	-2.83E+01	-6.14E-22	-7.14E+02	1.49E+02	5.90E+01
721	880	.006642	2.83E+01	56.03	50.03	2.31536E+02	1.80E-10	-2.83E+01	-6.14E-22	-7.14E+02	1.49E+02	5.90E+01
721	889	.054392	2.83E+01	48.56	48.56	2.24769E+02	1.80E-10	-2.83E+01	-6.14E-22	-7.14E+02	1.49E+02	5.90E+01
721	731	.029347	2.83E+01	58.27	51.98	8.91278E+01	1.80E-10	-2.83E+01	-6.14E-22	-7.14E+02	1.49E+02	5.90E+01
721	702	.002378	2.83E+01	14.99	75.02	2.47564E+02	1.80E-10	-2.83E+01	-6.14E-22	-7.14E+02	1.49E+02	5.90E+01
722	908	.023287	2.83E+01	49.38	54.01	2.64593E+02	-1.80E-10	2.83E+01	6.14E-22	-7.27E+02	1.49E+02	5.90E+01
722	901	.001077	2.83E+01	93.11	34.20	1.87559E+02	-1.80E-10	2.83E+01	6.14E-22	-7.27E+02	1.49E+02	5.90E+01
722	771	.000005	2.83E+01	86.76	85.82	8.72147E+02	-1.80E-10	2.83E+01	6.14E-22	-7.27E+02	1.49E+02	5.90E+01
722	773	.000034	2.83E+01	85.95	84.77	6.98101E+02	-1.80E-10	2.83E+01	6.14E-22	-7.27E+02	1.49E+02	5.90E+01
722	25	.000002	2.83E+01	89.01	89.01	3.60153E+01	-1.80E-10	2.83E+01	6.14E-22	-7.27E+02	1.49E+02	5.90E+01
722	2	.011091	2.83E+01	77.31	66.75	4.26163E+02	-1.80E-10	2.83E+01	6.14E-22	-7.27E+02	1.49E+02	5.90E+01
722	3	.024987	2.83E+01	55.67	59.44	3.05003E+02	-1.80E-10	2.83E+01	6.14E-22	-7.27E+02	1.49E+02	5.90E+01
722	144	.000840	2.83E+01	92.36	50.15	2.42447E+02	-1.80E-10	2.83E+01	6.14E-22	-7.27E+02	1.49E+02	5.90E+01
722	4	.007516	2.83E+01	100.68	9.23	1.69519E+02	-1.80E-10	2.83E+01	6.14E-22	-7.27E+02	1.49E+02	5.90E+01
722	765	.000597	2.83E+01	87.70	76.00	4.48402E+02	-1.80E-10	2.83E+01	6.14E-22	-7.27E+02	1.49E+02	5.90E+01
722	767	.000015	2.83E+01	86.70	82.45	7.91400E+02	-1.80E-10	2.83E+01	6.14E-22	-7.27E+02	1.49E+02	5.90E+01
723	730	.001618	2.83E+01	67.73	29.03	4.28472E+01	1.80E-10	-2.83E+01	-6.14E-22	-7.27E+02	1.49E+02	5.90E+01
723	732	.001960	2.83E+01	66.57	23.43	4.08095E+01	1.80E-10	-2.83E+01	-6.14E-22	-7.27E+02	1.49E+02	5.90E+01
723	734	.001619	2.83E+01	67.73	29.03	4.28472E+01	1.80E-10	-2.83E+01	-6.14E-22	-7.27E+02	1.49E+02	5.90E+01
723	901	.002954	2.83E+01	86.89	34.20	1.87559E+02	1.80E-10	-2.83E+01	-6.14E-22	-7.27E+02	1.49E+02	5.90E+01
723	31	.071108	2.83E+01	41.44	48.73	2.65294E+01	1.80E-10	-2.83E+01	-6.14E-22	-7.27E+02	1.49E+02	5.90E+01
723	32	.005333	2.83E+01	32.99	78.58	8.83009E+01	1.80E-10	-2.83E+01	-6.14E-22	-7.27E+02	1.49E+02	5.90E+01
723	33	.120622	2.83E+01	47.93	59.00	3.45785E+01	1.80E-10	-2.83E+01	-6.14E-22	-7.27E+02	1.49E+02	5.90E+01
723	34	.010080	2.83E+01	43.03	77.11	7.84044E+01	1.80E-10	-2.83E+01	-6.14E-22	-7.27E+02	1.49E+02	5.90E+01
723	26	.000417	2.83E+01	50.18	80.41	4.80163E+01	1.80E-10	-2.83E+01	-6.14E-22	-7.27E+02	1.49E+02	5.90E+01
723	800	.032954	2.83E+01	2.45	24.46	1.27891E+02	1.80E-10	-2.83E+01	-6.14E-22	-7.27E+02	1.49E+02	5.90E+01
723	801	.059628	2.83E+01	22.49	9.00	1.21069E+02	1.80E-10	-2.83E+01	-6.14E-22	-7.27E+02	1.49E+02	5.90E+01
723	805	.022083	2.83E+01	53.03	57.71	1.31155E+02	1.80E-10	-2.83E+01	-6.14E-22	-7.27E+02	1.49E+02	5.90E+01
723	806	.040964	2.83E+01	61.51	56.91	1.30151E+02	1.80E-10	-2.83E+01	-6.14E-22	-7.27E+02	1.49E+02	5.90E+01
723	810	.011693	2.83E+01	30.71	38.30	2.06776E+02	1.80E-10	-2.83E+01	-6.14E-22	-7.27E+02	1.49E+02	5.90E+01
723	811	.021730	2.83E+01	35.30	32.08	1.99012E+02	1.80E-10	-2.83E+01	-6.14E-22	-7.27E+02	1.49E+02	5.90E+01
723	222	.024360	2.83E+01	39.30	82.74	1.92231E+02	1.80E-10	-2.83E+01	-6.14E-22	-7.27E+02	1.49E+02	5.90E+01
723	22	.009691	2.83E+01	9.36	80.87	1.50057E+02	1.80E-10	-2.83E+01	-6.14E-22	-7.27E+02	1.49E+02	5.90E+01
723	417	.000038	2.83E+01	79.51	79.51	1.96524E+02	1.80E-10	-2.83E+01	-6.14E-22	-7.27E+02	1.49E+02	5.90E+01
723	15	.000000	2.83E+01	81.61	81.61	1.55992E+02	1.80E-10	-2.83E+01	-6.14E-22	-7.27E+02	1.49E+02	5.90E+01
723	143	.000081	2.83E+01	86.79	65.95	4.12831E+02	1.80E-10	-2.83E+01	-6.14E-22	-7.27E+02	1.49E+02	5.90E+01
723	144	.002264	2.83E+01	87.04	50.15	2.42447E+02	1.80E-10	-2.83E+01	-6.14E-22	-7.27E+02	1.49E+02	5.90E+01
723	4	.000726	2.83E+01	79.32	9.23	1.69519E+02	1.80E-10	-2.83E+01	-6.14E-22	-7.27E+02	1.49E+02	5.90E+01
723	326	.023431	2.83E+01	78.74	78.74	2.39724E+02	1.80E-10	-2.83E+01	-6.14E-22	-7.27E+02	1.49E+02	5.90E+01

MODEL = RIO STEP = 1 RCS ANALYSIS 4/9/75
PROCESSING OPERATIONS DATA

NODE I	NODE J	F(I,J)	AREA	THETI	THETJ	RADIUS	NORMAL VECTOR I			POSITION VECTOR I		
723	380	.006604	2.83E+01	50.82	50.82	2.394 59E+02	1.80E-10	-2.83E+01	-6.14E-22	-7.27E+02	1.49E+02	5.90E+01
723	385	.007910	2.83E+01	48.23	48.23	2.233 07E+02	1.80E-10	-2.83E+01	-6.14E-22	-7.27E+02	1.49E+02	5.90E+01
723	731	.029551	2.83E+01	55.05	58.74	8.181 19E+01	1.80E-10	-2.83E+01	-6.14E-22	-7.27E+02	1.49E+02	5.90E+01
723	732	.001735	2.83E+01	12.24	77.85	2.446 94E+02	1.80E-10	-2.83E+01	-6.14E-22	-7.27E+02	1.49E+02	5.90E+01
724	900	.021109	2.83E+01	56.41	54.78	2.706 77E+02	-1.80E-10	2.83E+01	6.14E-22	-7.40E+02	1.49E+02	5.90E+01
724	901	.000917	2.83E+01	92.98	37.28	1.957 77E+02	-1.80E-10	2.83E+01	6.14E-22	-7.40E+02	1.49E+02	5.90E+01
724	771	.000016	2.83E+01	86.80	85.88	8.894 06E+02	-1.80E-10	2.83E+01	6.14E-22	-7.40E+02	1.49E+02	5.90E+01
724	773	.000048	2.83E+01	86.02	84.87	7.114 96E+02	-1.80E-10	2.83E+01	6.14E-22	-7.40E+02	1.49E+02	5.90E+01
724	25	.000013	2.83E+01	88.46	88.46	2.300 84E+01	-1.80E-10	2.83E+01	6.14E-22	-7.40E+02	1.49E+02	5.90E+01
724	2	.010434	2.83E+01	77.66	67.26	4.386 91E+02	-1.80E-10	2.83E+01	6.14E-22	-7.40E+02	1.49E+02	5.90E+01
724	3	.022422	2.83E+01	56.70	60.25	3.133 85E+02	-1.80E-10	2.83E+01	6.14E-22	-7.40E+02	1.49E+02	5.90E+01
724	144	.000720	2.83E+01	92.26	51.96	2.529 07E+02	-1.80E-10	2.83E+01	6.14E-22	-7.40E+02	1.49E+02	5.90E+01
724	4	.016720	2.83E+01	100.38	12.51	1.742 83E+02	-1.80E-10	2.83E+01	6.14E-22	-7.40E+02	1.49E+02	5.90E+01
724	785	.000532	2.83E+01	87.76	70.97	4.609 54E+02	-1.80E-10	2.83E+01	6.14E-22	-7.40E+02	1.49E+02	5.90E+01
724	787	.000044	2.83E+01	86.72	82.57	8.042 56E+02	-1.80E-10	2.83E+01	6.14E-22	-7.40E+02	1.49E+02	5.90E+01
725	730	.003936	2.83E+01	70.40	39.27	4.840 87E+01	1.80E-10	-2.83E+01	-6.14E-22	-7.40E+02	1.49E+02	5.90E+01
725	732	.001618	2.83E+01	87.73	29.03	4.286 72E+01	1.80E-10	-2.83E+01	-6.14E-22	-7.40E+02	1.49E+02	5.90E+01
725	734	.001960	2.83E+01	66.57	23.43	4.086 95E+01	1.80E-10	-2.83E+01	-6.14E-22	-7.40E+02	1.49E+02	5.90E+01
725	901	.002513	2.83E+01	87.02	37.28	1.957 77E+02	1.80E-10	-2.83E+01	-6.14E-22	-7.40E+02	1.49E+02	5.90E+01
725	31	.025549	2.83E+01	56.92	33.17	3.643 91E+01	1.80E-10	-2.83E+01	-6.14E-22	-7.40E+02	1.49E+02	5.90E+01
725	32	.007002	2.83E+01	30.18	73.60	9.181 41E+01	1.80E-10	-2.83E+01	-6.14E-22	-7.40E+02	1.49E+02	5.90E+01
725	33	.008442	2.83E+01	53.59	44.36	4.262 76E+01	1.80E-10	-2.83E+01	-6.14E-22	-7.40E+02	1.49E+02	5.90E+01
725	34	.013843	2.83E+01	49.05	68.20	8.239 39E+01	1.80E-10	-2.83E+01	-6.14E-22	-7.40E+02	1.49E+02	5.90E+01
725	36	.003934	2.83E+01	38.38	78.23	3.922 45E+01	1.80E-10	-2.83E+01	-6.14E-22	-7.40E+02	1.49E+02	5.90E+01
725	800	.000278	2.83E+01	7.08	30.10	1.280 41E+02	1.80E-10	-2.83E+01	-6.14E-22	-7.40E+02	1.49E+02	5.90E+01
725	801	.000693	2.83E+01	16.64	5.13	1.174 33E+02	1.80E-10	-2.83E+01	-6.14E-22	-7.40E+02	1.49E+02	5.90E+01
725	805	.021538	2.83E+01	53.38	60.04	1.386 87E+02	1.80E-10	-2.83E+01	-6.14E-22	-7.40E+02	1.49E+02	5.90E+01
725	806	.004070	2.83E+01	60.06	56.84	1.251 75E+02	1.80E-10	-2.83E+01	-6.14E-22	-7.40E+02	1.49E+02	5.90E+01
725	810	.010940	2.83E+01	36.49	40.30	2.068 97E+02	1.80E-10	-2.83E+01	-6.14E-22	-7.40E+02	1.49E+02	5.90E+01
725	811	.023639	2.83E+01	33.72	31.99	1.952 62E+02	1.80E-10	-2.83E+01	-6.14E-22	-7.40E+02	1.49E+02	5.90E+01
725	232	.035516	2.83E+01	39.66	78.93	1.933 09E+02	1.80E-10	-2.83E+01	-6.14E-22	-7.40E+02	1.49E+02	5.90E+01
725	22	.077614	2.83E+01	13.97	76.11	1.581 61E+02	1.80E-10	-2.83E+01	-6.14E-22	-7.40E+02	1.49E+02	5.90E+01
725	437	.000006	2.83E+01	79.99	79.99	2.359 37E+02	1.80E-10	-2.83E+01	-6.14E-22	-7.40E+02	1.49E+02	5.90E+01
725	15	.000003	2.83E+01	81.09	81.09	1.977 61E+02	1.80E-10	-2.83E+01	-6.14E-22	-7.40E+02	1.49E+02	5.90E+01
725	143	.000333	2.83E+01	88.82	66.53	4.251 33E+02	1.80E-10	-2.83E+01	-6.14E-22	-7.40E+02	1.49E+02	5.90E+01
725	144	.001921	2.83E+01	87.74	51.96	2.529 07E+02	1.80E-10	-2.83E+01	-6.14E-22	-7.40E+02	1.49E+02	5.90E+01
725	4	.000101	2.83E+01	79.02	12.51	1.742 83E+02	1.80E-10	-2.83E+01	-6.14E-22	-7.40E+02	1.49E+02	5.90E+01
725	386	.020018	2.83E+01	79.26	79.26	2.508 18E+02	1.80E-10	-2.83E+01	-6.14E-22	-7.40E+02	1.49E+02	5.90E+01
725	391	.000613	2.83E+01	51.70	51.70	2.401 23E+02	1.80E-10	-2.83E+01	-6.14E-22	-7.40E+02	1.49E+02	5.90E+01
725	395	.000071	2.83E+01	48.07	48.07	2.222 96E+02	1.80E-10	-2.83E+01	-6.14E-22	-7.40E+02	1.49E+02	5.90E+01
725	731	.030253	2.83E+01	51.94	86.74	7.000 02E+01	1.80E-10	-2.83E+01	-6.14E-22	-7.40E+02	1.49E+02	5.90E+01
725	732	.001347	2.83E+01	9.94	80.75	2.429 87E+02	1.80E-10	-2.83E+01	-6.14E-22	-7.40E+02	1.49E+02	5.90E+01
726	900	.019101	2.83E+01	51.46	55.57	2.762 55E+02	-1.80E-10	2.83E+01	6.14E-22	-7.53E+02	1.49E+02	5.90E+01

MODEL = RIO STEP = 1 RCS ANALYSIS 4/9/75
PROCESSING OPERATIONS DATA

NODE I	NODE J	F(I,J)	AREA	THETI	THETJ	RADIUS	NORMAL VECTOR I			POSITION VECTOR I		
726	961	.000779	2.83E+01	92.86	40.11	2.04216E+02	-1.80E-10	2.83E+01	6.14E-22	-7.53E+02	1.49E+02	5.90E+01
726	771	.000019	2.83E+01	86.85	85.94	8.98765E+02	-1.80E-10	2.83E+01	6.14E-22	-7.53E+02	1.49E+02	5.90E+01
726	773	.000045	2.83E+01	86.09	84.96	7.24433E+02	-1.80E-10	2.83E+01	6.14E-22	-7.53E+02	1.49E+02	5.90E+01
726	29	.000414	2.83E+01	86.45	80.45	1.00192E+01	-1.80E-10	2.83E+01	6.14E-22	-7.53E+02	1.49E+02	5.90E+01
726	2	.009362	2.83E+01	78.80	67.74	4.50179E+02	-1.80E-10	2.83E+01	6.14E-22	-7.53E+02	1.49E+02	5.90E+01
726	3	.020126	2.83E+01	57.70	61.03	3.22479E+02	-1.80E-10	2.83E+01	6.14E-22	-7.53E+02	1.49E+02	5.90E+01
726	144	.000613	2.83E+01	92.17	53.64	2.63401E+02	-1.80E-10	2.83E+01	6.14E-22	-7.53E+02	1.49E+02	5.90E+01
726	4	.000937	2.83E+01	100.06	15.92	1.79863E+02	-1.80E-10	2.83E+01	6.14E-22	-7.53E+02	1.49E+02	5.90E+01
726	785	.000409	2.83E+01	87.82	77.32	4.73536E+02	-1.80E-10	2.83E+01	6.14E-22	-7.53E+02	1.49E+02	5.90E+01
726	787	.000342	2.83E+01	88.74	82.69	8.17117E+02	-1.80E-10	2.83E+01	6.14E-22	-7.53E+02	1.49E+02	5.90E+01
727	730	.000539	2.83E+01	73.28	48.41	5.64917E+01	1.80E-10	-2.83E+01	-6.14E-22	-7.53E+02	1.49E+02	5.90E+01
727	732	.003930	2.83E+01	71.40	39.27	4.84387E+01	1.80E-10	-2.83E+01	-6.14E-22	-7.53E+02	1.49E+02	5.90E+01
727	734	.001018	2.83E+01	67.73	29.03	4.28872E+01	1.80E-10	-2.83E+01	-6.14E-22	-7.53E+02	1.49E+02	5.90E+01
727	961	.002151	2.83E+01	87.14	40.11	2.04216E+02	1.80E-10	-2.83E+01	-6.14E-22	-7.53E+02	1.49E+02	5.90E+01
727	31	.011501	2.83E+01	65.44	24.63	4.78119E+01	1.80E-10	-2.83E+01	-6.14E-22	-7.53E+02	1.49E+02	5.90E+01
727	32	.003696	2.83E+01	40.12	63.33	9.69114E+01	1.80E-10	-2.83E+01	-6.14E-22	-7.53E+02	1.49E+02	5.90E+01
727	33	.004496	2.83E+01	61.31	34.43	5.27115E+01	1.80E-10	-2.83E+01	-6.14E-22	-7.53E+02	1.49E+02	5.90E+01
727	34	.014936	2.83E+01	49.32	60.37	8.79135E+01	1.80E-10	-2.83E+01	-6.14E-22	-7.53E+02	1.49E+02	5.90E+01
727	26	.001792	2.83E+01	22.61	76.10	3.33101E+01	1.80E-10	-2.83E+01	-6.14E-22	-7.53E+02	1.49E+02	5.90E+01
727	830	.026761	2.83E+01	12.90	35.05	1.31180E+02	1.80E-10	-2.83E+01	-6.14E-22	-7.53E+02	1.49E+02	5.90E+01
727	831	.000960	2.83E+01	10.40	3.16	1.14310E+02	1.80E-10	-2.83E+01	-6.14E-22	-7.53E+02	1.49E+02	5.90E+01
727	833	.002639	2.83E+01	53.56	82.65	1.33433E+02	1.80E-10	-2.83E+01	-6.14E-22	-7.53E+02	1.49E+02	5.90E+01
727	836	.004409	2.83E+01	58.78	57.11	1.20430E+02	1.80E-10	-2.83E+01	-6.14E-22	-7.53E+02	1.49E+02	5.90E+01
727	810	.010720	2.83E+01	30.05	42.49	2.66035E+02	1.80E-10	-2.83E+01	-6.14E-22	-7.53E+02	1.49E+02	5.90E+01
727	811	.024307	2.83E+01	32.38	32.28	1.92720E+02	1.80E-10	-2.83E+01	-6.14E-22	-7.53E+02	1.49E+02	5.90E+01
727	222	.045030	2.83E+01	40.30	75.13	1.95151E+02	1.80E-10	-2.83E+01	-6.14E-22	-7.53E+02	1.49E+02	5.90E+01
727	22	.009877	2.83E+01	18.49	71.53	1.56347E+02	1.80E-10	-2.83E+01	-6.14E-22	-7.53E+02	1.49E+02	5.90E+01
727	407	.000035	2.83E+01	80.44	80.44	2.15674E+02	1.80E-10	-2.83E+01	-6.14E-22	-7.53E+02	1.49E+02	5.90E+01
727	15	.000037	2.83E+01	81.81	81.81	1.59780E+02	1.80E-10	-2.83E+01	-6.14E-22	-7.53E+02	1.49E+02	5.90E+01
727	143	.000293	2.83E+01	88.86	67.07	4.37476E+02	1.80E-10	-2.83E+01	-6.14E-22	-7.53E+02	1.49E+02	5.90E+01
727	144	.001635	2.83E+01	87.83	53.64	2.63401E+02	1.80E-10	-2.83E+01	-6.14E-22	-7.53E+02	1.49E+02	5.90E+01
727	4	.005596	2.83E+01	79.94	15.92	1.79863E+02	1.80E-10	-2.83E+01	-6.14E-22	-7.53E+02	1.49E+02	5.90E+01
727	731	.000045	2.83E+01	89.06	81.68	4.65289E+02	1.80E-10	-2.83E+01	-6.14E-22	-7.53E+02	1.49E+02	5.90E+01
727	836	.017863	2.83E+01	79.73	79.73	2.62270E+02	1.80E-10	-2.83E+01	-6.14E-22	-7.53E+02	1.49E+02	5.90E+01
727	380	.000373	2.83E+01	52.65	52.65	2.45193E+02	1.80E-10	-2.83E+01	-6.14E-22	-7.53E+02	1.49E+02	5.90E+01
727	385	.090665	2.83E+01	48.08	48.08	2.22644E+02	1.80E-10	-2.83E+01	-6.14E-22	-7.53E+02	1.49E+02	5.90E+01
727	701	.023016	2.83E+01	49.49	75.89	7.21527E+01	1.80E-10	-2.83E+01	-6.14E-22	-7.53E+02	1.49E+02	5.90E+01
727	732	.000918	2.83E+01	7.06	83.09	2.40963E+02	1.80E-10	-2.83E+01	-6.14E-22	-7.53E+02	1.49E+02	5.90E+01
730	741	.000006	2.83E+01	37.22	87.20	2.19753E+02	0.	0.	-2.83E+01	-7.14E+02	1.33E+02	9.65E+01
730	903	.001624	2.83E+01	45.94	44.08	2.95329E+02	0.	0.	-2.83E+01	-7.14E+02	1.33E+02	9.65E+01
730	31	.007769	2.83E+01	8.46	83.43	3.93406E+01	0.	0.	-2.83E+01	-7.14E+02	1.33E+02	9.65E+01
730	32	.002200	2.83E+01	97.18	85.59	5.84399E+01	0.	0.	-2.83E+01	-7.14E+02	1.33E+02	9.65E+01
730	33	.382253	2.83E+01	24.37	79.19	2.39879E+01	0.	0.	-2.83E+01	-7.14E+02	1.33E+02	9.65E+01
730	34	.000206	2.83E+01	107.58	84.04	4.33677E+01	0.	0.	-2.83E+01	-7.14E+02	1.33E+02	9.65E+01

MODEL = R10 STEP = 1 RCS ANALYSIS 4/9/75
PROCESSING OPERATIONS DATA

NODE I	NODE J	F(I,J)	AREA	THETI	THETJ	RADIUS	NORMAL VECTOR I		POSITION VECTOR I			
730	25	.000340	2.83E+01	54.11	74.71	6.39675E+01	0.	0.	-2.83E+01	-7.14E+02	1.33E+02	9.65E+01
730	26	.000851	2.83E+01	48.32	48.32	6.84615E+01	0.	0.	-2.83E+01	-7.14E+02	1.33E+02	9.65E+01
730	800	.010220	2.83E+01	69.37	29.77	1.19655E+02	0.	0.	-2.83E+01	-7.14E+02	1.33E+02	9.65E+01
730	801	.009444	2.83E+01	73.50	26.09	1.17567E+02	0.	0.	-2.83E+01	-7.14E+02	1.33E+02	9.65E+01
730	805	.019445	2.83E+01	25.31	68.55	1.57257E+02	0.	0.	-2.83E+01	-7.14E+02	1.33E+02	9.65E+01
730	806	.032983	2.83E+01	33.76	69.16	1.60756E+02	0.	0.	-2.83E+01	-7.14E+02	1.33E+02	9.65E+01
730	807	.002022	2.83E+01	36.96	122.14	1.77910E+02	0.	0.	-2.83E+01	-7.14E+02	1.33E+02	9.65E+01
730	808	.002373	2.83E+01	46.62	122.09	1.94340E+02	0.	0.	-2.83E+01	-7.14E+02	1.33E+02	9.65E+01
730	810	.006737	2.83E+01	49.04	46.34	2.16475E+02	0.	0.	-2.83E+01	-7.14E+02	1.33E+02	9.65E+01
730	811	.011874	2.83E+01	51.01	43.34	2.12160E+02	0.	0.	-2.83E+01	-7.14E+02	1.33E+02	9.65E+01
730	222	.014851	2.83E+01	39.83	85.44	2.07732E+02	0.	0.	-2.83E+01	-7.14E+02	1.33E+02	9.65E+01
730	22	.004494	2.83E+01	70.94	83.54	1.94089E+02	0.	0.	-2.83E+01	-7.14E+02	1.33E+02	9.65E+01
730	15	.000008	2.83E+01	2.14	88.06	1.91734E+02	0.	0.	-2.83E+01	-7.14E+02	1.33E+02	9.65E+01
730	212	.000128	2.83E+01	80.32	65.58	1.44947E+02	0.	0.	-2.83E+01	-7.14E+02	1.33E+02	9.65E+01
730	701	.001438	2.83E+01	103.55	39.46	6.43927E+01	0.	0.	-2.83E+01	-7.14E+02	1.33E+02	9.65E+01
730	702	.000008	2.83E+01	85.67	76.58	2.31703E+02	0.	0.	-2.83E+01	-7.14E+02	1.33E+02	9.65E+01
731	32	.001579	2.83E+01	82.82	85.59	5.84699E+01	0.	0.	2.83E+01	-7.14E+02	1.33E+02	9.65E+01
731	34	.115669	2.83E+01	72.42	84.04	4.33677E+01	0.	0.	2.83E+01	-7.14E+02	1.33E+02	9.65E+01
731	380	.015257	2.83E+01	48.98	47.20	1.95191E+02	0.	0.	2.83E+01	-7.14E+02	1.33E+02	9.65E+01
731	385	.071304	2.83E+01	46.79	44.86	1.86934E+02	0.	0.	2.83E+01	-7.14E+02	1.33E+02	9.65E+01
731	701	.007731	2.83E+01	76.45	39.46	6.43927E+01	0.	0.	2.83E+01	-7.14E+02	1.33E+02	9.65E+01
731	702	.000001	2.83E+01	94.33	76.58	2.31703E+02	0.	0.	2.83E+01	-7.14E+02	1.33E+02	9.65E+01
732	740	.000033	2.83E+01	37.14	89.35	2.19717E+02	0.	0.	-2.83E+01	-7.27E+02	1.33E+02	9.65E+01
732	900	.014306	2.83E+01	46.78	50.32	2.99370E+02	0.	0.	-2.83E+01	-7.27E+02	1.33E+02	9.65E+01
732	31	.017843	2.83E+01	24.67	65.88	4.28265E+01	0.	0.	-2.83E+01	-7.27E+02	1.33E+02	9.65E+01
732	32	.000688	2.83E+01	96.89	73.30	6.08357E+01	0.	0.	-2.83E+01	-7.27E+02	1.33E+02	9.65E+01
732	33	.202886	2.83E+01	42.26	53.39	2.93464E+01	0.	0.	-2.83E+01	-7.27E+02	1.33E+02	9.65E+01
732	34	.000500	2.83E+01	106.34	67.92	4.65484E+01	0.	0.	-2.83E+01	-7.27E+02	1.33E+02	9.65E+01
732	25	.000038	2.83E+01	46.67	72.12	6.46826E+01	0.	0.	-2.83E+01	-7.27E+02	1.33E+02	9.65E+01
732	26	.001458	2.83E+01	40.46	40.46	5.98638E+01	0.	0.	-2.83E+01	-7.27E+02	1.33E+02	9.65E+01
732	800	.009605	2.83E+01	69.30	33.97	1.19761E+02	0.	0.	-2.83E+01	-7.27E+02	1.33E+02	9.65E+01
732	801	.010567	2.83E+01	72.59	23.14	1.11885E+02	0.	0.	-2.83E+01	-7.27E+02	1.33E+02	9.65E+01
732	805	.019503	2.83E+01	23.94	70.29	1.55143E+02	0.	0.	-2.83E+01	-7.27E+02	1.33E+02	9.65E+01
732	806	.037821	2.83E+01	30.43	69.54	1.54797E+02	0.	0.	-2.83E+01	-7.27E+02	1.33E+02	9.65E+01
732	807	.001431	2.83E+01	36.30	124.37	1.76697E+02	0.	0.	-2.83E+01	-7.27E+02	1.33E+02	9.65E+01
732	808	.002030	2.83E+01	45.25	124.08	1.89609E+02	0.	0.	-2.83E+01	-7.27E+02	1.33E+02	9.65E+01
732	810	.006629	2.83E+01	48.76	47.82	2.15635E+02	0.	0.	-2.83E+01	-7.27E+02	1.33E+02	9.65E+01
732	811	.012533	2.83E+01	50.04	43.29	2.07363E+02	0.	0.	-2.83E+01	-7.27E+02	1.33E+02	9.65E+01
732	222	.009761	2.83E+01	39.86	81.85	2.07126E+02	0.	0.	-2.83E+01	-7.27E+02	1.33E+02	9.65E+01
732	22	.002697	2.83E+01	71.15	78.34	1.42109E+02	0.	0.	-2.83E+01	-7.27E+02	1.33E+02	9.65E+01
732	15	.000008	2.83E+01	3.56	88.06	1.91871E+02	0.	0.	-2.83E+01	-7.27E+02	1.33E+02	9.65E+01
732	3	.006138	2.83E+01	52.93	55.32	3.36232E+02	0.	0.	-2.83E+01	-7.27E+02	1.33E+02	9.65E+01
732	4	.032097	2.83E+01	16.76	3.68	2.02428E+02	0.	0.	-2.83E+01	-7.27E+02	1.33E+02	9.65E+01
732	701	.002592	2.83E+01	106.29	46.15	5.38130E+01	0.	0.	-2.83E+01	-7.27E+02	1.33E+02	9.65E+01

MODEL = RIO STEP = 1 RCS ANALYSIS 4/9/75
PROCESSING OPERATIONS DATA

NODE I	NODE J	F(I,J)	AREA	THETI	THETJ	RADIUS	NORMAL VECTOR I		POSITION VECTOR I			
732	702	.000055	2.83E+01	85.61	79.60	2.28634E+02	0.	0.	-2.83E+01	-7.27E+02	1.33E+02	9.65E+01
733	32	.004322	2.83E+01	83.11	73.30	6.08857E+01	0.	0.	2.83E+01	-7.27E+02	1.33E+02	9.65E+01
733	34	.033851	2.83E+01	73.66	67.92	4.65484E+01	0.	0.	2.83E+01	-7.27E+02	1.33E+02	9.65E+01
733	380	.015138	2.83E+01	50.13	48.42	1.99561E+02	0.	0.	2.83E+01	-7.27E+02	1.33E+02	9.65E+01
733	385	.082823	2.83E+01	46.27	44.31	1.85174E+02	0.	0.	2.83E+01	-7.27E+02	1.33E+02	9.65E+01
733	701	.011880	2.83E+01	73.71	46.19	5.38130E+01	0.	0.	2.83E+01	-7.27E+02	1.33E+02	9.65E+01
734	740	.000012	2.83E+01	37.32	85.96	2.20549E+02	0.	0.	-2.83E+01	-7.40E+02	1.33E+02	9.65E+01
734	900	.017374	2.83E+01	47.66	51.00	3.04297E+02	0.	0.	-2.83E+01	-7.40E+02	1.33E+02	9.65E+01
734	31	.017762	2.83E+01	38.28	52.04	4.95793E+01	0.	0.	-2.83E+01	-7.40E+02	1.33E+02	9.65E+01
734	32	.000868	2.83E+01	96.38	62.39	6.58109E+01	0.	0.	-2.83E+01	-7.40E+02	1.33E+02	9.65E+01
734	33	.099383	2.83E+01	55.66	37.68	3.85384E+01	0.	0.	-2.83E+01	-7.40E+02	1.33E+02	9.65E+01
734	34	.000936	2.83E+01	104.36	54.74	5.28276E+01	0.	0.	-2.83E+01	-7.40E+02	1.33E+02	9.65E+01
734	25	.001155	2.83E+01	37.26	69.02	4.71152E+01	0.	0.	-2.83E+01	-7.40E+02	1.33E+02	9.65E+01
734	26	.002359	2.83E+01	31.80	30.80	5.30147E+01	0.	0.	-2.83E+01	-7.40E+02	1.33E+02	9.65E+01
734	800	.008612	2.83E+01	69.48	38.63	1.20279E+02	0.	0.	-2.83E+01	-7.40E+02	1.33E+02	9.65E+01
734	801	.011431	2.83E+01	71.80	21.30	1.07154E+02	0.	0.	-2.83E+01	-7.40E+02	1.33E+02	9.65E+01
734	805	.018920	2.83E+01	23.41	72.10	1.54905E+02	0.	0.	-2.83E+01	-7.40E+02	1.33E+02	9.65E+01
734	806	.042378	2.83E+01	27.11	70.08	1.49945E+02	0.	0.	-2.83E+01	-7.40E+02	1.33E+02	9.65E+01
734	807	.000770	2.83E+01	36.05	120.48	1.75434E+02	0.	0.	-2.83E+01	-7.40E+02	1.33E+02	9.65E+01
734	808	.001534	2.83E+01	44.04	120.05	1.85769E+02	0.	0.	-2.83E+01	-7.40E+02	1.33E+02	9.65E+01
734	810	.000420	2.83E+01	46.05	49.47	2.19175E+02	0.	0.	-2.83E+01	-7.40E+02	1.33E+02	9.65E+01
734	811	.013059	2.83E+01	49.19	43.45	2.04748E+02	0.	0.	-2.83E+01	-7.40E+02	1.33E+02	9.65E+01
734	222	.008034	2.83E+01	40.16	70.29	2.08134E+02	0.	0.	-2.83E+01	-7.40E+02	1.33E+02	9.65E+01
734	22	.048349	2.83E+01	71.51	73.30	1.44785E+02	0.	0.	-2.83E+01	-7.40E+02	1.33E+02	9.65E+01
734	15	.000008	2.83E+01	7.11	68.07	1.92186E+02	0.	0.	-2.83E+01	-7.40E+02	1.33E+02	9.65E+01
734	3	.013560	2.83E+01	53.88	56.11	3.43777E+02	0.	0.	-2.83E+01	-7.40E+02	1.33E+02	9.65E+01
734	4	.054493	2.83E+01	20.12	7.12	2.06126E+02	0.	0.	-2.83E+01	-7.40E+02	1.33E+02	9.65E+01
734	701	.004712	2.83E+01	109.31	56.09	4.45538E+01	0.	0.	-2.83E+01	-7.40E+02	1.33E+02	9.65E+01
734	702	.000039	2.83E+01	85.26	82.70	2.28670E+02	0.	0.	-2.83E+01	-7.40E+02	1.33E+02	9.65E+01
735	32	.005583	2.83E+01	83.62	62.39	6.58109E+01	0.	0.	2.83E+01	-7.40E+02	1.33E+02	9.65E+01
735	34	.031742	2.83E+01	75.04	54.74	5.28276E+01	0.	0.	2.83E+01	-7.40E+02	1.33E+02	9.65E+01
735	380	.043059	2.83E+01	51.37	49.74	2.05524E+02	0.	0.	2.83E+01	-7.40E+02	1.33E+02	9.65E+01
735	385	.081440	2.83E+01	46.02	44.04	1.84317E+02	0.	0.	2.83E+01	-7.40E+02	1.33E+02	9.65E+01
735	701	.016954	2.83E+01	70.19	56.09	4.45538E+01	0.	0.	2.83E+01	-7.40E+02	1.33E+02	9.65E+01
740	800	.001936	2.83E+01	96.16	94.51	1.34488E+02	-2.83E+01	-6.20E-10	-2.07E-10	-7.25E+02	1.17E-11	-7.85E+01
740	801	.012161	2.83E+01	71.51	96.78	1.54166E+02	-2.83E+01	-6.20E-10	-2.07E-10	-7.25E+02	1.17E-11	-7.85E+01
740	802	.001936	2.83E+01	90.16	94.51	1.34488E+02	-2.83E+01	-6.20E-10	-2.07E-10	-7.25E+02	1.17E-11	-7.85E+01
740	803	.012161	2.83E+01	71.51	96.78	1.54166E+02	-2.83E+01	-6.20E-10	-2.07E-10	-7.25E+02	1.17E-11	-7.85E+01
740	807	.095225	2.83E+01	69.23	41.14	4.66739E+01	-2.83E+01	-6.20E-10	-2.07E-10	-7.25E+02	1.17E-11	-7.85E+01
740	808	.074338	2.83E+01	33.57	67.50	7.90484E+01	-2.83E+01	-6.20E-10	-2.07E-10	-7.25E+02	1.17E-11	-7.85E+01
740	810	.095225	2.83E+01	69.23	41.14	4.66739E+01	-2.83E+01	-6.20E-10	-2.07E-10	-7.25E+02	1.17E-11	-7.85E+01
740	811	.074338	2.83E+01	33.57	67.50	7.90484E+01	-2.83E+01	-6.20E-10	-2.07E-10	-7.25E+02	1.17E-11	-7.85E+01

MODEL = RIO STEP = 1 RCS ANALYSIS 4/9/75
PROCESSING OPERATIONS DATA

NODE I	NODE J	F(I,J)	AREA	THETI	THETJ	RADIUS	NORMAL VECTOR I			POSITION VECTOR I		
740	701	.001270	2.83E+01	78.44	61.93	2.20134E+02	-2.83E+01	-6.20E-10	-2.07E-10	-7.25E+02	1.17E-11	-7.85E+01
740	702	.001563	2.83E+01	74.50	61.00	1.88444E+02	-2.83E+01	-6.20E-10	-2.07E-10	-7.25E+02	1.17E-11	-7.85E+01
741	31	.000020	2.83E+01	85.42	85.42	1.88612E+02	2.83E+01	6.20E-10	2.07E-10	-7.25E+02	1.17E-11	-7.85E+01
741	32	.000038	2.83E+01	85.65	85.65	1.97507E+02	2.83E+01	6.20E-10	2.07E-10	-7.25E+02	1.17E-11	-7.85E+01
741	33	.000062	2.83E+01	85.64	85.64	1.97353E+02	2.83E+01	6.20E-10	2.07E-10	-7.25E+02	1.17E-11	-7.85E+01
741	34	.000045	2.83E+01	85.90	85.90	2.09866E+02	2.83E+01	6.20E-10	2.07E-10	-7.25E+02	1.17E-11	-7.85E+01
741	800	.000787	2.83E+01	89.84	94.51	1.34488E+02	2.83E+01	6.20E-10	2.07E-10	-7.25E+02	1.17E-11	-7.85E+01
741	802	.000787	2.83E+01	89.84	94.51	1.34488E+02	2.83E+01	6.20E-10	2.07E-10	-7.25E+02	1.17E-11	-7.85E+01
741	222	.163980	2.83E+01	71.03	78.77	1.69289E+01	2.83E+01	6.20E-10	2.07E-10	-7.25E+02	1.17E-11	-7.85E+01
741	22	.001721	2.83E+01	88.97	88.32	1.30702E+02	2.83E+01	6.20E-10	2.07E-10	-7.25E+02	1.17E-11	-7.85E+01
900	24	.000034	1.49E+04	56.14	52.38	2.80446E+02	-4.62E+02	1.30E+03	1.48E+04	-6.17E+02	3.21E+02	-1.09E+02
900	27	.000033	1.49E+04	60.56	57.45	2.96742E+02	-4.62E+02	1.30E+03	1.48E+04	-6.17E+02	3.21E+02	-1.09E+02
900	701	.001269	1.49E+04	53.65	63.89	3.45752E+02	-4.62E+02	1.30E+03	1.48E+04	-6.17E+02	3.21E+02	-1.09E+02
901	24	.000004	4.78E+03	42.12	92.94	2.11194E+02	-1.48E+02	4.16E+02	4.76E+03	-6.17E+02	1.39E+02	-9.27E+01
901	25	.000011	4.78E+03	42.12	87.30	2.11194E+02	-1.48E+02	4.16E+02	4.76E+03	-6.17E+02	1.39E+02	-9.27E+01
901	27	.000100	4.78E+03	44.96	45.80	2.06122E+02	-1.48E+02	4.16E+02	4.76E+03	-6.17E+02	1.39E+02	-9.27E+01
901	701	.001969	4.78E+03	37.18	44.51	2.57226E+02	-1.48E+02	4.16E+02	4.76E+03	-6.17E+02	1.39E+02	-9.27E+01
771	24	.000000	1.18E+04	86.00	86.92	9.08701E+02	5.83E-08	-3.85E+03	1.11E+04	1.42E+02	1.98E+02	8.75E+00
773	24	.000000	1.18E+04	85.05	86.19	7.34345E+02	5.83E-08	-3.85E+03	1.11E+04	-3.25E+01	1.98E+02	8.75E+00
773	701	.000008	1.18E+04	80.12	79.05	7.49345E+02	5.83E-08	-3.85E+03	1.11E+04	-3.25E+01	1.98E+02	8.75E+00
31	25	.000405	4.14E+02	21.02	69.03	5.73136E+01	-4.14E+02	-6.69E-09	-2.46E-09	-7.10E+02	1.29E+02	5.76E+01
31	26	.000121	4.14E+02	12.35	83.13	5.49868E+01	-4.14E+02	-6.69E-09	-2.46E-09	-7.10E+02	1.29E+02	5.76E+01

MODEL = RIO STEP = 1 RCS ANALYSIS 4/9/75
PROCESSING OPERATIONS DATA

NODE I	NODE J	F(I,J)	AREA	THETI	THETJ	RADIUS	NORMAL VECTOR I			POSITION VECTOR I		
31	27	.0000+2	4.14E+02	13.35	96.87	5.498o8E+01	-4.14E+02	-6.69E-09	-2.46E-09	-7.1[illegible]E+02	1.29E+02	5.76E+01
31	701	.035407	4.14E+02	45.01	41.47	8.44355E+01	-4.14E+02	-6.69E-09	-2.46E-09	-7.1[illegible]E+02	1.29E+02	5.76E+01
32	25	.000275	8.95E+02	58.45	43.04	1.022[illegible]E+02	-8.95E+02	-6.79E-09	6.54E-09	-7.1[illegible]E+02	7.46E+01	1.04E+02
32	26	.000374	8.95E+02	51.94	52.52	8.67799E+01	-8.95E+02	-6.79E-09	6.54E-09	-7.1[illegible]E+02	7.46E+01	1.04E+02
32	701	.073214	8.95E+02	25.61	14.93	8.[illegible]375E+01	-8.95E+02	-6.79E-09	6.54E-09	-7.1[illegible]E+02	7.46E+01	1.04E+02
33	25	.000505	1.41E+03	29.37	65.06	8.15.98E+01	-1.41E+03	-3.87E-08	-8.60E-09	-7.1[illegible]E+02	1.23E+02	7.48E+01
33	26	.000747	1.41E+03	24.49	60.16	5.87[illegible]94E+01	-1.41E+03	-3.87E-08	-8.60E-09	-7.1[illegible]E+02	1.23E+02	7.48E+01
33	701	.060919	1.41E+03	35.63	33.84	7.28960E+01	-1.41E+03	-3.87E-08	-8.60E-09	-7.1[illegible]E+02	1.23E+02	7.48E+01
34	25	.000310	1.31E+03	55.19	51.79	9.37155E+01	-1.31E+03	-2.54E-09	6.50E-09	-7.1[illegible]E+02	9.14E+01	1.10E+02
34	26	.000513	1.31E+03	50.26	45.50	8.36[illegible]64E+01	-1.31E+03	-2.54E-09	6.50E-09	-7.1[illegible]E+02	9.14E+01	1.10E+02
34	701	.091934	1.31E+03	10.23	10.92	6.60[illegible]38E+01	-1.31E+03	-2.54E-09	6.50E-09	-7.1[illegible]E+02	9.14E+01	1.10E+02
24	2	.008601	2.83E+01	78.32	68.09	4.59[illegible]11E+02	-1.80E-10	2.83E+01	6.14E-22	-7.63E+02	1.49E+02	5.90E+01
24	3	.016517	2.83E+01	58.53	61.58	3.28962E+02	-1.80E-10	2.83E+01	6.14E-22	-7.63E+02	1.49E+02	5.90E+01
24	144	.000516	2.83E+01	92.23	54.82	2.71715E+02	-1.80E-10	2.83E+01	6.14E-22	-7.63E+02	1.49E+02	5.90E+01
24	4	.005204	2.83E+01	99.98	18.53	1.84770E+02	-1.80E-10	2.83E+01	6.14E-22	-7.63E+02	1.49E+02	5.90E+01
24	785	.000414	2.83E+01	87.94	77.55	4.83196E+02	-1.80E-10	2.83E+01	6.14E-22	-7.63E+02	1.49E+02	5.90E+01
24	787	.000638	2.83E+01	88.80	82.70	8.27[illegible]06E+02	-1.80E-10	2.83E+01	6.14E-22	-7.63E+02	1.49E+02	5.90E+01
25	26	.002047	2.83E+01	14.31	75.69	3.23[illegible]0E+01	1.80E-10	-2.83E+01	-6.14E-22	-7.63E+02	1.49E+02	5.90E+01
25	800	.023581	2.83E+01	16.96	39.70	1.34[illegible]32E+02	1.80E-10	-2.83E+01	-6.14E-22	-7.63E+02	1.49E+02	5.90E+01
25	801	.060718	2.83E+01	5.62	8.18	1.13[illegible]83E+02	1.80E-10	-2.83E+01	-6.14E-22	-7.63E+02	1.49E+02	5.90E+01
25	802	.010312	2.83E+01	53.75	64.57	1.32[illegible]81E+02	1.80E-10	-2.83E+01	-6.14E-22	-7.63E+02	1.49E+02	5.90E+01
25	806	.057962	2.83E+01	57.72	57.35	1.18[illegible]42E+02	1.80E-10	-2.83E+01	-6.14E-22	-7.63E+02	1.49E+02	5.90E+01
25	810	.010139	2.83E+01	30.94	44.19	2.07[illegible]82E+02	1.80E-10	-2.83E+01	-6.14E-22	-7.63E+02	1.49E+02	5.90E+01
25	811	.024429	2.83E+01	31.47	32.69	1.91158E+02	1.80E-10	-2.83E+01	-6.14E-22	-7.63E+02	1.49E+02	5.90E+01
25	222	.050270	2.83E+01	40.86	72.32	1.97[illegible]09E+02	1.80E-10	-2.83E+01	-6.14E-22	-7.63E+02	1.49E+02	5.90E+01
25	22	.003897	2.83E+01	21.76	68.24	1.60[illegible]30E+02	1.80E-10	-2.83E+01	-6.14E-22	-7.63E+02	1.49E+02	5.90E+01
25	407	.000005	2.83E+01	80.62	80.62	2.23[illegible]42E+02	1.80E-10	-2.83E+01	-6.14E-22	-7.63E+02	1.49E+02	5.90E+01
25	15	.000037	2.83E+01	81.73	81.73	1.62[illegible]14E+02	1.80E-10	-2.83E+01	-6.14E-22	-7.63E+02	1.49E+02	5.90E+01
25	143	.000283	2.83E+01	88.80	67.46	4.47[illegible]08E+02	1.80E-10	-2.83E+01	-6.14E-22	-7.63E+02	1.49E+02	5.90E+01
25	144	.001473	2.83E+01	87.77	54.82	2.71715E+02	1.80E-10	-2.83E+01	-6.14E-22	-7.63E+02	1.49E+02	5.90E+01
25	4	.005171	2.83E+01	80.02	18.53	1.84770E+02	1.80E-10	-2.83E+01	-6.14E-22	-7.63E+02	1.49E+02	5.90E+01
25	781	.000072	2.83E+01	85.07	81.79	4.75[illegible]8oE+02	1.80E-10	-2.83E+01	-6.14E-22	-7.63E+02	1.49E+02	5.90E+01
25	306	.015950	2.83E+01	79.94	79.94	2.71782E+02	1.80E-10	-2.83E+01	-6.14E-22	-7.63E+02	1.49E+02	5.90E+01
25	380	.017409	2.83E+01	53.80	53.80	2.49[illegible]27E+02	1.80E-10	-2.83E+01	-6.14E-22	-7.63E+02	1.49E+02	5.90E+01
25	385	.085720	2.83E+01	48.39	48.09	2.23.10E+02	1.80E-10	-2.83E+01	-6.14E-22	-7.63E+02	1.49E+02	5.90E+01
25	701	.010322	2.83E+01	48.08	83.61	7.10[illegible]12E+01	1.80E-10	-2.83E+01	-6.14E-22	-7.63E+02	1.49E+02	5.90E+01
25	702	.000066	2.83E+01	5.54	89.99	2.40[illegible]80E+02	1.80E-10	-2.83E+01	-6.14E-22	-7.63E+02	1.49E+02	5.90E+01

MODEL = RIO STEP = 1 RCS ANALYSIS 4/9/75
PROCESSING OPERATIONS DATA

26	800	.002640	2.83E+01	88.17	44.27	1.04977E+02	-9.53E-11	-6.97E-22	2.83E+01	-7.63E+02	1.18E+02	5.10E+01
26	801	.014055	2.83E+01	81.69	8.57	8.31962E+01	-9.53E-11	-6.97E-22	2.83E+01	-7.63E+02	1.18E+02	5.10E+01
26	22	.005103	2.83E+01	90.18	63.63	1.31940E+02	-9.53E-11	-6.97E-22	2.83E+01	-7.63E+02	1.18E+02	5.10E+01
26	380	.021745	2.83E+01	43.28	60.32	2.38403E+02	-9.53E-11	-6.97E-22	2.83E+01	-7.63E+02	1.18E+02	5.10E+01
26	385	.075639	2.83E+01	34.50	55.91	2.10837E+02	-9.53E-11	-6.97E-22	2.83E+01	-7.63E+02	1.18E+02	5.10E+01
26	701	.049862	2.83E+01	15.73	75.00	6.29488E+01	-9.53E-11	-6.97E-22	2.83E+01	-7.63E+02	1.18E+02	5.10E+01
26	702	.000179	2.83E+01	82.36	84.82	2.13992E+02	-9.53E-11	-6.97E-22	2.83E+01	-7.63E+02	1.18E+02	5.10E+01
27	800	.002289	2.83E+01	91.83	44.27	1.04977E+02	9.53E-11	6.97E-22	-2.83E+01	-7.63E+02	1.18E+02	5.10E+01
27	801	.008285	2.83E+01	98.31	8.57	8.31962E+01	9.53E-11	6.97E-22	-2.83E+01	-7.63E+02	1.18E+02	5.10E+01
27	805	.032715	2.83E+01	28.22	74.92	1.09995E+02	9.53E-11	6.97E-22	-2.83E+01	-7.63E+02	1.18E+02	5.10E+01
27	806	.109936	2.83E+01	25.44	69.87	9.74034E+01	9.53E-11	6.97E-22	-2.83E+01	-7.63E+02	1.18E+02	5.10E+01
27	810	.007038	2.83E+01	56.97	47.08	1.77307E+02	9.53E-11	6.97E-22	-2.83E+01	-7.63E+02	1.18E+02	5.10E+01
27	811	.015476	2.83E+01	56.81	35.57	1.60701E+02	9.53E-11	6.97E-22	-2.83E+01	-7.63E+02	1.18E+02	5.10E+01
27	222	.067854	2.83E+01	47.97	69.67	1.09935E+02	9.53E-11	6.97E-22	-2.83E+01	-7.63E+02	1.18E+02	5.10E+01
27	22	.006801	2.83E+01	89.82	63.63	1.31940E+02	9.53E-11	6.97E-22	-2.83E+01	-7.63E+02	1.18E+02	5.10E+01
27	437	.006001	2.83E+01	53.51	88.67	2.15263E+02	9.53E-11	6.97E-22	-2.83E+01	-7.63E+02	1.18E+02	5.10E+01
27	2	.007526	2.83E+01	72.90	69.74	4.64168E+02	9.53E-11	6.97E-22	-2.83E+01	-7.63E+02	1.18E+02	5.10E+01
27	3	.017068	2.83E+01	62.70	64.81	3.42529E+02	9.53E-11	6.97E-22	-2.83E+01	-7.63E+02	1.18E+02	5.10E+01
27	144	.007495	2.83E+01	58.20	57.03	2.68302E+02	9.53E-11	6.97E-22	-2.83E+01	-7.63E+02	1.18E+02	5.10E+01
27	4	.006947	2.83E+01	31.88	19.84	1.75131E+02	9.53E-11	6.97E-22	-2.83E+01	-7.63E+02	1.18E+02	5.10E+01
27	150	.000813	2.83E+01	77.87	60.02	4.43247E+02	9.53E-11	6.97E-22	-2.83E+01	-7.63E+02	1.18E+02	5.10E+01
800	701	.007986	3.44E+03	66.31	49.45	1.08434E+02	1.31E+03	3.18E+03	-2.31E+02	-7.29E+02	2.10E+01	5.43E+01
801	701	.007277	5.85E+03	39.76	76.79	8.17196E+01	1.36E+03	5.68E+03	-2.39E+02	-7.74E+02	3.03E+01	6.30E+01
805	701	.003520	3.44E+03	87.37	69.70	1.62597E+02	1.31E+03	3.18E+03	-2.31E+02	-7.42E+02	7.10E+01	-4.57E+01
806	701	.001737	5.85E+03	84.65	84.31	1.50956E+02	1.36E+03	5.68E+03	-2.39E+02	-7.91E+02	8.63E+01	-3.70E+01
807	701	.000506	3.44E+03	126.18	64.73	1.75473E+02	1.31E+03	-3.18E+03	-2.31E+02	-7.42E+02	2.90E+01	-4.57E+01
808	701	.000396	5.85E+03	119.88	80.47	1.74147E+02	1.36E+03	-5.68E+03	-2.39E+02	-7.91E+02	1.37E+01	-3.70E+01
810	701	.002278	3.44E+03	61.13	65.39	2.06443E+02	1.31E+03	3.18E+03	-2.31E+02	-7.42E+02	-2.90E+01	-4.57E+01
811	701	.001641	5.85E+03	54.33	79.65	1.89466E+02	1.36E+03	5.68E+03	-2.39E+02	-7.91E+02	-1.37E+01	-3.70E+01

MODEL = RIO STEP = 1 RCS ANALYSIS 4/9/75
PROCESSING OPERATIONS DATA

222	701	.000176	2.57E+04	61.54	59.53	2.07720E+02	-2.55E+04	-8.68E-08	3.47E+03	-7.19E+02	4.55E-13	-6.25E+01
22	701	.013038	1.63E+04	57.87	45.52	1.35196E+02	-1.62E+04	0.	2.09E+03	-7.04E+02	1.98E-10	5.06E+01
3	701	.000404	2.97E+04	57.99	53.76	3.86540E+02	-9.23E+02	2.59E+03	2.96E+04	-5.37E+02	3.21E+02	-1.66E+02
4	701	.004210	1.01E+04	15.25	53.72	2.21665E+02	-2.20E+03	8.61E+02	9.84E+03	-6.71E+02	1.17E+02	-9.77E+01

MODEL = RIO STEP = 1 RCS ANALYSIS 4/9/75
PROCESSING OPERATIONS DATA

380	701	.001257	2.81E+04	58.11	55.97	1.92437E+02	-2.18E-07	2.81E+04	-1.09E-07	-6.51E+02	-1.23E-08	2.25E+02
385	700	.000148	2.05E+04	48.51	96.13	1.53794E+02	-1.60E-07	2.05E+04	-7.99E-08	-7.46E+02	-1.31E-08	2.25E+02
385	701	.006541	2.05E+04	48.51	83.87	1.53794E+02	-1.60E-07	2.05E+04	-7.99E-08	-7.46E+02	-1.31E-08	2.25E+02
701	703	.000038	1.59E+03	78.80	89.16	1.95108E+02	1.52E+03	-3.03E+02	-3.51E+02	-7.61E+02	1.02E+02	1.12E+02